

A MULTI-CAUSAL FUNCTIONAL ANALYSIS OF HOMINID HIP MORPHOLOGY

A DISSERTATION

SUBMITTED TO THE DEPARTMENT OF ANTHROPOLOGICAL SCIENCES

AND THE COMMITTEE ON GRADUATE STUDIES

OF STANFORD UNIVERSITY

IN PARTIAL FULFILLMENT OF THE REQUIREMENTS

FOR THE DEGREE OF

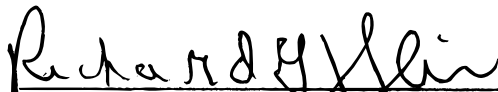
DOCTOR OF PHILOSOPHY

Timothy David Weaver

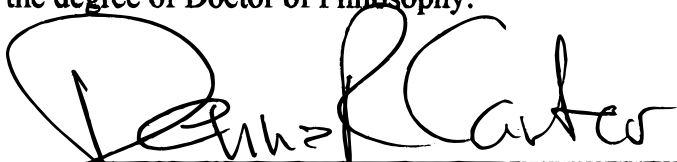
August 2002

© Copyright by Timothy David Weaver 2002
All Rights Reserved

I certify that I have read this dissertation and that, in my opinion, it is fully adequate in scope and quality as a dissertation for the degree of Doctor of Philosophy.


Richard G. Klein (Principal Advisor)

I certify that I have read this dissertation and that, in my opinion, it is fully adequate in scope and quality as a dissertation for the degree of Doctor of Philosophy.


Dennis R. Carter

I certify that I have read this dissertation and that, in my opinion, it is fully adequate in scope and quality as a dissertation for the degree of Doctor of Philosophy.


Joanna L. Mountain

Approved for the University Committee on Graduate Studies:

Abstract

The skeletal elements of the hip have factored prominently in discussions of the behaviors, life histories, and evolutionary histories of hominids from all time periods. Two particularly intriguing questions are what behavioral and life history differences, if any, existed between Neandertals and modern humans that could explain the demise of the Neandertals, and how rapidly and through what stages did bipedal gait evolve in australopiths? Hip form is functionally constrained by the mechanics of walking and childbirth, and variation between human populations in pelvic width and leg to trunk proportions is related to climate. Therefore, only a multi-causal model that simultaneously considers locomotor, obstetrical, and climatic constraints will be able to explain hominid hip morphology. This dissertation takes steps toward such a model through comprehensive 3-D landmark analyses of hip size and shape that are interpreted within a functional framework.

For comparison with fossil hominids, data were collected on matched sets of innominate, sacra, and femora — the skeletal elements of the hip — from a globally distributed sample of recent human skeletons. The data were considered as articulated anatomical units and by individual skeletal element. Novel methods and original software employing generalized procrustes analysis, principal component analysis, discriminant function analysis, and multiple regression were used to analyze the data; changes in form along multivariate axes of variation were explored using interactive computer visualization.

The results of these analyses suggest that features of the Neandertal hip that have been cited as evidence of extremely high activity levels or different life histories are more likely to be secondary mechanical and developmental consequences of hyper-arctic body proportions. Neandertal hip morphology is unique, but it is quantitatively and not qualitatively different from that of recent humans. In addition, while australopiths are outside the range of human variation in overall pelvic shape, many other features of their pelves can be predicted, at least in part, by human patterns of scaling related to birth canal depth versus breadth and iliac blade flaring. This dissertation illustrates the importance of considering the skeleton as an integrated whole that is shaped by both evolutionary and mechanically induced developmental adaptation.

*To my family and Teresa,
for your encouragement and love*

Acknowledgements

I would not have been able to complete this dissertation without much help and support. As I collected data at almost two dozen museums and universities in Africa, Europe, Israel, and the United States and required an expensive 3-D digitizer, the external funding I received for travel and equipment was essential. For generous financial support, I would like to thank the Louis S.B. Leakey Foundation, the Morrison Institute for Population and Resource Studies at Stanford University, the Andrew W. Mellon Foundation, and the Department of Anthropological Sciences at Stanford University. Phoebe Abt, Beth Bashore, Mary Cahill, Ellen Christianson, Shelly Coughlan, Jean Doble, Nancy Lonhart, Blanca Revuelta, and Roanne Shefte were very helpful in processing my grants, sometimes under difficult circumstances.

I especially would like to thank my primary advisor, Richard Klein, for his encouragement, help, and for always being available to discuss paleoanthropological or other topics with me. In the process, he also taught me that paleoanthropology is more than just studying hominid fossils — that for meaningful interpretation, the fossil record must be integrated with archaeology, genetics, paleoclimatology, geological context, and dating.

My two dissertation readers, Joanna Mountain and Dennis Carter, gave insightful comments on drafts of my thesis and imparted valuable knowledge and advice throughout my graduate career. Joanna Mountain taught me much of what I know about anthropological genetics, giving me the tools to evaluate journal articles in this important field of human evolutionary inquiry. I am very grateful to Dennis Carter for welcoming

me as an additional, if somewhat off-topic, member of his lab group, allowing me to learn fresh perspectives on the role of mechanics in skeletal development and evolution.

Robert Franciscus taught me most of what I know about the human skeleton, evolutionary anatomy, and practical aspects of data collection, giving me the tools I needed to collect my dissertation data. From Jean-Jacques Hublin, I learned about Neandertals, human evolution, and a commonly overlooked anatomical area above the hip — the skull. Gary Beaupré, Paul O’Higgins, and Christopher Ruff provided valuable discussions and suggestions about aspects of my project.

For their hospitality, help, and generosity in allowing me to study fossil and/or comparative material under their care, I especially would like to thank the following individuals: David Hunt (Smithsonian Institution); Ian Tattersal and Ken Mowbray (American Museum of Natural History); David Pilbeam and Gloria Greis (Harvard University); Graham Avery (South African Museum, Cape Town); Alan Morris (University of Cape Town Medical School); Phillip Tobias, Lee Berger, and Heather White (Wits Medical School, Johannesburg); Francis Thackeray and Rose Bellamy (Transvaal Museum, Pretoria); Yoel Rak (Tel Aviv University Medical School); Peter Schmid and Karin Isler (University of Zurich-Irchel); Christian Simon (l'Université de Genève); Pierre Vermeersch and Christine Charlier (Katholieke Universiteit te Leuven); Rosine Orban and Patrick Semal (Institut Royal des Sciences Naturelles de Belgique, Brussels); Louise Humphrey, Christopher Stringer, and Robert Kruszynski (Natural History Museum, London); Philip Powell (Oxford University); Hans-Eckart Joachim (Rheinisches Landesmuseum, Bonn); Robert Foley and Maggie Bellatti (University of Cambridge); Henry de Lumley and Dominique Grimaud-Hervé (Institut de Paléontologie

Humaine, Paris); A. Langaney, Philippe Menecier, and Mario Chech (Musée de l'Homme, Paris); G. Spedini and Giorgio Manzi (Universita' di Roma "La Sapienza"); Brunetto Chiarelli and Giuseppe D'Amore (Istituto di Antropologia, Florence); and S. Simone (Musée d'Anthropologie Préhistorique, Monaco). In addition, I would like to thank all of the graduate students and other individuals from these institutions who assisted me with my data collection. The Spy remains reside in the Institut Royal des Sciences Naturelles, Brussels, by courtesy of the family of Professor Max Lohest (1857-1926).

Jerome Cybulski, Christine Hanson, Trent Holliday, Marta Mirazon Lahr, Roberto Macchiarelli, Charles Merbs, Jacopo Moggi-Cecchi, Janet Monge, Susan Pfeiffer, Maria Teschler, and Douglas Ubelaker provided information that helped me track down skeletal collections. Brian and Lorna Kerr and Suhail and Trish Islam were wonderful with their hospitality and allowed me to stay with them in London; Pierre Le Breton generously rented me a room in his apartment for my stay in Paris; Roland Nespoulet kindly took the time to explain to me the stratigraphy of l'Abri Pautaud; and Francis Thackeray greatly enriched my data collection trip by giving me a tour of some of the South African australopith sites.

As fellow graduate students, Elizabeth Burson, Matt Jobin, Silvia Kembel, Richard Pocklington, Charles Roseman, Sandra Shefelbine, and Deborah Stratmann provided many stimulating discussions and much needed comic relief. Corey Karlin was very helpful with the initial stages of this project.

My extended family — the Bonellis — provided endless hospitality and entertainment and familiar faces during the six months that I was travelling. I especially

would like to thank my brothers, Ash and Chris, and my parents, David and Elena, for always being there for me with encouragement and love, even when I had the crazy idea of giving up my job as a computer software engineer to pursue a career in paleoanthropology. Finally, Teresa Steele contributed to this dissertation in ways that are too numerous to list — even though it was trying at times, we eventually made it together!

After six years, I truly am grateful to all these individuals, organizations, and institutions; I sincerely apologize for any inadvertent omissions. Of course, I take full responsibility for all the conclusions and any errors contained in this dissertation.

Table of contents

Abstract	iv
Acknowledgements.....	vii
Table of contents	xi
List of tables	xv
List of illustrations	xvi
Chapter 1. Introduction, background, and research questions.....	1
Introduction.....	1
Background.....	4
Fossil hominid hip morphology	4
Neandertals and their contemporaries.....	5
Primitive <i>Homo</i>	9
Australopiths	13
Constraints on hip morphology and explanations for fossil morphology.....	16
Climate	17
Locomotor biomechanics	21
Obstetrics	25
Other functional constraints	29
Developmental constraints	30
Hypotheses and research questions	32
Chapter 2. Materials: Comparative and fossil samples.....	33
Recent modern humans.....	33

Geographically variable sample	35
Sex balanced sample.....	36
Skeletal collections by geographic region of origin	36
Sub-Saharan Africa.....	37
Southern Asia.....	39
Pacific.....	39
Northern Africa.....	41
Northern Europe	41
Sub-Antarctic	41
Sub-Arctic	42
North America	42
Sex and age determination.....	43
Fossil hominids	44
Chapter 3. Methods: Data collection and analysis.....	46
Data collection and manipulation	46
Equipment and software	46
Specimen setup	47
Landmarks.....	48
Rearticulation and orientation	49
Standard measurements	50
Analytical techniques.....	51
Articulated hip analyses.....	51
Generalized Procrustes Analyses (GPA)	54
Discriminant function analyses	56
Multiple regression shape prediction	57
Original software	58
Precision of methods.....	58

Fossil hominid analyses.....	60
Chapter 4. Recent modern human analyses.....	62
Geographically variable sample.....	63
Articulated hip analyses.....	63
Hemi-pelvis analyses.....	66
Femur analyses.....	67
Innominate analyses.....	68
Relationship with climate and discriminant analyses.....	69
Sex balanced sample.....	72
Articulated hip analyses.....	72
Hemi-pelvis analyses.....	74
Femur analyses.....	75
Innominate analyses.....	75
Discriminant analyses.....	76
Discussion of the recent human baseline.....	77
Chapter 5. Fossil hominid analyses.....	83
Middle to Late Pleistocene fossils.....	84
Hemi-pelvis analyses.....	84
Femur analyses.....	87
Innominate analyses.....	88
Discussion of previous hypotheses.....	90
Australopiths.....	95
Hemi-pelvis analyses.....	95
Innominate analyses.....	96
Discussion of previous hypotheses.....	97

Chapter 6. Conclusions	101
A scenario for hominid hip evolution	101
Final thoughts and suggestions for future research	106
Appendices.....	108
A. Tables.....	109
B. Figures	119
C. List of fossil specimens analyzed	182
D. Detailed definitions of landmarks	184
Femoral landmarks	184
Pelvic landmarks.....	189
E. Methods for calculating standard measurements	197
F. Original software	203
Data collection	203
Rearticulation and anatomical orientation	204
Calculation of standard measurements	204
Morphometric analysis	205
Interactive visualization.....	205
Bibliography	207

List of tables

<u>Table</u>	<u>Title</u>	<u>Page</u>
1.1	Geologic timeline	110
2.1	Recent modern human skeletal samples	111
3.1	Landmarks used in this study	112
3.2	Calculated standard measurements	113
4.1	Correlation coefficients between standard measurements and the principal components of the geographically variable sample	114
4.2	Discriminant analyses for the geographically variable sample	115
4.3	Correlation coefficients between standard measurements and the principal components of the sex balanced sample	116
4.4	Discriminant analyses for the sex balanced sample	117
5.1	Multiple regression analyses of pelvic inlet shape, relative pelvic height, and pelvic morphology for the sex balanced sample	118

List of illustrations

<u>Figure</u>	<u>Title</u>	<u>Page</u>
1.1	Key fossil hominid pelves	120
1.2	Key fossil hominid femora	121
2.1	Geographic locations of recent human sub-samples	122
3.1	Landmarks used in this study	123
4.1	Geographically variable analysis: hip PC1	124
4.2	Geographically variable analysis: hip PC2	125
4.3	Geographically variable analysis: hip PC3	126
4.4	Geographically variable analysis: hip PC4	127
4.5	Geographically variable analysis: pelvis PC1	128
4.6	Geographically variable analysis: pelvis PC2	129
4.7	Geographically variable analysis: femur PC1	130
4.8	Geographically variable analysis: femur PC2	131
4.9	Geographically variable analysis: innominate PC1	132
4.10	Z-scores along PCA axes that reflect body proportions	133
4.11	Geographically variable analysis: hip discriminant function axis that separates populations by climate	134
4.12	Geographically variable analysis: pelvis discriminant function axis that separates populations by climate	135
4.13	Geographically variable analysis: femur discriminant function axis that separates populations by climate	136

4.14	Geographically variable analysis: innominate discriminant function axis that separates populations by climate	137
4.15	Sex balanced analysis: hip PC1	138
4.16	Sex balanced analysis: hip PC2	139
4.17	Sex balanced analysis: hip PC3	140
4.18	Sex balanced analysis: hip PC4	141
4.19	Sex balanced analysis: hip PC5	142
4.20	Sex balanced analysis: pelvis PC1	143
4.21	Sex balanced analysis: femur PC1	144
4.22	Sex balanced analysis: femur PC2	145
4.23	Sex balanced analysis: innominate PC1	146
4.24	Sex balanced analysis: hip discriminant function axis that separates males and females	147
4.25	Sex balanced analysis: pelvis discriminant function axis that separates males and females	148
4.26	Sex balanced analysis: innominate discriminant function axis that separates males and females	149
4.27	Biomechanical model of the adult human hip	150
4.28	Biomechanical model of the juvenile human hip	151
5.1	Geographically variable Middle to Late Pleistocene analysis: pelvis centroid size	152
5.2	Geographically variable Middle to Late Pleistocene analysis: pelvis PC1	153

5.3	Geographically variable Middle to Late Pleistocene analysis: pelvis PC2	154
5.4	Sex balanced Middle to Late Pleistocene analysis: pelvis centroid size	155
5.5	Sex balanced Middle to Late Pleistocene analysis: pelvis PC1	156
5.6	Geographically variable Middle to Late Pleistocene analysis: femur centroid size	157
5.7	Geographically variable Middle to Late Pleistocene analysis: femur PC1	158
5.8	Geographically variable Middle to Late Pleistocene analysis: femur PC2	159
5.9	Sex balanced Middle to Late Pleistocene analysis: femur centroid size	160
5.10	Geographically variable Middle to Late Pleistocene analysis: innominate centroid size	161
5.11	Geographically variable Middle to Late Pleistocene analysis: innominate PC1	162
5.12	Sex balanced Middle to Late Pleistocene analysis: innominate centroid size	163
5.13	Sex balanced Middle to Late Pleistocene analysis: innominate PC1	164
5.14	Superior pubic ramus length vs. bi-iliac breadth	165
5.15	Rak's ratio of antero-posterior acetabular positioning	166
5.16	Rak's posterior distance (sacral promontory to anterior acetabulum)	167
5.17	Rak's anterior distance (anterior acetabulum to superior pubic symphysis)	168

5.18	Medio-lateral acetabular angle	169
5.19	Antero-posterior sacral angle	170
5.20	Geographically variable australopith analysis: pelvis centroid size	171
5.21	Geographically variable australopith analysis: pelvis PC1	172
5.22	Geographically variable australopith analysis: pelvis PC2	173
5.23	Sex balanced australopith analysis: pelvis centroid size	174
5.24	Sex balanced australopith analysis: pelvis PC1	175
5.25	Geographically variable australopith analysis: innominate centroid size	176
5.26	Geographically variable australopith analysis: innominate PC1	177
5.27	Sex balanced australopith analysis: innominate centroid size	178
5.28	Sex balanced australopith analysis: innominate PC1	179
5.29	Prediction of pelvic shape based on AL 288-1's inlet shape	180
5.30	Prediction of pelvic shape based on AL 288-1's relative pelvic height	181

Chapter 1

Introduction, background, and research questions

Introduction

For more than a century, paleoanthropologists have frequently posed two questions: what behavioral and life history differences, if any, existed between Neandertals and modern humans, and how and in what exact form did human bipedal gait evolve? This dissertation addresses both of these questions, along with other issues, through analyses of recent human and fossil hominid hip morphology, but first, it is helpful to put these questions into context within the broader field of paleoanthropology.

Neandertals lived in Europe and western Asia between ca. 127-40 thousand years ago (kya), and their last common ancestor with modern humans probably lived 500-600 kya. Most paleoanthropologists now agree that Neandertals were predominately, if not completely, replaced by modern human populations originating in Africa during that last 50-200 thousand years. This growing consensus is based on genetics of the non-recombining portion of the Y-chromosome (e.g. Underhill et al. 2001), mitochondrial DNA (e.g. Ingman et al. 2000), and various autosomal regions in living humans (e.g. Knight et al. 1996, Tishkoff et al. 1996); ancient Neandertal mitochondrial DNA (e.g. Krings et al. 2000, Ovchinnikov et al. 2000); comparisons between Neandertal and fossil modern human cranial and post-cranial skeletons (e.g. Gambier 1989, Pearson 2000b); and a discontinuity at approximately 40 thousand years ago in the archaeological record of Europe (e.g. Klein 2000). Debate now centers on how much, if any, interbreeding

occurred between Neandertals and incoming modern humans, how rapidly Neandertals were replaced, and if Neandertals were behaviorally different from the African populations ancestral to modern humans. One interesting question that remains to be solved is: how were modern humans able to replace Neandertals so completely? — Especially given that Neandertals and their ancestors had been adapting to European environments for potentially 400-500 thousand years before modern humans arrived.

Neandertals could have been out-competed because they had altered life histories relative to later humans or because they used their bodies instead of technology to interface with the environment. If Neandertals had slightly different life histories than modern humans, they could have had lower birth rates or elevated death rates, and even small demographic discrepancies between modern humans and Neandertals could have resulted in population replacement over a number of generations (Zubrow 1989). In addition, the limited technological ability of Neandertals would have forced them to adapt physically instead of culturally to the glacial environments of Europe, potentially making them unable adapt as quickly as modern humans to changing climatic conditions leading up to the last glacial maximum. While some of these issues can be addressed with archaeological data, most can be directly tackled only by studying fossil anatomy.

Molecular and fossil evidence suggest that the last common ancestor of humans and chimpanzees lived 5-7 million years ago (mya). The australopiths were broadly speaking the first primates exclusively ancestral to humans, and in most respects they resembled living apes; they mainly differed from apes by walking on two legs instead of four. Various species of australopith lived in Africa from more than 4 mya to about 1 mya, and some australopith species coexisted with early members of the genus *Homo*.

While few dispute that these early hominids were bipedal, questions remain about the efficiency of their gait, their physical adaptations to tree climbing, and the influence of increasing brain size on the evolution of locomotor anatomy.

Many interesting questions about australopiths deal with the tempo and mode of evolutionary change and how to sort out which aspects of australopith skeletal morphology are adaptive and thus reflective of behavior. If the earliest hominids spent most of their time on the ground and walked in a manner indistinguishable from living humans, then the origin of our lineage was a punctuated event, perhaps because it is not an evolutionarily viable strategy to be intermediate between a quadruped and a biped. On the other hand, if these hominids initially retained many climbing adaptations and their bipedalism increased in efficiency over millions of years, hominid origins could be thought of as an evolutionarily more gradual event. These issues can only be addressed by determining which aspects of hominid skeletal anatomy accurately reflect locomotor behavior.

The skeletal elements of the hip have factored into discussions about both Neandertals and australopiths due to their crucial role in obstetrics and locomotion. Aspects of pelvic or femoral morphology have been used to support hypotheses of altered life histories, behavior, or gait of fossil hominids relative to modern humans, but often ranges and patterns of variation found in recent humans are not adequately considered. The hominid hip potentially is influenced by a combination of climatic, biomechanical, and obstetrical factors, but most studies have focused primarily on a single functional constraint. Also, even though the hip is functionally composed of both the pelvis and femur, usually these elements are studied separately.

This dissertation addresses these issues by 1) documenting geographic variation in recent human hip morphology as a comparative baseline for fossil hominid morphology; 2) considering multiple functional constraints simultaneously; 3) analyzing the hip as an anatomical unit in three-dimensions; and 4) relating shape trajectories to standard linear and angular measurements that have been discussed by previous researchers. My conclusion is a multi-causal functional scenario for the evolution of hominid hip morphology that can be further tested and refined by future research.

Background

Before discussing my research methods and results, I briefly describe fossil hominid hip morphology, starting with the Late Pleistocene and working back in time to the Pliocene and the Late Miocene (see Table 1.1 for a geologic timeline). Then, I discuss important functional constraints on the hominid hip and previous hypotheses to explain fossil morphology based on these constraints. Finally, I outline my objectives and research questions.

Fossil hominid hip morphology

Most descriptions of fossil hominid hip morphology are based on the relatively few well-preserved specimens that have been discovered, but these descriptions are often bolstered by the morphology of more fragmentary material. Starting with the bones of the pelvis and ending with the femur, I describe below many of the anatomical features that have been identified for Neandertals and their Late Pleistocene contemporaries, Late Pliocene and Early to Middle Pleistocene primitive *Homo*, and australopiths. Figures 1.1 and 1.2 show differences in hip morphology between fossil hominids and recent humans

on labeled illustrations of representative fossils. Table 1.1 defines relevant geologic time periods.

Neandertals and their contemporaries

This discussion of Neandertal pelvic morphology is based on descriptions of the right hemi-pelvis from the Mousterian layers of Kebara Cave, Israel (Kebara 2, see Fig. 1.1), because this specimen is the most complete yet discovered (Rak 1991, Rak and Arensburg 1987). I note my additional observations and those of other researchers about Kebara 2 or other Neandertal pelvises with citations. The descriptions that follow are relative to recent humans unless otherwise specified.

Kebara 2 has an extremely wide bi-iliac breadth that is surpassed only by the temporally earlier Pelvis 1 from the Sima de los Huesos (Arsuaga et al. 1999) and the Jinniushan pelvis (bi-iliac breadth estimated based on only a left innominate, Rosenberg, Zun'e, and Ruff 1999). According to Boule's (1912) reconstruction, La Chapelle-aux-Saints 1 also has a very wide bi-iliac breadth (Holliday 1997b). Kebara 2 has a spacious pelvic inlet (contra Rak 1991, Rak and Arensburg 1987), but its lower pelvic planes are very constricted (Tague 1992, Weaver et al. 1998). Although the pelvic inlet of Kebara 2 appears heart-shaped due to quite sagittally oriented pubic bones, its pelvic index is still that of a platypelloid pelvis. With its inlet held horizontally, Kebara 2 has acetabulae that face laterally and are positioned posteriorly relative to the pelvic inlet. These differences result in a narrow posterior acetabular surface (a short distance between the posterior margin of the acetabular rim and the anterior edge of the greater sciatic notch). Based on fragments, other Neandertals appear to have sagittally oriented pubic bones with arcuate/pectineal line curvatures that are similar to Kebara 2 (personal observation), but

interestingly, Krapina 209/212, which is assumed to be a female, may have a more coronally oriented pubic bone and a less laterally facing acetabulum (personal observation from Fig. 230, Radovic et al. 1988). Relative acetabular positioning is difficult to assess for more fragmentary Neandertal specimens.

Kebara 2 has a coronally facing posterior iliac blade, an elongated and medially pointing anterior-superior iliac spine, a pronounced and laterally concave anterior-inferior iliac spine, a deep inter-anterior spinal notch, a wide supra-acetabular shelf, and an anteriorly located iliac pillar with a large iliac tubercle. The ilia of Amud 1, Tabun C1, and Neandertal 1 are fragmentary, but they also appear to have prominent and concave anterior-inferior iliac spines and anteriorly located iliac pillars (Endo and Kimura 1970, Rosenberg 1986, personal observation). Other Neandertals also have large iliac tubercles (Rosenberg 1986); however, Amud 1 has a small iliac tubercle (Endo and Kimura 1970).

Kebara 2 has a constricted greater sciatic notch. Narrow greater sciatic notches are found in other Neandertals as well (Boule 1912, de Lumley 1972, Heim 1983), but Krapina 209/212 and 211, which are presumed to be females, have wider greater sciatic notches (Radovic et al. 1988) and so do Tabun C1 (McCown and Keith 1939) and La Ferrassie 2 (personal observation). Pronounced greater sciatic notch constriction in Kebara 2 causes its sacrum to have an extremely anteriorly rotated orientation from a lateral view, resulting in a sacral promontory that projects far superiorly to the plane of the pelvic inlet (personal observation). La Ferrassie 1 also appears to have a similar greater sciatic notch shape to Kebara 2 (personal observation from casts and photos).

The superior pubic ramus of Kebara 2 is long, supero-inferiorly thinned, and transversely wide, with a very tall, sharp pectineal crest. Posteriorly the pubic ramus of

Kebara 2 terminates in a weakly defined ilio-pubic eminence. Also, although universally considered a male individual, Kebara 2 has a wide sub-pubic angle. Even though they are fragmentary, Amud 1, La Ferrassie 1, Krapina 208, Krapina 209, Shanidar 1, Shanidar 3, and Tabun C1 all appear to have elongated and thinned pubic bones (Endo and Kimura 1970, Heim 1983, McCown and Keith 1939, Radovic et al. 1988, Rosenberg 1986, 1988, Smith 1978, Stewart 1960, Trinkaus 1984). Shanidar 4 displays pubic thinning but is too fragmentary to assess length (Rosenberg 1986). La Ferrassie 6 and the Dederiyeh infant also show that pubic elongation (but not thinning) is present early in Neandertal development (Akazawa et al. 1995, Tompkins and Trinkaus 1987). For the specimens currently available, purported male Neandertals have longer pubic bones than females (Rosenberg 1998), but given the small sample sizes presently available, it may be the case that male and female Neandertals have equally long pubic bones on average.

On Kebara 2 the groove for the tendon of M-obturator internus overrides the supero-medial aspect of the hamstring surface of the ischial tuberosity, potentially reflecting a different ischial orientation in Neandertals (but see Trinkaus 1996). This may occur because the ischial spine is very inferiorly placed and therefore close to the ischial tuberosity (personal observation).

Kebara 2 has a fairly wide and long sacrum with a fairly flat, as opposed to angled, superior surface of S1 (a high promontory angle). The sacra of other Neandertals are fairly wide in absolute dimensions (Rosenberg 1986). However, relative to pelvic breadth, Kebara 2 has a narrow sacrum (Tague 1992); this also is probably true for La Chapelle-aux-Saints 1 (Boule 1912).

In contrast to Neandertals, the Late Pleistocene near-modern Qafzeh-Skhul individuals from Israel and the early Upper Paleolithic people from Europe have pelvic morphologies similar to recent humans (Rak 1990, Trinkaus 1984). This assessment is based on Skhul 4, Qafzeh 9, and various Upper Paleolithic specimens. There also is new material from Omo (Kibish), Ethiopia, but it is still unpublished (Shea et al. 2002). The one potential exception is Skhul 9. This specimen has an elongated superior pubic ramus that is fairly thin (Rosenberg 1998) but not thinned to the same degree as for most Neandertals. The contemporaries of Neandertals generally have linear body forms based on proximal relative to distal limb length, limb length relative to trunk height (Holliday 1997a), and bi-iliac breadth relative to femur length (Ruff 1994), but in absolute dimensions at least some individuals have wide pelves. Both Skhul 4 and Grotte des Enfants 4 (Gravettian-associated modern human) have fairly wide bi-iliac breadths (data from Holliday 1995 and this dissertation).

Neandertal femora have large femoral heads and distal ends relative to femur length, rounded shafts that lack pilasters, antero-posterior shaft bowing, large gluteal tuberosities that are sometimes laterally buttressed, and low neck-shaft angles (Boule 1912, Trinkaus 1983, Trinkaus 1993a, Trinkaus 1995, Trinkaus 1997, Weidenreich 1941). One of the most extreme examples of these morphological features is the Spy 2 femur from Belgium (see Fig. 1.2), but other Neandertals from both western Asia and Europe approach this extreme. One potential exception is the Châtelperronian-associated Saint Césaire skeleton from France, which has a round sub-trochanteric shaft but a less rounded mid-shaft than other Neandertals (Trinkaus et al. 1998).

The femora of Qafzeh-Skhul and Upper Paleolithic individuals have antero-posteriorly reinforced shafts and large pilasters (Trinkaus 1983, Trinkaus, Ruff, and Churchill 1998). The Qafzeh-Skhul femora also have extremely high neck-shaft angles. The femora of Upper Paleolithic people are variable in neck-shaft angle (Trinkaus 1993a). Both Neandertals and their contemporaries tend to have thick femoral cortical bone relative to more recent humans (Trinkaus 1997). The right distal femoral fragment (Day, Twist, and Ward 1991) and mid-shaft reconstructed by Kennedy (1984) of Omo (Kibish) I from Ethiopia is indistinguishable in morphology and metrics from the femora of recent humans. Also, the KNM-ER 999 left proximal femur from Kenya has a clear pilaster and an extremely high neck-shaft angle (Trinkaus 1993b). Thus, these possible Late Pleistocene specimens from Africa appear to show closer affinities with the Qafzeh-Skhul individuals than with Neandertals. Recent humans groups are quite variable in robusticity, shaft shape, and neck-shaft angle.

Primitive Homo

For the purposes of this discussion, primitive *Homo* includes fossils classified as *Homo sp.*, *Homo habilis*, *Homo rudolfensis*, *Homo ergaster*, *Homo erectus*, *Homo heidelbergensis*, *Homo antecessor*, and late Middle Pleistocene archaic *Homo sapiens*. This categorization covers a broad temporal interval and undoubtedly contains much morphological and potential regional variation, but more specimens from this time period are needed for finer categorization. Also, it is sometimes difficult to make specific designations based on isolated postcranial elements. With these issues in mind, I discuss specimens in approximate chronological order to better highlight any patterns of morphological evolution.

The oldest relatively complete adult pelvic fragment from *Homo* is a partial right innominate, KNM-ER 3228, from the very end of the Pliocene of Kenya. The ilium and ischium of this specimen are preserved but the pubic region is missing. KNM-ER 3228 appears to have a laterally flaring and coronally oriented iliac blade, an elongated and possibly medially pointing anterior-superior iliac spine, an extremely robust iliac pillar and tubercle, a deep gluteal fossa, a shallow iliac fossa, a large acetabulum, a small and inferiorly located auricular surface, a large iliac tuberosity, and a laterally-twisted ischial tuberosity (Rose 1984). OH 28, the geologically much more recent Early Pleistocene left innominate fragment from Tanzania, also has a laterally flaring iliac blade, possibly an elongated anterior-superior iliac spine, a very robust iliac pillar, a shallow iliac fossa, a large acetabulum, a small and inferiorly located auricular surface, a rounded (as opposed to sharp) arcuate line, a large iliac tuberosity, and a laterally twisted ischial tuberosity. The main difference between these two innominates is that OH 28 has a much wider greater sciatic notch than KNM-ER 3228, presumably due to sexual dimorphism (Day 1971). Other than unpublished material from Dmanisi (Lordkipanidze and Vekua 2002), the only other reasonably complete pelvic material from this time period is the KNM-WT 15000 partial skeleton of a juvenile (Nariokotome, Kenya). The entire pelvic girdle has been reconstructed but only portions of unfused ilia and ischia from the left and right sides and sacral fragments are preserved, making any reconstruction very speculative. KNM-WT 15000 lacks a robust iliac pillar or tubercle, but this may be due to the individual's young age (Walker and Leakey 1993).

From the Middle Pleistocene, the Arago 44 left innominate from France is morphologically similar to the older KNM-ER 3228 and OH 28 innominates. It

preserves a prominent and anteriorly located iliac pillar, a medially located anterior-inferior iliac spine, a large supra-acetabular shelf, a marked medial deflection of the anterior iliac crest, and a shallow iliac fossa (Sigmon 1982). The E 719 right innominate from Broken Hill mine, Zambia, possibly of similar age to Arago 44, possesses an extremely thick iliac pillar (particularly the cortical bone). However, E 719 does not appear to have any of the other distinctive morphological features of KNM-ER 3228 and OH 28 (Stringer 1986). The E 688 sacrum from the same site also appears morphologically modern (personal observation). The geologically more recent (at least than Arago 44 and possibly E 719) fragmentary right innominate from Grotte du Prince, Italy, is generally robust, has an anteriorly located iliac pillar, a deep inter-anterior spinal notch, a laterally concave anterior-inferior iliac spine, a large supra-condylar shelf, a narrow posterior acetabular surface, and exhibits other morphological features that align it with Neandertals (de Lumley 1972).

By far the most complete pelvic remains from the Middle Pleistocene come from the Sima de los Huesos, Spain. One virtually complete pelvis (Pelvis 1, see Fig. 1.1) is preserved along with many other more fragmentary remains. Pelvis 1 has an extremely wide bi-iliac breadth that is partially produced by laterally flared ilia, and it is wide in all transverse dimensions. It also has elongated, medially pointing anterior-superior iliac spines, laterally concave anterior-inferior iliac spines, wide supra-acetabular shelves, robust iliac pillars and tubercles, and a long superior pubic ramus with a pronounced pectineal crest. Although Pelvis 1 is enormous, other fragmentary remains from the Sima de los Huesos appear to be similar in size (Arsuaga et al. 1999). The Jinniushan left innominate from China has a long pubic bone and is similar in morphology to Arago 44

but with a more gracile iliac pillar (Rosenberg 1998). However, neither of these specimens have superior pubic rami that are as thin as those of many Neandertals (Compare Figure 3 and Figure 2 in Arsuaga et al. 1999, Rosenberg 1998, respectively).

Femora from the earliest representatives of African *Homo* such as KNM-ER 1481 and OH 28 generally have long and antero-posteriorly flattened necks (McHenry and Corruccini 1978, Ruff 1995), low neck-shaft angles (Trinkaus 1993a), large gluteal tuberosities with lateral buttressing, relatively antero-posteriorly flattened versus medio-laterally wide shafts throughout their entire length, distal points of minimum shaft breadth, convex medial shaft borders, poorly developed pilasters, and very thick cortical bone that results in narrow medullary canals (Day 1971, Kennedy 1983, Kennedy 1984, Ruff 1995). It is important to note that medio-lateral buttressing of the shaft is mainly through increased cortical thickness as opposed to increased external dimensions. KNM-WT 15000 has only some of the features listed above, but this may be due to the individual's young age (Walker and Leakey 1993). The Middle Pleistocene Zhoukoudian femora from Asian *Homo erectus* appear morphologically similar to femora from primitive African *Homo* (Day 1971, Kennedy 1983, Kennedy 1984, Weidenreich 1941). The femora from Trinil appear morphologically more like those of recent humans, but there are questions about their age and their association with the Trinil cranial fragment (Day 1971, Kennedy 1983, Kennedy 1984, Weidenreich 1941).

Definite or supposed Middle Pleistocene femora from African and European sites such as Berg Aukas, Namibia, Broken Hill mine, Zambia (see Fig. 1.2), Aïn Maarouf, Morocco, and Sima de los Huesos, Spain tend to have shorter and rounder necks, more circular shafts, higher points of minimum shaft breadth, and larger pilasters than earlier

representatives of *Homo*. These femora also tend to have larger pilasters than Neandertals (Arsuaga et al. 1999, Grine et al. 1995, Hublin 1992, Kennedy 1984). However, there is quite a bit of femoral morphological diversity within the Middle Pleistocene, and different specimens approximate more or less the morphology of earlier *Homo*. The Broken Hill femora in particular appear morphologically very modern (Pearson 2000b). This diversity may be due to individual, temporal, or geographic variation. Because of the paucity of specimens, it is unclear whether or not there is any morphological divergence between geographic regions at this time.

Australopiths

For the purposes of this discussion, the category australopith includes fossils classified in the genera *Australopithecus* or *Paranthropus*. This categorization covers multiple species that may or may not have had different locomotor constraints due to differences in gait or habitual activities, but more specimens are needed to assess this potential variation. With this in mind, I discuss specimens in approximate chronological order.

The oldest relatively complete adult pelvic fragments from an australopith are from the AL 288-1 “Lucy” partial skeleton from Hadar, Ethiopia. They show many adaptations to bipedalism and are generally of human form. Therefore, I will note only morphological features that are different from or on the edge of recent human ranges of variation. AL 288-1 has a projecting and laterally pointing anterior-superior iliac spine, an iliac pillar just posterior to the apex of the anterior-superior iliac spine (that may or may not be homologous to the iliac pillar of recent humans), a pointed anterior limit of the lunate surface of the acetabulum, a fairly wide greater sciatic notch, a projecting

ischial spine, and long superior and inferior pubic rami (Johanson et al. 1982). In addition, AL 288-1 has a coronally facing posterior iliac blade, an ischial tuberosity that is separated from the acetabular rim by a large sulcus, a sharp angle between the hamstring and adductor surfaces of the ischial tuberosity, no clear falciform crest on the ischial tuberosity, a small pubic contribution to the lunate surface, a weakly defined ilio-pubic eminence, a sacrum that has a small amount of ventral concavity, a weakly developed transverse process of the sacral ala (Stern 2000, Stern and Susman 1983), and a high sacral promontory angle (Abitbol 1987a, Abitbol 1995a). The unique acetabular lunate surface morphology of AL 288-1 does not appear to be present on any South African australopiths (personal observation).

The other well-preserved australopith pelvis is from the Sts 14 partial skeleton from Sterkfontein, South Africa (see Fig. 1.2). Sts 14 has a pronounced acetabulo-spinous pillar that is the anterior portion of a wide, fan-shaped area of thickening of the iliac blade that continues posteriorly to meet a weakly developed iliac pillar. In addition, this specimen has a projecting and laterally pointing anterior-superior iliac spine, a laterally flaring iliac blade, a small auricular surface, a small acetabulum, a projecting ischial spine, an ischial tuberosity that is separated from the acetabular rim by a large sulcus, and a small sacral body relative to the alae. Sts 14 also has a low (or high if the supplementary angle is measured) pelvic torsion angle due to more coronally facing posterior iliac blades (Orban 1982, Robinson 1972, Segebarth-Orban 1977). The morphological features of Sts 14 are corroborated on other more fragmentary South African fossils (Lovejoy, Heiple, and Burstein 1973, McHenry 1975b, Robinson 1972, personal observation), and there do not appear to be major pelvic differences between

different australopith taxa (Lovejoy, Heiple, and Burstein 1973, McHenry 1975a). However, not all researchers agree (e.g. Sarmiento 1998).

In all three reconstructions of the Sts 14 pelvis, the pelvic aperture is wider transversely than it is sagittally at all pelvic planes (Abitbol 1995b, Häusler and Schmid 1995, Rosenman, Lovejoy, and Spurlock 1999). Robinson also reconstructed the Sts 14 pelvis, but unfortunately he never published obstetrical dimensions; nevertheless, Robinson's reconstruction appears platypelloid (Robinson 1972, Figs. 42-46, pp. 308-311). For the AL 288-1 pelvis, one reconstruction is platypelloid throughout the birth canal (Lovejoy 1979, Tague and Lovejoy 1986, Tague and Lovejoy 1998), another is transversely oval at the inlet and midplane but round at the outlet (Berge, Orban-Segebarth, and Schmid 1984, Häusler and Schmid 1995), and another is transversely oval at the inlet but larger sagittally at the midplane and outlet (Häusler and Schmid 1995). Thus, the majority of reconstructions of australopith pelves are wider or equal transversely than they are sagittally at all pelvic planes.

The proximal femora of australopiths tend to have small heads that are not much more than a hemisphere, long and antero-posteriorly flattened necks, low neck-shaft angles, laterally positioned lesser trochanters, and greater trochanters that are flush with the lateral shaft margin (Lovejoy, Heiple, and Burstein 1973, Lovejoy, Johanson, and Coppens 1982, McHenry and Corruccini 1978, Robinson 1972, Walker 1973, see Fig. 1.2). However, AL 288-1 and AL 333-3 both have higher neck shaft angles and shorter necks than other australopiths (Stern and Susman 1983), and most of the Hadar specimens have somewhat laterally flared greater trochanters (Lovejoy, Johanson, and Coppens 1982). Some australopith specimens also have pronounced gluteal tuberosities

with associated lateral buttressing (Lovejoy, Johanson, and Coppens 1982, Walker 1973). Some of this variation may reflect differences between taxa (McHenry and Corruccini 1978, Robinson 1972), but more specimens are needed to properly assess the ranges of variation for each taxon. The recently discovered late Miocene proximal femur from the Lukeino Formation, Kenya that has been assigned to the new genus and species *Orrorin tugenensis* shows many distinctive australopith features (Senut et al. 2001).

The shafts of australopith femora tend to be antero-posteriorly flattened subtrochanterically but round at the midshaft, and they generally have thick cortical bone (Ruff 1998, Walker 1973). The Hadar distal femora have weakly projecting lateral lips of the patellar groove and inferior widths of the medial condyle that are greater than those of the lateral condyle (Stern 2000, Stern and Susman 1983, Tardieu 1998). Distal femora from other australopiths are morphologically similar to those of recent humans (Robinson 1972, Walker 1973). Compared to living humans, australopith femora tend to be short relative to other dimensions (Stern 2000) and have high estimated bicondylar angles (Walker 1973).

Constraints on hip morphology and explanations for fossil morphology

Explanations for a particular morphological feature or group of features usually fall into two broad categories: phylogenetic (usually not adaptational) hypotheses or functional (adaptational) hypotheses. Phylogenetic hypotheses attempt to explain distinct anatomy as either due to historical inertia such as retention from an ancestor or due to stochastic processes such as genetic drift in a small, isolated population. Functional hypotheses posit that morphological features are adaptations to specific behaviors or activities and that they arise either through developmental adaptation during an

individual's lifetime or through evolutionary adaptation via natural selection. Many morphological features may also be the secondary consequences of changes to other regions coupled with the need to maintain developmental, biomechanical, or spatial integration of an anatomical region (Lovejoy, Cohn, and White 1999).

In general, only once developmental and functional constraints on an anatomical feature are understood can it be properly used for phylogeny (Lieberman 1995). Thus, taking primarily a functional approach to morphology is useful even if only to highlight those traits that are best to use for phylogenetic reconstruction. This is especially true for an anatomical region such as the hip, because the hip plays an integral role in both locomotion and obstetrics (Ruff 1995). Nevertheless, investigating functional hypotheses without attention to phylogeny also can lead to erroneous conclusions. With these theoretical considerations in mind, the following section discusses functional and developmental constraints on the hominid hip and explanations for fossil hominid and recent human hip morphology. I consider phylogenetic explanations in more detail in the concluding chapter.

Climate

From Bergmann (1847) and Allen (1877) to the present, numerous researchers have documented ecogeographical patterns in body size and limb proportions of warm-blooded animals that appear to be related to climate (reviewed by Ashton, Tracy, and de Queiroz 2000, Holliday 1995). Bergmann's "rule" states that members of a species living in cold climates will tend to be larger than those individuals living in warm climates. According to Allen's "rule", inhabitants of cold climates will tend to have shorter limbs than their warm climate counterparts. Although these ecological rules are

mainly empirical generalizations, they are based on the theoretical idea that it is advantageous to have a low ratio of body surface area to mass in cold climates to retain heat and a high ratio in warm climates to dissipate heat. The precise mechanism underlying these rules is not agreed upon by all researchers, but the observed patterns are remarkably strong (Ashton, Tracy, and de Queiroz 2000).

There is strong evidence that climate affects recent human morphology as well (Holliday 1995, Holliday 1997a, Roberts 1978, Ruff 1991, Ruff 1994, Steegmann 1975, Trinkaus 1981, Weaver 2000a). This is striking given the ability that humans have to buffer themselves culturally, at least to some extent, from the environment. The potential importance of thermoregulation as a selective agent is highlighted by the observation that humans usually die if core body temperature deviates from a narrow range of 35 to 41°C (Kormondy and Brown 1998). Humans living in cold climates tend to have wide bodies, short limbs relative to their trunks, and abbreviated distal limb segments, while people from warm climates show the reverse pattern. In the skeletal elements of the hip region these patterns manifest themselves most strikingly in differences in absolute bi-iliac breadth and ratios of bi-iliac breadth to femur length (i.e. “cold-adapted” and “warm-adapted” body proportions, Ruff 1991, Ruff 1994).

These differences in body proportions are primarily inherited (see Holliday 1997a, Ruff 1994) and are present very early in life. The few existing studies that have investigated juvenile body proportions show that infants already follow Bergmann and Allen’s rules. However, the exact proportions of infants are different from those of adults, because body proportions change throughout growth and development (Newman 1975). As an example of Bergmann’s rule, Roberts (1978) showed a significant inverse

correlation between infant birth weight and mean annual temperature. Although this relationship is strong, other factors such as nutritional deficiencies could influence this result. In a more direct study, Schultz (1926) documented that differences in body breadth and limb to trunk ratios between African-Americans and European-Americans appear as early as two years old. Y'Edynak (1978) found substantial differences in skeletal limb lengths and proportions of Western Eskimo and Aleut juveniles in comparison with European-Americans. As a proxy for limb to trunk proportions, the low sitting-height to stature ratio of Australian aborigines is present early in life (Eveleth and Tanner 1976). In addition, all of the relevant data on bi-iliac breadth and bi-acromial breadth for one year olds presented by Eveleth and Tanner (1976, 1990) show geographic patterning.

Based on Bergmann's and Allen's "rules", Ruff (1991) proposed that, as a first approximation, the hominid body can be modeled as a cylinder with bi-iliac breadth as the diameter and stature as the height. As a logical extension of this model, changes in stature will not affect surface area to mass ratios, because the height of the cylinder occurs in both the numerator and the denominator of the ratio. Consequently, parameters of body breadth (transverse dimensions) and depth (sagittal dimensions) would be expected to be most strongly related to climate. In support of the cylindrical model and of particular relevance to the hip complex, bi-iliac breadth is the body dimension which is most highly correlated with latitude in recent humans, and this relationship remains approximately the same when partial correlation coefficients are calculated holding stature and body weight constant. In contrast, stature is only weakly correlated with latitude, and the relationship is statistically insignificant (Ruff 1994).

Body proportions in fossil hominids appear to be related to climate as well. The remarkably complete Early Pleistocene KNM-WT 15000 skeleton has a projected adult pelvic width that is similar to recent human populations living in tropical environments (Walker and Leakey 1993). However, as discussed earlier, this pelvic reconstruction is fairly speculative. This aside, KNM-WT 15000 also has elongated distal limb segments like recent humans from tropical environments (Walker and Leakey 1993). The Broken Hill tibia is very long and therefore may reflect long distal limb segments in African Middle Pleistocene *Homo* (Kennedy 1984). Linear body forms and elongated distal limb segments reflecting probable African ancestry are found in the near-modern Qafzeh-Skhul individuals and early Upper Paleolithic people (Holliday 1995, Holliday 1997a). In addition, even though australopiths were very short in stature, AL 288-1 and STS 14 have approximately the same width pelvises as recent human populations living in tropical environments (Ruff 1991, Ruff 1993, Ruff 1994). However, australopiths have different front to hind limb proportions than recent humans (McHenry and Coffing 2000) which may have affected thermoregulation. In contrast, the Neandertals La Chapelle-aux-Saints 1 and Kebara 2 both have extremely wide bi-iliac breadths, probably related to ancestral cold climate adaptation (Holliday 1995, Holliday 1997b, Ruff 1994). The reconstructed bi-iliac breadth of Jinniushan from the Middle Pleistocene of northern China is very wide as well (Rosenberg, Zhen'e, and Ruff 1999). It is unclear whether or not the extremely wide bi-iliac breadth of Pelvis 1 from the Sima de los Huesos reflects cold climate adaptation (Arsuaga et al. 1999).

While differences in bi-iliac breadth, limb to trunk proportions, and distal to proximal limb lengths within and between fossil hominids and recent humans have been

well documented, the effects of ecogeographical patterning on other aspects of hip morphology have not been fully explored. It is likely that developmental and functional integration of the hip causes many other anatomical features to be affected by differences in body proportions.

Locomotor biomechanics

Numerous studies have shown that mechanical forces are a significant external constraint on the skeletons of all organisms that are continually subjected to the earth's strong gravitational field (e.g. Carter 1987, Carter and Beaupré 2001). In addition to gravity, the hominid hip is the attachment site for a number of large muscles that exert forces on and help determine the shape of its skeletal elements. Differences in habitual behavior between individuals can also result in skeletal changes (e.g. Ruff 2000). Changes in the shape of the skeleton are mainly produced during growth and development when the epiphyses are still open. Adult skeletons can change in internal architecture (e.g. Beaupré, Orr, and Carter 1990, Pauwels 1980) and cortical bone thickness (e.g. Ruff 2000, Ruff and Hayes 1983, Trinkaus, Churchill, and Ruff 1994), but in adults changes in gross shape are not usually possible except from degenerative changes such as osteoarthritis.

An example of mechanically driven shape change in the hip skeleton is the development of the human bicondylar angle (Shefelbine, Tardieu, and Carter 2002). Infants are born with bi-condylar angles of zero degrees and only develop adult angles by walking bipedally during growth and development; values of femoral obliquity close to those of adults are reached around the age of seven (Tardieu 1998). Adult humans also have lower femoral neck-shaft angles than newborns (Anderson and Trinkaus 1998,

Heimkes et al. 1993, Heimkes et al. 1997, Trinkaus 1993a). This change in angle arises because during development the capital growth-plate remains perpendicular to the habitual angle of the hip joint reaction force (Heimkes et al. 1993, Heimkes et al. 1997, Maquet 1985), and when infants begin to walk, hip joint reaction force becomes more horizontal due to the addition of abductor forces. This change in hip joint reaction force angle produces a lower neck-shaft angle. Individuals who are unable to walk with a normal gait continue to have high neck-shaft angles (Brien, Lane, and Healey 1995, Houston and Zaleski 1967, LaPlaza et al. 1993), because they are not habitually in one-legged stance.

In another region of the hip, Abitbol (1987a) has documented that the lumbosacral angle found in adult humans develops with the onset of bipedalism. The shape of the pelvic inlet may also be influenced by the degree of physical activity during adolescence and the age of acquisition of erect posture (Abitbol 1996), but in this case the exact nature of the interaction between mechanical forces and skeletal growth is unclear.

The skeletal changes discussed above are all achieved through developmental adaptation during the lifetime of an individual, but mechanical constraints also can result in evolutionary adaptation through natural selection over intergenerational time spans. In general, less drastic changes are probably achieved through developmental adaptation, because it is unlikely that the degeneration or increased energetic expenditure caused by slightly lower biomechanical efficiency would have significant enough effects on individual fitness to be selected against intraspecifically. In addition, most degenerative changes usually occur post-reproductively and therefore do not affect reproductive success. However, interspecifically there appear to be clear anatomical adaptations to

differences in locomotor biomechanics. The best example from the hip region is the extreme shortness of the human ilium relative to the ilia of other mammals. This change occurred to bring the human acetabulum and sacrum close together for efficient antero-posterior weight balance during bipedal locomotion (Lovejoy 1988, Lovejoy, Cohn, and White 1999, Lovejoy, Heiple, and Burstein 1973).

Many researchers have advanced biomechanical explanations for fossil hip morphology. Based on a relatively short femur, a wide tuberoacetabular sulcus, a weak iliopubic eminence, a small anterior horn of the lunate surface, a flat sacrum, evidence for weak sacral ligaments, a coronally oriented iliac blade, a non-projecting lateral lip of the patellar groove, and a relatively wide medial condyle (along with traits from other anatomical regions), Stern and Susman (1983) proposed that, relative to humans, AL 288-1 would have walked with less hip and knee extension and reduced weight transfer onto the medial part of the ball of the foot (a “bent-hip” and “bent-knee” gait). According to these authors, this gait would have allowed australopiths to maintain arboreal proficiency (Sarmiento 1998 sees some of these same features as compatible with terrestrial quadrupedalism). Berge (1994) presents a similar reconstruction to that of Stern and Susman (1983) for the gait of australopiths, with the addition that AL 288-1 would have walked with large pelvic and shoulder rotations (a “waddling” gait) due to a wide bi-acetabular breadth, coronally oriented iliac blades, a short femur, and a long femoral neck. Her conclusion is based in part on biomechanical arguments that AL 288-1 would have had ape-like gluteal musculature, but this conclusion overlooks what appear to be human-like gluteal lines on the AL 288-1 and Stw 441/465 ilia (Häusler and

Berger 2001, Johanson et al. 1982). There may also be part of an anterior gluteal line (human-like) on Stw 431 (personal observation).

Based on a biomechanical analysis of one-legged stance, Ruff concluded that AL 288-1 has a femoral head and iliac tubercle that are too small and a shaft with cortical bone that is too evenly distributed to be consistent with human-like bipedalism. As an explanation he proposes that australopiths may have walked with more lateral trunk bending and pelvic elevation than do recent humans (Ruff 1998). Alternatively, differences in the hip between australopiths and recent humans are simply changes necessary to maintain biomechanical equivalency of a human-like gait in the context of different obstetrical constraints (Lovejoy 1988, Lovejoy, Heiple, and Burstein 1973).

Ruff (1995) suggests that the long necks, low neck-shaft angles, and medial-laterally thickened shafts of the femora of primitive *Homo* are an evolutionary adaptation to minimize hip joint reaction forces while still maintaining a relatively wide true pelvis for non-rotational birth. Trinkaus and colleagues (Trinkaus 1997, Trinkaus, Ruff, and Churchill 1998, Trinkaus et al. 1998) propose that the general robusticity, circular cross-sections, cortical thickness, and low neck-shaft angles of Neandertal femora are the result of increased mechanical loading due to elevated activity levels (Trinkaus 1983, Trinkaus 1993a). Alternatively, the medial-lateral thickening of Neandertal femora may be due to differences in mechanical loading due to “hyper-arctic” body proportions (Trinkaus, Ruff, and Churchill 1998) or a non-mechanical consequence of climatic adaptation (Pearson 2000a).

Rak (1993) argues based on the presumably male Kebara 2 pelvis that Neandertals had a less efficient gait relative to modern humans because their acetabulae

were positioned closer to their sacra (relative to the total sagittal dimensions of their pelvic inlets). However, male and female recent humans have similar absolute distances between their acetabulae and sacra, and Kebara 2 falls within the narrow range of recent human variation. In addition, while different from males, the relative positioning the Kebara 2 acetabulum is only between one and two standard deviations from the mean for recent human females (Weaver 2000b, Weaver et al. 1998).

Obstetrics

Given differences in the degree of encephalization between hominid taxa (Ruff, Trinkaus, and Holliday 1997), the importance of obstetrics in determining hip anatomy must have changed dramatically throughout the course of human evolution (Tague 2000). The usefulness of obstetrical constraints for explaining variation in pelvic dimensions between recent human populations and by extension Neandertal and other Late Pleistocene pelvises has been questioned (Abitbol 1987b, Baskerville 1989); however, it is clear that parturition has the potential to be a powerful selective force, because cephalopelvic disproportion can result in infant and/or maternal mortality (Rosenberg 1989, Rosenberg 1992).

Although circumstantial, the most convincing evidence for natural selection acting on pelvic dimensions is pronounced sexual dimorphism in pelvic shape between recent human males and females. Although most dimensions of the birth canal are affected, most sexual dimorphism in pelvic shape in humans is achieved by separating bony elements. Therefore, sexual dimorphism occurs primarily at the pelvic midplane and outlet and the posterior spaces of all pelvic planes. Females, relative to males, have wider subpubic angles, wider bispinous and bituberous diameters, more angled sacra,

wider greater sciatic notches, increased inlet, midplane, and outlet posterior space, larger midplane and outlet sagittal diameters, and increased midplane and outlet circumferences. For dimensions of the pelvic inlet, females usually have longer pubic lengths than males, but sexual dimorphism in pubic length is population dependant and less extreme than midplane and outlet dimensions (this summary of sexual dimorphism is based on Arsuaga and Carretero 1994, Hager 1996, LaVelle 1995, Rosenberg 1986, Rosenberg 1988, Segebarth-Orban 1980, Tague 1992).

Pelvic differences caused by obstetrical constraints between males and females do not appear to affect femoral morphology. Similar to other anatomical regions the femora of males and females differ primarily in size, with male femora being larger. This size dimorphism in the femur is reflected in differences in length, head diameter, shaft dimensions, and distal end size (Steele and Bramblett 1988, Van Gerven 1972).

Even though many researchers have discussed australopith parturition (e.g. Abitbol 1995b, Berge, Orban-Segebarth, and Schmid 1984, Häusler and Schmid 1995, Rosenman, Lovejoy, and Spurlock 1999, Tague and Lovejoy 1986), none have proposed primarily obstetrical explanations for the hip morphology of these early hominids. However, there has been some debate about the sex of AL 288-1 and the mechanism of birth in australopiths (Häusler and Schmid 1995, Häusler and Schmid 1998, Tague and Lovejoy 1986, Tague and Lovejoy 1998, Wood and Quinney 1996).

Tague and Lovejoy (Tague and Lovejoy 1986) argue that in australopiths the fetus would have passed through the birth canal by aligning the long axes of its head and shoulders transversely throughout the process of parturition. This explanation has been debated (Häusler and Schmid 1995), but given the platypelloid configuration of not only

the inlet but also the midplane and outlet dimensions of the majority of the reconstructions of australopith birth canals (Abitbol 1995b, Berge, Orban-Segebarth, and Schmid 1984, Häusler and Schmid 1995, Rosenman, Lovejoy, and Spurlock 1999, Tague and Lovejoy 1986), it is likely to be correct. Birth in australopiths would not have been easy, but obstetrical constraints were probably not primarily involved in determining the shape of their pelves, because their infants were not highly encephalized (Rosenberg 1992, Tague and Lovejoy 1986). This conclusion is important because it follows that comparisons of australopiths with other hominids may help sort out which aspects of hip morphology are primarily due to obstetrics.

For early Pleistocene primitive *Homo*, analysis is complicated by the fact that the best-preserved pelvis (KNM-WT 15000) comes from a juvenile male (Walker and Leakey 1993). Based on the curvature of the arcuate line in fragments of adult specimens, Ruff (1995) proposed that primitive *Homo* is characterized by pelves that are similar to those of australopiths in their extreme platypelloidy, and non-rotational birth may have persisted until at least the Middle Pleistocene. Walker and Ruff (1993) argued that an overly constricted birth canal and increased encephalization in primitive *Homo* would have resulted in the human pattern of “secondary altriciality” (where approximately one year of fetal brain growth is delayed until after birth, presumably to allow for successful parturition). However, this conclusion is based on a fairly speculative reconstruction of a juvenile male (KNM-WT 15000).

The discovery of Pelvis 1 from the Sima de los Huesos led Arsuaga and colleagues (Arsuaga et al. 1999) to propose that the infants of these Middle Pleistocene hominids would have rotated within the birth canal as in recent humans. This conclusion

is based on their reconstruction that the sagittal diameter is greater than the transverse diameter at the midplane. Unfortunately, Pelvis 1 is likely to be from a male individual, making any conclusions about obstetrics less secure. Given that a human infant could easily pass through the “birth canal” of Pelvis 1 and that the Sima hominids were less encephalized than later hominids, it is unlikely that obstetrical constraints are primarily responsible for the shape of the Sima pelves (Arsuaga et al. 1999).

The relationship between obstetrical constraints and Neandertal pelvic morphology is a topic that has been debated extensively. Before the discovery of the Kebara 2 pelvis, elongated superior pubic rami in Neandertals were sometimes assumed to be a reflection of enlarged birth canals due to longer gestation periods (Trinkaus 1984), accelerated fetal growth (Dean, Stringer, and Bromage 1986), or relatively large infants because Neandertals were heavy for their short stature (Rosenberg 1986, Rosenberg 1988). However, all of these hypotheses have been called into question, because it has been shown that the long superior pubic ramus in the Kebara 2 specimen is not accompanied by a proportionally larger birth canal (Rak 1991, Rak and Arensburg 1987), at least at the midplane and outlet (Tague 1992). In addition, when confidence intervals are accounted for in regression equations between brain size and gestation length, there is no evidence that Neandertals would have had different gestation lengths than recent humans (Gelvin and Albrecht 1989). These obstetrical explanations also do not address the observation that Neandertal males appear to have even longer superior pubic rami than females (Rosenberg 1998). While obstetrical constraints may not be the primary reason for the special pelvic anatomy of Neandertals, they must have played an important

role in determining differences in pelvic morphology between Neandertals (and recent humans) and earlier hominids.

Other functional constraints

In addition to climate, locomotor biomechanics, and obstetrics there are numerous other functional constraints that could help explain a portion of the variation in hip morphology found in recent humans and fossil hominids. Some possibilities are sexual selection, thorax shape related to lung capacity, and visceral support. There are undoubtedly many other factors that could be added to the list. Of these possible constraints perhaps visceral support is the most important (Robinson 1972, Tague and Lovejoy 1986), but little comparative research has been conducted on the influence of viscera on pelvic morphology in either recent humans or other primates.

The important question is not whether or not there are other factors that could potentially affect hip morphology. More important is the significance of these factors relative to climate, locomotor biomechanics, and obstetrics and the explanatory power they add to any functional model of hip morphology. A scientific model has no value if it is as complicated as the sum of all empirical observations, and depending on the particular question, simplicity must be balanced in some way with realism. Therefore, in this dissertation I focus on climatic, locomotor, and obstetric constraints as a first approximation for explaining recent human and fossil hominid hip morphology, because these factors clearly play an important role.

Developmental constraints

If the functions of the hip are thought of as external constraints on morphology, then constraints on the raw material and mechanisms on which natural selection has to act to produce adaptive morphology can be thought of as internal constraints. These internal influences on morphology are often called developmental or phylogenetic constraints, and they reflect the realization that while genotypes are inherited, natural selection usually acts on phenotypes, and therefore the mechanistic links between genes and morphology cannot be ignored.

Recent advances in evolutionary developmental biology have greatly improved our understanding of the mechanisms underlying morphogenesis: the transition from genotype to phenotype (Arthur 2002, Cohn and Bright 2000, Gilbert, Opitz, and Raff 1996, Lovejoy, Cohn, and White 1999, Lovejoy, Cohn, and White 2000); although, there is still much work left to be done before we can completely define generally applicable principles (Arthur 2002). It now appears that most anatomical traits are not independently inherited, and therefore they cannot be separately selected for in a “particulate” Mendelian fashion (Lovejoy, Cohn, and White 1999, Lovejoy, Cohn, and White 2000). This has two major implications for interpreting skeletal morphology. First, an adaptive change in a particular aspect of morphology will necessarily produce a number of other correlated changes (secondary consequences) which were not directly selected for and may or may not have any adaptive value (Lovejoy, Cohn, and White 1999, Lovejoy, Cohn, and White 2000). Second, most evolutionary change between closely related species occurs by developmental shifts either in timing or initial conditions (analagen specification), and a hierarchical system of local chemical or

mechanical interactions between different levels of modules, down to the level of individual cells, works to produce an integrated organism (Arthur 2002, Cohn and Bright 2000, Gilbert, Opitz, and Raff 1996, Lovejoy, Cohn, and White 1999, Lovejoy, Cohn, and White 2000). Even for the cranium, local interactions at the cellular level during cell migration are important for determining the size, shape, and orientation of skeletal elements (Pasqualetti and Rijli 2002). These insights mean that it is no longer necessary to posit individual selective mechanisms for each feature of an adaptive complex, because local interactions between modules can produce a suite of adaptive features without any further genetic changes. In other words, local interactions at the cellular level during development necessarily produce integrated anatomical units.

Lovejoy and colleagues (1999, 2000) and McCollum (1999a, 1999b) have argued that insights from evolutionary developmental biology rule out any possibility of “particulate” evolution of individual traits (contra Churchill 1996 and others). However, a multitude of population genetics experiments have shown that at least some traits are independently inherited, and we may need an even better understanding of morphogenesis before we can completely dismiss the possibility of independent inheritance. The realization that a simple change in one trait can produce a cascade of secondary changes does not conversely rule out the possibility that small shifts in hierarchically lower developmental modules could produce independent anatomical change. Of course a strong argument can still be made that the influence of a slight change in an individual trait on the fitness of an individual is so low that it is unlikely to have been naturally selected for. However, this argument does not apply to changes in trait frequency produced by genetic drift. Therefore, although integration is likely based

on evidence from evolutionary developmental biology, any hypothesis of integration should be tested empirically.

Hypotheses and research questions

This dissertation has the following specific objectives:

1. To statistically explore geographic variation and interrelationships within recent human hip morphology to establish a comparative baseline for fossil hominids.
2. To propose hypotheses based on climatic, biomechanical, obstetrical, and developmental constraints on the hip to explain empirical patterns of variation in the hip morphology of recent humans.
3. To determine to what extent the hyper “cold-adapted” body proportions of Neandertals can explain other purportedly unique aspects of their hip morphology.
4. To determine to what extent the supero-inferiorly short pelves with platypelloid birth canals of australopiths can explain other purportedly unique aspects of their hip morphology.
5. To develop a multi-causal functional scenario for hominid hip evolution.
6. To suggest avenues for future research.

Chapter 2

Materials: Comparative and fossil samples

Recent modern humans

The recent human skeletons analyzed for this dissertation were selected to encompass enough variation in size and shape to be suitable for examining allometric patterns in the human hip. Individuals were chosen to appropriately represent diverse climatic zones with the corresponding variation in body proportions (shape), differences in body mass (size), and a range of statures (size and shape). Skeleton choice also was strongly limited by availability. Even in the best collections, post-crania are much scarcer than crania, and data could not be collected on 85-100% of the individuals with post-crania due to missing, fragmentary, or at least partially damaged sacra, innominates, or femora.

The individuals in the recent human samples come from eight broad geographic regions: Sub-Saharan Africa, southern Asia, the Pacific, northern Africa, northern Europe, the Sub-Antarctic, and the Sub-Arctic, listed roughly from equatorial to polar regions, and African-Americans from North America (Table 2.1, Fig. 2.1). The major geographic gaps in the dataset are in central and southern Europe, eastern and western Asia, northwest Africa, and the New World. As a general rule, New World populations were avoided because humans have not been living in the Americas long enough for strong climate-induced patterns in body proportions to appear. Although not ideal, to my

knowledge the recent human skeletal dataset used in this dissertation constitutes the most comprehensive sampling of matched pelvic and femoral measurements yet collected.

The total number of different individuals included is 270, collected from repositories around the world. However, for analysis the complete dataset is broken into two samples to better control for unbalanced sex ratios and other potential biases. The first sample is used for geographic comparisons (geographically variable sample, Table 2.1a) and contains mainly larger, more-representative populations that can be explicitly related to climate. It also contains only males to help control for sex biases and the confounding effects of sexual dimorphism on analyses of body proportions and pelvic morphology. The second sample (sex balanced sample, Table 2.1b) includes individuals from all of the geographic regions for which data could be collected on approximately equal numbers of males and females.

Each individual's population or sub-group and geographic region was determined from documentation associated with the skeleton remains. Most of skeletons come from either older archeological excavations or anatomical collections from the nineteenth century and tend to be sparsely documented. While more precise records would have been preferable, older collections have the advantage that they were collected before modern patterns of more frequent and extensive human migration. Thus, they should better reflect regional differences between populations. The following sections discuss the compositions of the geographically variable and sex balanced samples, the context (whenever possible) and repository institution for each individual (listed by geographic region), and methods for sex and age assessment.

Geographically variable sample

The geographically variable sample consists of matched sets of innominates, sacra, and femora from 127 adult, male individuals (Table 2.1a). Only males are included to prevent patterns related to body size and proportions from being confounded by sexual dimorphism. The sample includes a few individuals with some missing data, but no more than 5% of the sample is ever excluded from an analysis.

The strongest geographic distinctions are between the Sub-Saharan, eastern and southern African “Bantu” and Khoi-San groups and the Sub-Arctic, Aleutian Islander and Inuit groups. The Australian Aborigine group is important because these individuals are genetically divergent from Sub-Saharan Africans but are still from a warm climate; the northern European group serves as a similar comparison with the Sub-Arctic groups. The Egyptian/Nubian group is from the mid-latitudes. Also included are a few Mbuti, Anadaman Islander, and Philippine “Negrito” individuals, because they are from the low end of the human size range, and Tierra del Fuegians, because of the extensive literature on their extreme cranial size and robusticity (e.g. Lahr 1995). More individuals from eastern Asia such as China or Japan would have been useful, but large postcranial samples of eastern Asians do not exist outside of eastern Asia. Eastern Asians are intermediate in bi-iliac breadth (similar to some Europeans) and tend to have abbreviated lower limbs (Ruff 1994). Nevertheless, the sample used here is adequate for investigating major differences in body proportions.

Sex balanced sample

The sex balanced sample consists of matched sets of innominates, sacra, and femora from 242 adult individuals (126 males and 117 females), with approximately equal numbers of males and females from each population (no more than 67% of one sex from a geographic region). Overall, the sample is 52% male and 48% female (Table 2.1b). There are a few individuals with some missing data, but no more than 5% of the sample is ever excluded from an analysis.

As for the geographically variable sample, individuals from diverse geographic regions with very different body proportions, statures, and body masses are represented. This is important because many studies of sexual dimorphism are conducted on fairly homogenous samples, and the results are then generalized to all recent humans. However, visual inspection of pelves from different regions suggests that there may be differences in hip sexual dimorphism between populations, and understanding these differences is especially important when further comparisons are made with fossil hominids.

Skeletal collections by geographic region of origin

This section contains information about the repository institution and brief documentation, when available, for all of the individuals in the dataset. The skeletons are grouped by geographic region, proceeding from warm to cold climates.

Sub-Saharan Africa

Sub-Saharan Africa is represented by a total of eighty-two individuals from central, eastern, and southern Africa and Madagascar. Madagascar is discussed here because it is geographically part of Sub-Saharan Africa, even though its genetic and linguistic affinities are with Indonesia. In Table 2.1, Khoisan and Mbuti (a central African “pygmy” group) individuals are listed separately even though they are from southern Africa and central Africa respectively, because they are both hunter-gatherer groups and are physically distinct from their regional counterparts.

The thirty-three Khoi-San individuals are primarily from collections housed in the South African Museum, Cape Town (n=25) and the University of Cape Town (n=5), with two individuals from the British Museum of Natural History, London and one individual from Department of Biological Anthropology, Cambridge University. The skeletons housed in Cape Town are for the most part fairly well documented and come from a broad geographic area, including Namibia, the southern Kalahari Desert, the western and southern coasts of South Africa, the Cape Peninsula, and inland regions of the ex-Cape Province of South Africa. The skeletons are dated from 2090 BP to early in the last century. The three Khoi-San individuals from Great Britain are less precisely documented. One of the skeletons from the British Museum is said to be from the Cape of Good Hope, and the provenience of the other skeleton is unclear. The skeleton stored in Cambridge is said to have come from Knysna, on the southern coast of South Africa.

The seven Mbuti individuals are from collections at the Université de Genève (n=5) and the Institut Royal des Sciences Naturelles de Belgique, Brussels (n=2). The Geneva and Brussels skeletons are documented to be respectively from the Wamba and

Irumu localities in the Ituri forest of the northeastern Republic of the Congo (formerly Zaire). The skeletons from Geneva are extensively documented and certainly belong to Mbuti individuals, and the skeletons from Brussels come from a region of the Ituri forest historically inhabited by the Mbuti (Turnbull 1983).

The remainder of the Sub-Saharan sub-sample is composed of thirty-nine “Bantu” individuals from various localities and three individuals from Madagascar. Central Africans (n=4, excluding the Mbuti) are represented by four individuals housed in the British Museum of Natural History, London and documented to be from Mission Hottot in the Lake Chad region of Nigeria. Southern Africans (n=11, excluding the Khoisan) are represented by five Mozambicans from the Musée de l’Homme, Paris, five Zulus from the American Museum of Natural History, New York, and one Zulu from the British Museum of Natural History, London. As with many older collections, the only documentation available for these fourteen southern African skeletons is that they come from Mozambique and South Africa respectively. Eastern Africans (n=24) are represented by six Haya individuals from Tanzania, five Somalians, and ten Sudanese from collections at the Department of Biological Anthropology, Cambridge University and three Masai individuals from the American Museum of Natural History, New York. The Haya skeletons were excavated from various cave sites on Musira Island, Lake Victoria. The Somalians come from the Ogaden region that is currently part of Ethiopia (along the disputed border between Somalia and Ethiopia); they are casualties of war and therefore all males. The exact provenience of the Masai individuals is not documented, but it is presumably somewhere in southern Kenya or northern Tanzania. The Sudanese sample comes from the site of Kerma, located in Upper Nubia near the third cataract of

the Nile and just south of the Nubian Desert in the modern nation of Sudan.

Geographically the Sudanese collection is from the border between Sub-Saharan Africa and northern Africa and therefore could be placed in either geographic region. The three skeletons from Madagascar are poorly documented. Two come from Tananarive, and the locality of the other skeleton is undocumented.

Southern Asia

Southern Asia is represented by twelve individuals from Anadaman Islander (n=2) and Philippine “Negrito” (n=10) hunter-gatherer populations. The majority of these skeletons are from collections housed at the Musée de l’Homme, Paris, but two Anadaman Islanders are from the British Museum of Natural History, London, and two Philippine “Negritos” are from the Smithsonian, Washington DC. The documentation for all of these skeletons is limited, but it is sufficient to establish ancestry and provenience to the Anadaman and Philippine Islands. Philippine “Negrito” groups were the aboriginal inhabitants of the Philippines. The Anadaman Islands are located south of Burma. No non-hunter-gatherer populations from southern Asia are represented in the recent human samples used in this dissertation.

Pacific

The sample contains twenty-six individuals from the Pacific, coming from Australia and Melanesia. The Australian Aborigine skeletons come from collections housed at the Istituto di Antropologia, Florence (n=2), the Department of Biological Anthropology, Cambridge University (n=1), the Institut Royale des Sciences Naturelles de Belgique, Brussels (n=1), the British Museum of Natural History, London (n=3), the

Musée de l'Homme, Paris (n=3), the American Museum of Natural History, New York (n=3), and the Smithsonian, Washington DC (n = 2). The provenience is as follows. One of the Australian Aborigine skeletons housed in Florence comes from Cape York, Northeastern Australia. The skeleton stored in Brussels comes from Flinders Island (a small island situated between Tasmania and mainland Australia). Two of the skeletons from Paris come from Queensland, Northeastern Australia and from one of the small islands in the northern Torres Strait between New Guinea and the Cape York Peninsula of Australia. One of the skeletons from the Smithsonian is documented to come from Murray River, southern Australia, and the other one comes from the vicinity of Melbourne. The other nine skeletons are purportedly from Australian Aborigines, but their localities of origin are not precisely documented.

The Melanesians are from collections housed at the Musée de l'Homme, Paris (n=7) and the British Museum of Natural History, London (n=4). Three of the skeletons from Paris come from Vanuatu, a group of islands east of Australia. Two of the other skeletons are from New Caledonia, a group of islands located south of Vanuatu. Another two skeletons from the Musée de l'Homme come from New Britain, a large island just east of New Guinea. Two of the skeletons stored at the British Museum are from the Kingsmill Islands (now Gilbert Islands), located to the northeast of Australia and currently part of the independent republic of Kiribati. Another skeleton housed in the Natural History Museum comes from the Isle of Pines, New Guinea. The remaining skeleton from London is documented to be from a Papuan individual, but no further details are given.

Northern Africa

Northern Africa is represented by a total of twenty-seven individuals from Egypt (n=4) and ancient Nubia (n=23). All of these individuals come from collections housed in the Department of Biological Anthropology, Cambridge University, and are from various archaeological contexts and time-periods. Data were collected on all of the skeletons in the Duckworth Collection from Egypt and Nubia with fully preserved hip elements.

Northern Europe

Northern Europe is represented by thirty-six individuals from the British Isles that come from collections housed at the British Museum of Natural History, London. The bulk of the skeletons come from the eighteenth to early nineteenth century Spitalfields crypt in London (n=30). Some individuals in the Spitalfields collection had ancestry outside of Great Britain, because London was already a very cosmopolitan city, but judging from the names on the coffin plates it is likely that all of the skeletons included are of European descent. All of the Spitalfields individuals included in this dissertation are of known sex, age, and identity. The remaining six individuals are purportedly of Norse ancestry from archaeological excavations at Newark Bay, Orkney Island (just north of the northernmost tip of Scotland).

Sub-Antarctic

The Sub-Antarctic geographic region is represented entirely by Tierra del Fuegians (n=12) from collections housed at the Istituto di Antropologia, Florence (n=5)

and the University of Rome (n=7). Tierra del Fuegians are included because many researchers have described their crania as extremely robust (e.g. Lahr 1995), but very few studies of their post-crania have been published. All of the skeletons come from various localities in the vicinity of Cape Horn at the southern tip of South America.

Sub-Arctic

The Sub-Arctic is represented by Aleutian Islanders (n=28) from collections housed at the Smithsonian, Washington, D.C. and Inuit (n=17) from the American Museum of Natural History, New York. The Aleutian Islanders come from archaeological excavations of cave sites on Kagamil, Shiprock, and Umnak islands off the western coast of mainland Alaska. The Inuit come from a variety of sites in the vicinity of Point Hope, Northwestern Alaska, with one individual from Smith Sound, northern Greenland.

North America

North America is represented by African-Americans (n= 30) from the Terry Collection. These individuals are included to increase the number of taller individuals with relatively narrow hips in the sex balanced sample (especially females), because African-Americans have body proportions that are intermediate between those of Europeans and Sub-Saharan African groups (Ruff and Walker 1993). The skeletons in the Terry collection come from the Missouri Medical College and are mainly from individuals who died in the St. Louis area during the late nineteenth and early twentieth century. Data was not collected on individuals who died of protracted illnesses such as tuberculosis that might have affected their skeletal morphology.

Sex and age determination

Only fully adult individuals (based on complete epiphyseal closure for both the innominate and femur) were included in the recent human dataset. Care was taken to exclude clearly pathological or extremely old individuals from the sample as well. No precise attempts were made to age the skeletons, but approximate age classes were determined based on pubic symphysis morphology and degenerative changes (e.g. ribs, vertebrae).

The skeletons from the Spitalfields and Terry collections, and a few other individuals, are of known sex. However, for the majority of the skeletons sex had to be determined based on pelvic morphology (in some cases supplemented by cranial features). The sex of each individual was determined by the author using the features described by Phenice (1969), supplemented by observations of other features such as the presence or absence of a preauricular sulcus, the width of the greater sciatic notch, the subpubic angle, acetabular size, and the general shape of the birth canal. In the case of the thirty known-sex individuals from the Spitalfields crypt, my visual sex determinations agreed with the true sex of the individual in all but one case (97% accuracy). This degree of accuracy is consistent with that of Molleson and Cox (1993) for the entire known-sex portion of the Spitalfields collection. With the Terry Collection, it was not always possible to determine the sex of a skeleton before becoming aware of the individual's documented sex, because in many cases a male or female symbol is marked on the outside of the storage drawer. When I was able to perform a blind-test, my determinations agreed with the documentation. My accuracy may have been slightly less for individuals from other populations, given differences in sexual dimorphism and body

proportions, but sex determination based on the pelvis has been found to be accurate more than 95% of the time (Steele and Bramblett 1988, White and Folkens 1995). Because most mistakes in sex determination occur in the middle of the distribution of pelvic morphology, sexual dimorphism will tend to be slightly underestimated.

Fossil hominids

The fossil specimens included in this dissertation were selected based primarily on the degree of preservation of hip region skeletal elements. Ideally a specimen would preserve the sacrum and at least one innominate and one femur, but given the fragmentary nature of the fossil record, the majority of the individuals were less complete. Specimens also were chosen to cover as much temporal, geographic, and phylogenetic variation as possible for a broad perspective on hominid hip morphology. Appendix C contains a complete list of the specimens included in at least one analysis, along with information on geological age, missing/estimated landmarks (if any), and whether or not the original or a cast was analyzed. Appendix C also contains the three-letter abbreviations for each specimen that are used in Figures 5.1-5.28. In addition to the specimens listed in Appendix C, I made notes and observations on many more fragmentary specimens to make sure that the morphology of more complete specimens was representative of other individuals. Some of these observations are discussed in the introductory chapter.

For the pelvis, although I made observations and in many cases collected data on original fossils, in some cases I analyzed reconstructions instead. This was done because distortion or fragmentation prevents the originals from being used for three-dimensional data analysis. A good example of this problem is the AL 288-1 pelvis, which is crushed

and has been reconstructed to correct this distortion. Refer to Appendix C for more information about the specific reconstructions that were used.

Chapter 3

Methods: Data collection and analysis

Data collection and manipulation

I discuss my data collection and manipulation techniques in some detail because many aspects are either fairly novel or newly developed for my research questions. The motivation behind these methods is first, to consider the hip anatomical region as a functional unit that includes the femur; second, to quantify the three-dimensional spatial relationships within the skeletal elements of the hip; and third, to examine the relationships between hip skeletal elements with respect to anatomical orientation.

Equipment and software

A Microscribe 3DX digitizer (Immersion Corporation, 2158 Paragon Drive, San Jose, CA 95131, USA), a Macintosh PowerBook G3 laptop computer, and original software (see Appendix F for further details about the software) were used to collect the three-dimensional coordinate locations of landmarks on the skeletal elements of the hip. The digitizer consists of a fine-tipped stylus attached to five mechanical linkages that together can move with six degrees of freedom through a 127 cm spherical reach. The 3DX model records the three-dimensional coordinate location of the stylus with an accuracy of 0.23 mm. The digitizer automatically re-calibrates itself on startup and is not sensitive to changes in temperature, humidity, atmospheric pressure, or magnetic field. Data points are recorded by placing the stylus on a landmark and pushing the left button

of the foot pedal. Points are confirmed by pushing the right foot pedal button. At the end of each digitizing session the x-y-z coordinates of all of the landmarks that were digitized are output into an ASCII text file for further manipulation.

I carried the digitizer at all times in a heavily padded hard-plastic case to avoid damaging it during transport. Nevertheless, I checked the equipment periodically for damage. Proper functioning of the mechanical linkages was tested using visual observations of arm movement and the two self-tests found on the Immersion Corporation web-site. The accuracy and precision of the digitizer was further verified by digitizing the location of dots that had been measured out on a piece of paper and confirming that the distances and angles between the dots as calculated from the digitized points agreed with measured distances and angles. None of these tests ever indicated problems with the digitizer.

Specimen setup

The innominates, sacra, and femora were digitized separately. Nothing could be moved during the digitizing process, so points that were difficult or impossible to locate visually while digitizing were first marked with self-adhesive dots on which an "X" had been written at the midpoint of the dot. Once all of the points had been marked, the particular skeletal element was secured, using elastic plastic ribbons, in a stable orientation to a padded board that had been taped to a desk or table. This setup was chosen to be portable, flexible when dealing with fragmentary fossils, and to prevent damage to specimens during the digitizing process. After all of the landmarks were digitized, three or four points (depending on the skeletal element) were digitized a second time to confirm that nothing had moved during digitizing.

Landmarks

The three-dimensional coordinate locations of 42 landmarks were collected on matched sets of innominates, sacra, and femora (Fig. 3.1, Table 3.1). Whenever possible the right innominate and femur were used, but if only the left side was present or the right side was fragmentary, the left side was digitized and the data were mathematically mirrored. Also, some supplementary points for calculating approximations of certain standard osteometric measurements were digitized (Table 3.2). The complete definitions of the landmarks and the calculation procedures for the standard measurements are described in Appendices D and E respectively.

Bookstein (1991) categorizes landmarks as type I, II, or III, from most to least precisely specified. Type I landmarks are defined by a discrete juxtaposition of tissues such as a junction of two sutures; type II corresponds to local maxima such as the tip of a structure; and type III landmarks include extremal points and mathematically constructed points. Using this classification system, the majority of the pelvic landmarks are of type I or II; type III landmarks are more common on the femur due its more rounded geometry. In practice, mathematically constructed type III landmarks may actually be more precisely defined than some type I or II landmarks. The mean precision for the femoral analyses (2.3% error) was actually better than that for the pelvis (5.8% error) even though the femur has more type III landmarks. The details of determining methodological precision are discussed below.

Rearticulation and orientation

For a number of calculations the separately digitized skeletal elements are rearticulated and oriented in standard anatomical position as defined by Gray's Anatomy (Williams 1995) with the specifics of orientation modified from other researchers (Brand et al. 1982, Delp 1990). (Note that as will be discussed below, rearticulation is only performed for some analyses and calculations.) The goal of this procedure is to mathematically manipulate the individual hip elements so that the coordinate locations of their landmarks correspond to those of a properly oriented physically articulated skeleton. For this purpose, the x-axis is defined to be antero-posterior with coordinate values becoming larger moving more anteriorly, the y-axis is oriented medio-laterally (right to left) with medial (left) being larger, and the z-axis corresponds to supero-inferior with superior being larger (Fig. 3.1).

The first step is to re-articulate the hemi-pelvis using a combination of manual articulation and visual marking of points with mathematical rearticulation later using these visually marked points. During data collection, the sacrum is manually articulated with the innominate and points 15, 16, and 17 (Table 3.1) are marked on the innominate. At the same time, three points on the sacrum that exactly match up with points 15, 16, and 17 of the innominate are marked on the sacrum. Care is taken to make sure all three pairs match up precisely when the hemi-pelvis is manually articulated. Each set of three points describes a triangle that defines a plane. To re-articulate the hemi-pelvis these two planes are mathematically transformed so that the mean error at all three pairs of points is minimized. The mean error for the entire dataset (both geographically variable and sex balanced samples) is 0.50 mm. Given the amount of play at the sacro-iliac joints of

skeletons, this amount of error is well within the range of reasonable articulations. Once the sacrum and innominate are rearticulated they can be transformed as a complete hemipelvic unit. Following other researchers (Tague and Lovejoy 1986), no allowance is made for soft tissue at either the pubic symphyses or the sacro-iliac joints.

The next step is to orient the hemipelvis in standard anatomical position. The midpoint of the sacral promontory is rotated to be directly posterior to the pubic symphysis, the sacrum is oriented straight up and down, and the anterior-superior iliac spine and the pubic symphysis are rotated to be in the same frontal plane. More precisely, points 40 and 18 are lined up along an XZ-plane (equal y coordinates), points 40 and 41 are lined up along an XZ-plane (equal y coordinates), and points 18 and 29 are lined up along a YZ-plane (equal x coordinates).

Next, the femur is orientated as if the inferior femoral condyles had been placed on a table, the posterior condyles had been squared off, and the center of the femoral head had been rotated to be even in an antero-posterior direction with the midpoint of the epicondyles. More specifically, points 10 and 11 are lined up along an XY-plane (equal z coordinates), points 12 and 13 are lined up along a YZ-plane (equal x coordinates), and points 1 and 14 are lined up along a YZ-plane (equal x coordinates).

The final step is to mathematically translate the femur so that the center of the femoral head (point 1) exactly matches up with the center of the acetabulum (the mean of points 24, 25, 26, and 27).

Standard measurements

To provide comparability with other research, a number of additional points for calculating approximations for standard linear or angular measurements were digitized; a

list of the measurements along with references is found in Table 3.2, and Appendix E contains complete descriptions of these calculations. The absolute values of the linear measurements are not always exactly the same as distances taken with calipers, because digitized landmarks cannot always be defined in precisely the same way as the endpoints of standard measurements (e.g. maximum or minimum measurements cannot be duplicated exactly using landmarks). Nevertheless, the relative distances are similar and internally consistent for this dissertation.

Analytical techniques

In this section I discuss only the more novel aspects of my data analysis. I also use standard univariate, bivariate, and multivariate techniques such as Analysis of Variance (ANOVA), correlation and partial correlation, least-squares regression, Principal Component Analysis (PCA), discriminant analysis, and multiple regression (following Johnson and Wichern 1998, Sokal and Rohlf 1995).

Articulated hip analyses

For the articulated hip analysis, the entire hip is investigated as a unit. The methods described for this analysis are an attempt to understand variation in an anatomical region as opposed to a single bone. Many important anatomical regions straddle mobile joints, and the articulated hip analysis illustrates a method for dealing with these regions. In this case, an important aspect of size and shape variation in the hip region is differences in body proportions, or non-isometric scaling of the pelvis and femur relative to each other (i.e. wide pelvises tend to be associated with short femora), and these relative proportions cannot be examined easily by considering the shapes of

innominates, sacra, and femora in isolation or by combining the results of separate analyses after the fact. Therefore, the articulated hip analysis is an attempt to consider body proportions explicitly.

The steps of the articulated hip analysis are as follows. First, the raw coordinate data for each individual are mathematically transformed to rearticulate the skeletal elements and orient the hip joint in standard anatomical position (as discussed above). (Note that orienting is done for each individual without reference to the rest of the sample, so that the coordinate values are homologous variables and therefore measure the same thing across individuals in the same way that standard osteometric measurements are homologous.) Next, for each individual, all of the landmarks are translated so that the origin is at the mean of the landmark coordinates (the centroid). Then, for each of the landmarks, the residuals from the mean location are calculated to center the x, y, and z coordinate values (to set the mean equal to zero); this has no effect on the covariance matrix but makes the visualization calculations easier. Next, the transformed x, y, and z coordinate values are analyzed with PCA. Finally, the size and shape changes along each principal component axis are visualized using interactive computer graphics by adding multiples of the eigenvectors back into the mean configuration (Dryden and Mardia 1998, O'Higgins 2000, O'Higgins and Jones 1998). In the articulated hip analysis the mean configuration is synonymous with the mean for each of the x, y, z coordinates. The percentage variance explained by each of the principal components is used to determine which components to examine (based on a scree plot). The first principal component is not included in this determination, because it mainly reflects size and therefore explains a much larger percentage of the variance than do any of the shape components.

The purpose of this analysis is to examine the whole hip joint as a unit. Although the methods described above are similar to those of geometric morphometrics (= landmark based shape analysis), the goal of this analysis is not exactly the same. In this case, shape as defined by Kendall (= the properties of an object that remain when location, rotation, and scale have been removed, Kendall 1984) per se is not the quantity of interest. The goal is to examine the differences between individuals with highly variable body proportions with their hip joints oriented in an anatomically and biomechanically meaningful position. Location is removed but scale and rotation (in Kendall's sense) remain; and the coordinate axes have physical meanings: the x-axis is antero-posterior, the y-axis is medio-lateral, and the z-axis is supero-inferior, during two-legged stance.

Bookstein (1996) touches briefly on the problem of comparing articulated linkages (articulated skeletal elements are a subset of this category) when discussing different definitions of shape, but he concludes surprisingly that geometric morphometrics on linked objects will not give any more insight than intuitive distance ratios and biomechanical indices. It is probably true that for statistical testing similar results could be reached using a large enough set of ratios or indices, but perhaps the greatest strength of geometric morphometrics is lost: the ability to actually visualize a sample's pattern of variation instead of having to pour over principal component loadings or other similar tables of numbers to try to mentally conceptualize the changes along each multivariate axis.

Many researchers have pointed out (Bookstein 1991, 1996, Dryden and Mardia 1998) that edge superposition techniques (= lining objects up along an edge) may

introduce spurious correlations into a dataset, because the mid-point of the edge becomes the axis of rotation of the object. Small discrepancies along the edge will cause all the other points to rotate similarly, introducing covariation, especially far away from the edge. While not exactly edge superposition, orienting a hip joint in anatomical position is mathematically very similar and could result in similar problems. Spurious correlations are potentially a serious problem when an arbitrary baseline is chosen, as with Bookstein coordinates, but in the case of hip orientation the fixing of certain landmarks is defined by anatomical knowledge. As pointed out by Dryden and Mardia (1998) in reference to Bookstein coordinates, edge superposition will not produce spurious correlations if there is some reason to believe that certain points are fixed. Even so, in life clearly not every individual has a hip joint that conforms exactly to standard anatomical position, making it necessary to be cautious when interpreting the results of a PCA on anatomically oriented hip coordinates.

Generalized Procrustes Analyses (GPA)

The data are investigated further by analyzing the individual skeletal elements of the hip separately without any rearticulation or orientation, and therefore these analyses are independent of any assumptions about anatomical position. Since no mobile joints are crossed for these analyses, standard techniques of geometric morphometrics can be applied.

For all analyses of individual skeletal elements (hemi-pelvis, innominate, sacrum, femur), the steps are as follows. First, all of the raw coordinates are superimposed using Generalized Procrustes Analysis (GPA, Dryden and Mardia 1998, Gower 1975), leaving an estimation of shape as defined by Kendall (1984). It is important to emphasize that

one of the steps of GPA is to scale each individual by centroid size, preserving only shape information. Then, for each landmark, each individual's residuals from the mean configuration are calculated. Next, these residuals are analyzed using PCA. Finally, the shape changes along each principal component axis are visualized using interactive computer graphics (as described above for the articulated hip analysis). As with the articulated hip analysis, scree plots of the percentage variance explained by each of the principal components are used to determine which components to examine. The first principal component is included in this plot, because size already has been removed.

Briefly, the GPA algorithm uses the following steps. First, all of the specimens are centered and scaled by centroid size (= the square root of the sum of the squared Euclidean distances from each landmark to the centroid, Bookstein 1991, Dryden and Mardia 1998). Centroid size is a standard size measure used with landmark data, and it is roughly analogous to the geometric mean in traditional morphometrics. Then, in an iterative procedure, each specimen is superimposed on the mean configuration such that the total least squared error between the points is minimized. At the end of each iteration a new mean configuration is calculated, and the procedure ends when the change in total least squared error between iterations becomes extremely small. There are a few variants of the GPA algorithm, but the basic procedure is always essentially the same.

The space of objects for which location, rotation, and scale has been removed is named Kendall's shape space (Rohlf 1999) after David Kendall who first proposed it (1984), and it has a non-Euclidean geometry. Fortunately for practical applications, as long as the shapes are tightly clustered in space, as is almost always the case for similar biological objects (Rohlf 1999), distances between shapes can be approximated in an

Euclidean space tangent to Kendall's shape space. This tangent space can be thought of as similar to making a flat map projection of a globe (Bookstein 1996, O'Higgins and Jones 1998). In the analyses in this dissertation, tangent coordinates are approximated by calculating the residuals at each coordinate from the mean location of each landmark (Dryden and Mardia 1998).

Discriminant function analyses

For some of the analyses, discriminant functions are calculated using multiple regression of the principal component scores on group membership, following the methods of Penin and Baylac (1999) that are further discussed by Hennessy and Stringer (2002). In the analyses that follow, the groups are either sex (male or female) or climatic zone (warm, mid-latitude, or cold).

To calculate each discriminant function, the dependent variable of the multiple regression model (Y) codes for group membership (either -1, 1 for female and male for the sex balanced analysis or -1,0,1 for warm, mid-latitude, and cold climatic zone for the geographically variable analysis) and the independent variables (X_1, \dots, X_n) are the principal component scores (following discussion of discriminant functions in Sokal and Rohlf 1995). Principal components are included in a forward, stepwise manner with the probability necessary to enter equal to 0.05 (probability $> F$ of 0.05 or smaller) and the probability necessary to leave equal to 0.1 (probability $> F$ of 0.10 or larger). Only principal components explaining greater than 2.5% of the total sample variance are considered for inclusion in the regression model. The stepwise procedure and the exclusion of principal components that explain 2.5% or less of the total sample variance are both done to minimize the effects of any noise in the dataset on the discriminant axes.

Other combinations of principal components also are experimented with to determine the sensitivity of the results to the stepwise procedure.

As with visualization of the individual principal components, shapes along the discriminant function axes are visualized using interactive computer graphics by adding multiples of the eigenvectors for each of the included principal components, weighted by their multiple regression coefficients, back into the x, y, z coordinates of the mean form. The images generated by this procedure describe the shape changes along the discriminant function axes.

Multiple regression shape prediction

In a few cases for the fossil analyses, multiple regression equations that describe the hip morphologies (shapes) that best predict specific standard measurements (e.g. inlet dimensions) are calculated. The exact calculations are very similar to those for the discriminant analyses.

For these analyses, the dependent variable of the multiple regression model (Y) is the standard measurement and the independent variables (X_1, \dots, X_n) are the principal component scores. Principal components are included in the same stepwise manner with the same cutoff of variance explained as for the discriminant analyses. Likewise, shapes along the multiple regression axes are visualized using interactive computer graphics by adding multiples of the eigenvectors for each of the included principal components, weighted by their multiple regression coefficients, back into the x, y, z coordinates of the mean form. In this way, the shapes that correspond to changes in the particular standard measurement can be visualized.

This type of analysis allows one to evaluate whether or not, based on extensions of recent human patterns of variation, a recent human individual with the same value of a particular standard dimension as a fossil specimen would necessarily have many of the other morphological features of this fossil specimen. Thus, this technique allows hypotheses of integration for fossil hominid morphology to be directly tested using statistical shape analysis.

Original software

All of the calculations and visualization were performed using original software written for Macintosh computers (see Appendix F for more details). The accuracy of this GPA and PCA software was tested by comparisons with other existing programs. Standard univariate and bivariate statistics, discriminant analyses, and multiple regression analyses were computed using JMP 3.2 for the Macintosh (SAS Institute Inc., SAS Campus Drive, Cary, NC 27513, USA).

Precision of methods

For prudent interpretation of results, it is important to distinguish between those differences among specimens that are meaningful and those that could be simply due to methodologically induced noise. Essentially, what values for a particular variable are equivalent given the precision of the methodology?

Therefore, the precision of the multivariate methods used in this dissertation was tested, following O'Higgins and Jones (1998), by recollecting data multiple times on the same individuals. A full set of data was collected on three different individuals, three times, on different days. Then, all analyses were recalculated, including rearticulation

and orientation, using both the geographically variable and sex balanced samples combined with the nine repeats.

The repeats cluster tightly relative to the total sample variation along each principal component axis for every analysis. This visual assessment is confirmed mathematically by dividing the mean range of the repeats for the three individuals by the full range of variation for the sample. The mean value of this calculation for the principal components discussed in this dissertation is 5.4% of the sample range for the geographically variable analyses and 4.3% of the sample range for the sex balanced analyses. These percentages are comparable to a mean of approximately 7% for two principal components of cranial variation discussed by O'Higgins and Jones (1998:260, their Fig. 4). The error magnitude is similar between the two studies, which is encouraging given that pelvic and femoral landmarks are usually more difficult to define precisely than cranial ones. This procedure is one of the best ways to assess the effect of measurement error on multivariate results because data collection error can be magnified by the multiplication and addition involved in multivariate procedures. Smith (1996) discusses the problem of error propagation in a different context.

Using the same set of repeats, the precision of the measurements listed in Table 3 can be assessed by calculating the mean deviation from the repeat mean divided by the repeat mean (White and Folkens 1995). Using this standard procedure, all of the linear measurements have errors of less than 3% of the repeat mean. The mean errors for neck-shaft, torsion, and bicondylar angle are less than one degree, which is comparable to Trinkaus' (1993a) mean error for neck-shaft angles calculated using traditional methods.

Therefore, the error from data collection, rearticulation, and orientation is only a small fraction of the sample variation.

One additional issue of potential concern is the extent to which the analyses are influenced by the specific superimposition technique or a combination of measurement error and superimposition (Lele 1991, Lele and Richtsmeier 2001, Rohlf and Slice 1990). If variation in a dataset using n landmarks in p dimensions is small relative to all the possible shapes that could be described by n p -dimensional landmarks, all reasonable superimposition techniques should produce similar results, especially as $n \cdot p$ increases (Dryden and Mardia 1998, Rohlf 1999). Intuitively, these conditions would appear to hold for the analyses in this dissertation, because they deal with intraspecific variation in hominids and between 14-42 landmarks in three dimensions are used ($n \cdot p = 42-126$). Superimposition issues also are addressed empirically in this dissertation, because two very different superimposition techniques are used; the articulated hip analyses use “anatomical superimposition” and the hemi-pelvis, innominate, and femoral analyses use GPA superimposition. If these analyses point to similar conclusions, then the results are likely to be biologically meaningful.

Fossil hominid analyses

In most cases, the purpose of the analyses in this dissertation is to establish whether or not fossil morphology deviates from recent human patterns of variation. Therefore, for the fossil analyses, all calculations of principal components, correlation coefficients, and regression equations are done using only recent human individuals. In actuality, because the ratio of fossil specimens to recent humans in the sample is small, including fossil specimens in all calculations probably would not have changed the

results significantly. The one exception is that the fossil specimens are included in calculations of procrustes mean shape, because otherwise it would be impossible to compare them in shape space to the recent humans. However, including the fossil specimens in the generalized procrustes calculations does not significantly change the shape estimates for the recent humans and the resulting principal components.

Chapter 4

Recent modern human analyses

The changes along each principal component axis are visualized via stick figures that correspond mathematically to negative three standard deviations (left) and positive three standard deviations (right) from the mean configuration (Figs. 4.1-4.9 for the geographically variable analysis, Figs. 4.15-4.23 for the sex balanced analysis, and Figs. 4.11-4.14 and 4.24-4.26 for the discriminant analyses). The points (landmarks) and connections in the stick figures correspond to those in Figure 3.1 and Table 3.1. One of the major advantages of landmark-based analyses that preserve geometry is the ability to actually visualize changes along multivariate axes. On the computer it is possible to interactively flip back and forth between stick figures and view them from all directions, but for the figures in this dissertation viewing angles were chosen that best illustrate similarities and differences. To further understand changes along each principal component axis and for easier comparison with other studies, correlation coefficients with the standard measurements listed in Table 3.2 and centroid size are tabulated in Tables 4.1 (geographically variable analysis) and 4.3 (sex balanced analysis). It is important to note that these correlation coefficients, like loadings in traditional principal component analysis, do not reflect multivariate relationships in the sample and are thus not a substitute for careful examination of the changes occurring in Figures 4.1-4.9 and 4.15-4.23.

Geographically variable sample

The individuals included in the geographically variable sample analyses are those listed in Table 2.1a. As discussed in the materials chapter, this sample is composed entirely of males to prevent sexual differences from being confounded with geographic differences. A separate analysis that includes both males and females (sex balanced analysis) is discussed later in this chapter. The purpose of these analyses is to illuminate the shape differences that characterize the hip regions of people from warm versus cold climates.

Articulated hip analyses

The first four principal components of the geographically variable articulated hip analysis explain 61.9%, 13.1%, 6.5%, and 4.9% respectively (totaling 86.4%) of the sample variation. Principal component 1 (PC1G, the 'G' designates that the analysis is for the geographically variable sample) is a size component, indicated by the extremely large percentage of the variance that it explains and its relationship with centroid size (Table 4.1). The percentage variance explained by each shape principal component (PC2G onward) shows a clear flattening out at PC5G, so only the first four principal components are discussed (scree plot is not shown).

PC1G mainly reflects differences in femur length and height of the pelvis (Fig. 4.1, Table 4.1). Because PC1G has an extremely strong inverse relationship with femur length, and femur length is the best single predictor of stature (Steele and Bramblett 1988), PC1G probably also reflects changes in stature. In agreement with Ruff (1991), bi-iliac breadth is only moderately correlated with PC1G, showing that changes in stature

(using femur length as a proxy) are not necessarily associated with large changes in body breadth; however, there is a stronger inverse relationship between PC1G and pelvic depth. PC1G also has strong inverse relationships with measurements of weight-bearing joint size and shaft dimensions such as femoral head diameter, epicondylar width, acetabular size, and mid-shaft size; sagittal pelvic aperture dimensions; and ischial length (reflecting pelvic height) and superior pubic ramus length. The changes in pubic length appear to be due to more sagittally oriented pubic bones (Fig. 4.1). Essentially, this component reflects that, on average, taller people are heavier and have larger pelves, but the relationship between stature and pelvic size (particularly breadth) is fairly weak.

PC2G describes changes in bicondylar angle that are only weakly correlated with any other skeletal changes (Fig. 4.2, Table 4.1). Even though only bicondylar angle is changing, PC2G explains a high percentage of the variation, because many landmarks move with a change in bicondylar angle. There are two possible explanations for PC2G: either there is a great deal of random variation between individuals in their knee angles *in vivo*, or the standard measurement of bicondylar angle is not a very good proxy for an individual's knee angle *in vivo*. The second explanation seems more biologically reasonable, because an actual change in knee angle would affect the mechanical stresses of the hip region and therefore would produce other correlated skeletal changes. Bicondylar angle only measures a portion of the anatomy that produces an angle at the knee in living humans; the orientation of the tibial plateau contributes as well (Ruff 1995), and differences in cartilage thickness could be important. Van Gerven's (1972) PCA of linear and angular measurements of the femur also resulted in a principal component on which only bicondylar angle loaded highly. A study of radiological data

from living humans could assess actual differences in knee angle *in vivo* between individuals.

PC3G can be interpreted in a similar way to PC2G. The main changes along PC3G are in antero-posterior rotation of the entire hemi-pelvis (Fig. 4.3). As expected, PC3G is strongly correlated with pelvic depth, because all else being equal a change in rotation of the pelvis will result in a change in depth. There also are relationships between mid-plane and outlet dimensions and these differences in pelvic orientation. As for PC2G, a large amount of variation is produced through the movement of so many landmarks. This is likely another case of standard anatomical orientation not corresponding exactly to orientation during life for every individual.

PC4G describes changes in body proportions (Fig. 4.4, Table 4.1); it is strongly correlated with bi-iliac breadth ($r = -0.69$) and the ratio of bi-iliac breadth to femur length ($r = -0.70$). Not surprisingly, PC4G also has strong inverse relationships with transverse pelvic aperture dimensions (particularly medio-lateral inlet width), body weight moment arm, pubic length, and sacral breadth. Pelvic depth and sagittal aperture dimensions (especially antero-posterior inlet depth) are not as strongly correlated with PC4G, showing that while people with wide pelves have slightly deeper trunks, the main changes are in a transverse direction. PC4G is also inversely related to weight-bearing joint size (as discussed for PC1G), ischial length, pubic breadth, and femoral medio-lateral mid-shaft thickness. A close examination of Figure 4.4 shows that people with more linear bodies (positive scores) have more medially pointing anterior-superior iliac spines, more superiorly positioned sacral bodies, and less flared ilia.

PC4G further shows that people with relatively wide pelves tend to have lower neck-shaft angles, smaller torsion angles, and longer biomechanical neck lengths. Bicondylar angle also is inversely related to PC4G; however, as discussed above, this angle may not be a good proxy for knee angle *in vivo*. Van Gerven (1972) also found similar relationships between neck-shaft angle, torsion angle, and bicondylar angle. He further suggested that patterns of femoral variation may correspond to differences in pelvic breadth, but his study was only of the femur, making it impossible to relate femoral measurements to pelvic dimensions.

Hemi-pelvis analyses

The first two principal components of the hemi-pelvis GPA analysis for the geographically variable sample explain 12.4% and 9.3% respectively (totaling 21.7%) of the sample shape variation. The percentage variance explained by each of the principal components of this analysis has a flat portion after PC2G, so only PC1G and PC2G are discussed (scree plot is not shown).

Both PC1G and PC2G reflect differences in posterior iliac blade rotation, pubic bone orientation, and anterior-superior iliac spine orientation (Figs. 4.5 and 4.6). PC1G is strongly correlated with bi-iliac breadth and moderately correlated with the ratio of bi-iliac breadth to femur length (Table 4.1), which could reflect geographic differences in body proportions; however, PC2G is equally strongly correlated with the ratio of bi-iliac breadth to femur length as PC1G. This suggests that both components reflect independent aspects of pelvic variation that are related to differences in body proportions.

PC1G has moderate to strong direct relationships with pelvic depth, pubic breadth, pubic length, ischial length, transverse inlet diameter, and body weight moment

arm. PC2G has moderate to strong direct relationships with transverse mid-plane and outlet dimensions and body weight moment arm (Table 4.1). One main difference between the two components is that for PC1G changes in iliac blade rotation, supero-inferior sacral body position, pubic bone orientation, and anterior-superior iliac spine orientation are correlated with sacral shape, and for PC2G these same changes are correlated with sacral sagittal orientation and curvature (Figs. 4.5 and 4.6). Another difference is that PC1G reflects differences in iliac flare and inlet breadth, whereas PC2G more strongly reflects differences in the mid-plane and outlet (Fig. 4.5, Table 4.1). PC2G more strongly reflects acetabular orientation (Fig. 4.5) and femur length (Table 4.1) than PC1G. Neither principal component is strongly correlated with sagittal pelvic aperture dimensions, showing that most shape variation in the pelvis is due to changes in transverse dimensions. Both components also show that coronally facing posterior iliac blades, laterally facing anterior-superior iliac spines, and medially oriented pubic bones tend to co-occur.

Femur analyses

The first two principal components of the femur GPA analysis for the geographically variable sample explain 33.9% and 14.3% respectively (totaling 48.2%) of the sample shape variation. The percentage variance explained by each of the principal components of this analysis has a flat portion after PC2G, so only PC1G and PC2G are discussed (scree plot is not shown).

PC1G is related to differences in body proportions. It is strongly correlated with the ratio of bi-iliac breadth to femur length ($r = 0.67$). PC1 also is inversely correlated with femur length, but when partial correlation analysis is performed, its relationship with

the ratio of bi-iliac breadth to femur length remains strong ($r = 0.58$), but its relationship with just femur length disappears ($r = -0.18$). Therefore, the shape changes along PC1G are mainly due to differences in body proportions and not simply femur length. PC1G represents changes in neck-shaft angle, torsion angle, biomechanical neck length, and relative joint size (Fig. 4.7, Table 4.1). PC1G also has moderate direct relationships with transverse pelvic aperture dimensions and body weight moment arm. Most of the changes along PC1G of the femur also occur along PC4G of the articulated hip analysis (Fig. 4.4).

PC2G primarily reflects differences in torsion angle and also smaller changes in neck-shaft angle (Fig. 4.8, Table 4.1) that have a moderate inverse relationship with the ratio of bi-iliac breadth to femur length. Neck-shaft angle has a stronger relationship with PC1G than with PC2G, and PC1G explains more than twice the variance as PC2G, so neck-shaft angle is primarily related to body proportions in the manner discussed for PC1G. However, PC2G shows that some variation in neck-shaft angle remains to be explained. Possibly PC2G reflects differences in activity levels (Anderson and Trinkaus 1998, Trinkaus 1993a), but no clear pattern of this sort is evident in this dataset.

Innominate analyses

PC1G of the innominate GPA analysis for the geographically variable sample explains 11.5% of the sample shape variation and has a much stronger relationship with body proportions than any other innominate principal component. There is no clear cutoff in the percentage variance explained by each of the principal components of this analysis, so only the first principal component is examined (scree plot is not shown). PC1G is strongly correlated with bi-iliac breadth ($r = 0.64$) and the ratio of bi-iliac

breadth to femur length ($r = 0.66$). As with the articulated hip analysis, transverse pelvic aperture dimensions, body weight moment arm, sacral breadth, and pubic length are strongly correlated with PC1G, and sagittal pelvic dimensions are weakly correlated with PC1G (Table 4.1). PC1G is also moderately correlated with pelvic depth. Figure 4.9 displays anterior (top) and antero-superior (bottom) views of changes along PC1G. The antero-superior view in particular shows that as the pelvis gets wider medio-laterally, sagittal dimensions do not change much, resulting in morphological changes. The dorsal iliac blades become more posteriorly rotated, the pubic bones become more medially oriented, the anterior-superior iliac spine points more medially, and the iliac pillar becomes more anteriorly located. Most of these changes can also be seen along PC4G of the articulated hip analysis (Fig. 4.4), albeit less clearly due to the viewing angle and scale.

Relationship with climate and discriminant analyses

Figure 4.10 is a plot of Z-scores along the three principal components that reflect differences in body proportions (hip PC4G, femur PC1G, and innominate PC1G). There is no clear relationship between body proportions and any single principal component of the hemi-pelvis analysis (as discussed above). The histogram bars show the mean Z-scores for the eight largest geographic samples in Table 2.1a. The signs of scores along PC4G of the articulated hip are reversed so that positive corresponds to wide trunks and relatively short limbs and negative corresponds to linear bodies for all analyses. The low latitude groups have negative Z-scores for all three principal components plotted in Figure 4.10, and the high latitude groups have positive Z-scores; the mid-latitude Egyptian/Nubian group has a mix of negative and positive Z-scores. This plot shows

that, within the geographically variable sample, aspects of hip morphology related to body proportions are also related to climate. This is not surprising given that many other researchers have documented relationships between body proportions and climate in other samples (as discussed in the introductory chapter).

In addition, these three principal components are strongly correlated with latitude (by means for the 8 largest groups in Table 2.1a). PC4G of the articulated hip has an inverse relationship with latitude ($r = -0.85$), PC1G of the innominate has a direct relationship with latitude ($r = 0.66$), and PC1G of the femur has an inverse relationship with latitude ($r = 0.81$).

Discriminant analyses serve as a further test of the relationship between climatic zone, body proportions, and the other shape changes discussed above as correlated with body proportions. Table 4.2 and Figures 4.11-4.14 describe the results of discriminant analyses for the articulated hip, hemi-pelvis, femur, and innominate. As discussed in the methods chapter, the discriminant axes are calculated using stepwise, multiple regression of codes for group membership on principal component scores for the eight largest geographic groups in Table 2.1a (-1 for eastern African “Bantu”, Khoi-San, southern African “Bantu”, and Australian; 0 for Egyptian/Nubian; and 1 for British, Aleutian Islander, and Inuit). Experimentation with the specific multiple regression parameters did not significantly change the results. In all of the figures (Figs. 4.11-4.14) negative three standard deviations (left) represents shape change in the direction of people from warm environments, and positive three standard deviations (right) represents shape change in the direction of people from cold environments.

The percentage variance explained by the discriminant function (r^2) is moderate to high for all four analyses (Table 4.2), confirming that there are pronounced shape differences in hip morphology between people from different climatic zones. Also, for the articulated hip, femur, and innominate analyses, PC4G, PC1G, and PC1G respectively contribute most to group discrimination (Table 4.2). Not surprisingly, these three principal components also are those that are strongly correlated with body proportions (as discussed earlier and in Fig. 4.10). In fact, there are only slight differences between the shape changes along the three discriminant axes (Figs. 4.11, 4.13, and 4.14) and those along the corresponding principal components that reflect differences in body proportions (Figs. 4.4, 4.7, and 4.9).

For the pelvis, both PC1G and PC2G contribute strongly to group discrimination, along with smaller contributions from other principal components. This is consistent with the comparably strong relationships for both components with the ratio of bi-iliac breadth to femur length. Also, the shape changes along the hemi-pelvis discriminant axis (Fig. 4.12) are an amalgam of the shape changes along PC1G (Fig. 4.5) and PC2G (Fig. 4.6). The changes in innominate shape along the hemi-pelvis discriminant axis are similar to and confirm those along the articulated hip and innominate discriminant axes as well as those along PC4G of the articulated hip and PC1G of the innominate. The sacral shape changes along the hemi-pelvis discriminant axis show that people from warm climates, relative to individuals from cold climates, tend to have first sacral bodies that are superiorly located relative to the auricular surface and more vertically oriented sacra. However, the results of the hemi-pelvis principal component analysis show that sacral shape (PC1G) and sacral angulation (PC2G) are both independently correlated

with the innominate features that differentiate people with narrow or wide pelves. This point will become more important for the fossil hominid analyses.

Sex balanced sample

The individuals included in the sex balanced sample analyses are those listed in Table 2.1b. As discussed in the materials chapter, this sample is composed of both males and females with an approximately equal sex ratio for all populations. The purpose of the following analyses is to examine sexual dimorphism in the hip in a geographically diverse sample.

Articulated hip analyses

The first five principal components of the sex balanced articulated hip analysis explain 52.1%, 17.0%, 8.7%, 4.7%, and 2.8% respectively (totaling 85.3%) of the sample variation. As for PC1G of the geographically variable analysis, the first principal component of the sex balanced analysis (PC1S, the 'S' designates that the analysis is of the sex balanced sample) is a size component, indicated by the extremely large percentage of the variance that it explains and its relationship with centroid size (Table 4.3). For the first four principal components, only differences between this analysis and the geographically variable analysis are highlighted. The percentage variance explained by each of the principal components of sex balanced articulated hip analysis flattens out at PC5, which would argue for excluding PC5, but this component reflects sexual dimorphism so it is considered anyway (scree plot is not shown).

PC1S mainly reflects differences in femur length, height of the pelvis, and probably stature (Fig. 4.15, Table 4.3) and is broadly similar to PC1G (Fig. 4.1, Table

4.1). However, males and females are significantly different ($p < 0.0001$) along PC1S using a standard t-test due to sexual dimorphism in stature. Therefore, PC1S reflects sexual dimorphism as well as stature. PC1S differs from PC1G primarily in its weaker inverse relationships with bi-iliac breadth, sagittal inlet and midplane dimensions, and pubic ramus length and its stronger inverse relationship with pubic breadth (compare Tables 4.1 with 4.3). Females have lower scores along PC1S than males, and they have larger sagittal pelvic aperture dimensions and pubic lengths than males. This means that the relationships between PC1G and sagittal midplane and outlet dimensions and pubic length are cancelled out for PC1S. Similarly, females have narrower pubic breadths than males, so the relationship between PC1G and pubic breadth is canceled out for PC1S. The difference between the two analyses in correlation coefficients with bi-iliac breadth is smaller (-0.40 for PC1G and -0.26 for PC1S); this difference may simply reflect slightly narrower bi-iliac breadths in females due to smaller body mass.

There are only slight differences between PC2S and PC2G and PC3S and PC3G (compare Fig. 4.2 with Fig. 4.16 and Fig. 4.3 with Fig. 4.17). Comparing PC4S (Fig. 4.18) with PC4G (Fig. 4.4), there are slight differences in the magnitudes of the correlation coefficients with bi-condylar angle, pubic breadth, sagittal outlet dimensions, and pelvic depth (compare Table 4.1 with Table 4.3). This likely reflects changes in sample composition, because the sex balanced sample is not as evenly distributed geographically as the geographically variable sample. For all three of these principal components none of the discrepancies significantly change the biological interpretation.

PC5S reflects sexual dimorphism (Fig. 4.19, Table 4.3). Males and females are significantly different along this component ($p < 0.0001$) using a standard t-test. PC5S

has strong direct relationships with both sagittal and transverse midplane and outlet dimensions and with antero-posterior inlet depth. Interestingly, PC5 is only weakly correlated with medio-lateral inlet width. This component also is inversely related to pubic ramus breadth, reflecting increased male robusticity. Males have more laterally oriented acetabulae than do females, and females have more anteriorly facing obturator foramina and relatively smaller distal femora than do males (Fig. 4.19).

Hemi-pelvis analyses

The first principal component of the hemi-pelvis GPA analysis for the sex balanced sample explains 20.2% of the sample shape variation. The percentage variance explained by each of the principal components of this analysis clearly flattens out at the second principal component, so only PC1S is discussed (scree plot is not shown).

PC1S primarily reflects the larger midplane and outlet dimensions of females contrasted with the more pronounced robusticity of males (Fig. 4.20, Table 4.3). Males and females are significantly different along this component ($p < 0.0001$) using a standard t-test. Interestingly, like PC5S of the articulated hip analysis, PC1S does not reflect differences in inlet dimensions. Tague (1992) also found that across different human populations, sexual dimorphism in the pelvic midplane and outlet is more consistent than sexual dimorphism in the pelvic inlet. PC1S has strong direct relationships with femur length, pubic breadth, femoral head diameter, epicondylar width, acetabular diameter, ischial length, and mid-shaft dimensions. These measurements all reflect either sexual differences in stature or robusticity. Males have more laterally facing acetabulae and obturator foramina than females (Fig. 4.20, confirming PC5 of the sex balanced articulated hip analysis). Females also have wider greater sciatic notches, more elongated

pubic bodies, wider and shorter sacra, and many other features previously noted to be sexually dimorphic in humans (Fig. 4.20, see introductory chapter).

Femur analyses

The first two principal components of the femur GPA analysis for the sex balanced sample explain 31.5% and 15.3% respectively (totaling 46.8%) of the sample shape variation. The percentage variance explained by each of the principal components of this analysis has a flat portion after PC2S, so only PC1S and PC2S are discussed (scree plot is not shown).

In general PC1S and PC2S are similar to the first two principal components of the geographically variable femur analysis (compare Fig. 4.7 with Fig. 4.21 and Fig. 4.8 with Fig. 4.22). This is not surprising because most sexual differences in the femur are in size (Steele and Bramblett 1988, Van Gerven 1972). Comparing PC1S with PC1G, there are small differences in correlation coefficients with bi-iliac breadth, femur length, transverse inlet breadth, body weight moment arm, and centroid size, and larger differences for transverse mid-plane and outlet widths (Tables 4.1 and 4.3). The last differences are probably because females with wide pelves also have wide mid-planes and outlets. There are only minor differences between PC2S and PC2G.

Innominate analyses

The first principal component of the innominate GPA for the sex balanced sample explains 14.8% of the sample shape variation and reflects aspects of sexual dimorphism similar to those reflected in the first principal component of the sex balanced pelvis analysis (Fig. 4.23, Table 4.3) and the fifth principal component of the sex balanced

articulated hip analysis (Fig. 4.19, Table 4.3). The percentage variance explained by each of the principal components of this analysis clearly flattens out at the second principal component, so only PC1S is discussed (scree plot is not shown). Males and females are significantly different ($p < 0.001$) along this component using a standard t-test. The standard measurements with strong positive relationships with PC1S are transverse mid-plane and outlet width and antero-posterior inlet and mid-plane depth. The standard measurements with strong inverse relationships with PC1S are measures of robusticity such as iliac pillar breadth, superior pubic ramus breadth, femoral head size, acetabular size, epicondylar width, and mid-shaft dimensions. Males also tend to have longer ischia and femoral biomechanical neck lengths (Table 4.3). Most of the correlation coefficients are similar to those for PC1S for the hemi-pelvis and PC5S for the articulated hip, although the magnitudes differ somewhat. The sex related shape changes in analyses of the innominate (Fig. 4.23), the pelvis (Fig. 4.20), and the articulated hip (Fig. 4.19) are very similar.

Discriminant analyses

Table 4.4 and Figures 4.24-4.26 describe the results of discriminant analyses for the articulated hip, hemi-pelvis, femur, and innominate for the sex balanced sample. As discussed in the methods chapter, the discriminant axes are calculated using stepwise, multiple regression of principal component scores on codes for group membership. In this case the grouping is by sex (-1 for female and 1 for male). Experimentation with the specific multiple regression parameters did not significantly change the results. In all the figures (Figs. 4.24-4.26), negative three standard deviations (left) represents shape

change in the direction of females, and positive three standard deviations (right) represents shape change in the direction of males.

The percentage variance explained by the discriminant function (r^2) is moderate to high for the articulated hip, hemi-pelvis, and innominate analyses (Table 4.4), confirming pronounced shape differences in pelvic morphology between males and females. In contrast, the small percentage variance explained by the femur analysis suggests that the shape of the femur does not distinguish well between males and females (no figure is shown due to the lack of discrimination). For the pelvis and innominate analyses the first principal component, which reflects pelvic aperture size in both analyses (Figs. 4.20 and 4.23), contributes most to group discrimination (Table 4.4) and this is reflected in the changes along the discriminant axes. For the articulated hip, PC5 that reflects pelvic aperture size (Fig. 4.19), PC1 that reflects stature (Fig. 4.15), and PC2 that reflects bi-condylar angle (Fig. 4.16) all contribute strongly to discrimination between males and females. The principal component contributions to the articulated hip discriminant function made intuitive sense, because females have larger pelvic apertures, are shorter, and have slightly higher bi-condylar angles.

Discussion of the recent human baseline

Even though the results of the individual analyses are slightly different, they are generally consistent and agree upon a number of points. There are few completely novel conclusions from the analyses of sexual dimorphism in the hip, but it is reassuring that the results of the analyses in this dissertation are consistent with those of other studies. It appears that sexual dimorphism, particularly for the mid-plane and outlet of the pelvic aperture, is similar across diverse human populations. Sexual dimorphism in the size and

shape of the inlet and in pubic length is less consistent. The results from the geographically variable analyses are more novel, and therefore I discuss them extensively below.

The one area related to sexual dimorphism and obstetrics that warrants further discussion is Rosenberg's (1988) study of birth canal dimensions between different recent human populations. She found that birth canal dimensions are more strongly correlated with femoral head size (a proxy for body weight) than they are with femoral length (a proxy for stature). Interestingly, she also found that populations that are relatively heavy as compared with stature have disproportionately long pubic lengths and wide birth canals. She postulated that large female birth canal dimensions are produced by natural selection for an adequately sized birth canal for heavy and therefore large infants to pass through. The relationship between adult body weight and birth canal size was explained as a secondary consequence of the link between maternal weight and infant weight.

A correspondence between absolute body weight and birth canal dimensions seems logical, but the importance of relative body weight in determining birth canal dimensions is more puzzling unless one considers that individuals with high relative body weight tend to be "cold-adapted." The results of this dissertation show that it is not body weight per se that is important for determining birth canal dimensions but body breadth. People with high body weights because they are tall tend to have slightly wider body breadths and birth canal dimensions, but the main differences in birth canal dimensions (excluding sexual dimorphism) occur between "cold-adapted" and "warm-adapted" individuals who primarily differ in relative body weight. Interesting in this regard,

Rosenberg's tall-light group has "warm-adapted" body proportions and her short-heavy category is composed of groups with "cold-adapted" body forms.

It is possible that birth canal dimensions are the result of combined selection due to infant size and climatic adaptation, but a number of researchers have questioned the relationship between infant size and birth canal dimensions in recent humans (Abitbol 1987b, Baskerville 1989). At least for transverse dimensions, a simple direct link between climate-induced body breadth and birth canal size seems to be more plausible than a multi-causal explanation.

Most of the pelvic differences between people with "cold-adapted" and "warm-adapted" body proportions appear to be either the direct consequence of variation in pelvic width or the secondary consequence of uneven scaling of pelvic transverse dimensions versus sagittal dimensions. People with wider pelves have wider sacra, increased biacetabular distances, longer pubic lengths, and larger transverse pelvic inlets, because all of these dimensions are oriented predominately in transverse planes. However, the sagittal pelvic inlets of people with wide pelves tend to be similar in size to those of people with narrow pelves. This uneven scaling results in people with wide pelves having more posteriorly rotated dorsal iliac blades, more anteriorly located iliac pillars, and more laterally pointed anterior-superior iliac spines. These geometric scaling relationships can be seen clearly in Figure 4.9 (geographically variable innominate PC1), but it is unclear exactly why transverse dimensions show more geographic patterning than sagittal dimensions. One possible hypothesis is that sagittal variation is more constrained, because sagittally deep hips would be difficult to balance during bipedal locomotion. This idea needs to be explored further with biomechanical models based on

data from living humans, and other sagittal constraints on the hip such as developmental constraints should be examined as well.

Most of the femoral differences between people with “cold-adapted” and “warm-adapted” body proportions appear to be either the direct consequence of variation in relative body weight or the secondary consequences of the interaction between body proportions and mechanical stress. People from high latitudes have large joints relative to femur length. Other researchers have noted this relationship, and it probably reflects greater body weight relative to stature at high latitudes (Holliday 1997a, Pearson 2000a, Ruff 1994). People from high latitudes tend to have lower femoral neck-shaft angles than those individuals from low latitudes (Figs. 4.4 and 4.7). This difference in neck shaft angle is likely due to the interaction between body proportions and mechanical stress, but the exact biomechanical explanation is unclear. Figures 4.27 and 4.28 illustrate two alternate hypotheses to explain differences in neck-shaft angle; one is based on evolutionary adaptation (Fig. 4.27), and the other is based on developmental adaptation (Fig. 4.28).

The top picture in Figure 4.27 shows a simplified model of the forces acting on the adult hip (modified from Ruff 1995). In both the left and right bottom pictures the pelvis has been widened, and body weight acts at an increased distance from the hip joint, producing a larger moment (rotation) about the hip. The only way to counteract this increased moment without increasing the abductor force and the joint reaction force is for the abductor muscles to act at an increased distance as well. This can be accomplished either by lengthening the femoral neck without changing the neck-shaft angle (Fig. 4.27, bottom, left) or by lowering the neck-shaft angle without changing the neck length (Fig.

4.27, bottom, right). Lowering the neck-shaft angle is a better solution for preventing fracture of the femoral neck. Therefore, according to the hypothesis illustrated in Figure 4.27, a lower neck-shaft angle is biomechanically adaptive for people with wide hips, because it maintains equivalence in hip joint reaction force. The main problem with this evolutionary hypothesis is that it seems unlikely that degenerative changes caused by higher hip joint reaction force would have a significant enough effect on individual fitness to be naturally selected against, at least intraspecifically within humans. These degenerative changes would probably occur post-reproductively and not affect reproductive success. It also is unlikely that variation in neck-shaft angle is genetically controlled (see introductory chapter).

An alternate hypothesis is based on developmental adaptation during an individual's lifetime as opposed to evolutionary adaptation. As discussed in the introductory chapter, adult humans have lower femoral neck-shaft angles than newborns, and this difference is the result of a change in the angle of the hip joint reaction force with the onset of bipedal locomotion (Heimkes et al. 1993, Heimkes et al. 1997). The left picture in Figure 4.28 shows a simple model of the forces acting on the juvenile hip (modified from Heimkes et al. 1993), and the right figure shows changes in orientation of the hip joint reaction force. Infants and adults who are unable to walk with a normal gait have high neck-shaft angles, because they have joint reaction forces oriented more like R_1 . People with joint reaction forces oriented more like R_2 would be predicted to have low neck-shaft angles.

Body proportions are primarily inherited and differences between populations appear very early in life (see the introductory chapter). Therefore, it is possible that

“cold-adapted” versus “warm-adapted” body proportions produce different angles of hip joint reaction force, starting from a very early age, that ultimately result in differences in adult neck-shaft angle. Trying to model this idea precisely becomes complicated very quickly, because assumptions have to be made about juvenile morphology, pelvic tilt, and femur abduction or adduction during one-legged stance. The hip biomechanics of living human children with divergent body proportions needs to be investigated more fully to formally model this hypothesis.

Chapter 5

Fossil hominid analyses

The purpose of the fossil hominid analyses is to determine where individual fossil specimens fall relative to patterns of variation in recent humans. To make these comparisons, the fossil specimens are included in the generalized procrustes fitting (so that they can be compared to recent humans) but not in the calculations to generate the principal components (discussed in more detail the methods chapter). Including the fossil specimens in the procrustes fitting leads to principal components that are almost indistinguishable from those for the recent human only analyses (where the fitting did not include any fossil specimens). Therefore, the images (Figs. 4.1-4.9 and 4.15-4.23) and correlation coefficients (Tables 4.1 and 4.3) from the recent human only analyses apply equally well to the principal components discussed in this section.

For the figures in this chapter of principal components from the geographically variable analyses (Figs. 5.1-5.3, 5.6-5.8, 5.10, 5.11, 5.20-5.22, 5.25, 5.26), recent humans are grouped into three categories: those individuals from fairly warm climates (Sub-Saharan Africa, southern Asia, the Pacific), colder regions (northern Europe, the Sub-Antarctic, and the Sub-Arctic), or mid-latitudes (northern Africans), with the sample composition as given in Table 2.1a. For the figures in this chapter of the principal component from the sex balanced analyses (Figs. 5.4, 5.5, 5.9, 5.12, 5.13, 5.23, 5.24, 5.27, 5.28), males and females are grouped separately. In these same figures, fossil hominids are grouped either as Neandertal, Skhul, australopith, or modern (Upper

Paleolithic and Holocene specimens). Each specific fossil also is labeled with a three-letter abbreviation found in Appendix C.

All principal components discussed for the recent human hemi-pelvic, femoral, and innominate analyses also are discussed for the Middle to Late Pleistocene fossils, with the exception of PC1 and PC2 of sex balanced femur GPA which are essentially the same as PC1 and PC2 of the geographically variable femur GPA. For the australopiths, only the hemi-pelvis and innominate principal components are discussed due to incomplete femoral preservation. Also, none of the articulated hip principal components are discussed for any fossil specimens, because the only fossil that could have been included is from the Upper Paleolithic (Grotte des Enfants 4). Plots of centroid size (overall size) are discussed as well.

In the graphs in Figures 5.1-5.28, the overall sample mean is the dotted horizontal line, and the group means are the solid, gray horizontal lines in the middle of the gray means diamonds. The solid, black lines indicate positive and negative standard deviations from each group mean. If the tips of their means diamonds do not overlap, two groups are statistically different from each other ($p < 0.05$). The fossils are plotted as solid, black dots with adjacent labels.

Middle to Late Pleistocene fossils

Hemi-pelvis analyses

There is a clear trend of increasing overall pelvic size (hemi-pelvis centroid size) with cooler climate for males in the geographically variable recent human sample (Fig. 5.1). The warm climate mean is significantly smaller than the cold climate mean

(signified by the non-overlapping means diamonds in Figure 5.1). The northern African mean is intermediate and not statistically different from the other two means; this lack of statistical significance is partly due to small sample size for northern Africans ($n = 14$). Both Grottes des Enfants 4 (modern) and Kebara 2 (Neandertal) have large pelves, but in overall pelvic size the Upper Paleolithic modern human has a larger pelvis than the Neandertal, in spite of the fact that Kebara 2 has a wider pelvis (Holliday 1995). This result obtains because the Kebara 2 pelvis is wide but not particularly tall (superoinferiorly).

For PC1 of the geographically variable hemi-pelvis analysis, warm and cold climate males have statistically different means (Fig. 5.2), but northern Africans have an even higher, although not statistically different, mean than the cold climate group. Positive scores along PC1 reflect more posteriorly rotated iliac blades, more medially oriented pubic bones, more laterally pointing anterior-superior iliac spines, and flared ilia. Individuals with positive scores also tend to have superior first sacral bodies that are set low relative to their iliac blades (Fig. 4.5). This component has a strong direct relationship with bi-iliac breadth, transverse inlet width, and body weight moment arm (Table 4.1). Both Grotte des Enfants 4 and Kebara 2 have similarly high scores along PC1, consistent with their relatively wide bi-iliac breadths. However, based solely on bi-iliac breadth, Kebara 2 would be predicted to have a higher score than Grotte des Enfants 2, suggesting that Kebara 2 does not have a typically shaped pelvis for an individual with a wide bi-iliac breadth.

Figure 5.3 shows scores along PC2 of the geographically variable hemi-pelvis analysis. Once again, the warm and cold climate group means are statistically different

from each other, but in this case, the northern Africans are more like warm climate males. Recall from the recent human analyses that this principal component reflects similar changes to hemi-pelvis PC1 in iliac blade rotation, pubic bone orientation, and anterior-superior iliac spine orientation, but these shape changes are associated with antero-posterior sacral rotation as opposed to changes in sacral shape. Individuals with negative scores have more anteriorly rotated sacra, less posteriorly rotated iliac blades, more sagittally oriented pubic bones, more medially facing anterior-superior iliac spines (Fig. 4.6), and smaller transverse midplane and outlet dimensions (Table 4.1) than people with positive scores. Grotte des Enfants 4 falls slightly below the overall sample mean, but Kebara 2 has a score that is more than one standard deviation below the warm climate mean. Instead of falling with cold climate individuals, Kebara 2 is more extreme in shape than the average warm climate individual.

The results from PC1 and PC2 for the geographically variable hemi-pelvis analysis suggest that the Kebara 2 pelvis is a combination of pelvic features not commonly found together in recent human groups; the closest recent human group is the northern African sample. Kebara 2 has a wide pelvis with flaring and posteriorly rotated iliac blades, but these features are combined with sagittally oriented pubic bones, an anteriorly rotated sacrum, medially pointing anterior superior iliac spines, and a constricted pelvic outlet. Consequently, Kebara 2 has a lower than expected score for its bi-iliac breadth along PC1 and a “warm-adapted” score along PC2.

Figure 5.4 is a plot of hemi-pelvis centroid size for the sex balanced analysis. Interestingly, males and females are not statistically different in the overall sizes of their pelvises, as for the geographically variable hemi-pelvis analysis, because in some

dimensions males are larger but in others females are larger. Recent human sexual dimorphism in the pelvis is in shape as opposed to size. The centroid sizes for the fossils are exactly the same as for the geographically variable analysis.

PC1 of the sex balanced hemi-pelvis analysis reflects sexual dimorphism in shape (Fig. 5.5), with males having significantly larger scores than females. Both Kebara 2 and Grotte des Enfants 4 fall at the top of the male section of the graph due to their constricted pelvic mid-planes and outlets, large acetabular sizes, and general robusticity (see Fig. 4.20 and Table 4.3 for the changes along this principal component).

Femur analyses

People from warmer climates tend to have femora with larger centroid sizes than people from colder climates (Figure 5.6), although there are no significant differences between the groups. Femur centroid size mainly reflects differences in femur length ($r = 0.99$). The two Neandertals (Neandertal 1 and Spy 2) have shorter than average femora, and the two near-moderns (Skhul 4 and Skhul 5) have very long femora. Grotte des Enfants 4 has the longest femur of the Upper Paleolithic and Holocene fossils. Oakhurst 14 and Gough's Cave 1 have short femora, and Paviland 1, Afalou 2, and Ohalo 2 have long femora relative to recent humans but intermediate relative to the other fossils.

Along PC1 of the geographically variable femur analysis warm and cold climate groups show significant separation (Fig. 5.7). Along this component, northern Africans appear more like the warm climate group. Positive scores correspond to relatively large joints, low neck-shaft angles, and low torsion angles (Fig. 4.7, Table 4.1). The Neandertals have very high scores, although Neandertal 1 is within one standard deviation of the cold climate mean. The other fossil hominids have scores that cluster

around the recent human mean. There is clear separation between the near-moderns (Skhul 4 and Skhul 5) and the Neandertals (Neandertal 1 and Spy 2). The changes in shape reflected along this component are not simply size related, because within the modern human fossils there does not appear to be any relationship between centroid size and scores along PC1.

PC2 of the geographically variable femur analysis corresponds primarily to differences in torsion angle with smaller changes in neck-shaft angle (Fig. 4.8, Table 4.1). Individuals with positive scores tend to have low torsion angles. The warm climate group has a significantly higher score along this component than the cold climate group (Fig. 5.8). The Neandertals have low scores, which means that although they have low neck-shaft angles, they do not have particularly low torsion angles. Skhul 4 and 5 and the left and right femora of Grotte des Enfants 4 have fairly low torsion angles. The other Upper Paleolithic and Holocene fossils have variable scores.

Figure 5.9 is a plot of femur centroid size for the sex balanced sample. The fossils plot in exactly the same locations as for the geographically variable analysis. Females have significantly different centroid sizes than males, reflecting that, on average, females have shorter femora than males.

Innominate analyses

There is a clear trend of increasing innominate size with cooler climate (Figure 5.10). The warm and cold climate groups are significantly different in centroid size, and the pattern is similar to that for pelvis centroid size (Fig. 5.1). Most of the fossils have fairly large innominates, with the exception of the very small Oakhurst 14 innominate from the Holocene of South Africa. Kebara 2 has a large innominate, but there are a

number of fossils that have larger innominates. Once again, although the Kebara 2 pelvis is wide, it is not exceptionally large, at least relative to other fossil hominids.

Warm and cold climate groups are significantly different along PC1 of the innominate geographically variable analysis (Fig. 5.11); northern Africans have high scores like cold climate individuals. Most of the Upper Paleolithic and Holocene fossils cluster around the overall recent human mean. Oakhurst 14 groups with warm climate individuals. Skhul 4 has the highest score for the fossils, and Kebara 2 is similar to the cold climate and northern African means. Positive scores along this principal component correspond to posteriorly rotated iliac blades, medially oriented pubic bones, laterally facing anterior superior iliac spines, and anteriorly located iliac pillars (Fig. 4.9). Based on Figure 5.11, Skhul 4 is the most extreme in this morphology. However, remember from the above discussion of the hemi-pelvis that Kebara 2 has an unusual mix of pelvic features; this likely accounts for its less extreme position along this component.

Figure 5.12 is a plot of innominate centroid size for the sex balanced sample. Males have significantly larger innominates than females. The fossils plot in exactly the same locations as for the geographically variable analysis (Fig. 5.10). Most of the fossils have fairly large innominates relative to recent humans.

PC1 of the innominate sex balanced analysis reflects sexual dimorphism in shape (Fig 4.23, Table 4.3), and males and females are significantly different along this component. One standard deviation below the female mean is still a higher score than one standard deviation above the male mean. All of the fossils group closer to the male mean than to the female mean, with the exception of Gough's Cave 1. Unfortunately, the position of Gough's Cave 1 may be related to difficulty in locating landmarks along its

auricular surface, because its innominates were glued to its sacrum. Skhul 4 and Grotte des Enfants 4 have hyper-male-shaped pelvises according to their scores along this component, likely reflecting relatively long ischial lengths. Kebara 2 falls close to the recent human mean, because in the anterior pelvis, Kebara 2 is more like a female in morphology, but in the posterior pelvis, midplane, and outlet, Kebara 2 is more like a male in morphology.

Discussion of previous hypotheses

The results discussed above show that Late Pleistocene and Holocene fossil hominids tend to follow recent human patterns of variation in the hip, although there are some exceptions. For the femur, the Neandertals are extreme in their morphology, but their large femoral heads and distal ends and low neck-shaft angles are consistent with their “cold-adapted” body proportions (Fig. 5.7). In fact, when PC1 of the femur for the geographically variable analysis is regressed on the ratio of bi-iliac breadth to femur length ($r^2 = 0.45$), Spy 1 and Neandertal 1, using Ruff’s (1994) estimate of the ratio of bi-iliac breadth to femur length for Kebara 2, fall well within the 95% confidence intervals for recent human individuals. Therefore, most if not all aspects of Neandertal femoral morphology are direct consequences of their “cold-adapted” body proportions. In contrast, the individuals from Skhul and early Upper Paleolithic people have femoral shapes that correspond to their “warm-adapted” body proportions (Fig. 5.7). These results strongly support those of Pearson (2000a, 2000b) that show that body proportions are a better predictor of postcranial robusticity than activity levels.

For the pelvis, the situation is a bit more complicated. As discussed above, Kebara 2 combines some features of “cold-adapted” pelvises with other aspects of “warm-

adapted” pelvis (Figs. 5.2 and 5.3). The Kebara 2 innominate (without considering the sacrum) also is somewhat intermediate in shape. Consequently, it is instructive to investigate the Kebara 2 pelvis in more detail.

Figure 5.14 is a plot of superior pubic ramus length against bi-iliac breadth. The gray diamonds represent males in the geographically variable sample. The solid line is the least-squares regression line, and the dashed lines are the 95% confidence intervals for recent human individuals. The black diamonds with adjacent labels show the locations of fossil specimens. The coefficient of determination was calculated for the recent humans only. Ruff’s (1994) estimate for the bi-iliac breadth of Skhul 4 is used (the sacrum is not preserved). The Middle Pleistocene pelvis 1 from the Sima de los Huesos, Spain and the left innominate from Jinniushan from China are included based on measurements taken from the literature (Arsuaga et al. 1999, Rosenberg, Zun’er, and Ruff 1999). All of the fossils appear to follow the recent human relationship with the exception of Kebara 2, which is just above the upper 95% confidence interval line. Interestingly, Jinniushan has a pubic length that would be expected for its bi-iliac breadth, and Sima pelvis 1 actually has a short superior pubic ramus relative to its bi-iliac breadth. Although both these fossils have absolutely long superior pubic rami (Arsuaga et al. 1999, Rosenberg, Zun’er, and Ruff 1999), this is expected given their extremely wide pelvises.

Kebara 2 is the only fossil specimen that deviates notably from the recent human regression line. Even after its wide bi-iliac breadth is accounted for, its superior pubic ramus is still slightly long. One possible explanation proposed by Rak (1991, 1993) is that Kebara’s pelvic inlet is more anteriorly located relative to its acetabulae. In order to

quantify inlet location, Rak oriented the pelvis so that the inlet rim was horizontal, and by dropping perpendiculars, he computed the ratio of the distance from the posterior edge of the inlet to the anterior edge of the acetabulae to the total sagittal dimensions of the inlet. This procedure was replicated mathematically by rotating the pelvic inlet so that the sacral promontory and the superior edge of the pubic symphysis were aligned in a horizontal plane.

Figure 5.15 shows the results of these calculations, which are very similar to those of Rak (1991, p. 152). High values of the ratio correspond to relatively posterior acetabular location. Males have significantly higher ratios than females, and Kebara 2 has an extremely low ratio that is closer to the mean for recent human females than males. Interestingly, Grotte des Enfants 4 has an extremely high ratio, possibly explaining its hyper-male position in Figure 5.13 (innominate sexual dimorphism). Ohalo 2 and Oakhurst 14 are both within one standard deviation of the recent human male mean.

When just the distance between the sacrum and acetabulum is plotted, however, males and females are statistically indistinguishable (Fig. 5.16), suggesting that this distance is biomechanically constrained (Weaver 2000b, Weaver et al. 1998). Kebara 2 plots just below the overall recent human mean. Ohalo 2 is the most deviant fossil hominid from the recent human mean, having a fairly large distance between its sacrum and acetabulum.

When just the anterior distance between the acetabulum and the pubic symphysis is plotted, the results are similar to those for the ratio (Fig. 5.17 is approximately the

inverse of Fig. 5.15). Therefore, male and female differences and the low ratio of Kebara 2 are primarily due to variation anterior to the acetabulum.

One possible reason why Kebara 2 has a more spacious anterior pelvic inlet is because its acetabulae are more laterally oriented (Rak 1991). With the pelvis rotated as for quantifying inlet location, acetabular angle was calculated as the angle between a sagittal plane and the line between the anterior and posterior edges of the acetabulum (following Rak 1991). Figure 5.18 shows the results of this calculation. Males have significantly more laterally oriented acetabulae than females, and Kebara 2 has an extremely laterally oriented acetabulum. Grotte des Enfants 4 also has a fairly lateral orientation, and Ohalo 2 and Oakhurst 14 have orientations within one standard deviation of the recent human male mean.

PC4 of the geographically variable hemi-pelvis analysis shows that within recent humans, people with more laterally oriented acetabulae also tend to have more anteriorly rotated sacra (Fig. 4.6). Therefore, Kebara 2 would be predicted to have an extremely anteriorly rotated sacrum to go along with its laterally facing acetabulae. With the pelvis rotated as for quantifying inlet location, sacral angle was calculated as the angle between a coronal plane and the line between the sacral promontory and the transverse line between the fourth and fifth sacral vertebrae. A sacrum with an angle of zero lies in a coronal plane; positive angles correspond to anteriorly rotated sacra, and negative angles correspond to posteriorly rotated sacra. Figure 5.19 shows the results of this calculation. Males have significantly more anteriorly rotated sacra than females. Also, as expected based on acetabular orientation, Kebara 2 has an extremely anteriorly rotated sacrum. Both Grotte des Enfants 4 and Oakhurst 14 fall closer to the overall recent human mean.

In summary, the long pubic bone, posteriorly rotated iliac blade, and anterior located iliac pillar of the Kebara 2 hemi-pelvis primarily appear to be the secondary consequences of a wide bi-iliac breadth. These features are usually found in “cold-adapted” individuals, although in a less extreme form than for Kebara 2. However, unlike most “cold-adapted” people, Kebara 2 has a laterally facing acetabulum, an anteriorly rotated sacrum, a sagittally oriented pubic bone, and a medially pointing anterior-superior iliac spine. These features are usually found in “warm-adapted” individuals, although in a less extreme form than for Kebara 2. The sagittally oriented pubic bone and laterally oriented acetabulum of Kebara 2 result in a low value for Rak’s ratio of sagittal acetabular positioning and in pubic bones that are slightly longer than would be predicted from bi-iliac breadth. The recent human group that most closely approximates Kebara 2 in pelvic shape is the Egyptian/Nubian sample from northern Africa, but these pelves are much smaller in overall size than the Kebara 2 pelvis. Interesting in this regard, like Neandertals (Rosenberg 1998), the Egyptian/Nubian males have longer superior pubic rami than females (male mean = 67.7 mm, female mean = 65.8). The Egyptian/Nubian sample size is small (n = 26), but this result merits further investigation. The only individual feature of the pelvis that appears to be truly unique to Neandertals is an extremely thin pubic bone in cross section. It is possible that thin pubic bones are the biomechanical consequence of the unique mix of pelvic features found in Neandertals (features found in both “cold” climate and “warm” climate recent humans) in combination with a very large pelvis.

Australopiths

Hemi-pelvis analyses

Figure 5.20 is a plot of centroid size for the geographically variable hemi-pelvis analysis. Two different reconstructions of the AL 288-1 hemi-pelvis are plotted alongside recent humans. Not surprisingly, AL 288-1 has an extremely small pelvis in overall size and the two reconstructions group very closely together.

Along PC1 for the geographically variable hemi-pelvis analysis, large positive scores reflect more posteriorly rotated iliac blades, more medially oriented pubic bones, and more laterally pointing anterior-superior iliac spines. Individuals with positive scores also tend to have superior first sacral bodies that are set low relative to their iliac blades (Fig. 4.5). Figure 5.21 shows the location of AL 288-1 along this principal component. Both reconstructions of AL 288-1 have fairly high scores, which is similar to the Late Pleistocene fossils with wide pelvises. In absolute dimensions, AL 288-1 does not have a particularly wide pelvis (Ruff 1994); however, in pelvic shape it is similar to recent humans with wide pelvises.

Figure 5.22 shows scores along PC2 of the geographically variable pelvis analysis. It is important to note, however, that the scores along this component are reversed relative to Figure 5.3 for the Middle to Late Pleistocene hominids; reversals in sign commonly occur when principal component analyses are re-run. Interestingly, unlike Kebara 2, AL 288-1 more closely follows recent human patterns by grouping with people from cold climates along both PC1 and PC2 of the geographically variable pelvis analysis. Therefore, AL 288-1 has a pelvis that is shaped like those of “cold-adapted”

individuals (see the right-hand images in Figure 4.12 from the hemi-pelvis discriminant analysis for separating individuals by climatic zone).

There is almost no difference in centroid size between males and females (Fig. 5.23), and as for the geographically variable analysis, the AL 288-1 pelvis has a very small centroid size.

Along PC1 of the sex balanced hemi-pelvis analysis, which reflects sexual dimorphism primarily in midplane and outlet dimensions (Fig. 4.20, Table 4.3), AL 288-1 falls with recent human males (Fig. 5.24).

Innominate analyses

Figure 5.25 is a plot of centroid size for the geographically variable innominate analysis. The two reconstructions of AL 288-1 and reconstructions of the left and right sides of Sts 14 all group together and are extremely small relative to recent humans. This result is consistent with that for pelvic centroid size for AL 288-1 (Figs. 5.20 and 5.23).

Along PC1 for the geographically variable innominate analysis, positive scores correspond to posteriorly rotated iliac blades, medially oriented pubic bones, laterally facing anterior superior iliac spines, and anteriorly located iliac pillars (Fig. 4.9). All of the australopiths cluster together and have extremely high scores along this component (Fig. 5.26). In recent humans, PC1 is strongly correlated with bi-iliac breadth. Therefore, although australopiths have small innominates overall and not particularly wide bi-iliac breadths, in shape their innominates are like recent humans with wide pelves. This is consistent with the results for AL 288-1 along PC1 and PC2 of the geographically variable hemi-pelvis analysis (Figs. 5.21 and 5.22).

Figure 5.28 is a plot of centroid size for the sex balanced innominate analysis. All of the australopiths have extremely small innominates based on innominate centroid size. This is consistent with results for the geographically variable innominate analysis (Fig. 5.25) and the hemi-pelvic analyses (Figs. 5.20 and 5.23).

Interestingly, along PC1 of the sex balanced analysis, which reflects sexual dimorphism (Fig. 4.23), all the australopiths appear more like recent human females (Fig. 5.28). This is in contrast the position of AL 288-1 in the hemi-pelvis analysis (Fig. 5.24). The position of the australopiths along PC1 of the innominate for the sex balanced analysis likely reflects their long pubic bones, short ischia, and wide greater sciatic notches. For the PC1 of the sex balanced pelvis analysis, AL 288-1 groups with males due to its constricted pelvic midplane and outlet.

Discussion of previous hypotheses

The results of the above analyses suggest that in general australopiths follow recent human patterns of variation in pelvic shape consistent with their relatively wide hips (as compared to sagittal dimensions and height of the pelvis), but in absolute size australopith pelves are extremely small. Nevertheless, more extreme morphological differences between australopiths and recent humans may be masked in the analyses discussed above, because they are based only on recent human patterns of variation.

There has been extensive debate over the exact nature of australopith locomotion (see the introductory chapter). On one side of the debate, Lovejoy and colleagues (Lovejoy, Cohn, and White 1999, Lovejoy, Heiple, and Burstein 1973, Tague and Lovejoy 1986) argue that none of the purportedly unique anatomical features of australopiths are due to fundamental differences between their form of bipedal

locomotion and that of recent humans. They further argue that there is no evidence for the continued importance to australopiths of tree climbing. They suggest instead that any differences between australopiths and recent humans either are due to different obstetrical constraints combined with flaring ilia to increase the area for visceral support or are the developmental consequence of supero-inferior shortening of the pelvis in the transition from quadrupedalism to bipedalism. It is important to examine these hypotheses in detail before moving on to hypotheses that posit differences in gait between australopiths and recent humans.

By extending patterns of variation in recent humans, it is possible to predict hypothetical forms given particular dimensions of the AL 288-1 pelvis. These forms then can be visualized using computer graphics and compared to the actual form of the AL 288-1 pelvis. In this way, hypotheses that posit scaling relationships as explanations for australopith morphology can be tested.

The middle two images in Figure 5.29 show predicted pelvic shape based on recent human patterns of variation given the ratio of medio-lateral inlet width to antero-posterior inlet depth found in AL 288-1. The predicted shape was generated by multiple regression of medio-lateral to antero-posterior inlet shape on principal components from the hemi-pelvis GPA for the sex-balanced sample. The specific techniques are discussed in more detail in the methods chapter. Table 5.1a gives the details of the multiple regression analysis. The top pictures in Figure 5.29 show the mean shape for the entire recent human sex balanced sample, and the bottom pictures are of Häusler and Schmid's (1995) reconstruction of AL 288-1. The predicted pelvis (middle images) has more coronally oriented posterior iliac blades, more medially oriented pubic bones, and a wider

sacrum than the mean pelvis (top images). In these features it approximates AL 288-1 (bottom images). However, AL 288-1 has a more anteriorly rotated sacrum, a more anteriorly located iliac pillar, and flared iliac blades than the predicted pelvis. Thus, the extremely platypelloid pelvic inlet of AL 288-1 partially explains other morphological features of australopith pelvises, but not all of the differences between AL 288-1 and recent humans.

The middle two images in Figure 5.30 show predicted pelvic shape based on recent human patterns of variation given the ratio of bi-iliac breadth to pelvic height (from the iliac crest to the ischial tuberosity) found in AL 288-1. This ratio is used as a proxy for relative supero-inferior shortening of the pelvic girdle. Table 5.1b gives the details of the multiple regression analysis. The top pictures in Figure 5.30 show the mean shape for the entire recent human sex balanced sample, and the bottom pictures are of Häusler and Schmid's (1995) reconstruction of AL 288-1. The predicted pelvis (middle image) has a more anteriorly located iliac pillar, a more flaring anterior-superior iliac spine, and flared iliac blades relative to the sample mean (top image). However, AL 288-1 is still more extreme in these features (bottom image).

The predicted shapes in Figures 5.29 and 5.30 illustrate the importance of the hypotheses put forth by Lovejoy and colleagues for explaining aspects of australopith pelvic morphology (Lovejoy, Cohn, and White 1999, Lovejoy, Heiple, and Burstein 1973, Tague and Lovejoy 1986), because they show that many features of australopith pelvises can be explained, at least in part, by extending recent human scaling relationships. Nevertheless, based on the analyses in this dissertation, scaling relationships are still inadequate as an explanation for all aspects of australopith pelvic morphology. The

remaining differences could be due to altered locomotor behavior (Berge 1994, Stern 2000, Stern and Susman 1983) or possibly developmental timing.

Chapter 6

Conclusions

A scenario for hominid hip evolution

In this section, I hypothesize a scenario for the evolution of the hominid hip and discuss important morphological features found in fossil hominids. Whenever possible I try to frame my discussion in a phylogenetic context as well as a functional one.

Although the ideas in this section stem from the data and analyses in the preceding chapters of this dissertation, many of them also are based on hypotheses proposed by other researchers that are outlined and referenced in the introductory chapter. Most of these ideas need to be tested further by new fossil discoveries, because we have very few specimens to study; the skeletal elements of the hip region, particularly the pelvis, are very fragile. We also need a better understanding of extant human and ape patterns of adult and juvenile variation in the hip and a greatly amplified understanding of the developmental bases of the morphological features of the hip. Nonetheless, I try to present a plausible and consistent sequence of events based on my interpretation of the current state of our knowledge about hominid hip morphology. Table 1.1 defines the geologic time periods that I refer to in this section.

With the first bipedal apes (hominids) emerging probably 5-7 million years ago and definitely 4 million years ago, there were fundamental shifts in hip morphology. Assuming that the last common ancestor of chimpanzees and humans had a pelvis shaped more like that of a great ape, the major change with the shift to bipedalism was a supero-

inferior shortening of the ilia to position the sacrum and the vertebral column over the acetabulae and legs. In fact, my analyses suggest that the location of the sacrum relative to the acetabulae continues to be constrained in recent humans. Males and females are statistically indistinguishable in sacral-acetabular distance even though their pelves differ dramatically in features related to parturition. As further evidence of continued sacral-acetabular constraints, medio-lateral breadth of the pelvis shows more geographical patterning than antero-posterior depth. In the anthropological and biomechanical literature constraints on hip morphology in a frontal plane are widely discussed. However, hip constraints in a sagittal plane may be more important, because there are fewer musculo-skeletal avenues to compensate for antero-posterior changes than there are for medio-lateral changes.

Based on complete fossils of australopiths, supero-inferior shortening of the ilia resulted in a relatively wide but short pelvis with an extremely platypelloid pelvic aperture and likely non-rotational birth. This pelvic shape is most similar to that of recent humans from cold climates, even though australopiths are closer to Sub-Saharan Africans in pelvic width, meaning that australopith pelvic shape is not simply an allometric consequence of small size. The analyses presented in this dissertation show that platypelloid and short pelves are necessarily associated with coronally oriented posterior iliac blades, medially oriented and long pubic bones, laterally flared ilia, laterally pointing anterior superior iliac spines, and anteriorly located iliac pillars and tubercles. These features are not independent of pelvic shape, and therefore, caution should be exercised before ascribing any of them to gait differences between australopiths and recent humans. However, australopith morphology is still more extreme than would be

predicted from recent human patterns of variation. This discrepancy could either be because our understanding of pelvic morphology is still far from complete (particularly development) or because australopith pelvic morphology results from the combination of scaling relationships and gait differences.

It is important to be wary of making the teleological assumption that recent human pelvic morphology is ideally adapted to bipedal locomotion. This assumption is implicitly made when any difference between australopith, or even Neandertal, and recent human pelvic morphology is assumed to be because the bipedal gait of fossil hominids was less efficient than that of recent humans. Because all researchers would agree that australopiths differed from recent humans in obstetrical constraints and likely in the length and timing of growth and development, these non-locomotor constraints on the hip must be accounted for before examining behavioral hypotheses. We can be sure that the gait of australopiths would have appeared strange to us due to their funnel shaped rib cages, relatively short lower limbs, and diminutive stature, but it is unclear whether or not their locomotion was fundamentally different or less efficient than that of recent humans.

In the early phases of hominid evolution, hip morphology was shaped primarily by locomotor constraints. Climate may have been an important additional constraint, but its influence will be difficult to detect given the limited geographic distribution of australopiths. The narrowness of australopith pelvises in absolute dimensions could be used as evidence of warm climate adaptation, but australopiths more closely resemble cold climate recent humans in their ratios of bi-iliac breadth to femur length and in pelvic shape. Thus, the thermoregulatory implications of australopith body shape are unclear.

Constraints due to visceral support need to be investigated further before they can be established as important determinants of pelvic shape.

During the Early to Middle Pleistocene, dramatic changes in hip morphology must have occurred to modify the birth canal to keep pace with increasing brain size. As obstetrical constraints became more important, the birth mechanism likely changed from non-rotational to rotational. Rotational birth originated because after a certain pelvic breadth is reached there are more morphological avenues for sagittal expansion in the pelvic midplane and outlet; however, the inlet remained wider medio-laterally to maintain similar sacral-acetabular positioning. Because the infant's head always aligns itself along the path of least resistance, rotational birth results from a pelvic inlet that is largest medio-laterally at the inlet but largest antero-posteriorly at the midplane and outlet. Unfortunately, there are few fossils from the Early Pleistocene, and the ones we do have are fragmentary and thus inconclusive. Definitely by the Middle Pleistocene pelvic morphology in all regions of the world appears to be fundamentally modern in form relative to australopiths, and femoral morphology suggests that obstetrical changes had not yet started to occur by the Early Pleistocene. More complete innominates and sacra are necessary, however, to pin down the exact timing of these changes. Birth canal changes probably coincided with large increases in brain size that occurred around the Early/Middle Pleistocene boundary, but this evidence is only circumstantial.

As hominids expanded out of Africa into more geographic regions for the first time, climatic constraints must have become more important. As discussed in the introductory chapter, there is good evidence that fossil hominids follow geographical patterns in body shape similar to those found in recent humans, at least for limb

proportions. However, it is important to note that most Middle Pleistocene pelvises are fairly large in size and wide, and the overall body size of all of these hominids may have been large relative to recent humans. As a consequence, most Middle Pleistocene specimens have fairly long pubic bones relative to recent humans. Long pubic length should not be defined in absolute dimensions but instead by whether or not a fossil has a pubic length that is longer than expected for its pelvic width, and discussion of whether or not long pubic bones are phylogenetically primitive is not very useful. Pubic length is not a unique character; it is the consequence of a particular pelvic size and shape.

There has been much discussion about whether or not aspects of Neandertal pelvic morphology are uniquely derived or are primitive features of all Middle to Late Pleistocene hominids (excluding near-modern and early-modern humans). Although many fossils from this time period have long pubic bones, as discussed above, this should not be used as evidence that Neandertal pelvic morphology is primitive. In fact, Neandertals appear to be derived in their pubic bone cross sections, because the Middle Pleistocene Sima Pelvis 1 and Jinniushan are not as extreme in this feature as most Neandertals. Also, based on photographs and published measurements, Sima Pelvis 1 does not appear to have a sacrum that is as anteriorly rotated as Kebara 2 or pubic bones that are as sagittally oriented. I suspect that many aspects of Neandertal pelvic morphology are actually derived relative to the primitive condition for large-brained hominids. This conclusion would support arguments based on cranial morphology that Neandertals were on a separate evolutionary trajectory from their African and Asian contemporaries. The unique features of the Neandertal hip may be due to the combination of physical adaptation to the cold climates of glacial Europe combined with

genetic isolation. The differences between Neandertal and recent human hips are quantitative rather than qualitative, because Neandertal morphology appears to follow recent human patterns of variation. More Middle Pleistocene fossils are needed to determine the phylogenetic polarity of many pelvic features and to fully understand the Neandertal hip.

Final thoughts and suggestions for future research

This dissertation illustrates the importance of taking into account scaling relationships and the functional links between different skeletal elements when interpreting skeletal morphology. This can be done effectively by combining empirical studies of variation in size and shape with formal biomechanical modeling. In this vein, there needs to be more research into developing methods for examining the geometry of size and shape changes in skeletal regions that include mobile joints.

Extensive research needs to be done on living humans to better understand developmental changes in the hip and the exact orientations of different skeletal elements in life. We need to fully understand the biomechanical and developmental bases for features such as femoral head size, iliac pillar size and location, and femoral neck length, along with many other morphological features. Surprisingly little is known about these features, yet they are commonly used as markers of similarity or difference in gait between fossil hominids, apes, and recent humans.

This dissertation shows empirically that there are uneven scaling relationships in the pelvis and that variation in pelvic breadth results in many cascading morphological differences. Additionally, many differences in femoral shape are related to variation between populations in body proportions. These results illustrate the importance of

considering the skeleton as an integrated whole that is shaped by both evolutionary and mechanically induced developmental adaptation.

Appendices

A. Tables

Table 1.1 Geologic timeline¹

Era	Period	Epoch	Thousands of years ago (kya)
			0
		Holocene	
			10
	Quaternary	Late	
			127
		Pleistocene	
		Middle	
			780
		Early	
			1750
		Pliocene	
			5200
		Miocene	
	Tertiary		23500

¹Based on Klein (1999).

Table 2.1 Recent modern human skeletal samples

a. Geographically variable male sample

Sub-Saharan Africa	M	Northern Africa	M
E. African "Bantu"	18	Egyptian/Nubian	14
Khoi-San	20	Northern Europe	
Mbuti	4	British	15
S. African "Bantu"	11	The Sub-Antarctic	
Southern Asia		Tierra del Fuegian	4
Anadaman Islander	2	The Sub-Arctic	
Philippine "Negrito"	4	Aleutian Islander	16
The Pacific		Inuit	9
Australian	10		
Total		127 Males	

b. Sex balanced sample

Sub-Saharan Africa	M	F	Northern Africa	M	F
C. African "Bantu"	2	2	Egyptian/Nubian	14	13
E. African "Bantu"	4	6	Northern Europe		
Khoi-San	20	13	British	15	15
Madagascan	2	1	Norse	2	4
Mbuti	4	3	The Sub-Antarctic		
Southern Asia			Tierra del Fuegian	4	8
Philippine "Negrito"	4	6	The Sub-Arctic		
The Pacific			Aleutian Islander	16	12
Australian	10	5	Inuit	9	8
Melanesian	5	6	North America		
			African-American	15	15
Total		126 Males	117 Females		

Table 3.1 Landmarks used in this study

Femoral landmarks	
1.	Center of the hemispherical articular surface of the femoral head
2.	Center of the midpoint of the femoral neck
3.	Middle of the insertion area for gluteus minimus
4.	Middle of the insertion area for gluteus medius
5.	Tip of the lesser trochanter
6.	Center of the femoral shaft at the eighty percent of the total shaft length level
7.	Center of the femoral shaft at the mid-shaft level
8.	Tip of the adductor tubercle
9.	Midpoint of the antero-superior edge of the patellar surface of the distal femur
10.	Midpoint of the medial edge of the inferior surface of the medial condyle
11.	Midpoint of the lateral edge of the inferior surface of the lateral condyle
12.	Midpoint of the medial edge of the posterior surface of the medial condyle
13.	Midpoint of the lateral edge of the posterior surface of the lateral condyle
14.	Midpoint of the line between the medial and lateral epicondyles

Pelvic landmarks	
15.	Point where the inferior sacral auricular surface meets the superior edge of the sciatic notch
16.	Most postero-superior point on the auricular surface of the ilium
17.	Point where the arcuate line meets the auricular surface of the ilium
18.	Most superior point on the superior edge of the medial aspect of the pubic symphysis
19.	Most inferior point on the inferior edge of the medial aspect of the pubic symphysis
20.	Center of the obturator groove on the inferior surface of the superior pubic ramus
21.	Center of the notch on the superior surface of the inferior margin of the obturator foramen
22.	Center of the posterior obturator tubercles along the posterior margin of obturator foramen
23.	Center of inflection point on postero-lateral surface of the anterior margin of the obturator foramen
24.	Point on the superior edge of acetabular notch next to the lunate surface
25.	Point on the acetabular margin furthest away from the superior edge of the acetabular notch
26.	Inflection point on the inferior edge of the acetabular margin
27.	Point on acetabular margin furthest away from the inflection point on the inferior acetabular margin
28.	Apex of the anterior-inferior iliac spine
29.	Apex of the anterior-superior iliac spine
30.	Midpoint of the supero-lateral edge of the cristal tubercle
31.	Point where the lateral margin of the iliac crest meets the superior end of the posterior gluteal line
32.	Apex of the posterior-superior iliac spine
33.	Point of maximum curvature in the greater sciatic notch
34.	Tip of the ischial spine
35.	Point where the transverse ridge meets the medial edge of the ischial tuberosity
36.	Center of the more proximal hamstring facet
37.	Center of the more distal hamstring facet
38.	Point where the ischio-pubic ramus meets the ischial tuberosity
39.	Point of maximum curvature on the arcuate line of ilium (most lateral point in anatomical position)
40.	Midpoint of the anterior edge of the superior surface of the first sacral body
41.	Midpoint of the transverse line between the fourth and fifth sacral vertebrae
42.	Midpoint of the antero-inferior edge of the apex of the sacrum

Table 3.2 Calculated standard measurements

Measurement		Reference
BIBR	Bi-iliac breadth of the pelvis	(Steele and Bramblett 1988)
PELVD	Pelvic depth (PSIS spine to ASIS with pelvis in anatomical position)	(Ruff 1998)
FEML	Bicondylar length of the femur	(Steele and Bramblett 1988)
MLIN	Transverse diameter of the pelvic inlet	(Tague and Lovejoy 1986)
MLMID	Transverse diameter of the pelvic mid-plane	(Tague and Lovejoy 1986)
MLOUT	Transverse diameter of the pelvic outlet	(Tague and Lovejoy 1986)
APIN	Sagittal diameter of the pelvic inlet	(Tague and Lovejoy 1986)
APMID	Sagittal diameter of the pelvic mid-plane	(Tague and Lovejoy 1986)
APOUT	Sagittal diameter of the pelvic outlet	(Tague and Lovejoy 1986)
SACBR	Maximum breadth between the margins of the sacral alae	(Steele and Bramblett 1988)
ILBR	Maximum breadth of the iliac crest	(Ruff 1995)
PUBH	Superior pubic ramus height	(Rosenberg 1988)
PUBB	Superior pubic ramus breadth	(Rosenberg 1988)
NECK	Femoral neck-shaft angle	(Van Gerven 1972)
TORS	Femoral torsion angle	(Van Gerven 1972)
BICON	Femoral bicondylar angle	(Van Gerven 1972)
NECKL	Femoral biomechanical neck length	(Ruff 1995)
FHDIA	Femoral head diameter	(Steele and Bramblett 1988)
EPIBR	Epicondylar width	(Steele and Bramblett 1988)
RAML	Superior pubic ramus length	(Rosenberg 1988)
PUBL	Pubic length	(Rosenberg 1988)
ISCHL	Ischium length	(Steele and Bramblett 1988)
BWMA	Body weight moment arm (distance from the center of the acetabulum to the mid-line)	(McLeish and Charnley 1970)
ACET	Acetabulum diameter	(Steele and Bramblett 1988)
MLMS	Transverse femoral mid-shaft diameter	(Steele and Bramblett 1988)
APMS	Antero-posterior femoral mid-shaft diameter	(Steele and Bramblett 1988)

Table 4.1 Correlation coefficients between standard measurements and the principal components of the geographically variable sample¹

Measurement	Hip PC1G	Hip PC2G	Hip PC3G	Hip PC4G	Pelvis PC1G	Pelvis PC2G	Femur PC1G	Femur PC2G	Innom PC1G
BIBR	-0.40	-0.22	-0.01	-0.69	0.56	0.20	0.30	-0.21	0.64
PELVD	-0.48	-0.26	-0.56	-0.37	0.44	-0.00	0.18	-0.02	0.40
FEML	-0.99	-0.05	-0.07	0.02	0.10	-0.34	-0.43	0.29	-0.04
BIBR:FEML	0.41	-0.19	0.05	-0.70	0.46	0.45	0.67	-0.43	0.66
MLIN	-0.21	-0.25	-0.11	-0.70	0.52	0.34	0.41	-0.21	0.64
MLMID	0.04	-0.19	-0.46	-0.44	0.17	0.64	0.41	-0.03	0.47
MLOUT	0.01	-0.20	-0.48	-0.45	0.30	0.56	0.38	-0.15	0.60
APIN	-0.56	-0.09	0.20	-0.20	-0.28	-0.31	-0.12	0.05	-0.14
APMID	-0.45	-0.08	-0.07	-0.46	-0.17	0.26	0.16	0.07	0.08
APOUT	-0.34	-0.05	-0.04	-0.41	-0.25	0.38	0.17	0.05	0.10
SACBR	-0.34	-0.26	-0.10	-0.58	0.34	0.25	0.31	-0.20	0.50
ILBR	-0.33	-0.25	-0.19	-0.02	0.24	-0.10	-0.05	0.02	0.02
PUBH	-0.23	-0.01	-0.05	-0.20	0.14	-0.06	0.11	0.03	0.04
PUBB	-0.31	-0.10	-0.22	-0.42	0.43	-0.06	0.24	0.13	0.23
NECK	0.00	0.09	0.17	0.49	-0.04	-0.21	-0.53	-0.48	-0.04
TORS	-0.02	0.01	0.31	0.44	-0.14	-0.24	-0.56	-0.65	-0.15
BICON	-0.06	0.77	-0.11	-0.43	0.12	0.13	0.14	0.11	0.12
NECKL	-0.27	-0.30	-0.20	-0.70	0.19	0.20	0.65	0.33	0.23
FHDIA	-0.53	-0.18	-0.12	-0.62	0.39	0.08	0.29	-0.12	0.38
EPIBR	-0.58	-0.21	-0.20	-0.53	0.35	0.05	0.28	-0.05	0.35
RAML	-0.42	-0.26	-0.02	-0.71	0.45	0.18	0.32	-0.10	0.52
PUBL	-0.36	-0.29	-0.05	-0.70	0.42	0.22	0.37	-0.13	0.51
ISCHL	-0.44	-0.04	-0.18	-0.66	0.44	0.08	0.25	0.00	0.38
BWMA	-0.28	-0.25	-0.30	-0.75	0.54	0.40	0.44	-0.15	0.66
ACET	-0.60	-0.11	-0.09	-0.57	0.31	0.03	0.17	0.07	0.26
MLMS	-0.40	-0.22	-0.29	-0.49	0.38	0.09	0.31	-0.00	0.38
APMS	-0.51	-0.18	-0.01	-0.25	0.15	0.02	0.03	0.08	0.09
CENTSIZE	-1.00	-0.06	-0.03	-0.05	0.34	0.14	-0.46	0.34	0.39

¹Correlation coefficients with an absolute value of 0.40 or greater are boldfaced.

Table 4.2 Discriminant analyses for the geographically variable sample**a. Hip geographically variable analysis**

Principal component	F ratio	Probability > F
PC1	13.37	0.0004
PC2	5.55	0.0204
PC3	17.57	<0.0001
PC4	237.79	<0.0001
$r^2 = 0.75$ n = 107 variance explained ₁ = 86%		

b. Pelvis geographically variable analysis

Principal component	F ratio	Probability > F
PC1	32.49	<0.0001
PC2	50.25	<0.0001
PC3	9.96	0.0021
PC6	13.99	0.0003
PC7	7.81	0.0062
PC10	18.14	<0.0001
$r^2 = 0.57$ n = 107 variance explained ₁ = 43%		

c. Femur geographically variable analysis

Principal component	F ratio	Probability > F
PC1	162.12	<0.0001
PC2	13.20	0.0004
PC6	8.11	0.0053
PC9	14.47	0.0002
$r^2 = 0.66$ n = 113 variance explained ₁ = 55%		

d. Innominate geographically variable analysis

Principal component	F ratio	Probability > F
PC1	56.96	<0.0001
PC2	13.35	0.0004
PC4	9.42	0.0027
$r^2 = 0.44$ n = 109 variance explained ₁ = 28%		

¹Percentage of the total sample variance that is explained by the included principal components.

Table 4.3 Correlation coefficients between standard measurements and the principal components of the sex balanced sample¹

Measurement	Hip PC1S	Hip PC2S	Hip PC3S	Hip PC4S	Hip PC5S	Pelvis PC1S	Femur PC1S	Femur PC2S	Innom PC1S
BIBR	-0.26	-0.29	0.15	0.68	-0.16	0.27	0.42	-0.22	-0.23
PELVD	-0.42	-0.15	-0.60	0.41	0.03	0.15	0.17	-0.16	-0.13
FEML	-0.99	-0.05	-0.07	-0.02	-0.01	0.43	-0.34	0.02	-0.36
BIBR:FEML	0.48	-0.23	0.18	0.63	-0.12	-0.07	0.64	-0.20	0.06
MLIN	0.08	-0.08	-0.00	0.67	0.20	-0.23	0.34	-0.08	0.16
MLMID	0.26	0.10	-0.36	0.40	0.58	-0.63	0.13	0.08	0.43
MLOUT	0.16	0.13	-0.45	0.41	0.52	-0.52	0.10	-0.03	0.40
APIN	-0.15	0.02	0.08	0.24	0.52	-0.37	-0.04	0.06	0.49
APMID	-0.02	0.05	-0.01	0.43	0.71	-0.64	0.09	0.07	0.42
APOUT	0.04	0.09	-0.01	0.36	0.70	-0.67	0.07	0.07	0.39
SACBR	-0.18	-0.14	-0.09	0.58	0.06	0.08	0.30	-0.25	-0.10
ILBR	-0.30	-0.17	-0.20	0.16	-0.20	0.33	0.09	-0.09	-0.40
PUBH	-0.34	-0.12	-0.07	0.26	-0.06	0.26	0.16	-0.16	-0.31
PUBB	-0.54	-0.24	-0.12	0.27	-0.40	0.68	0.21	-0.17	-0.72
NECK	-0.07	0.23	0.02	-0.43	0.12	-0.12	-0.58	-0.42	0.23
TORS	0.01	0.11	0.07	-0.40	0.08	-0.15	-0.54	-0.62	0.20
BICON	-0.08	0.78	0.03	0.36	-0.19	-0.06	-0.05	0.08	-0.06
NECKL	-0.25	-0.41	-0.14	0.62	-0.18	0.38	0.71	0.18	-0.44
FHDIA	-0.58	-0.32	-0.05	0.50	-0.31	0.65	0.34	-0.34	-0.69
EPIBR	-0.61	-0.31	-0.12	0.43	-0.29	0.62	0.33	-0.30	-0.63
RAML	-0.16	-0.15	-0.04	0.75	0.19	-0.02	0.35	-0.13	-0.01
PUBL	-0.09	-0.16	-0.03	0.71	0.26	-0.07	0.35	-0.16	0.05
ISCHL	-0.57	-0.18	-0.10	0.52	-0.22	0.52	0.24	-0.23	-0.59
BWMA	-0.18	-0.14	-0.27	0.79	0.15	0.01	0.38	-0.19	-0.15
ACET	-0.62	-0.27	-0.03	0.47	-0.20	0.57	0.25	-0.25	-0.62
MLMS	-0.41	-0.31	-0.17	0.45	-0.22	0.41	0.37	-0.19	-0.49
APMS	-0.54	-0.28	-0.06	0.18	-0.15	0.51	0.14	-0.10	-0.48
CENTSIZE	-0.99	-0.08	-0.01	0.06	0.03	0.17	-0.38	0.09	-0.32

¹Correlation coefficients with an absolute value of 0.40 or greater are boldfaced.

Table 4.4 Discriminant analyses for the sex balanced sample**a. Hip sex balanced analysis**

Principal component	F ratio	Probability > F
PC1	92.40	<0.0001
PC2	43.33	<0.0001
PC5	171.35	<0.0001
$r^2 = 0.57$ n = 231		variance explained ₁ = 72%

b. Pelvis sex balanced analysis

Principal component	F ratio	Probability > F
PC1	652.92	<0.0001
PC2	27.75	<0.0001
PC3	47.08	<0.0001
PC4	26.15	<0.0001
PC5	15.24	0.0001
PC6	9.18	0.0027
PC8	14.45	0.0002
PC9	15.90	<0.0001
PC10	6.09	0.0143
PC11	6.82	0.0096
$r^2 = 0.79$ n = 231		variance explained ₁ = 66%

c. Femur sex balanced analysis

Principal component	F ratio	Probability > F
PC1	7.53	0.0065
PC2	8.10	0.0048
PC4	13.32	0.0003
PC6	11.77	0.0007
PC9	4.44	0.0362
$r^2 = 0.16$ n = 242		variance explained ₁ = 60%

d. Innominate sex balanced analysis

Principal component	F ratio	Probability > F
PC1	585.13	<0.0001
PC2	105.56	<0.0001
PC3	113.09	<0.0001
PC4	5.69	0.0179
PC6	12.50	0.0005
PC7	4.77	0.0300
PC9	10.86	0.0011
PC11	6.45	0.0118
$r^2 = 0.79$ n = 238		variance explained ₁ = 53%

¹Percentage of the total sample variance that is explained by the included principal components.

Table 5.1 Multiple regression analyses of pelvic inlet shape, relative pelvic height, and pelvic morphology for the sex balanced sample

a. Inlet shape (ratio of medio-lateral inlet breadth to antero-posterior inlet depth)

Principal component	F ratio	Probability > F
PC1	6.60	0.0109
PC2	29.23	<0.0001
PC3	429.94	<0.0001
PC4	12.47	0.0005
PC5	11.53	0.0008
PC6	31.41	<0.0001
PC7	48.21	<0.0001
PC8	7.69	0.0060
PC9	19.72	<0.0001
PC11	4.81	0.0294
<hr/>		
$r^2 = 0.73$	n = 230	variance explained ₁ = 67%

b. Relative pelvic height (ratio of bi-iliac breadth to pelvic height)

Principal component	F ratio	Probability > F
PC1	23.84	<0.0001
PC2	56.24	<0.0001
PC3	247.90	<0.0001
PC4	43.79	<0.0001
PC6	14.15	0.0002
PC7	13.45	0.0003
PC8	11.03	0.0011
PC9	29.82	<0.0001
PC10	11.95	0.0007
PC11	25.22	<0.0001
<hr/>		
$r^2 = 0.69$	n = 230	variance explained ₁ = 64%

¹Percentage of the total sample variance that is explained by the included principal components.

B. Figures

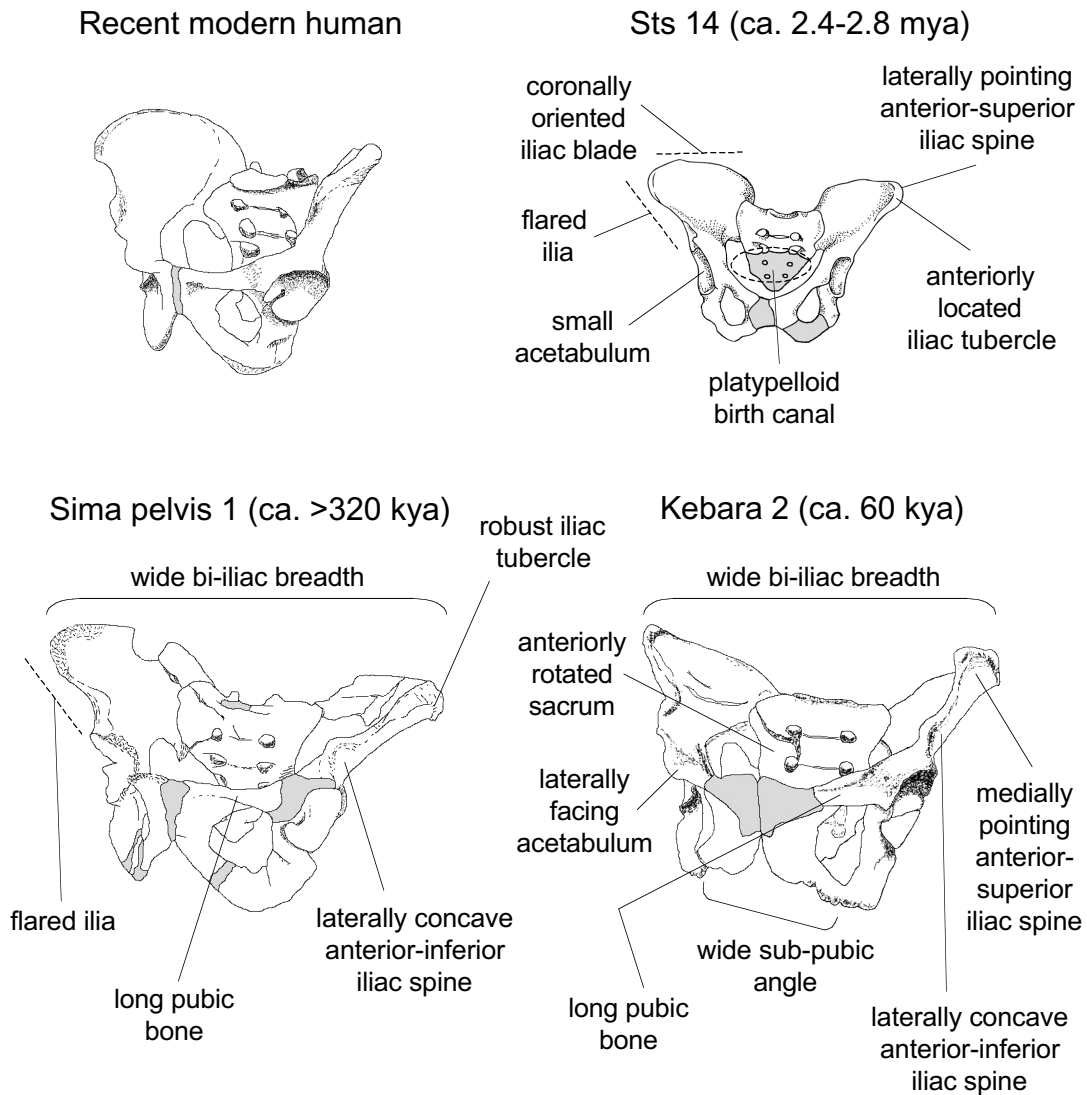


Figure 1.1 Key fossil hominid pelvises

From the top left, moving clockwise, are illustrations of articulated pelvises from a recent modern human male, an australopith (Sts 14), a Neandertal (Kebara 2), and Middle Pleistocene primitive *Homo* (Sima pelvis 1). Sima Pelvis 1 comes from a population that in the broad sense was ancestral to Neandertals. Unfortunately, earlier pelvises from primitive *Homo* are all much more fragmentary. The illustrated pelvises are drawn approximately to scale, and all the labeled features are relative to recent human pelvic morphology. The gray, shaded areas are reconstructed anatomical regions, and the left side of the Kebara 2 pelvis is a mirror image of the right side. The picture of Sts 14 is modified slightly from a drawing by R. Klein.

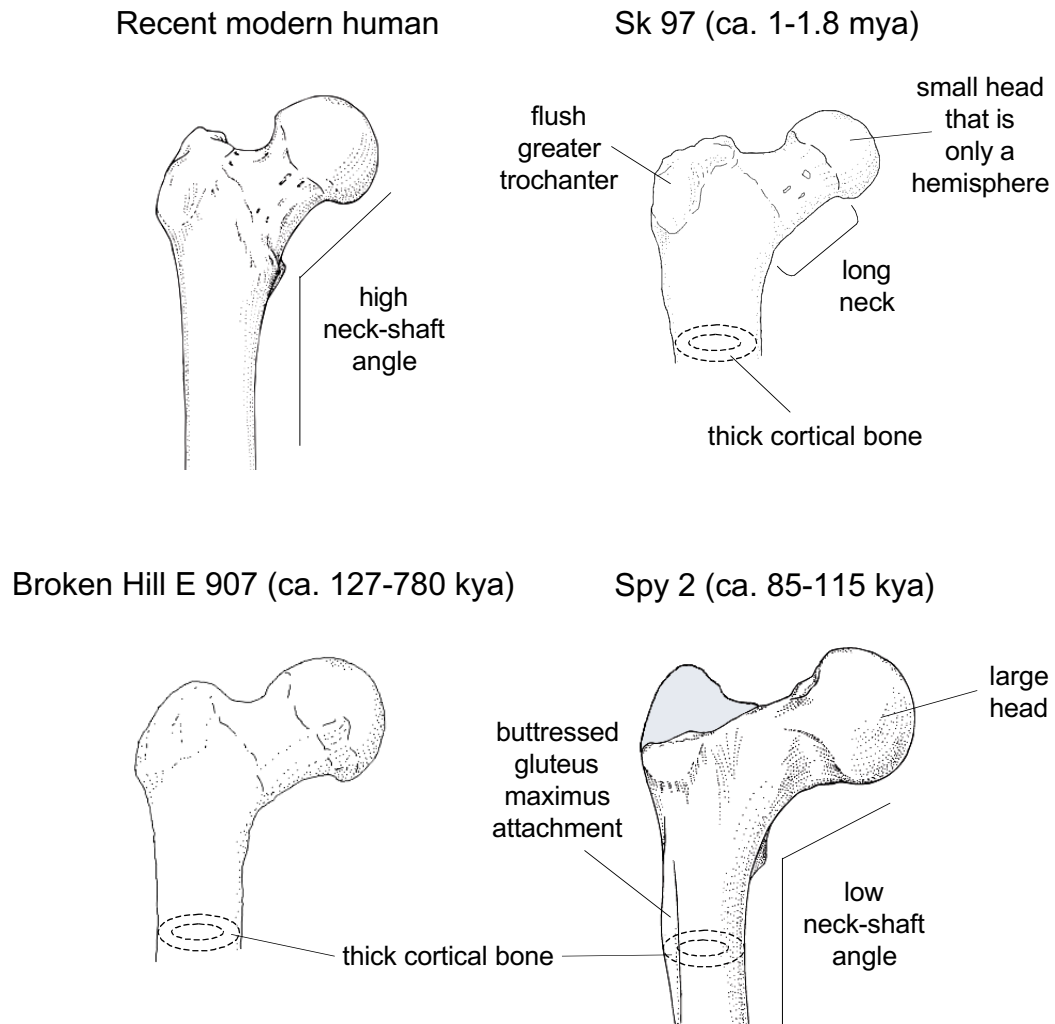


Figure 1.2 Key fossil hominid femora

From the top left, moving clockwise, are illustrations of femora from a recent modern human male, an australopith (Sk 97), a Neandertal (Spy 2), and Middle Pleistocene primitive *Homo* (Broken Hill E 917). E 917 comes from an African population that in the broad sense was probably ancestral to modern humans; however, the geological context of this fossil is poorly known, making its dating somewhat speculative. It also is important to note that the femora of Middle Pleistocene primitive *Homo* are morphologically very variable. The illustrated femora are drawn approximately to scale. The gray, shaded areas are reconstructed anatomical regions. The pictures of Spy 2 and the recent modern human are modified slightly from drawings by R. Klein.

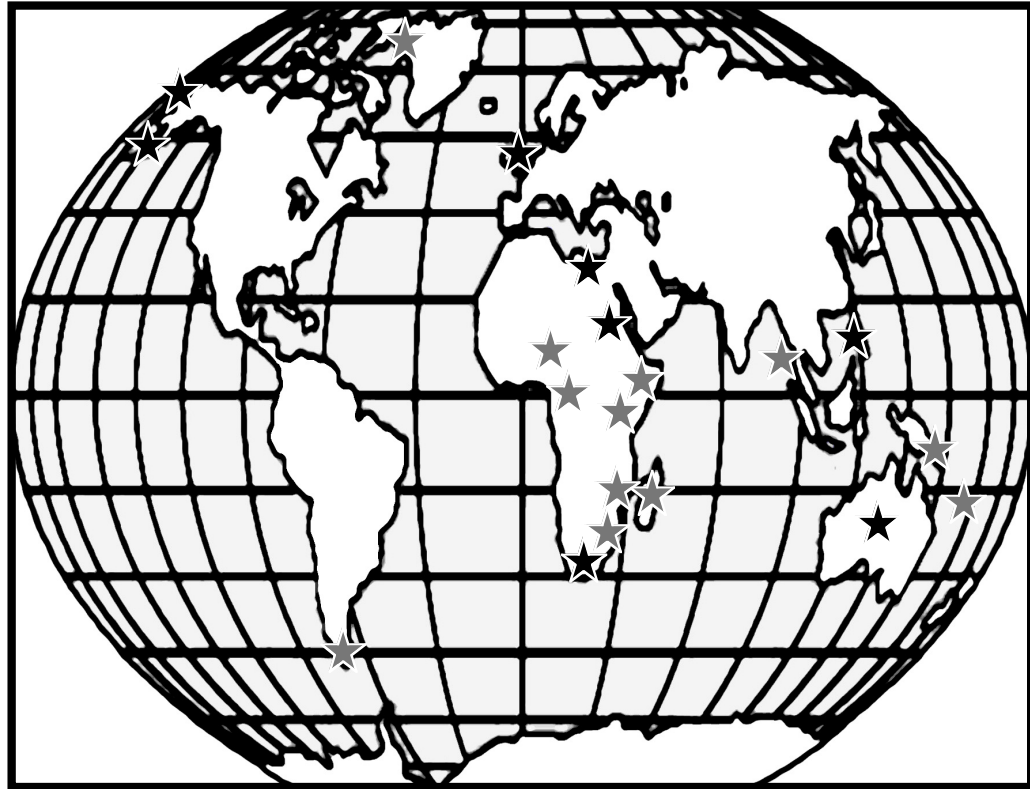


Figure 2.1 Geographic locations of recent human sub-samples

The stars show the geographic distribution of the individuals in the recent human comparative dataset used in this dissertation. Black stars signify at least 10 individuals, and gray stars signify less than 10 individuals. Refer to Table 2.1 and the text for more details about the exact composition of the geographically variable and sex balanced samples and how individuals were grouped together. The African-American sub-sample is not included in this plot.

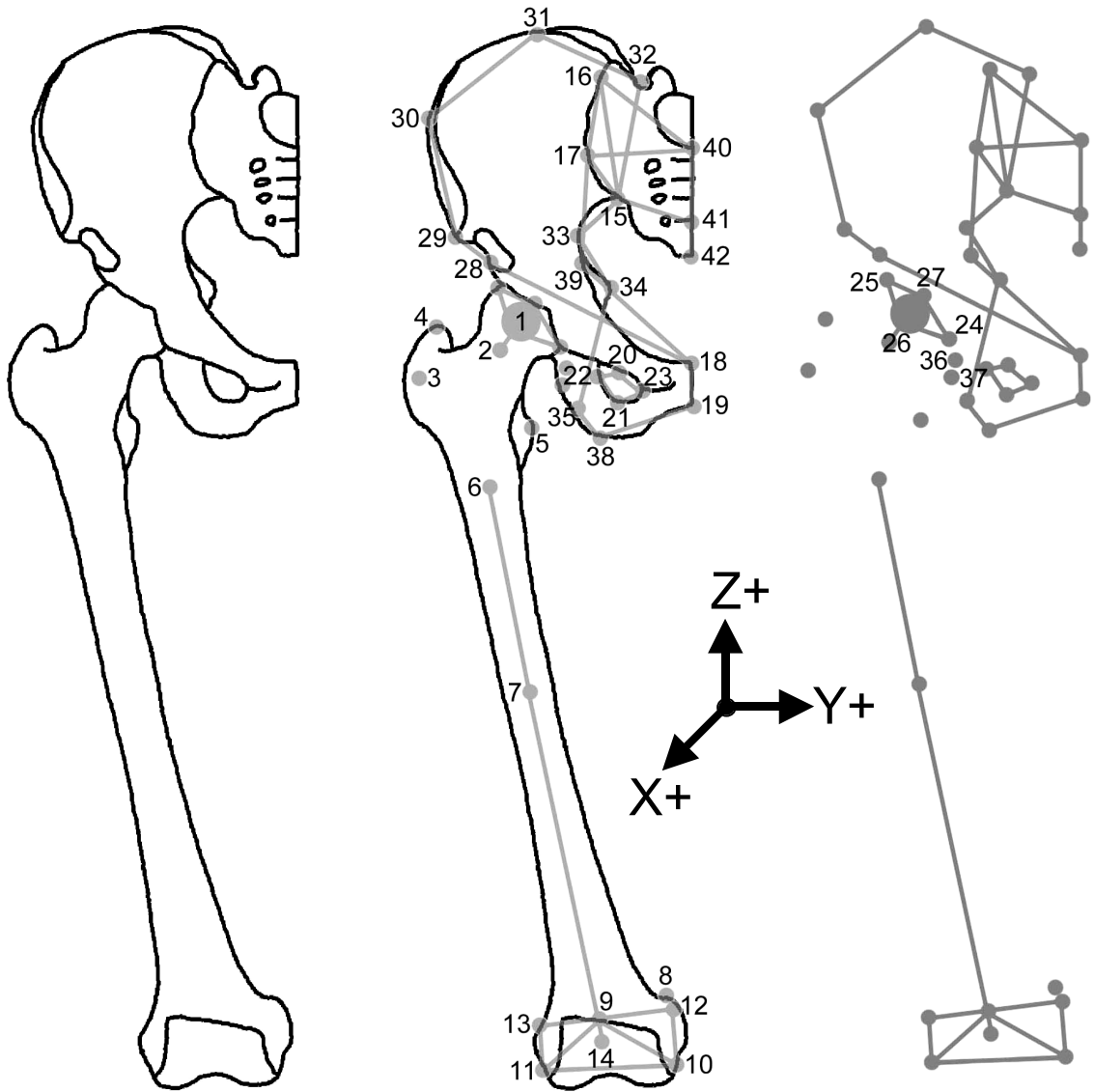


Figure 3.1 Landmarks used in this study

On the left is a picture of half of an articulated hip; on the right is a stick figure representation of the same hip created by linking together the landmarks in Table 3.1. In the middle is the stick figure overlain on top of the hip picture. The landmark numbers correspond with those in Table 3.1. As shown by the coordinate axes, x is posterior to anterior, y is lateral to medial, and z is inferior to superior. The landmarks and connections of the stick figures in Figures 4.1-4.9, 4.11-4.26, 5.29, and 5.30 correspond with those shown here.

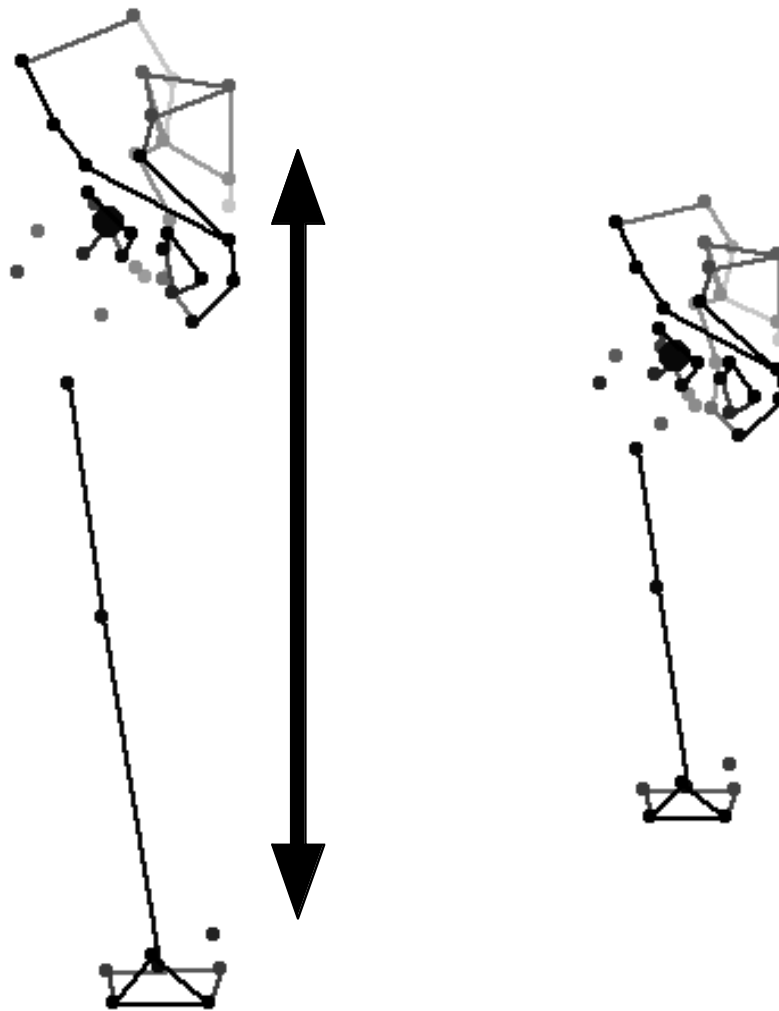


Figure 4.1 Geographically variable analysis: hip PC1

Anterior view

The left stick figure shows negative three and the right stick figure shows positive three standard deviations from the sample mean along PC1 from the geographically variable articulated hip analysis (assuming no changes along any of the other principal component axes). Lighter shading indicates greater depth in the stick figures. Notice the large changes in femur length and pelvic height coupled with only limited changes in pelvic breadth.

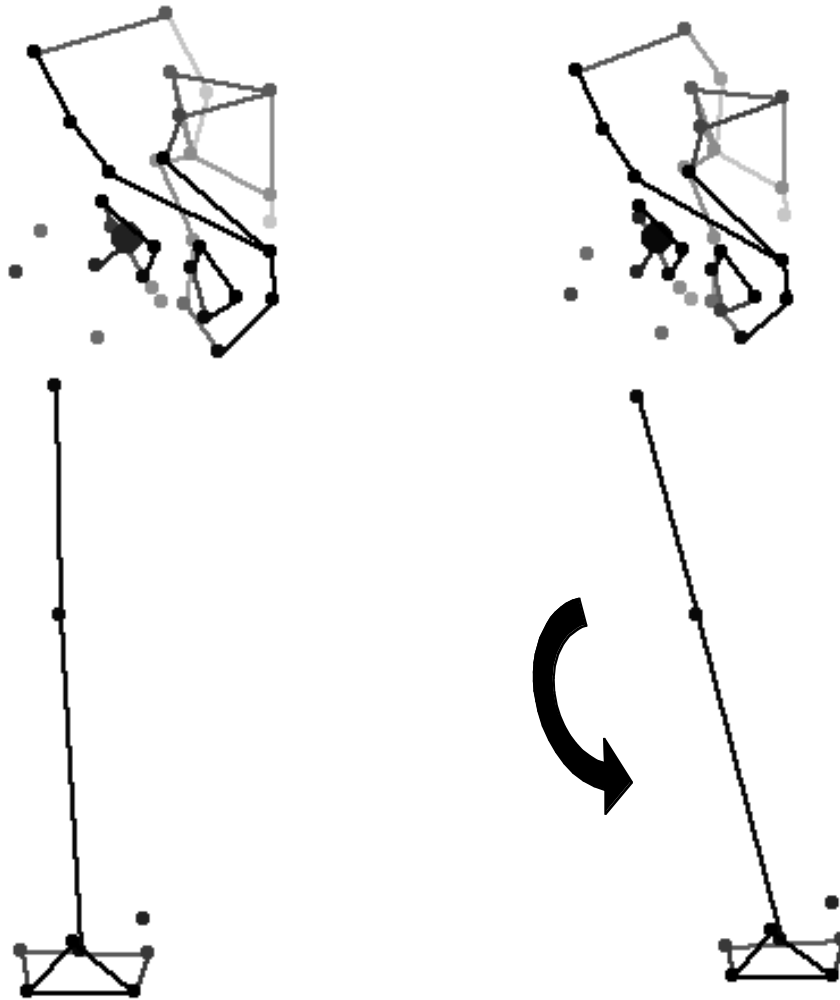


Figure 4.2 Geographically variable analysis: hip PC2

Anterior view

The left stick figure shows negative three and the right stick figure shows positive three standard deviations from the sample mean along PC2 from the geographically variable articulated hip analysis (assuming no changes along any of the other principal component axes). Lighter shading indicates greater depth in the stick figures. Notice the large changes in bicondylar angle with almost no other changes.

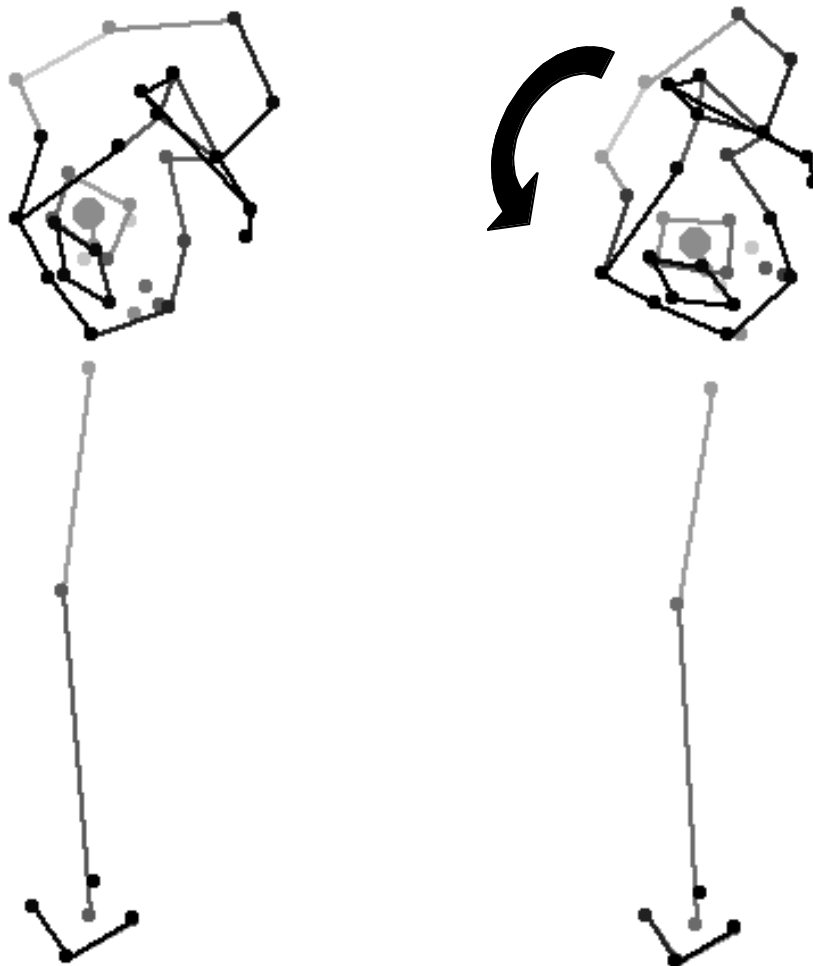


Figure 4.3 Geographically variable analysis: hip PC3

Medial view

The left stick figure shows negative three and the right stick figure shows positive three standard deviations from the sample mean along PC3 from the geographically variable articulated hip analysis (assuming no changes along any of the other principal component axes). Lighter shading indicates greater depth in the stick figures. Notice the large changes in antero-posterior rotation of the entire pelvic girdle with almost no other changes.

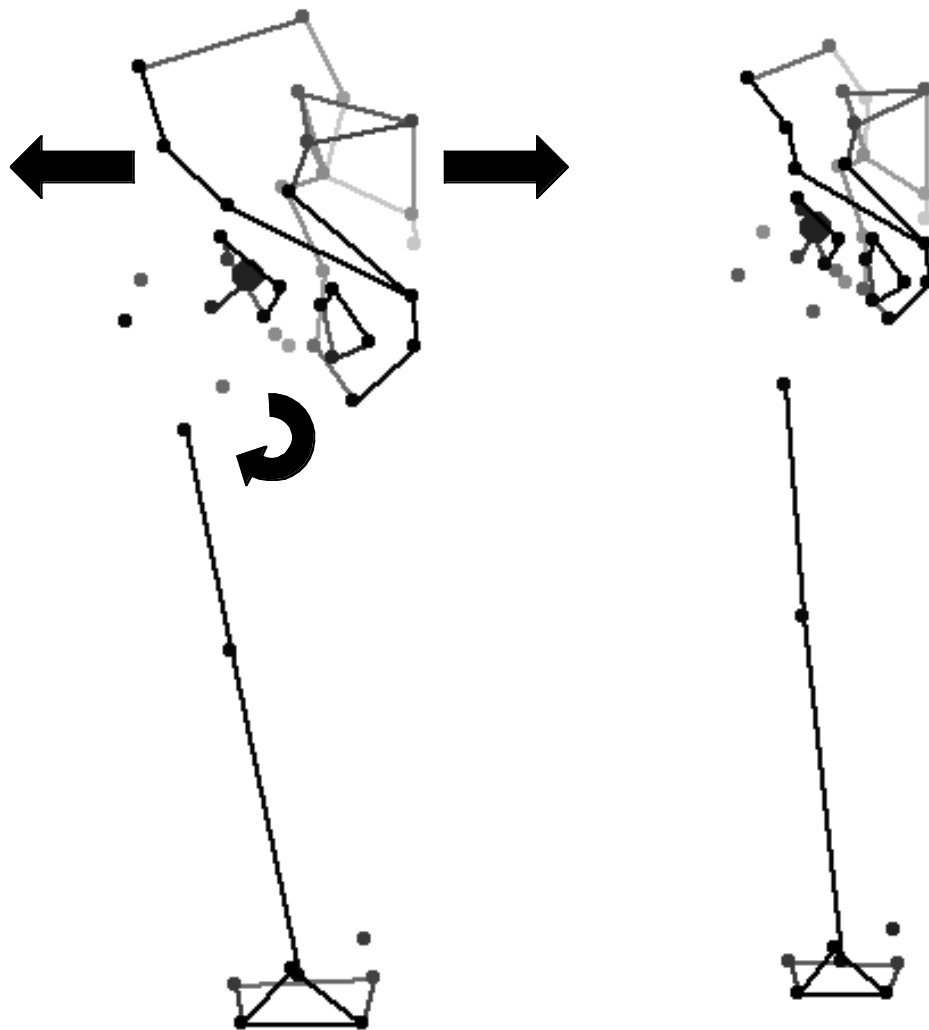


Figure 4.4 Geographically variable analysis: hip PC4

Anterior view

The left stick figure shows negative three and the right stick figure shows positive three standard deviations from the sample mean along PC4 from the geographically variable articulated hip analysis (assuming no changes along any of the other principal component axes). Lighter shading indicates greater depth in the stick figures. The left stick figure has a wide body and relatively short limbs, and the right stick figure has a linear body form. Notice the differences in pelvic aperture size, shape of the pelvis, neck-shaft angle, and bicondylar angle.

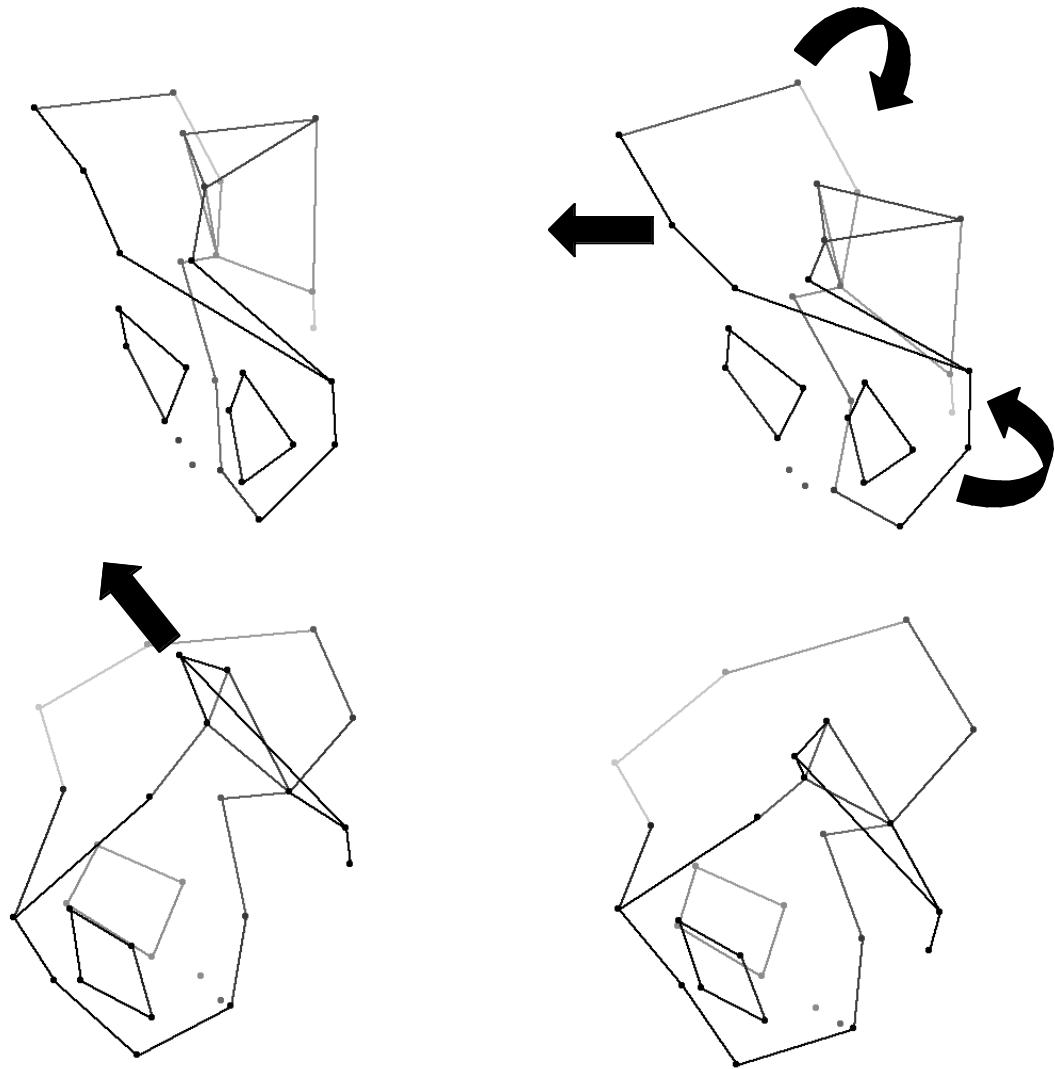


Figure 4.5 Geographically variable analysis: pelvis PC1

Anterior (top) and medial (bottom) views

The left stick figures show negative three and the right stick figures show positive three standard deviations from the sample mean along PC1 from the geographically variable pelvis GPA (assuming no changes along any of the other principal component axes). Lighter shading indicates greater depth in the stick figures. Notice the differences in posterior iliac blade rotation, pubic bone orientation, anterior-superior iliac spine orientation, first sacral body shape, and lateral iliac blade flaring.

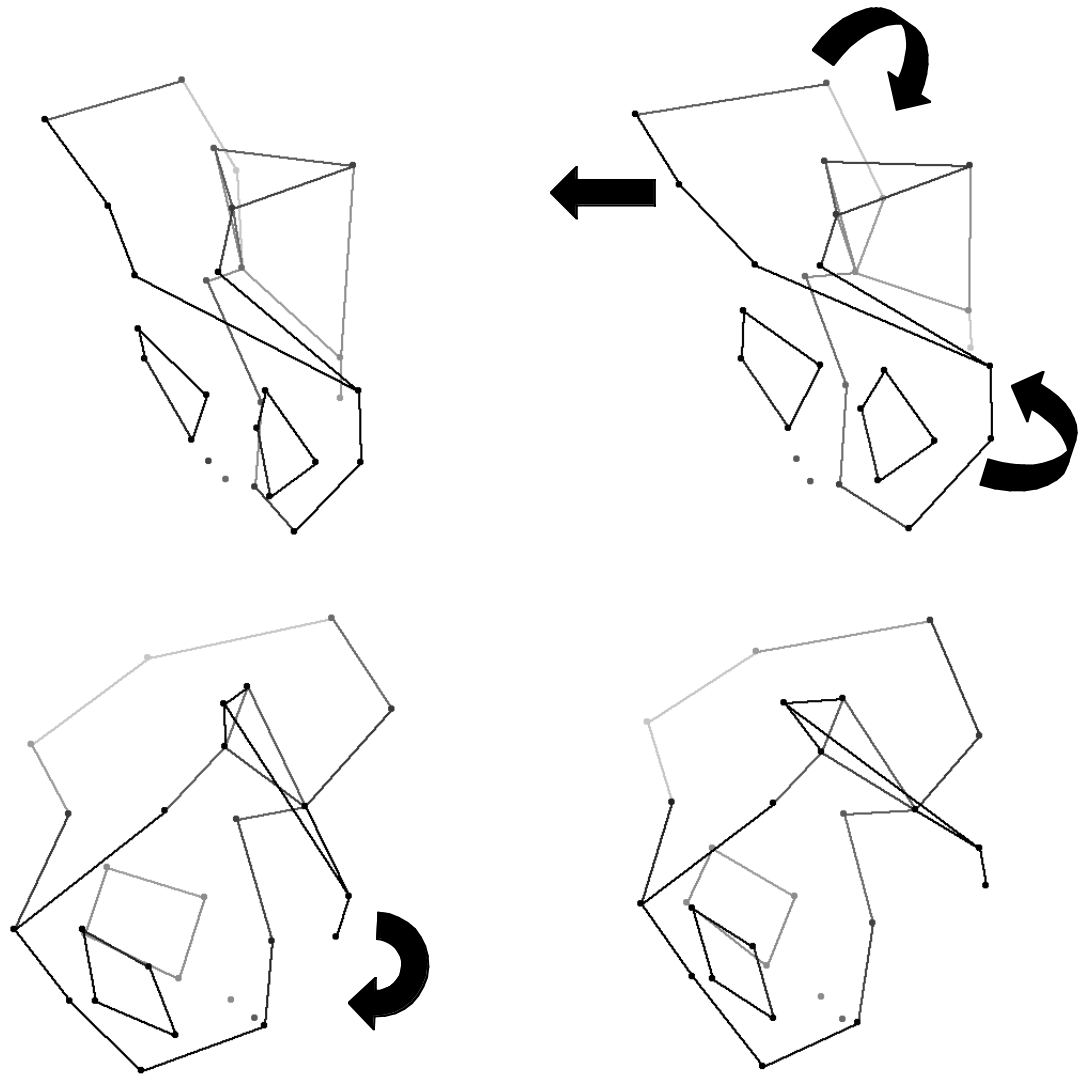


Figure 4.6 Geographically variable analysis: pelvis PC2

Anterior (top) and medial (bottom) views

The left stick figures show negative three and the right stick figures show positive three standard deviations from the sample mean along PC2 from the geographically variable pelvis GPA (assuming no changes along any of the other principal component axes). Lighter shading indicates greater depth in the stick figures. Notice the differences in posterior iliac blade rotation, pubic bone orientation, anterior-superior iliac spine orientation, acetabular orientation, and sacral angle and curvature.

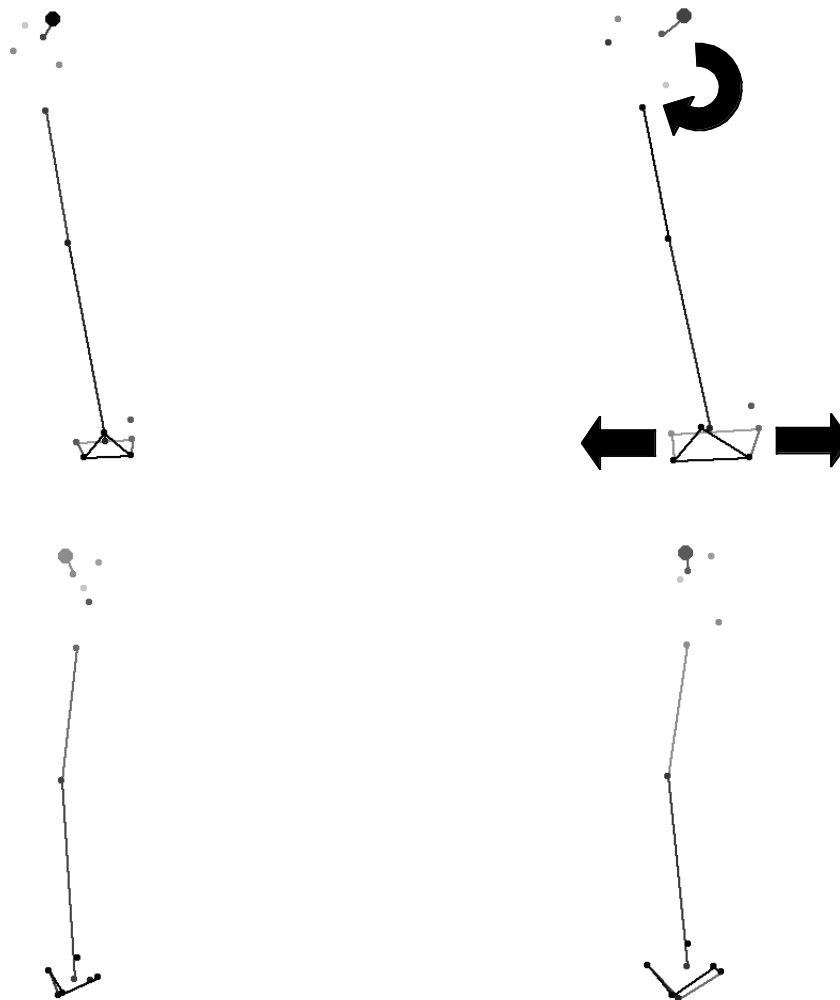


Figure 4.7 Geographically variable analysis: femur PC1

Anterior (top) and medial (bottom) views

The left stick figures show negative three and the right stick figures show positive three standard deviations from the sample mean along PC1 from the geographically variable femur GPA (assuming no changes along any of the other principal component axes). Lighter shading indicates greater depth in the stick figures. The left stick figure corresponds to a low ratio of bi-iliac breadth to femur length, and the right stick figure corresponds to a high one. Notice the differences in relative joint size, neck-shaft angle, and torsion angle.

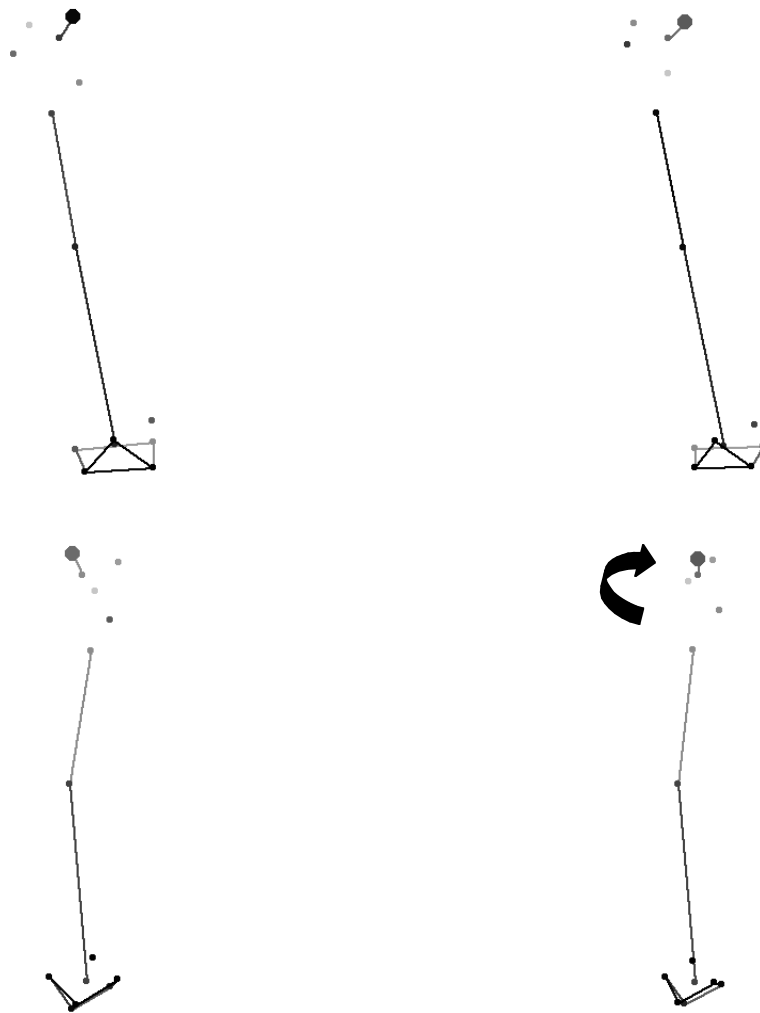


Figure 4.8 Geographically variable analysis: femur PC2

Anterior (top) and medial (bottom) views

The left stick figures show negative three and the right stick figures show positive three standard deviations from the sample mean along PC2 from the geographically variable femur GPA (assuming no changes along any of the other principal component axes). Lighter shading indicates greater depth in the stick figures. Notice the pronounced differences in torsion angle and the moderate differences in neck-shaft angle.

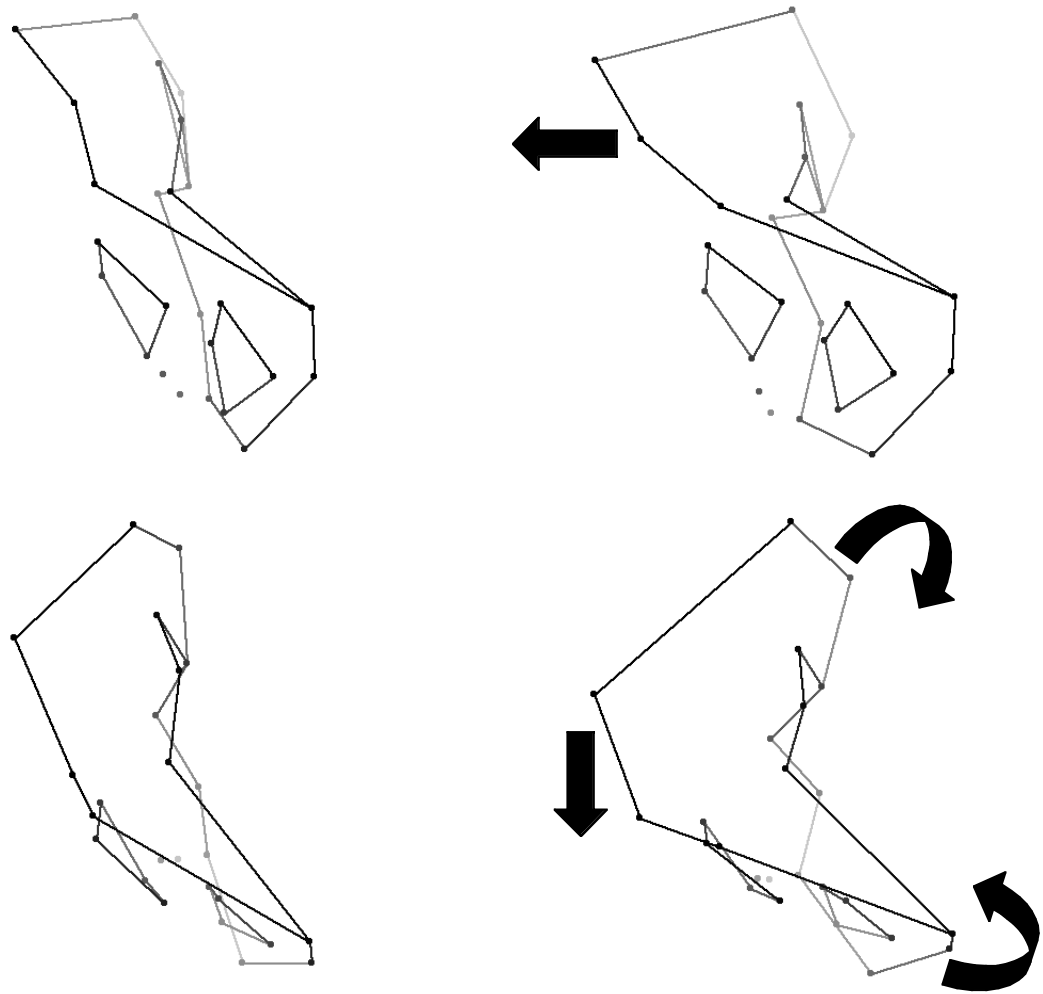


Figure 4.9 Geographically variable analysis: innominate PC1

Anterior (top) and antero-superior (bottom) views

The left stick figures show negative three and the right stick figures show positive three standard deviations from the sample mean along PC1 from the geographically variable innominate GPA (assuming no changes along any of the other principal component axes). Lighter shading indicates greater depth in the stick figures. The left stick figure shows the shape of a narrow pelvis, and right stick figure shows the shape of a wide pelvis. Notice the differences in posterior iliac crest rotation, pubic bone orientation, transverse relative to sagittal pelvic dimensions, anterior-superior iliac spine orientation, and relative location of the iliac tubercle.

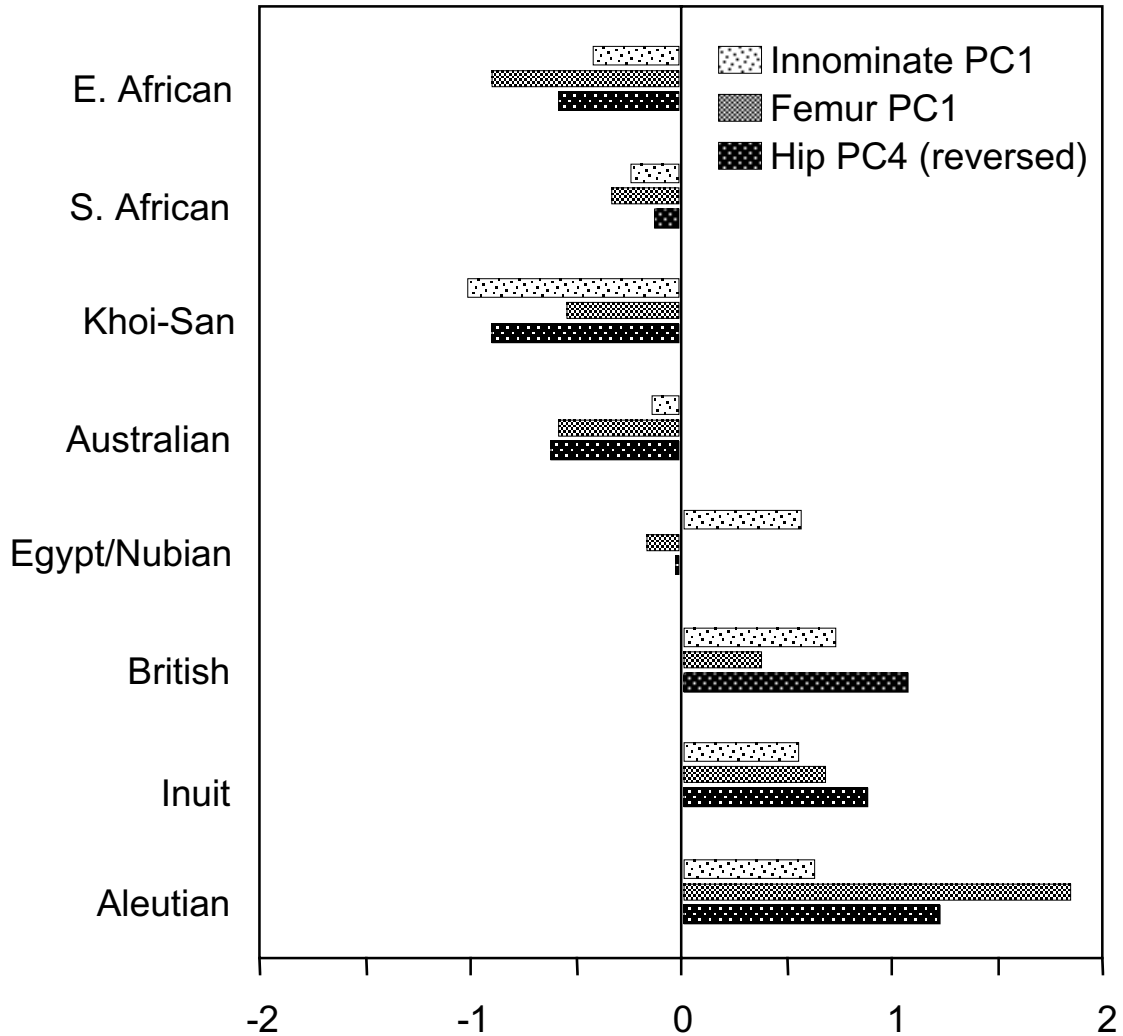


Figure 4.10 Z-scores along PCA axes that reflect body proportions
 The histogram bars show the mean Z-scores for the eight largest samples in the geographically variable analysis along PC4 of the articulated hip, PC1 of the femur GPA, and PC1 of the innominate GPA. The signs of the scores along PC4 of the articulated hip are reversed so that positive corresponds to wide trunks and relatively short limbs and negative corresponds to linear bodies along all analyses. The low latitude groups have negative Z-scores for all three principal components, and the high latitude groups have positive Z-scores; the mid-latitude Egyptian/Nubian group has a mix of negative and positive Z-scores.

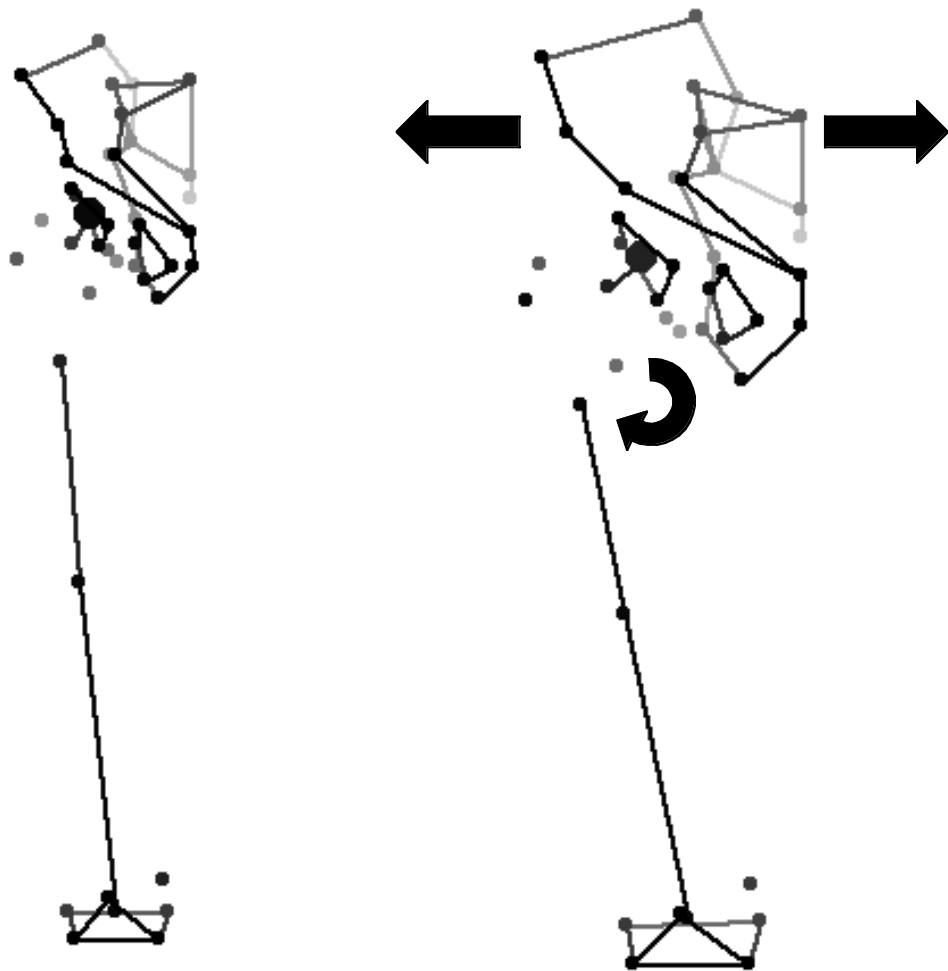


Figure 4.11 Geographically variable analysis: hip discriminant function axis that separates populations by climate

Anterior view

The left stick figure shows negative three and the right stick figure shows positive three standard deviations from the sample mean along a discriminant function axis calculated to separate warm, mid-latitude, and cold climate populations. The discriminant function was calculated using principal components from the geographically variable articulated hip analysis. Lighter shading indicates greater depth in the stick figures. The right stick figure has a wide body and relatively short limbs (cold climate), and the left stick figure has a linear body form (warm climate). Notice the differences in pelvic aperture size, anterior-superior iliac spine orientation, iliac flaring, sacral shape, and neck-shaft angle.

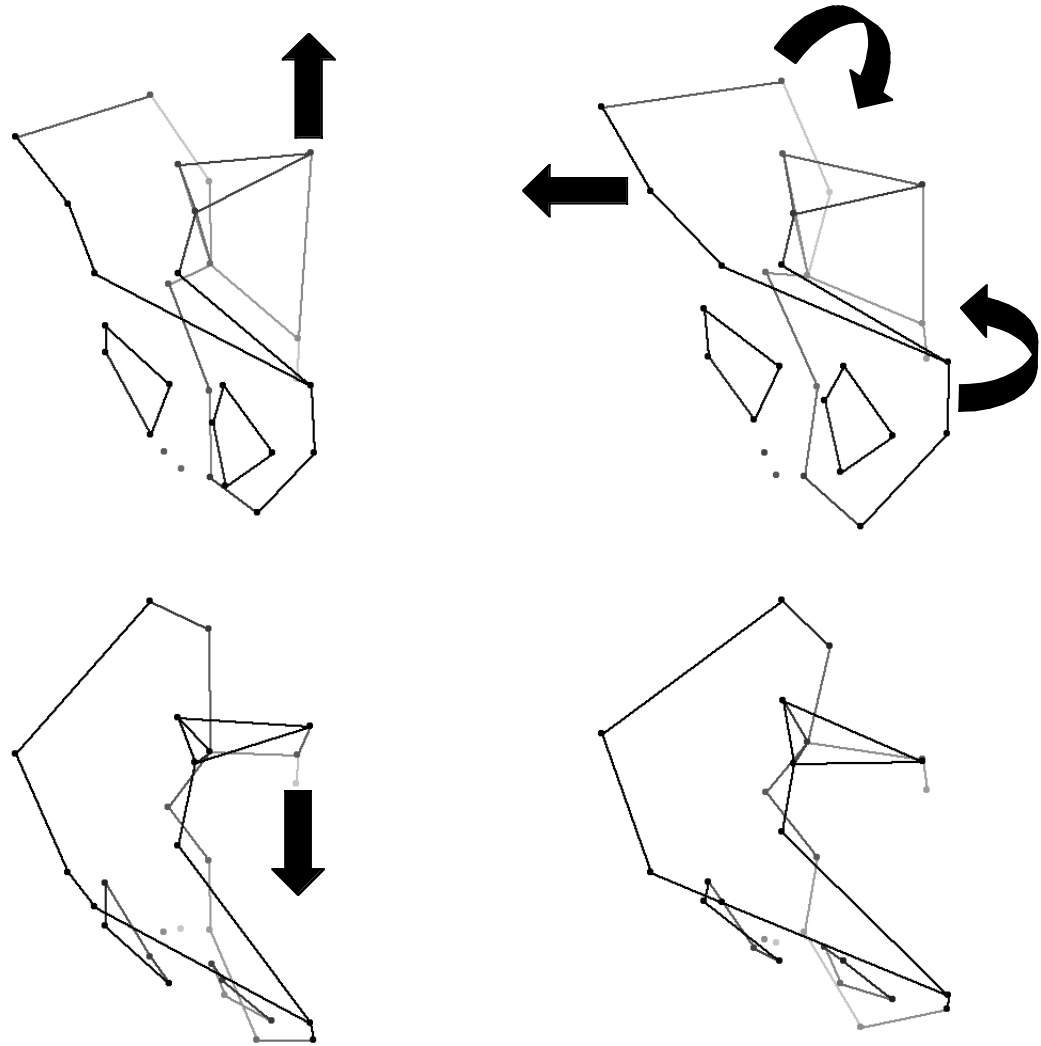


Figure 4.12 Geographically variable analysis: pelvis discriminant function axis that separates populations by climate

Anterior (top) and antero-superior (bottom) views

The left stick figure shows negative three and the right stick figure shows positive three standard deviations from the sample mean along a discriminant function axis calculated to separate warm, mid-latitude, and cold climate populations. The discriminant function was calculated using principal components from the geographically variable pelvis GPA. Lighter shading indicates greater depth in the stick figures. The left stick figure is the shape of a narrow pelvis (warm climate), and the right stick figure is the shape of a wide pelvis (cold climate). Notice differences in iliac rotation, pubic orientation, transverse to sagittal pelvic dimensions, anterior-superior iliac spine and acetabular orientation, and sacral shape and orientation.

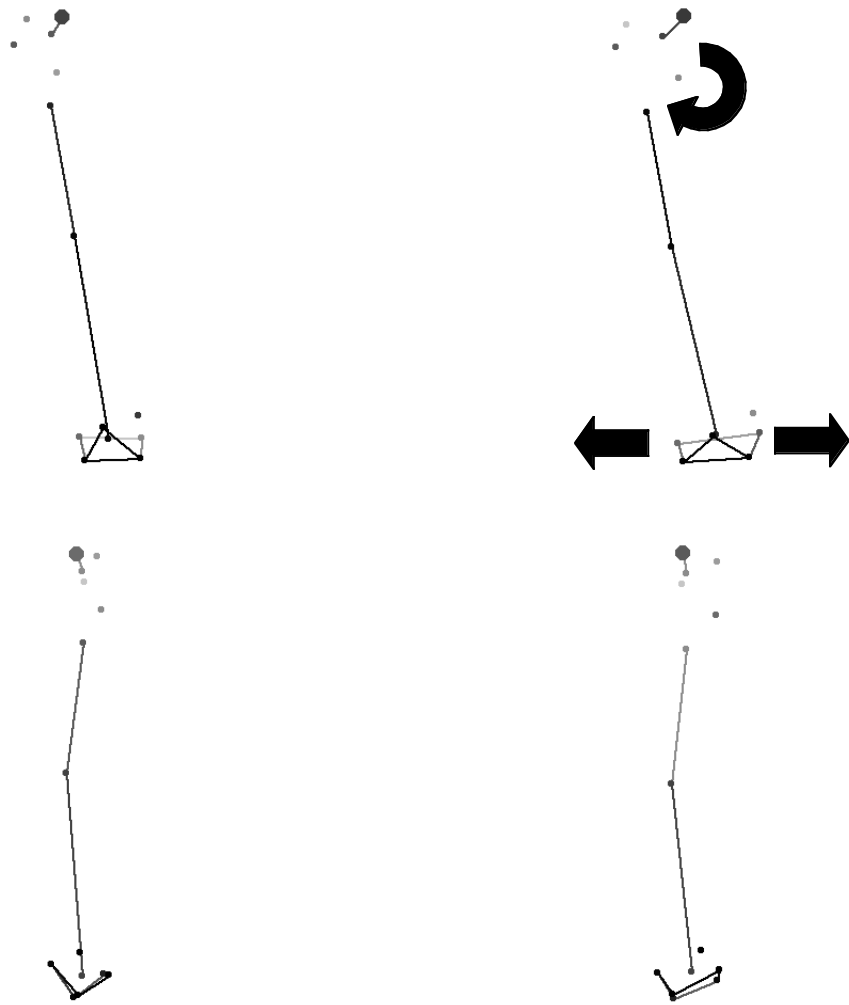


Figure 4.23 Geographically variable analysis: femur discriminant function axis that separates populations by climate

Anterior (top) and medial (bottom) views

The left stick figure shows negative three and the right stick figure shows positive three standard deviations from the sample mean along a discriminant function axis calculated to separate warm, mid-latitude, and cold climate populations. The discriminant function was calculated using principal components from the geographically variable femur GPA. Lighter shading indicates greater depth in the stick figures. Notice the differences in relative joint size and neck-shaft angle between warm (left) and cold (right) climate individuals.

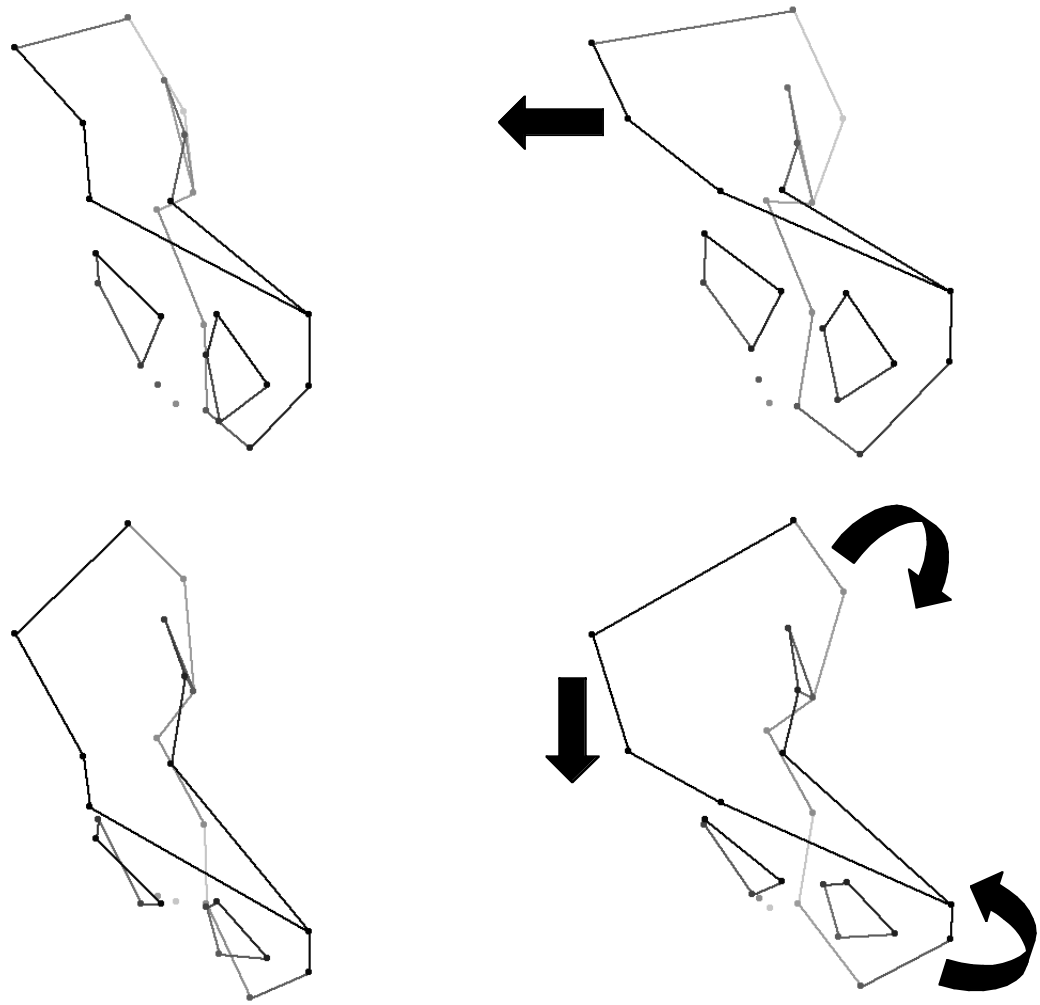


Figure 4.14 Geographically variable analysis: innominate discriminant function axis that separates populations by climate

Anterior (top) and antero-superior (bottom) views

The left stick figure shows negative three and the right stick figure shows positive three standard deviations from the sample mean along a discriminant function axis calculated to separate warm, mid-latitude, and cold climate populations. The discriminant function was calculated using principal components from the geographically variable innominate GPA. Lighter shading indicates greater depth in the stick figures. The left stick figure shows the shape of a narrow pelvis (warm climate), and right stick figure shows the shape of a wide pelvis (cold climate). Notice the differences in posterior iliac crest rotation, pubic bone orientation, anterior-superior iliac spine orientation, and relative location of the iliac tubercle.

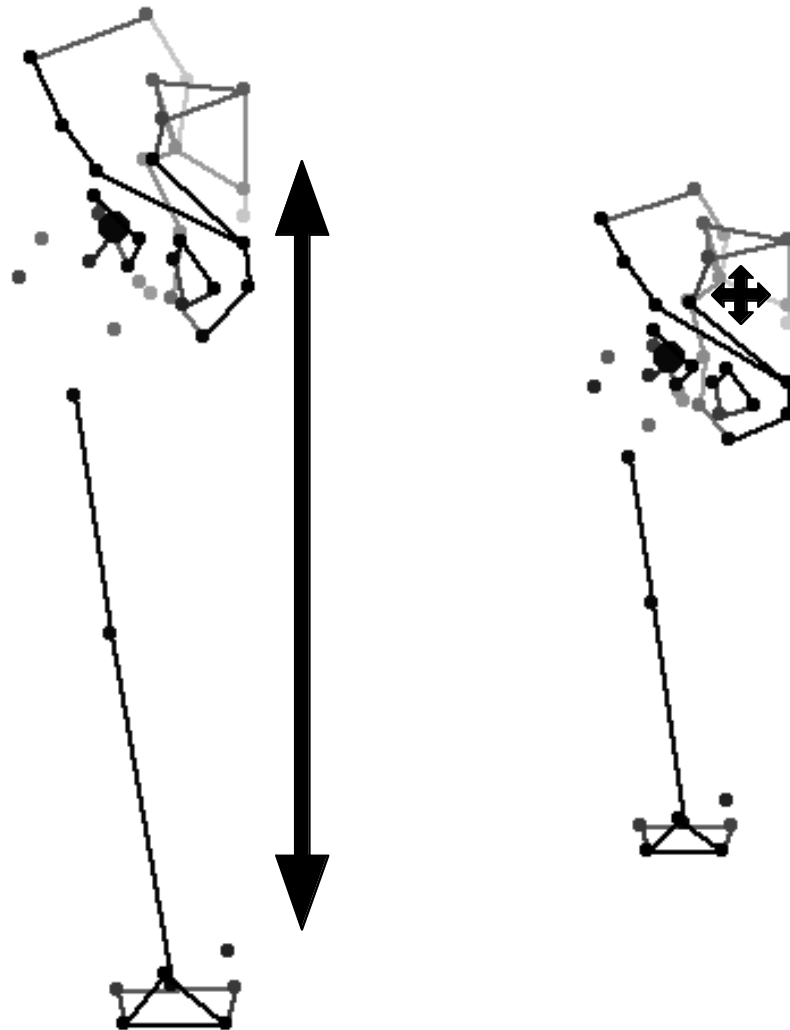


Figure 4.15 Sex balanced analysis: hip PC1

Anterior view

The left stick figure shows negative three and the right stick figure shows positive three standard deviations from the sample mean along PC1 from the sex balanced articulated hip analysis (assuming no changes along any of the other principal component axes). Lighter shading indicates greater depth in the stick figures. Notice the large changes in femur length and pelvic height coupled with only limited changes in pelvic breadth. Also, notice the changes in pelvic aperture size and shape.

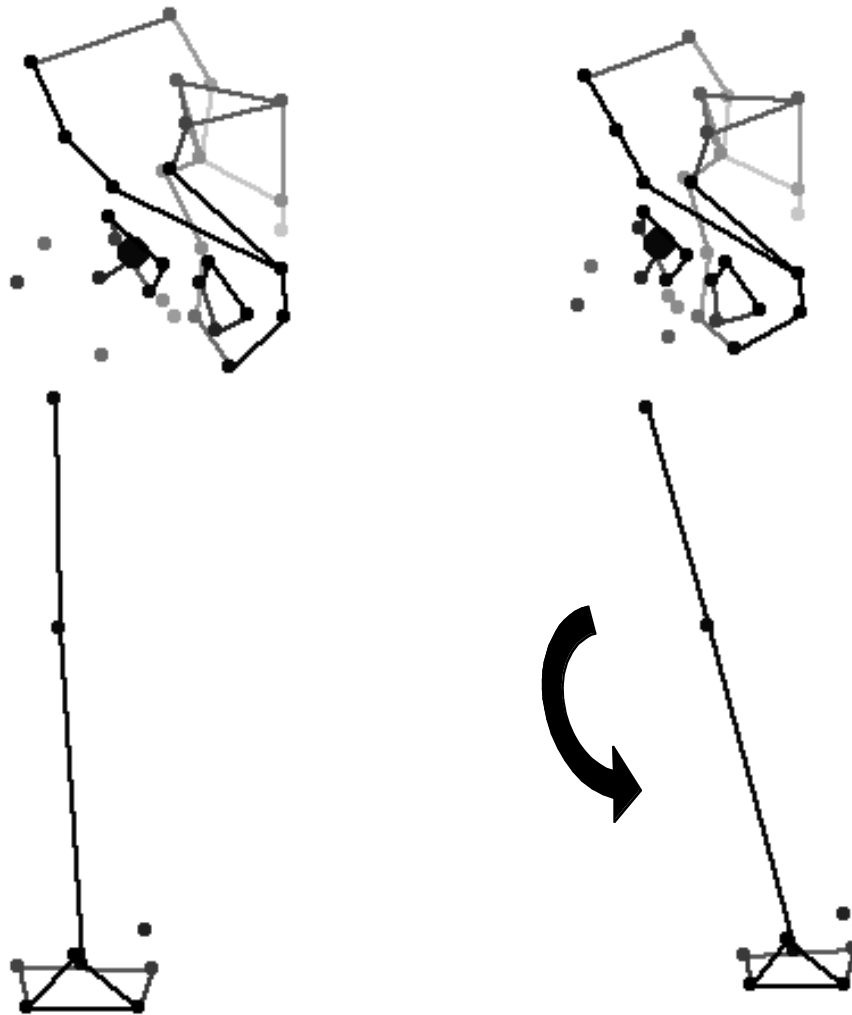


Figure 4.16 Sex balanced analysis: hip PC2

Anterior view

The left stick figure shows negative three and the right stick figure shows positive three standard deviations from the sample mean along PC2 from the sex balanced articulated hip analysis (assuming no changes along any of the other principal component axes). Lighter shading indicates greater depth in the stick figures. Notice the large changes in bicondylar angle with almost no other changes.

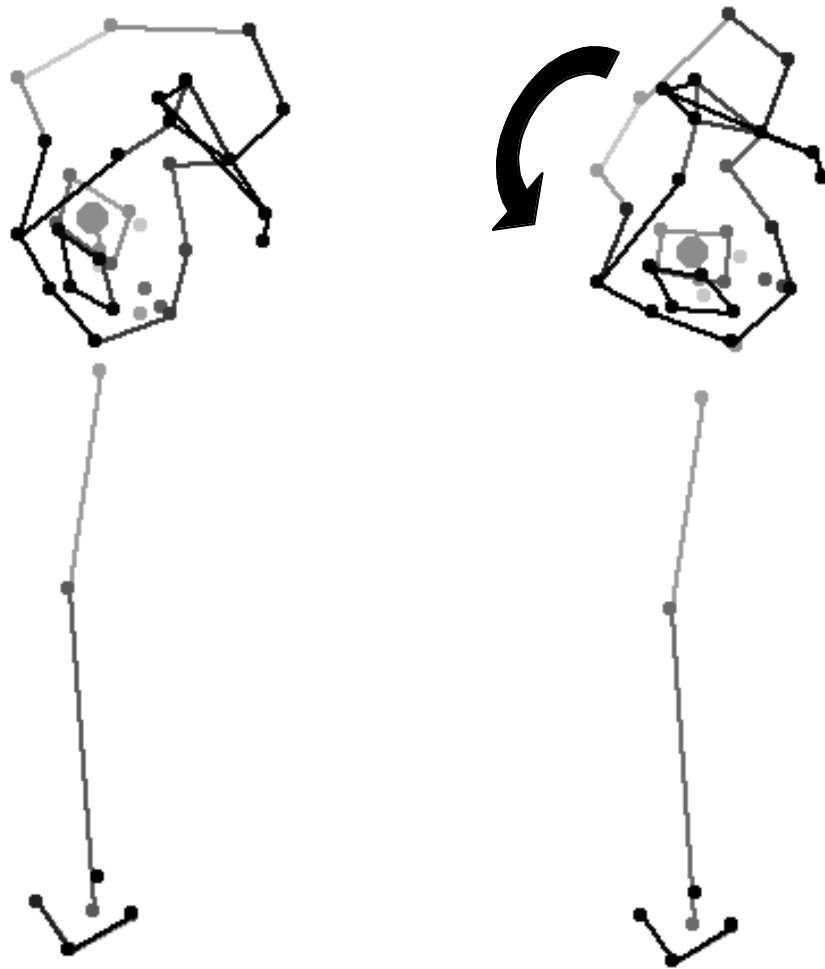


Figure 4.17 Sex balanced analysis: hip PC3

Medial view

The left stick figure shows negative three and the right stick figure shows positive three standard deviations from the sample mean along PC3 from the sex balanced articulated hip analysis (assuming no changes along any of the other principal component axes). Lighter shading indicates greater depth in the stick figures. Notice the large changes in antero-posterior rotation of the entire pelvic girdle with almost no other changes.

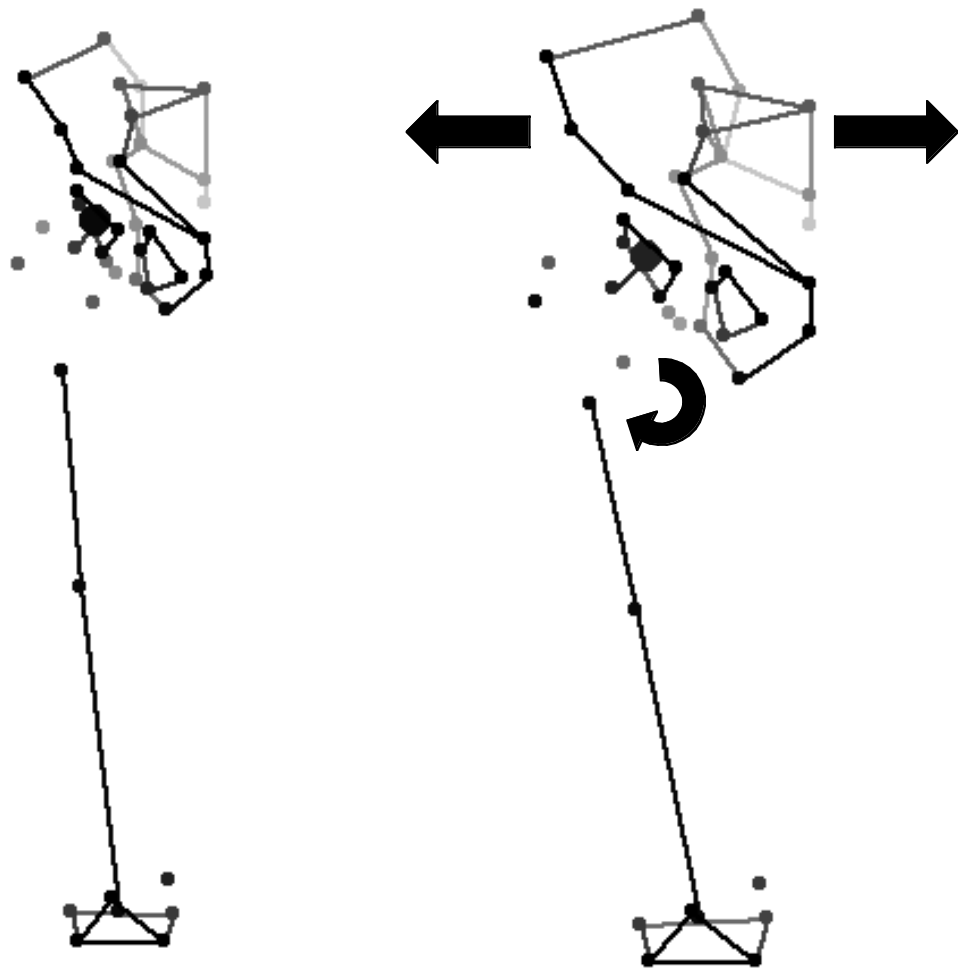


Figure 4.18 Sex balanced analysis: hip PC4

Anterior view

The left stick figure shows negative three and the right stick figure shows positive three standard deviations from the sample mean along PC4 from the sex balanced articulated hip analysis (assuming no changes along any of the other principal component axes). Lighter shading indicates greater depth in the stick figures. The left stick figure has a linear body form, and the right stick figure has a wide body with relatively short limbs. Notice the differences in pelvic aperture size, shape of the pelvis, neck-shaft angle, and bicondylar angle.

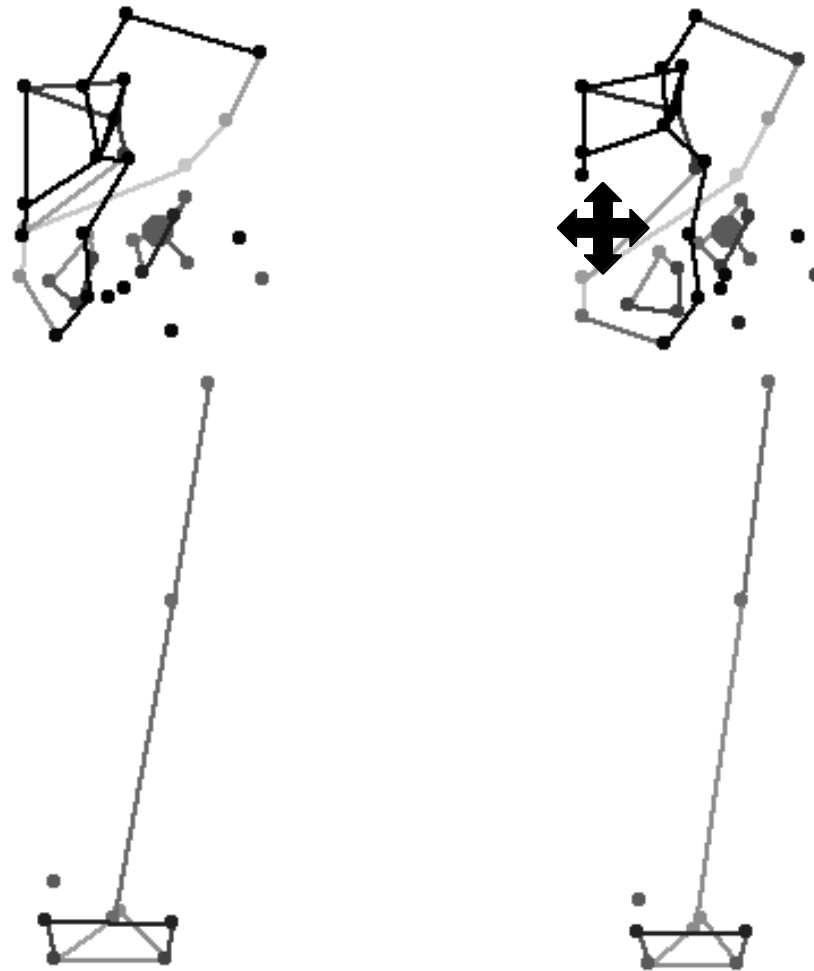


Figure 4.19 Sex balanced analysis: hip PC5

Posterior view

The left stick figure shows negative three and the right stick figure shows positive three standard deviations from the sample mean along PC5 from the sex balanced articulated hip analysis (assuming no changes along any of the other principal component axes). Lighter shading indicates greater depth in the stick figures. Notice the differences in pelvic aperture size, particularly at the mid-plane and outlet, sacral shape, acetabular orientation, obturator foramen orientation, and pubic bone orientation.

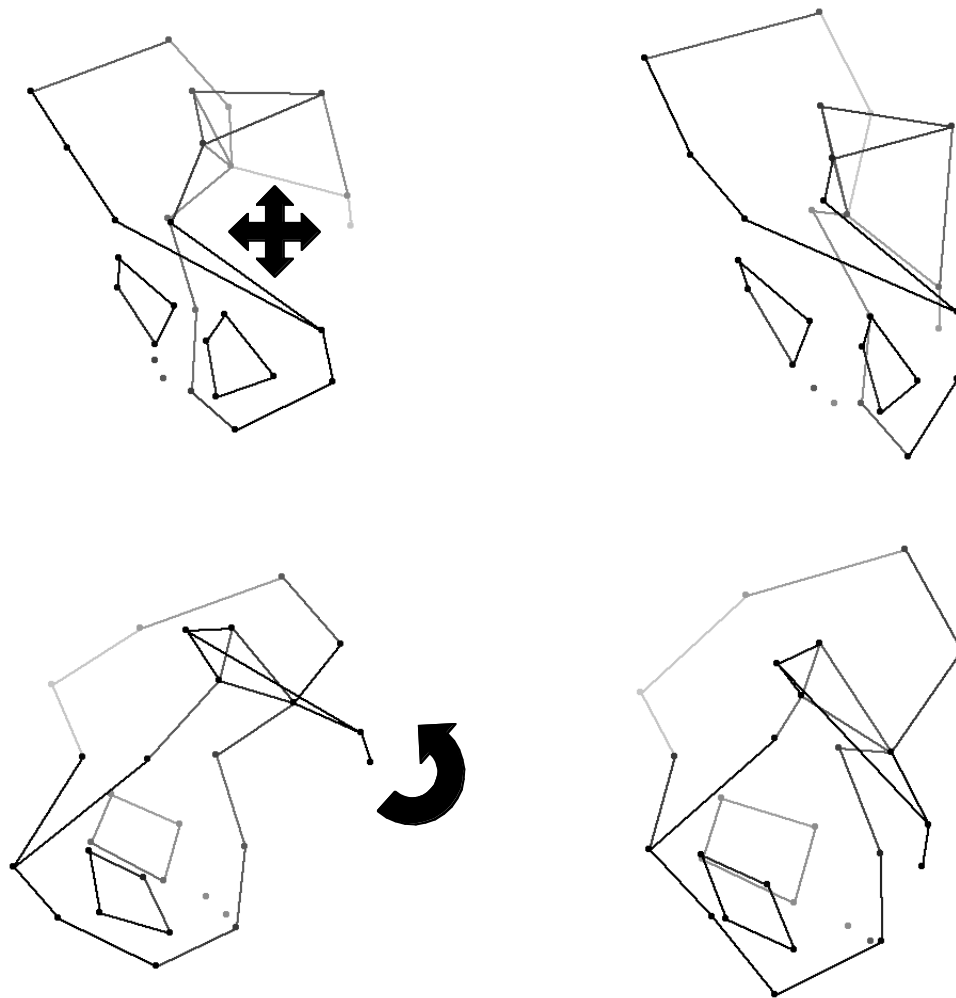


Figure 4.20 Sex balanced analysis: pelvis PC1

Anterior (top) and medial (bottom) views

The left stick figures show negative three and the right stick figures show positive three standard deviations from the sample mean along PC1 from the sex balanced pelvis GPA (assuming no changes along any of the other principal component axes). Lighter shading indicates greater depth in the stick figures. Notice the differences in pelvic aperture size, particularly at the midplane and outlet, sacral shape and angle, and pubic bone orientation and shape.

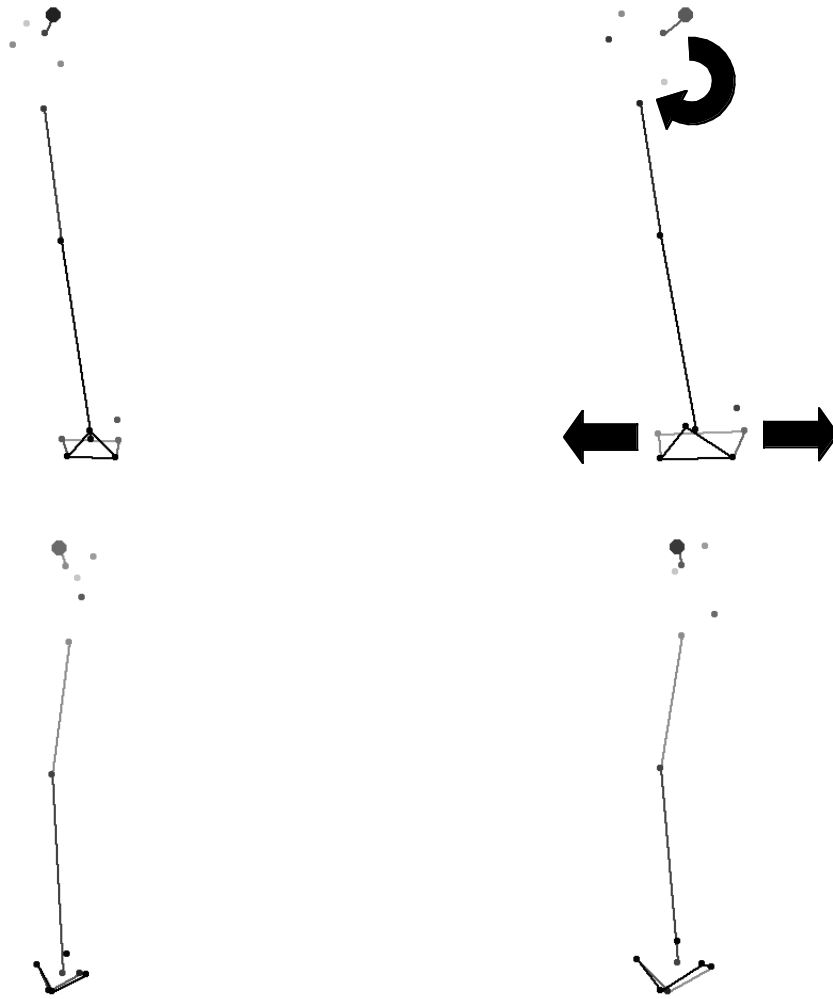


Figure 4.21 Sex balanced analysis: femur PC1

Anterior (top) and medial (bottom) views

The left stick figures show negative three and the right stick figures show positive three standard deviations from the sample mean along PC1 from the sex balanced femur GPA (assuming no changes along any of the other principal component axes). Lighter shading indicates greater depth in the stick figures. The left stick figure corresponds to a low ratio of bi-iliac breadth to femur length, and the right stick figure corresponds to a high one. Notice the differences in relative joint size, neck-shaft angle, and torsion angle.

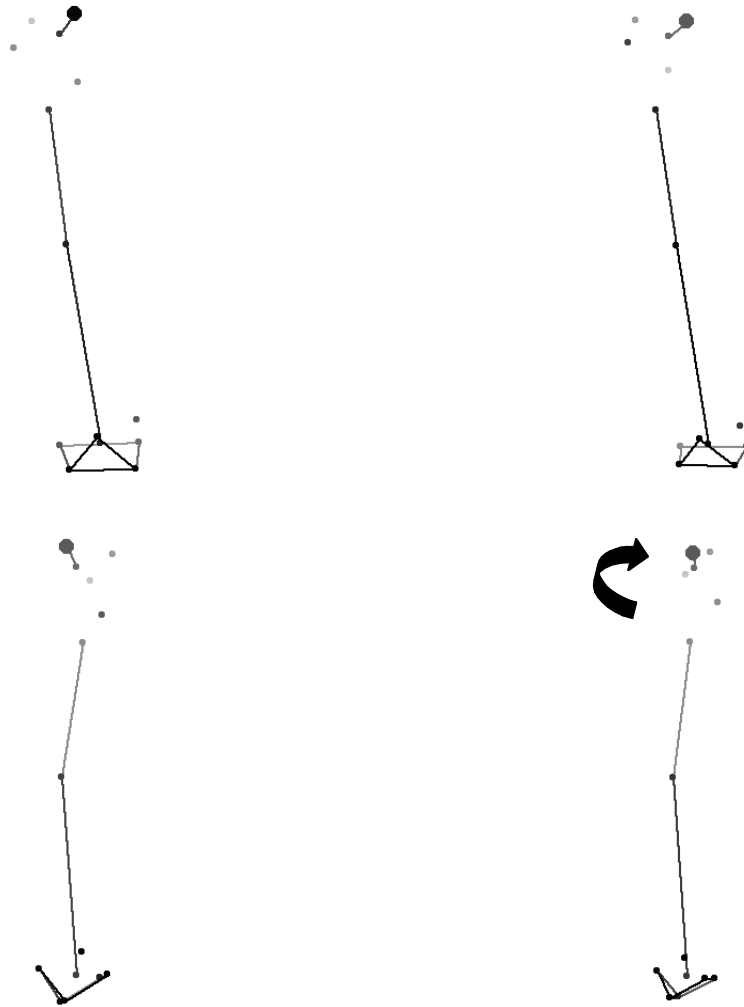


Figure 4.22 Sex balanced analysis: femur PC2

Anterior (top) and medial (bottom) views

The left stick figures show negative three and the right stick figures show positive three standard deviations from the sample mean along PC2 from the sex balanced femur GPA (assuming no changes along any of the other principal component axes). Lighter shading indicates greater depth in the stick figures. Notice the pronounced differences in torsion angle and the moderate differences in neck-shaft angle.

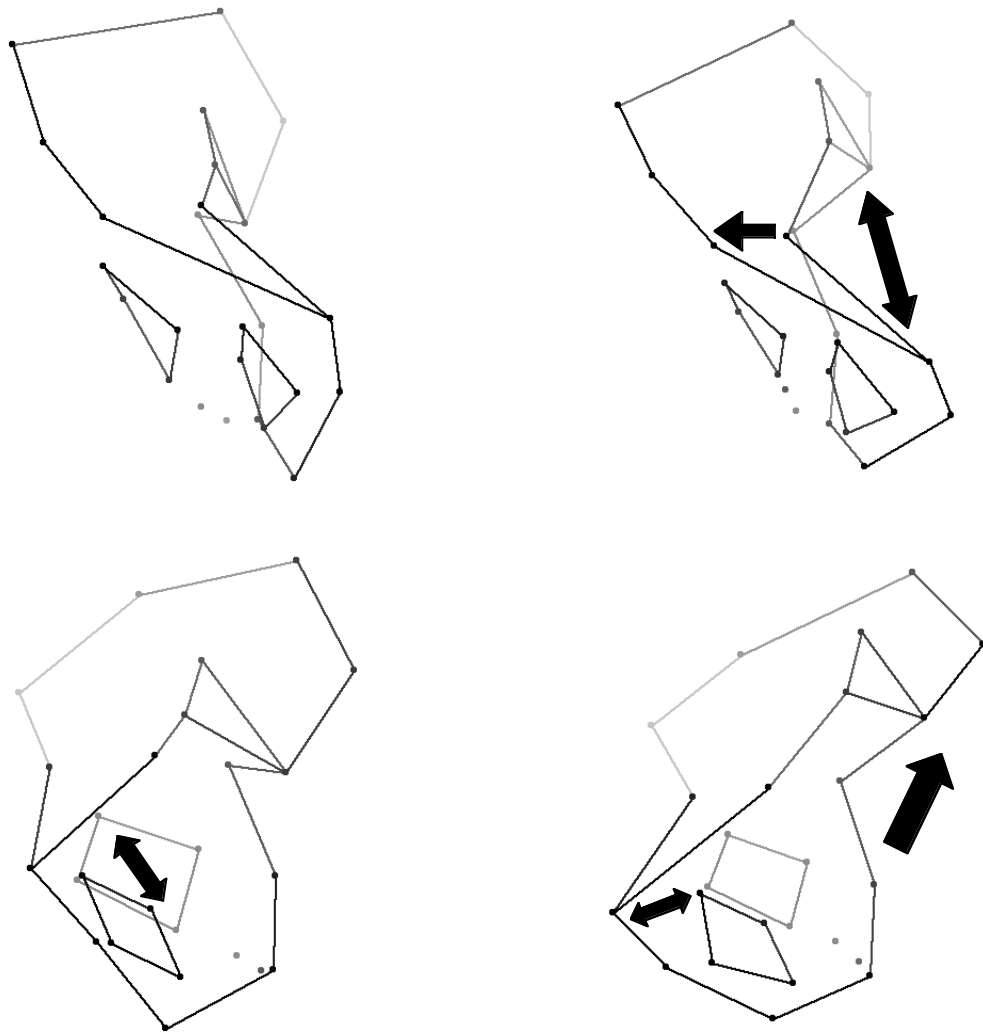


Figure 4.23 Sex balanced analysis: innominate PC1

Anterior (top) and medial (bottom) views

The left stick figures show negative three and the right stick figures show positive three standard deviations from the sample mean along PC1 from the sex balanced innominate GPA (assuming no changes along any of the other principal component axes). Lighter shading indicates greater depth in the stick figures. Notice the differences in greater sciatic notch width, pubic bone shape, iliac blade shape, and acetabular size.

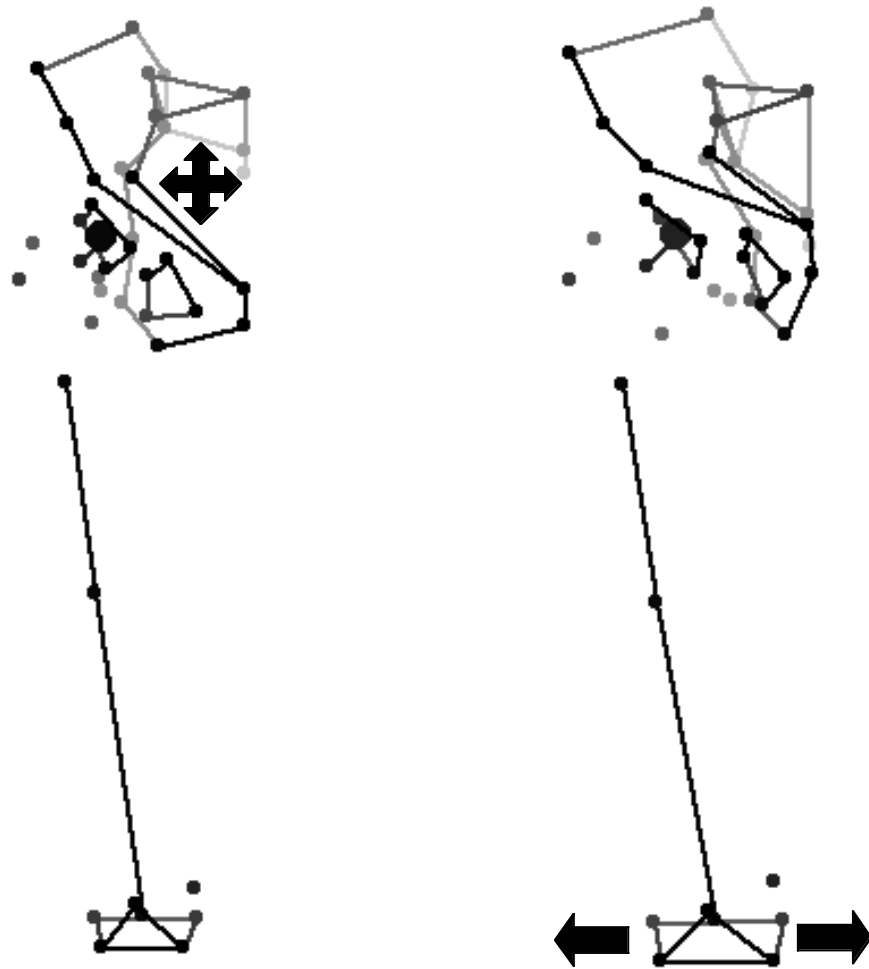


Figure 4.24 Sex balanced analysis: hip discriminant function axis that separates males and females

Anterior view

The left stick figure shows negative three and the right stick figure shows positive three standard deviations from the sample mean along a discriminant function axis calculated to separate males and females. The discriminant function was calculated using principal components from the sex balanced articulated hip analysis. Lighter shading indicates greater depth in the stick figures. The left stick figure is the shape of a female hip, and the right stick figure is the shape of a male hip. Notice the differences in pelvic aperture size, particularly at the mid-plane and outlet, sacral shape, acetabular orientation, pubic bone orientation, and size of the distal end of the femur.

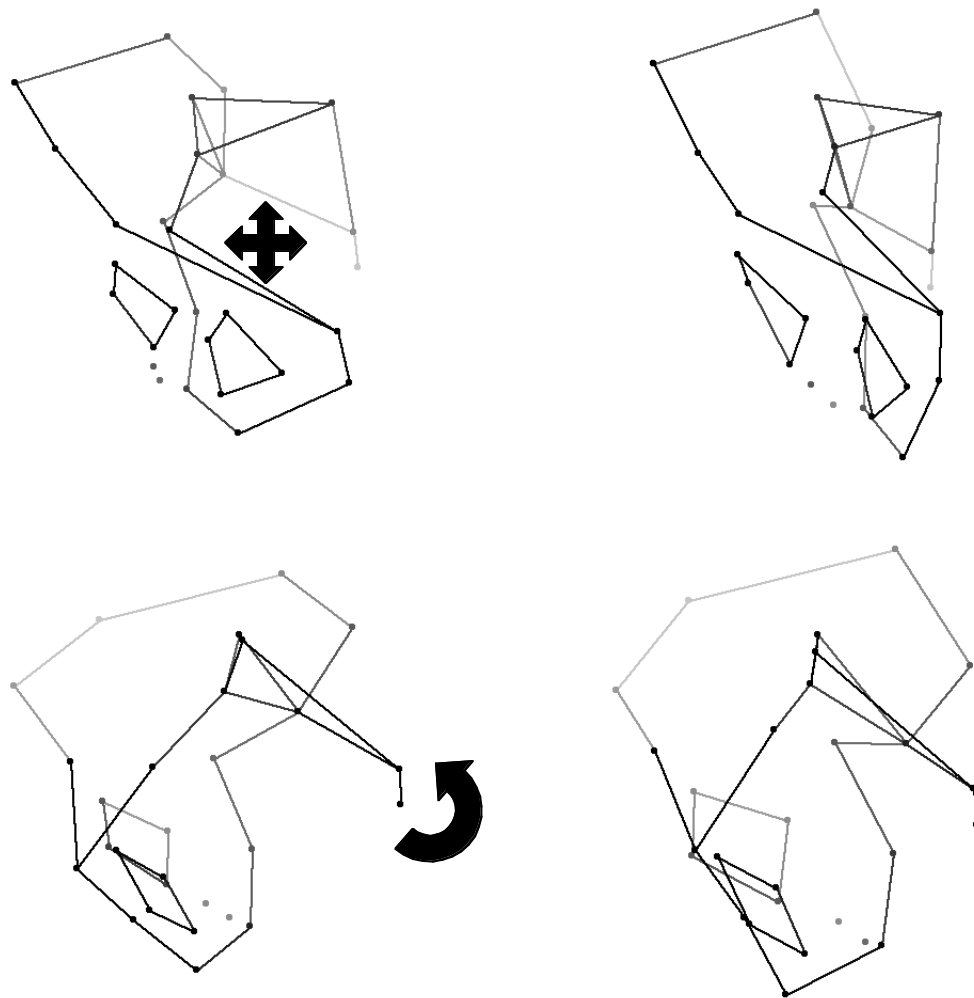


Figure 4.25 Sex balanced analysis: pelvis discriminant function axis that separates males and females

Anterior (top) and medial (bottom) views

The left stick figure shows negative three and the right stick figure shows positive three standard deviations from the sample mean along a discriminant function axis calculated to separate males and females. The discriminant function was calculated using principal components from the sex balanced pelvis GPA. Lighter shading indicates greater depth in the stick figures. The left stick figure is the shape of a female pelvis, and the right stick figure is the shape of a male pelvis. Notice the differences in pelvic aperture size, particularly at the mid-plane and outlet, sacral angle, and pubic bone orientation and shape.

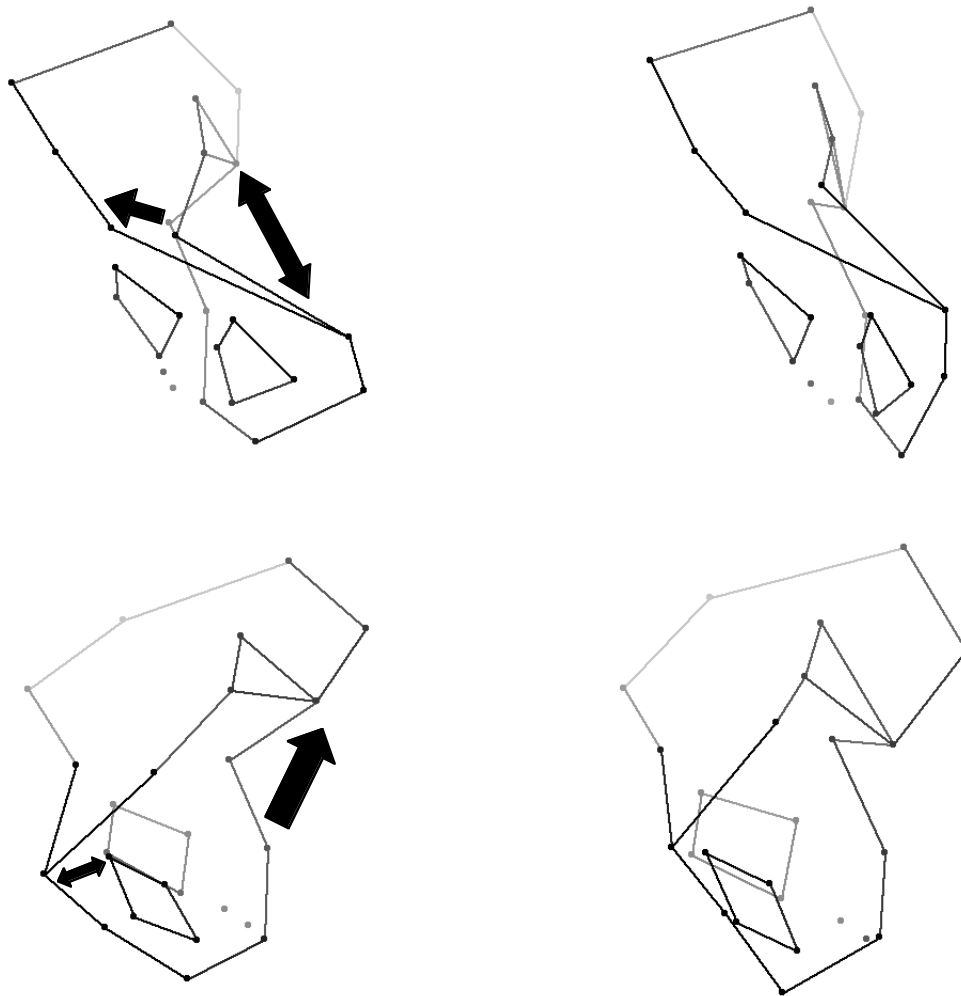


Figure 4.26 Sex balanced analysis: innominate discriminant function axis that separates males and females

Anterior (top) and medial (bottom) views

The left stick figure shows negative three and the right stick figure shows positive three standard deviations from the sample mean along a discriminant function axis calculated to separate males and females. The discriminant function was calculated using principal components from the sex balanced innominate GPA. Lighter shading indicates greater depth in the stick figures. The left stick figure is the shape of a female innominate, and the right stick figure is the shape of a male innominate. Notice the differences in greater sciatic notch width, pubic bone shape, and iliac blade shape.

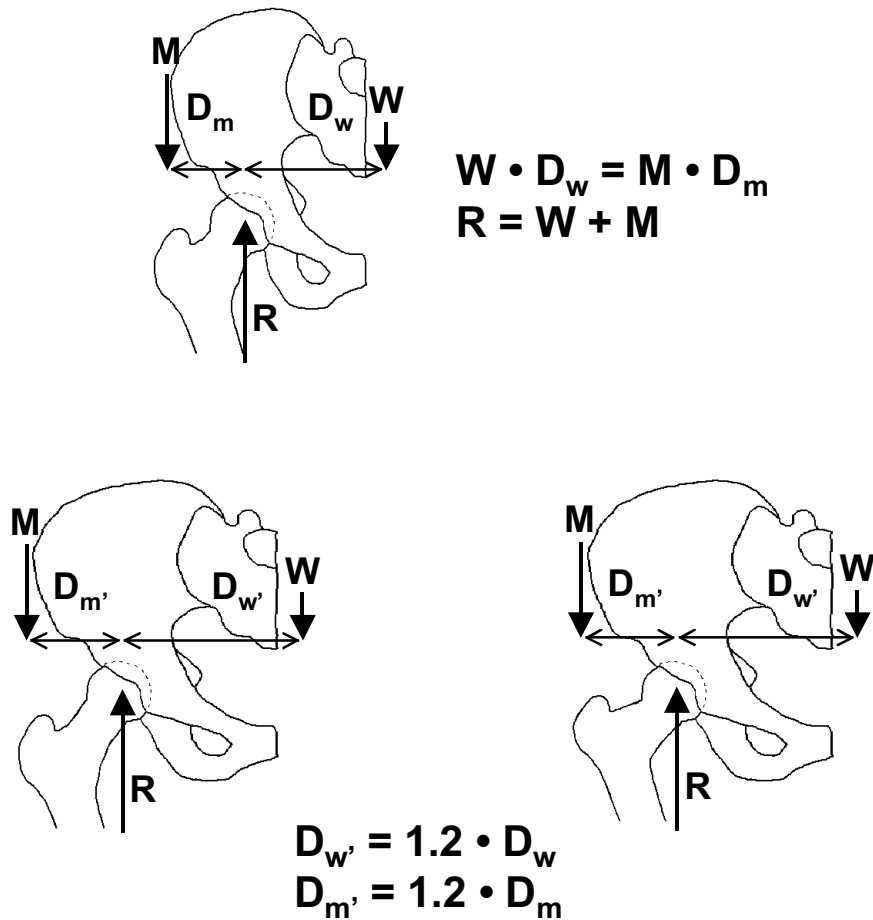


Figure 4.27 Biomechanical model of the adult human hip

The top picture shows a simplified model of the forces acting on the adult hip (modified from Ruff, 1995). Body weight (W) acts at a distance from the joint center (D_w) and therefore produces a moment (rotation) that is opposed by abductor force (M) also acting at a distance from the joint center (D_m). The sum of these two forces is opposed by hip joint reaction force (R). In both the left and right bottom pictures the pelvis has been widened, and body weight (W) acts at an increased distance ($D_{w'}$), producing a larger moment about the hip. The only way to counteract this increased moment without increasing the abductor force (M) and the joint reaction force (R) is for the abductor muscles to act at an increased distance ($D_{m'}$) as well. This can be accomplished either by lengthening the femoral neck without changing the neck-shaft angle (bottom, left) or by lowering the neck-shaft angle without changing the neck length (bottom, right). Lowering the neck-shaft angle is a better solution for preventing fracture of the femoral neck.

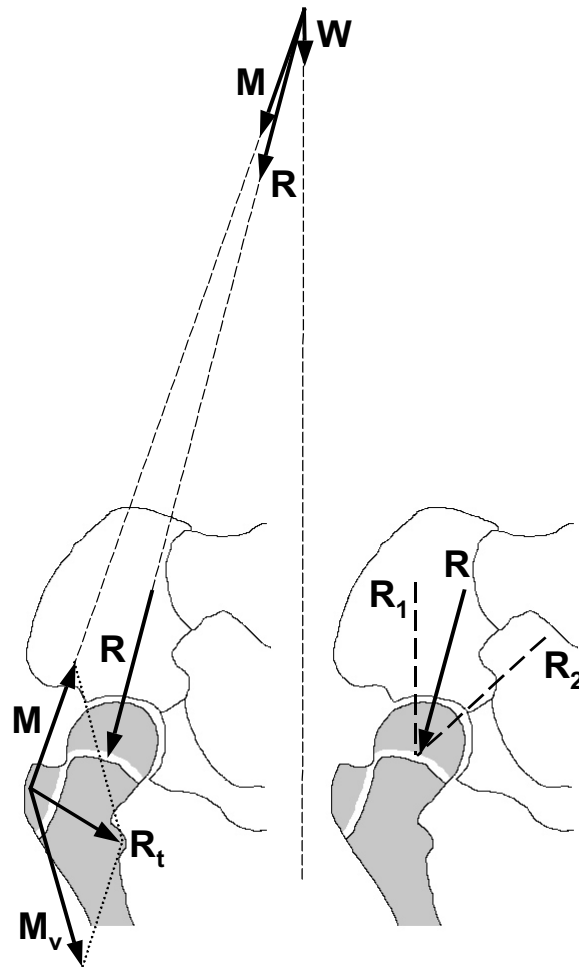


Figure 4.28 Biomechanical model of the juvenile human hip

The left picture shows body weight (W), abductor force (M), vastus lateralis force (M_v), hip joint reaction force (R), and greater trochanteric growth-plate normal force (R_t) acting on a juvenile hip (modified from Heimkes et al., 1993). The right figure shows changes in orientation of the hip joint reaction force that would produce a higher (R_1) or lower (R_2) neck-shaft angle. A change in neck-shaft angle could also be produced by a different amount of abduction or adduction of the femur during gait without changing the orientation of the hip joint reaction force (R).

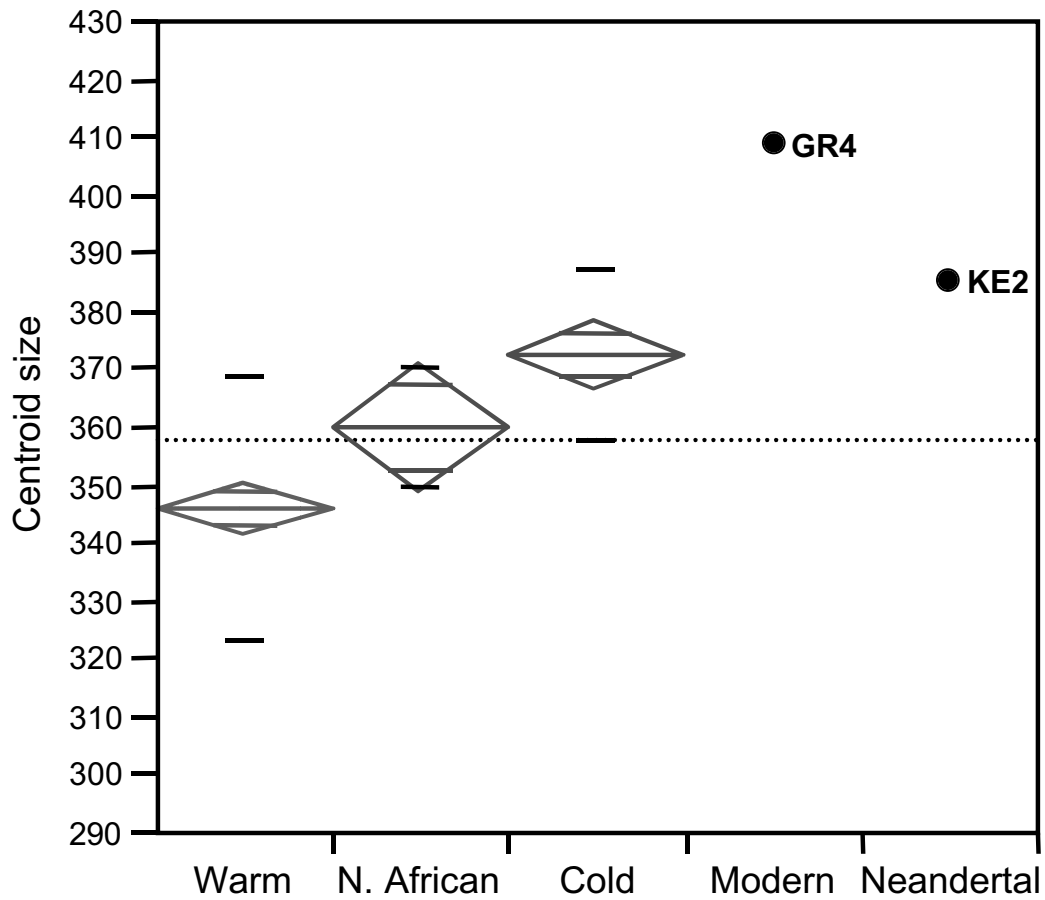


Figure 5.1 Geographically variable Middle to Late Pleistocene analysis: pelvis centroid size

The dotted horizontal line is the overall sample mean, and the solid, gray lines in the middle of the gray means diamonds are the group means. Non-overlapping means diamonds indicate statistical significance ($p < 0.05$). The solid, black lines are positive and negative standard deviations. Notice the clear trend in increasing pelvic size with cooler climate. Both fossil specimens have large pelvises, but Grotte des Enfants 4 has a larger pelvis than Kebara 2.

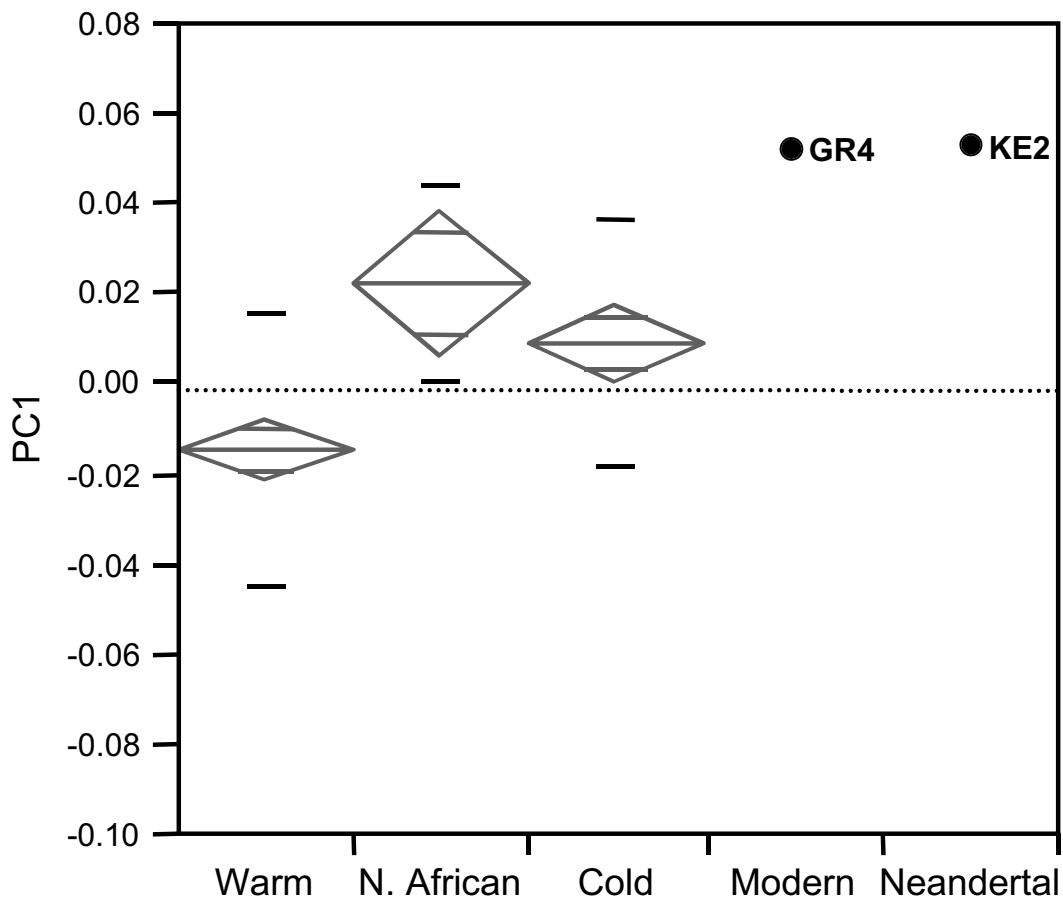


Figure 5.2 Geographically variable Middle to Late Pleistocene analysis: pelvis PC1

The dotted horizontal line is the overall sample mean, and the solid, gray lines in the middle of the gray means diamonds are the group means. Non-overlapping means diamonds indicate statistical significance ($p < 0.05$). The solid, black lines are positive and negative standard deviations. The cold climate individuals and the northern Africans have statistically higher means than the warm climate individuals. Both fossils have similarly high scores along this principal component. Refer to Figure 4.5 for shape changes along PC1.

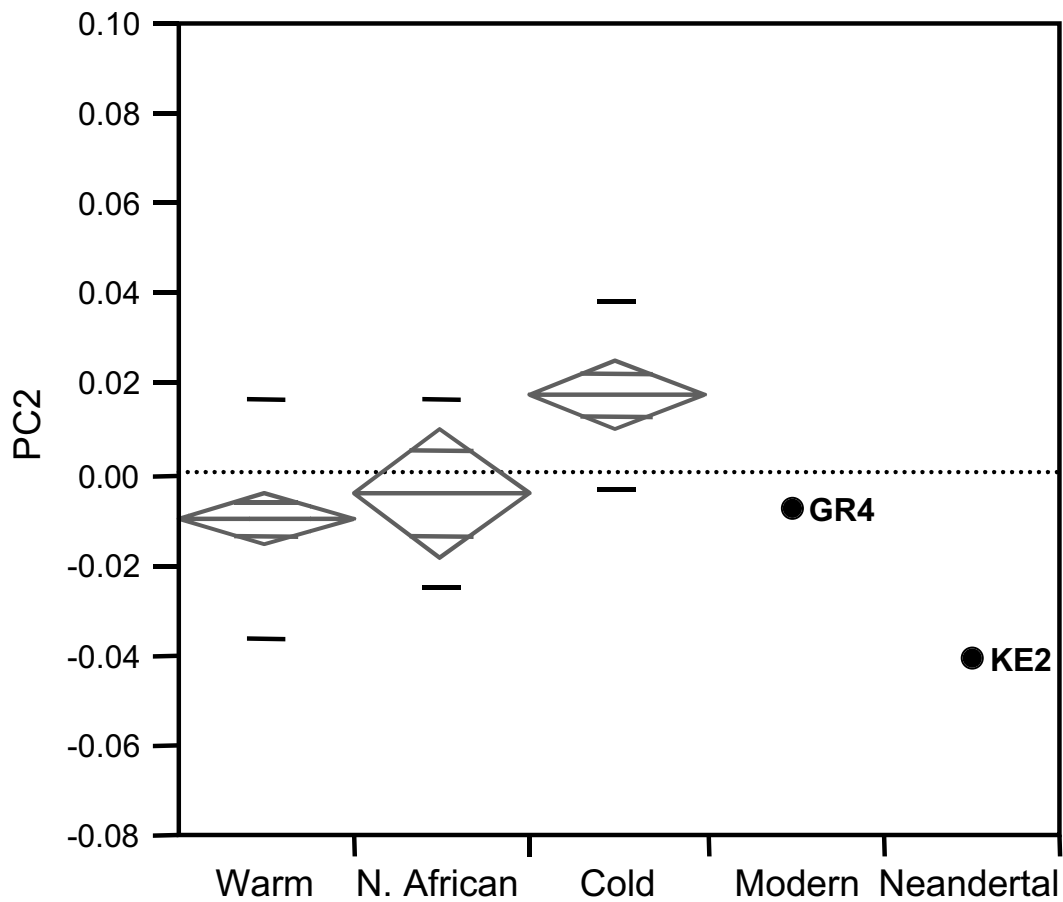


Figure 5.3 Geographically variable Middle to Late Pleistocene analysis: pelvis PC2

The dotted horizontal line is the overall sample mean, and the solid, gray lines in the middle of the gray means diamonds are the group means. Non-overlapping means diamonds indicate statistical significance ($p < 0.05$). The solid, black lines are positive and negative standard deviations. There is a clear trend of increasing scores with cooler climate. Grotte des Enfants 4 falls near the overall recent human mean, but Kebara 2 has a very negative score. Refer to Figure 4.6 for shape changes along PC2.

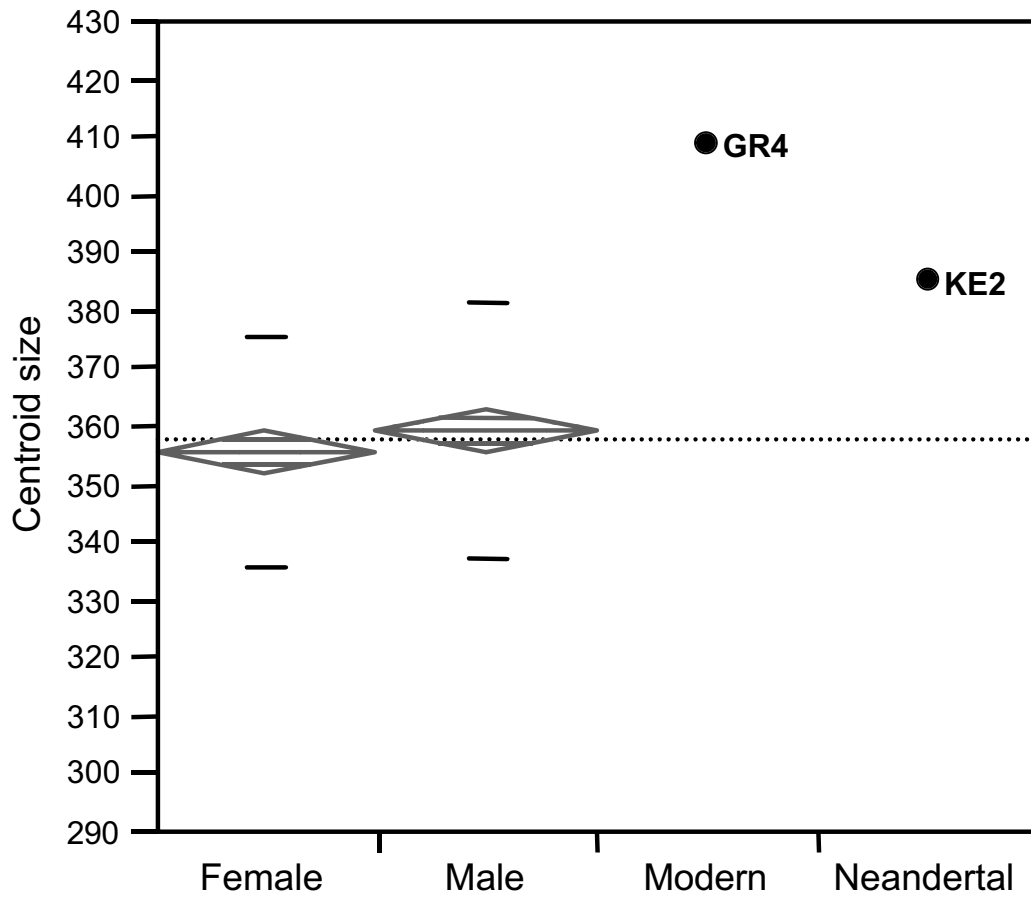


Figure 5.4 Sex balanced Middle to Late Pleistocene analysis: pelvis centroid size

The dotted horizontal line is the overall sample mean, and the solid, gray lines in the middle of the gray means diamonds are the group means. Non-overlapping means diamonds indicate statistical significance ($p < 0.05$). The solid, black lines are positive and negative standard deviations. Notice the lack of sexual dimorphism in overall pelvic size between males and females. Both fossils have very large pelvises.

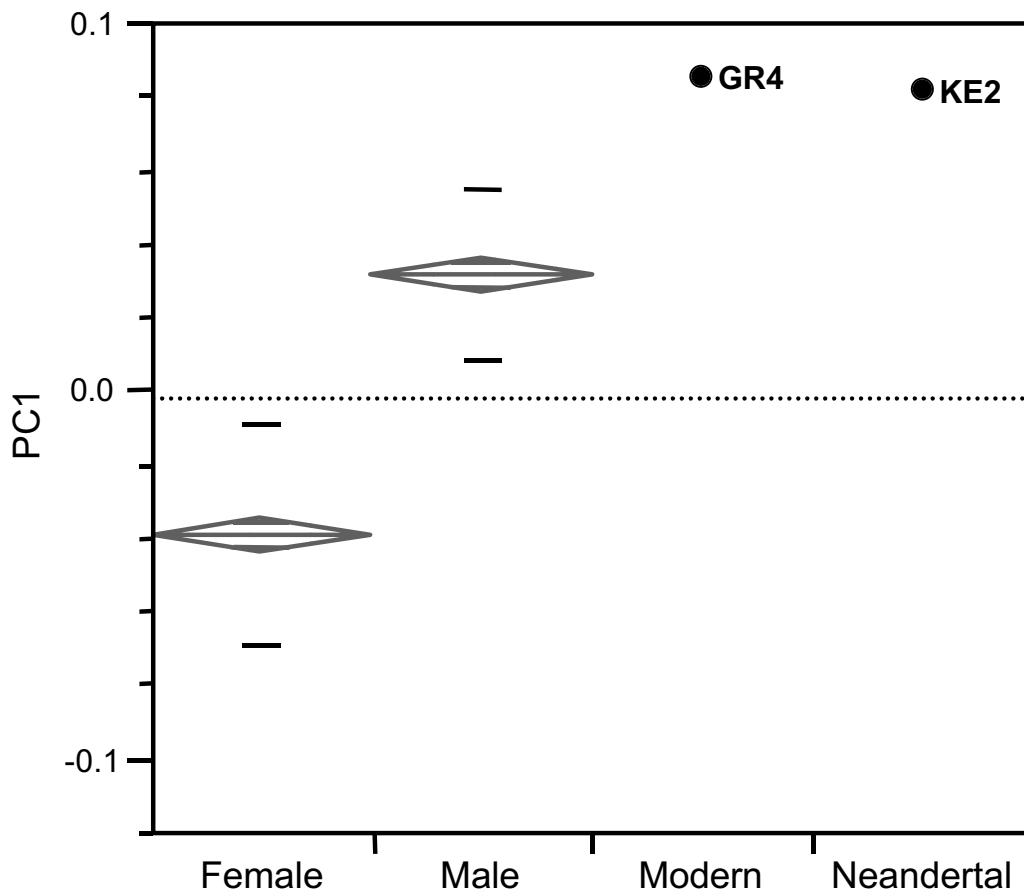


Figure 5.5 Sex balanced Middle to Late Pleistocene analysis: pelvis PC1

The dotted horizontal line is the overall sample mean, and the solid, gray lines in the middle of the gray means diamonds are the group means. Non-overlapping means diamonds indicate statistical significance ($p < 0.05$). The solid, black lines are positive and negative standard deviations. Males and females are extremely different along this principal component. Both fossils fall more than one standard deviation above the male mean. Refer to Figure 4.15 for shape changes along PC1.

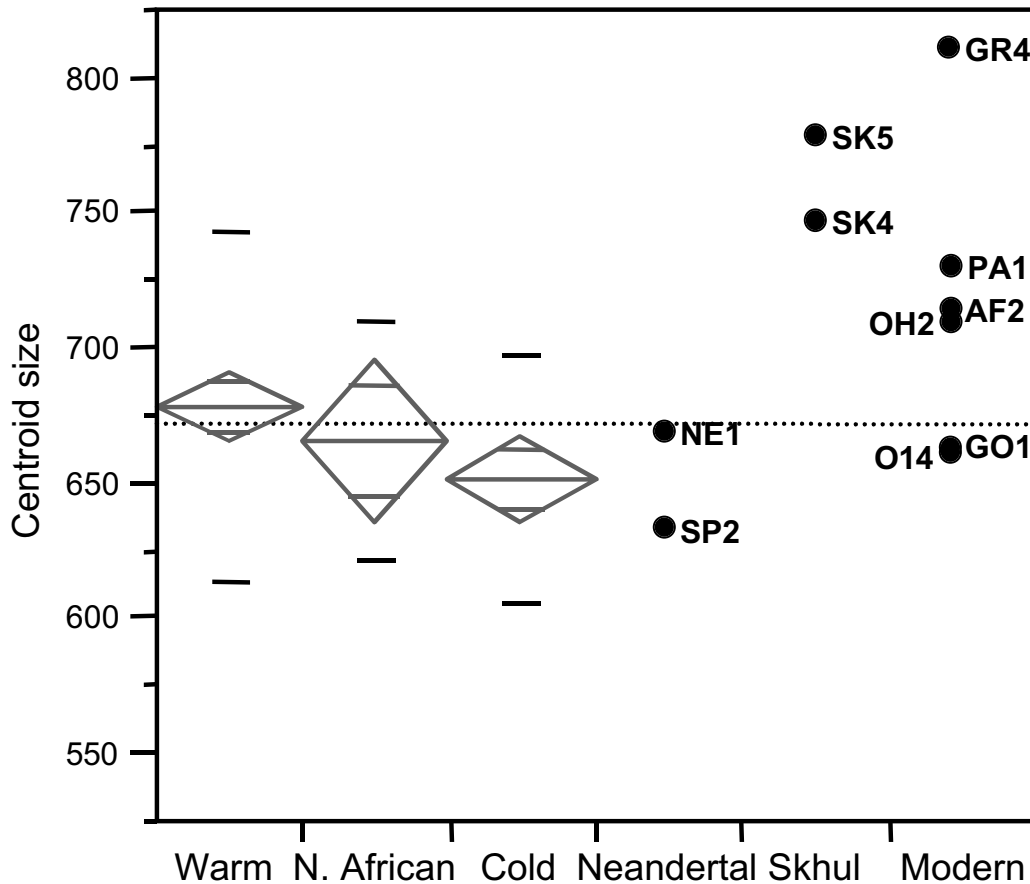


Figure 5.6 Geographically variable Middle to Late Pleistocene analysis: femur centroid size

The dotted horizontal line is the overall sample mean, and the solid, gray lines in the middle of the gray means diamonds are the group means. Non-overlapping means diamonds indicate statistical significance ($p < 0.05$). The solid, black lines are positive and negative standard deviations. People from warmer climates tend to have femora with larger centroid sizes (lengths) than people from colder climates. The Neandertals have much shorter femora than the Near Modern humans (SK4 and SK5). The early Upper Paleolithic human from Grotte des Enfants 4 has an extremely long femur.

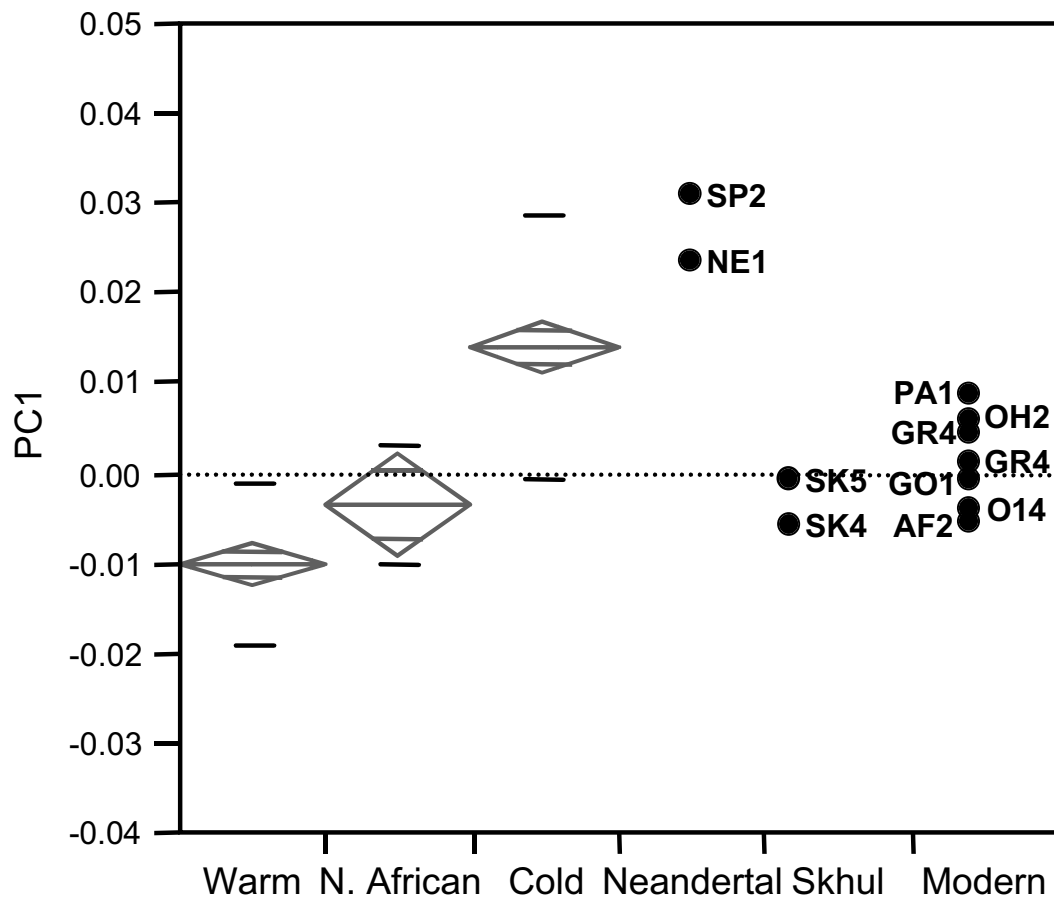


Figure 5.7 Geographically variable Middle to Late Pleistocene analysis: femur PC1

The dotted horizontal line is the overall sample mean, and the solid, gray lines in the middle of the gray means diamonds are the group means. Non-overlapping means diamonds indicate statistical significance ($p < 0.05$). The solid, black lines are positive and negative standard deviations. There is a clear trend of increasing scores with cooler climate. Notice the separation between the Neandertals and the other fossil hominids. Refer to Figure 4.7 for shape changes along PC1.

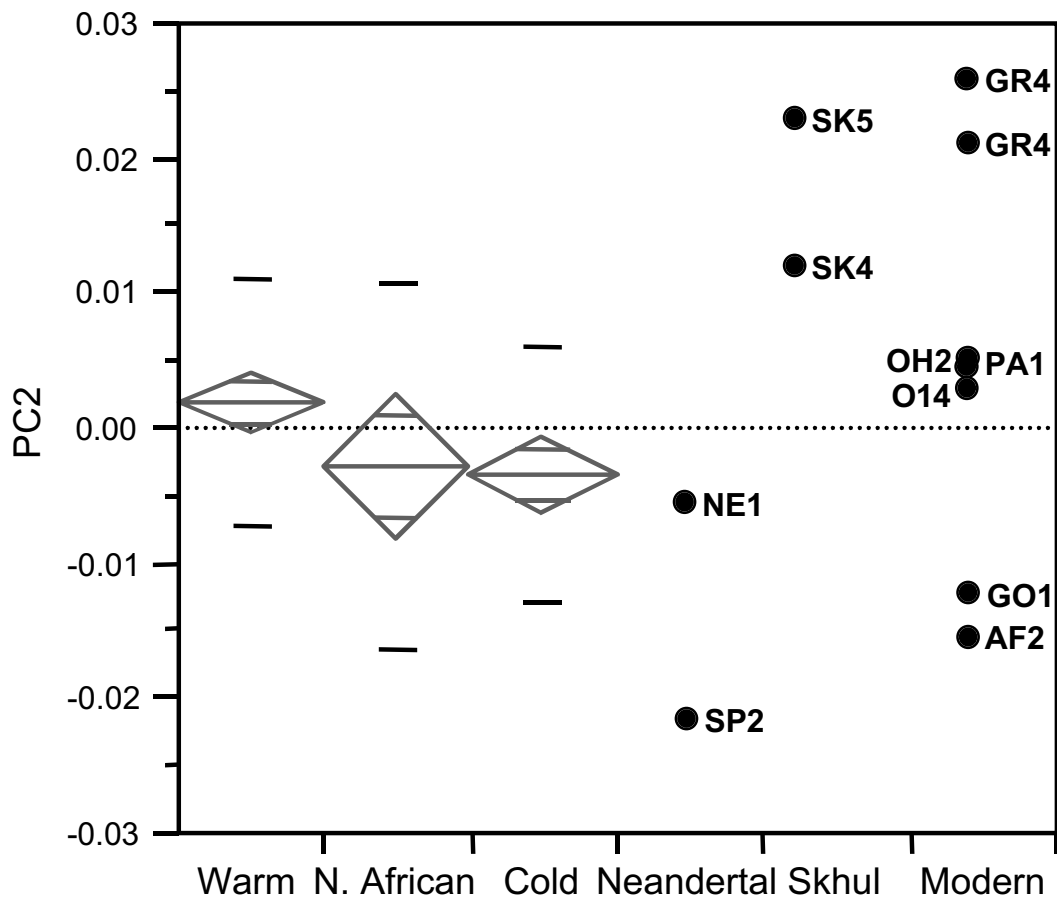


Figure 5.8 Geographically variable Middle to Late Pleistocene analysis: femur PC2

The dotted horizontal line is the overall sample mean, and the solid, gray lines in the middle of the gray means diamonds are the group means. Non-overlapping means diamonds indicate statistical significance ($p < 0.05$). The solid, black lines are positive and negative standard deviations. Refer to Figure 4.8 for shape changes along PC2.

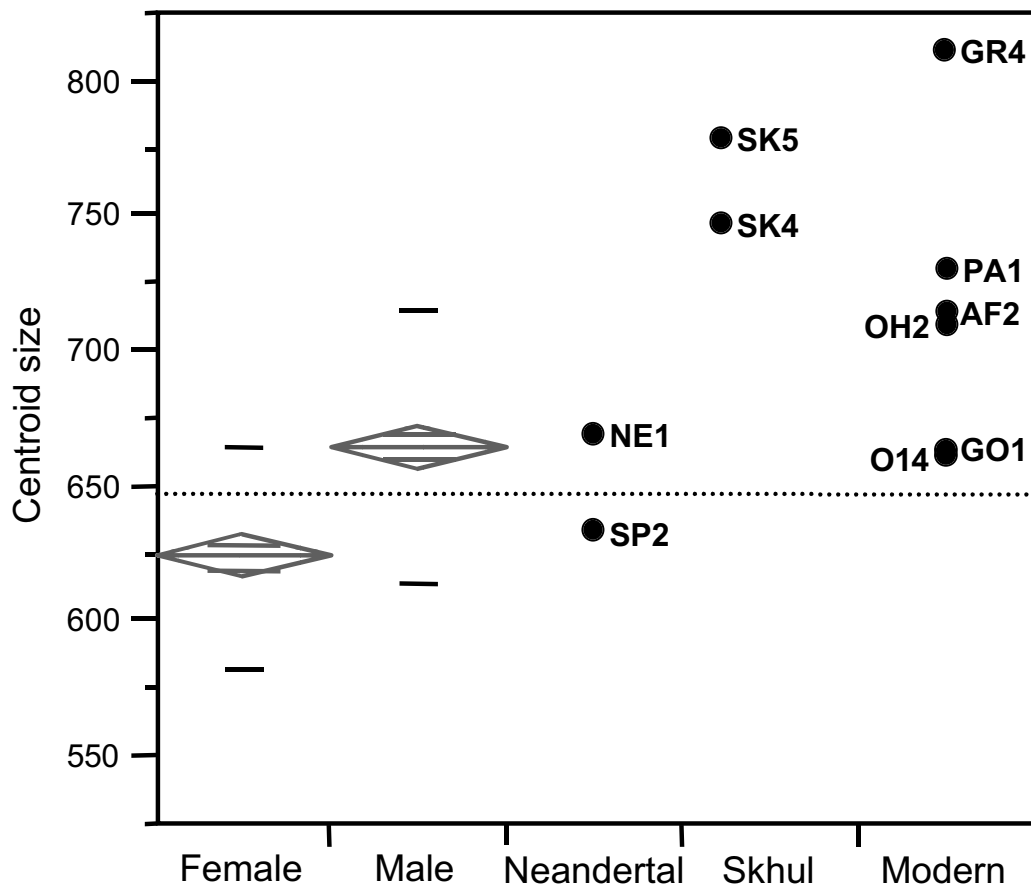


Figure 5.9 Sex balanced Middle to Late Pleistocene analysis: femur centroid size

The dotted horizontal line is the overall sample mean, and the solid, gray lines in the middle of the gray means diamonds are the group means. Non-overlapping means diamonds indicate statistical significance ($p < 0.05$). The solid, black lines are positive and negative standard deviations. Females have smaller centroid sizes of their femora (lengths) than males.

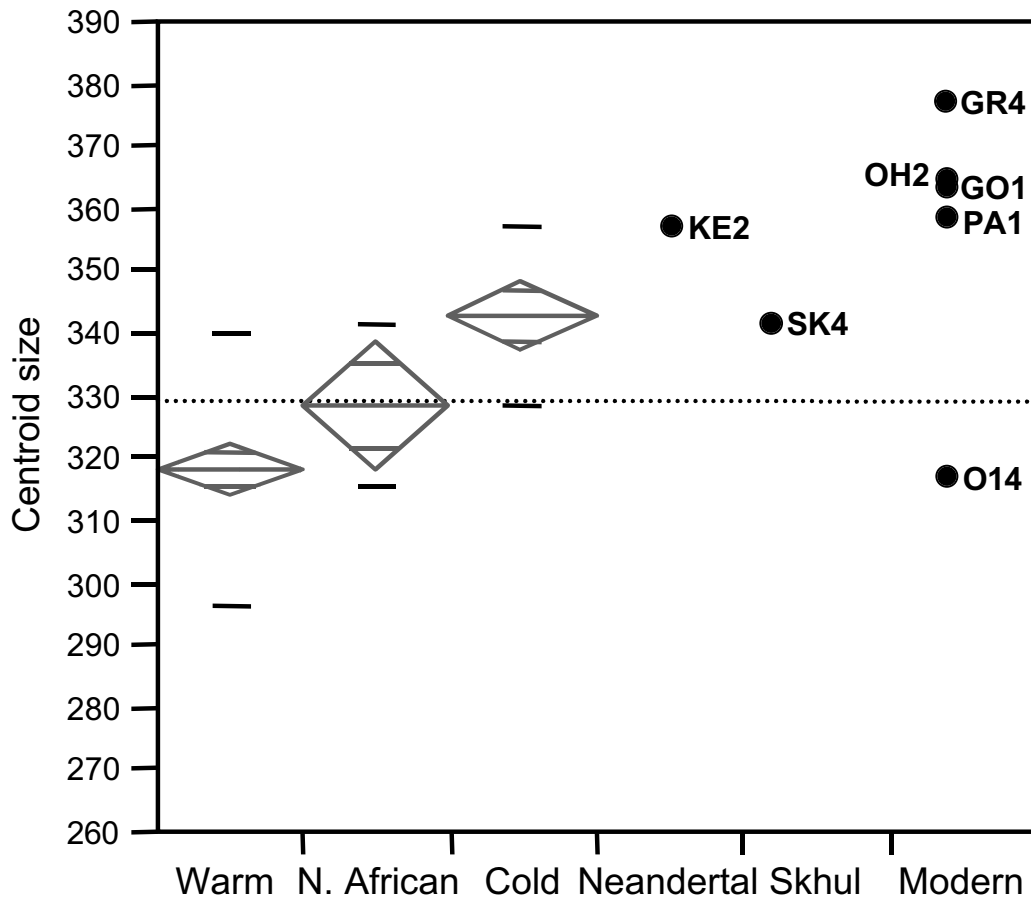


Figure 5.10 Geographically variable Middle to Late Pleistocene analysis: innominate centroid size

The dotted horizontal line is the overall sample mean, and the solid, gray lines in the middle of the gray means diamonds are the group means. Non-overlapping means diamonds indicate statistical significance ($p < 0.05$). The solid, black lines are positive and negative standard deviations. There is a clear trend of increasing centroid size with cooler climate. Most of the fossil hominids have large innominates relative to recent humans.

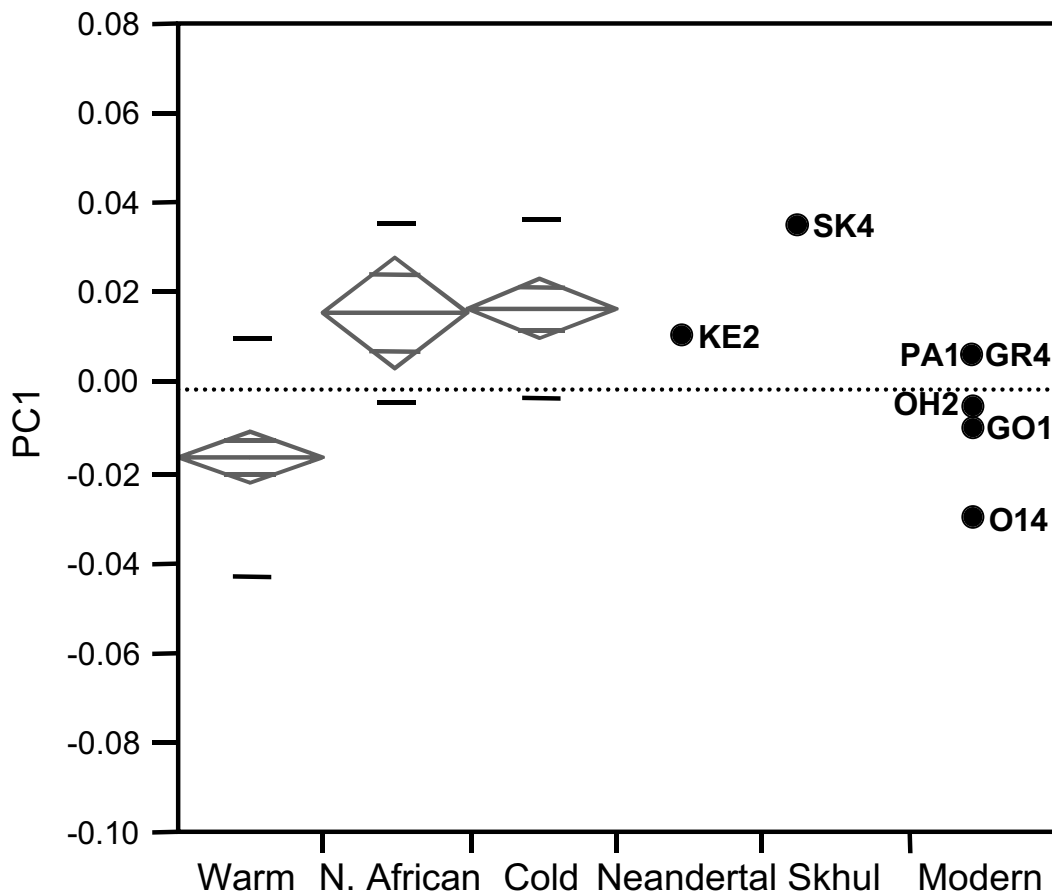


Figure 5.11 Geographically variable Middle to Late Pleistocene analysis: innominate PC1

The dotted horizontal line is the overall sample mean, and the solid, gray lines in the middle of the gray means diamonds are the group means. Non-overlapping means diamonds indicate statistical significance ($p < 0.05$). The solid, black lines are positive and negative standard deviations. The cold climate and northern African means are significantly different than the warm climate mean. Most of the fossils cluster around the recent human mean, with the exception of Skhul 4 (high score) and Oakhurst 14 (low score). Kebara 2 does not have a particularly high score. Refer to Figure 4.9 for shape changes along PC1.

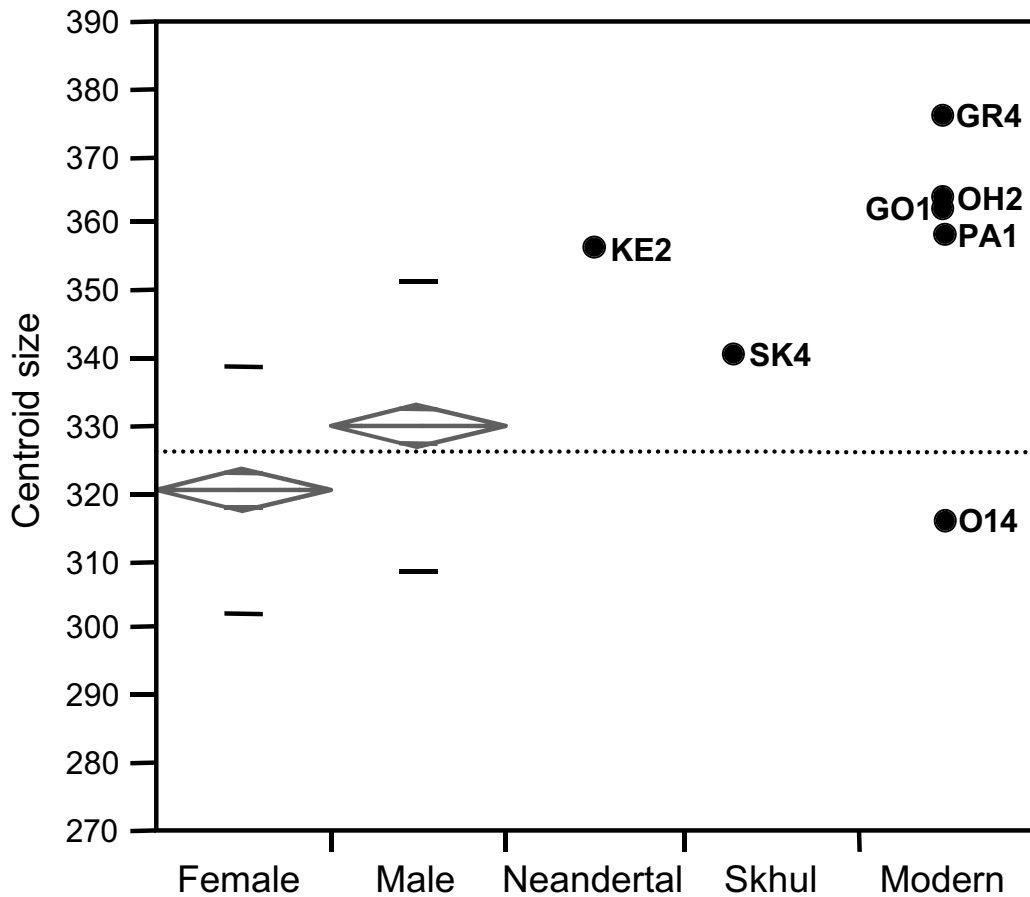


Figure 5.12 Sex balanced Middle to Late Pleistocene analysis: innominate centroid size

The dotted horizontal line is the overall sample mean, and the solid, gray lines in the middle of the gray means diamonds are the group means. Non-overlapping means diamonds indicate statistical significance ($p < 0.05$). The solid, black lines are positive and negative standard deviations. Males have significantly larger innominates than females. Most fossil hominids also have much larger innominates than recent humans.

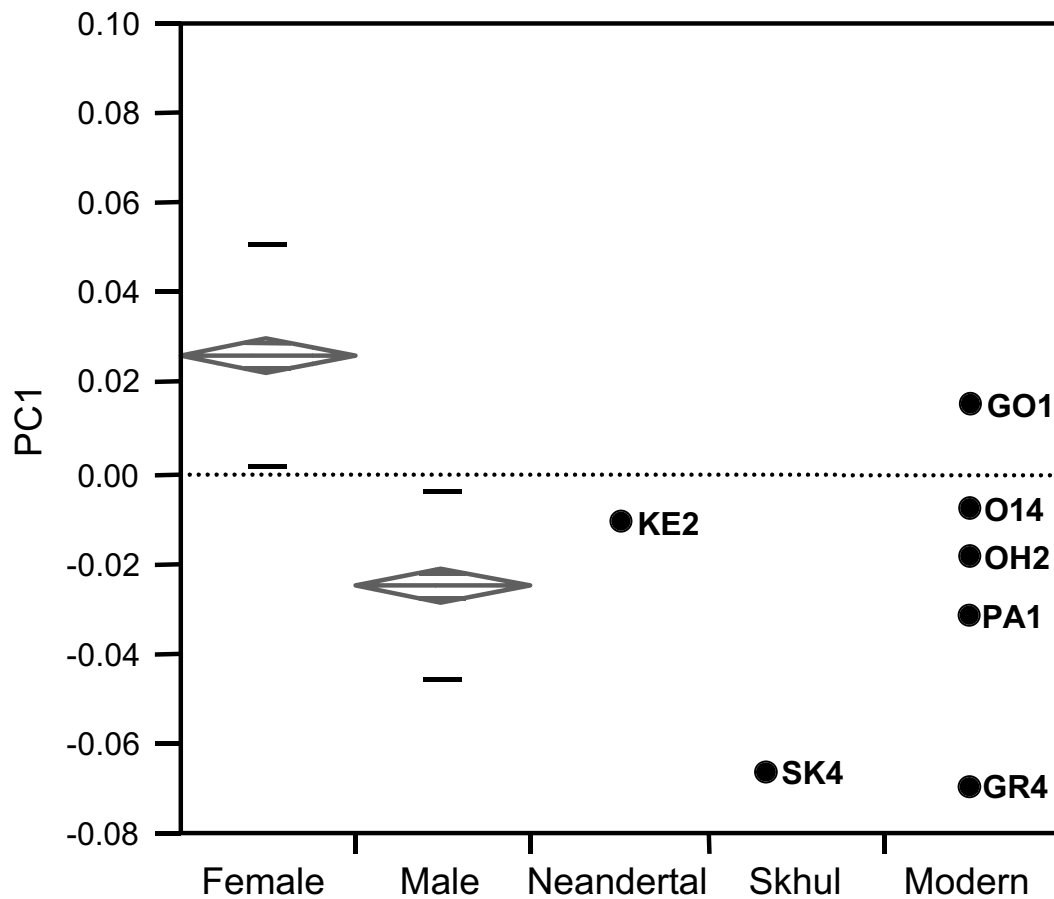


Figure 5.13 Sex balanced Middle to Late Pleistocene analysis: innominate PC1

The dotted horizontal line is the overall sample mean, and the solid, gray lines in the middle of the gray means diamonds are the group means. Non-overlapping means diamonds indicate statistical significance ($p < 0.05$). The solid, black lines are positive and negative standard deviations. Males and females are significantly different along this principal component. Most fossil hominids appear more like males. Refer to Figure 4.18 for shape changes along this principal component.

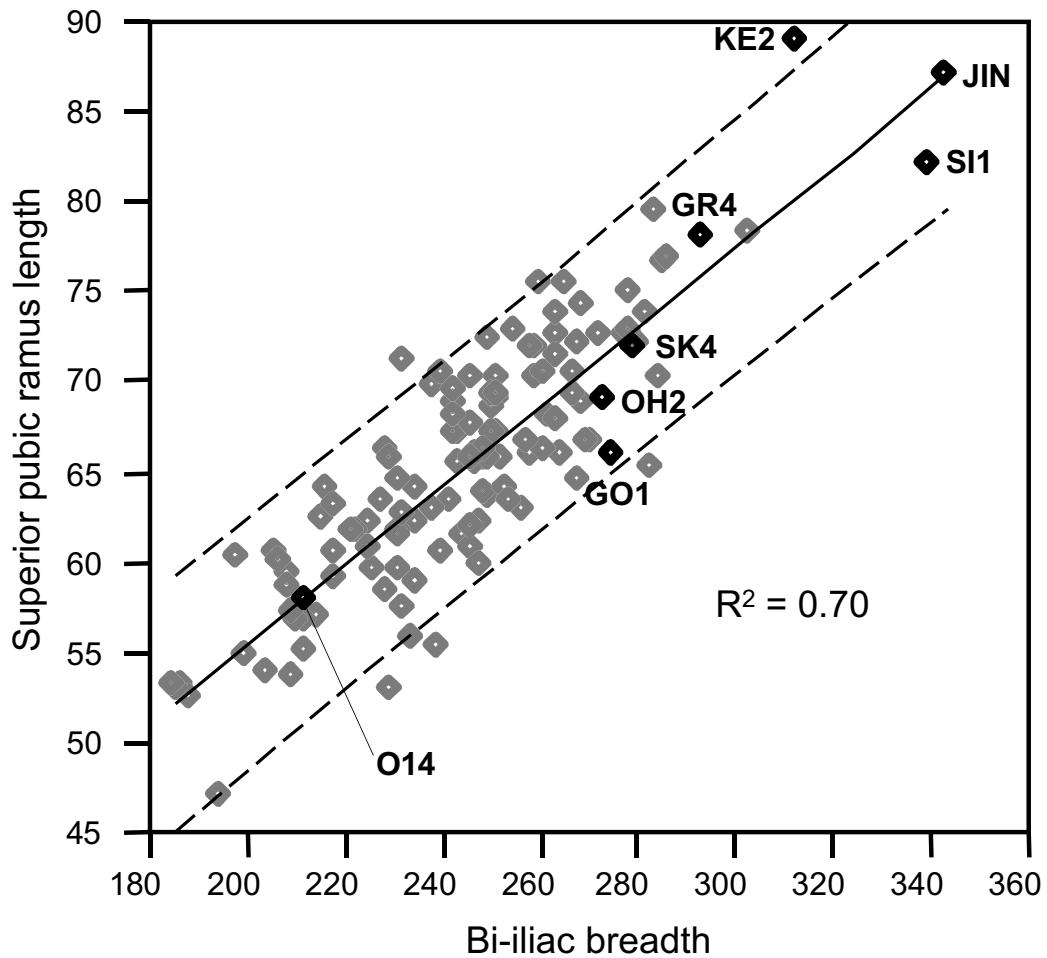


Figure 5.14 Superior pubic ramus length vs. bi-iliac breadth

The gray diamonds are recent humans, and the black diamonds are fossil hominids. The least-squares regression line (solid line), the 95% confidence intervals for individuals (dashed lines), and the coefficient of determination are for the recent humans only. Note the strong relationship between pubic length and bi-iliac breadth. All of the fossil hominids appear to follow the recent human relationship, with the exception of Kebara 2 which is just above the upper 95% confidence interval.

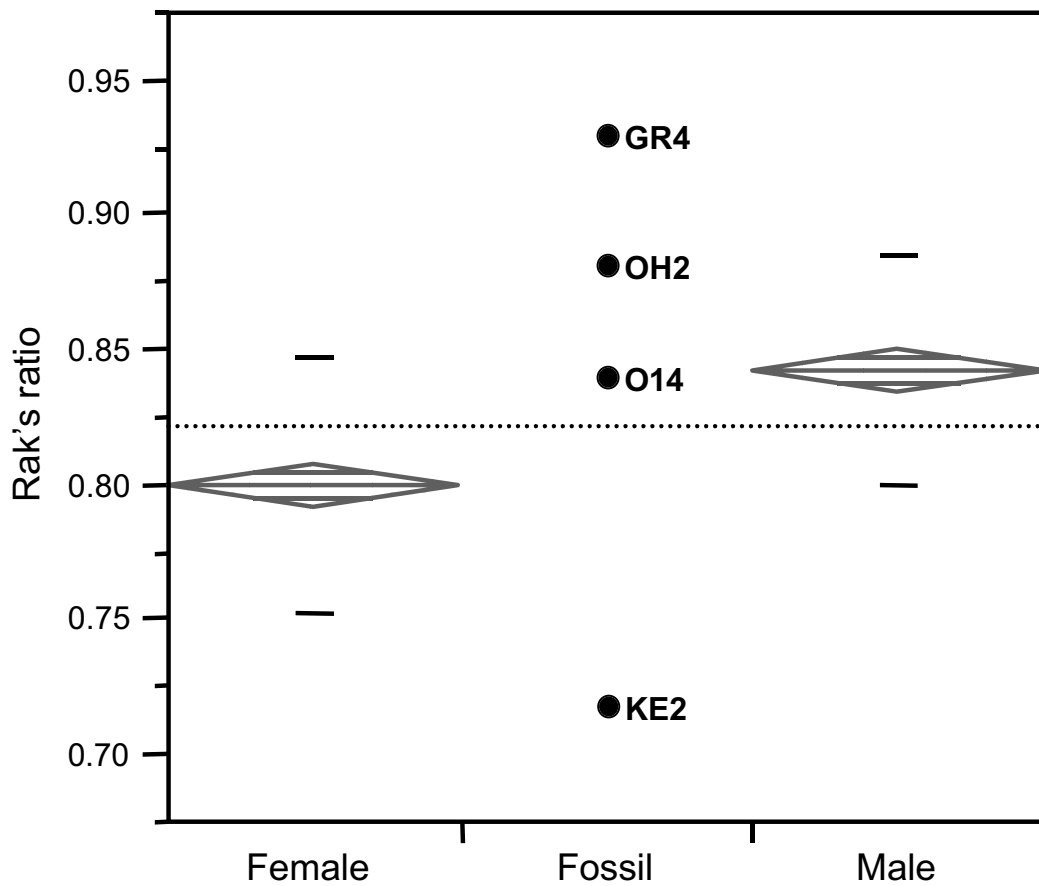


Figure 5.15 Rak's ratio of antero-posterior acetabular positioning
 The dotted horizontal line is the overall sample mean, and the solid, gray lines in the middle of the gray means diamonds are the group means. Non-overlapping means diamonds indicate statistical significance ($p < 0.05$). The solid, black lines are positive and negative standard deviations. Males have significantly higher ratios than females. Kebara 2 has an extremely low ratio, and Grotte des Enfants has a very high ratio.

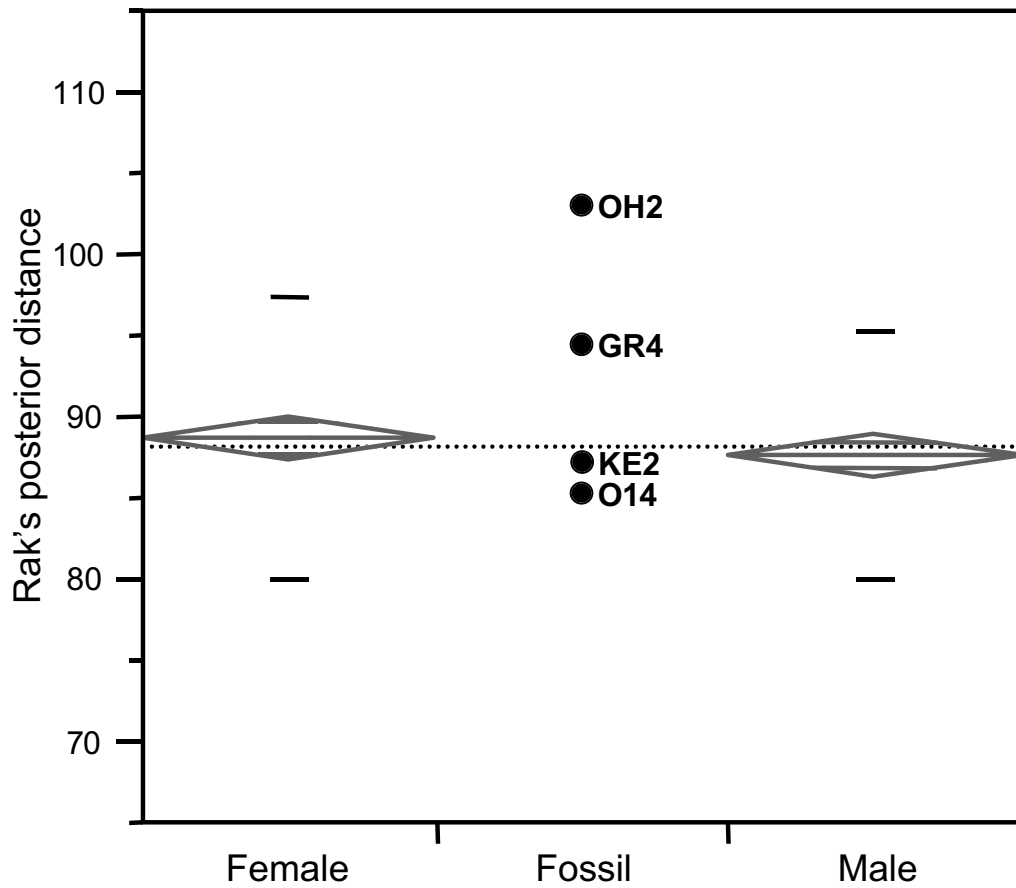


Figure 5.16 Rak's posterior distance (sacral promontory to the anterior acetabulum)

The dotted horizontal line is the overall sample mean, and the solid, gray lines in the middle of the gray means diamonds are the group means. Non-overlapping means diamonds indicate statistical significance ($p < 0.05$). The solid, black lines are positive and negative standard deviations. Males and females have very similar distances even though they have very differently shaped pelves. Kebara 2 plots very close to the overall recent human mean.

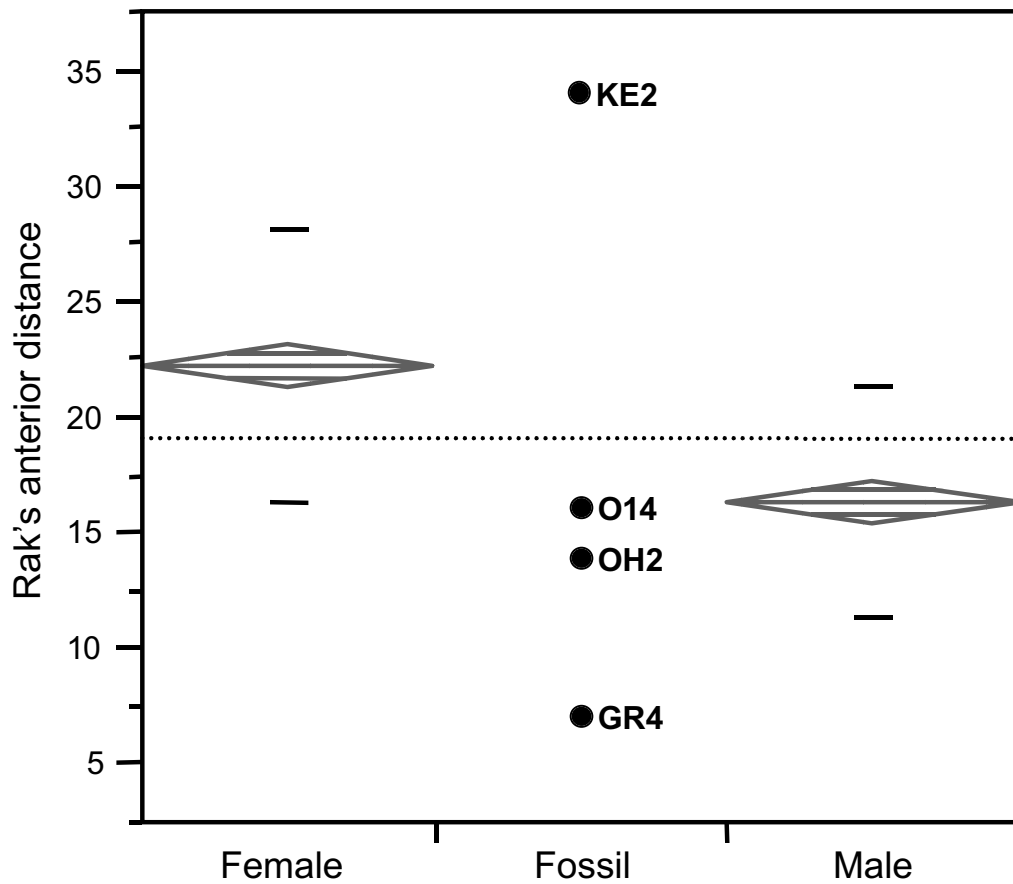


Figure 5.17 Rak's anterior distance (anterior acetabulum to superior pubic symphysis)

The dotted horizontal line is the overall sample mean, and the solid, gray lines in the middle of the gray means diamonds are the group means. Non-overlapping means diamonds indicate statistical significance ($p < 0.05$). The solid, black lines are positive and negative standard deviations. Females have more spacious anterior inlets than males. Kebara 2 has an extremely large anterior distance, and Grotte des Enfants 4 has a fairly small distance.

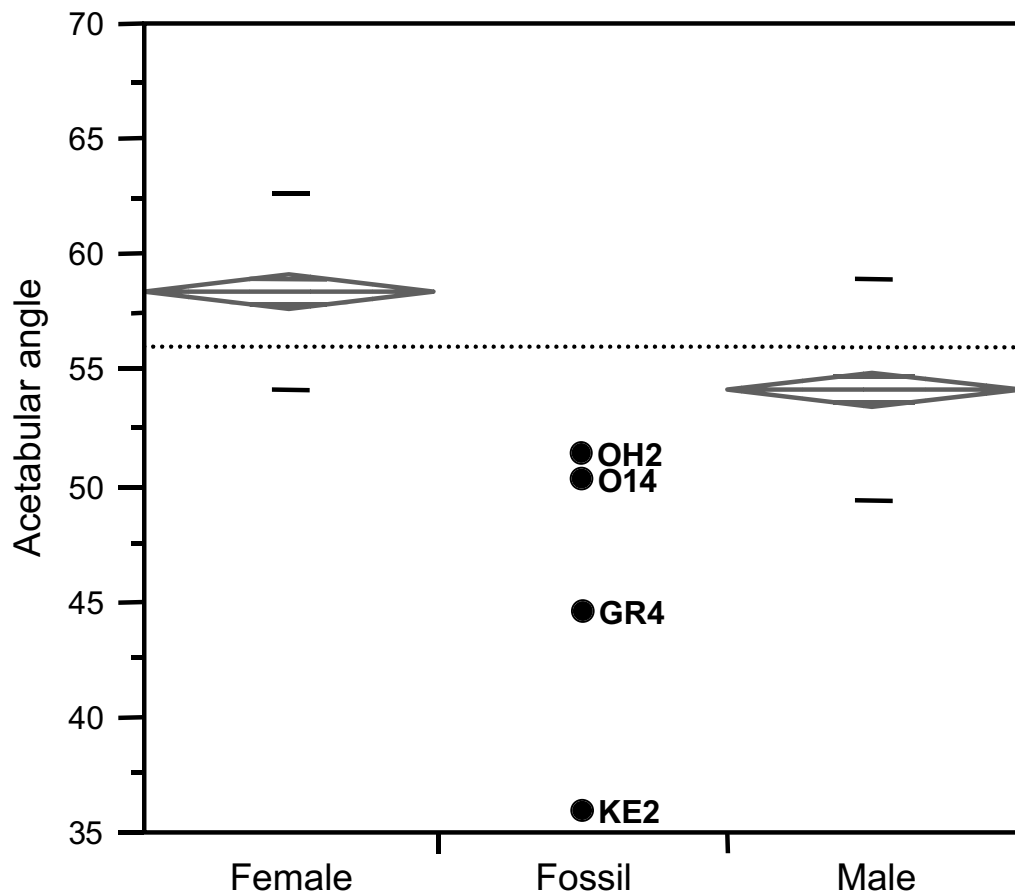


Figure 5.18 Medio-lateral acetabular angle

The dotted horizontal line is the overall sample mean, and the solid, gray lines in the middle of the gray means diamonds are the group means. Non-overlapping means diamonds indicate statistical significance ($p < 0.05$). The solid, black lines are positive and negative standard deviations. Males have more laterally facing acetabulae than females, and Kebara 2 has an extremely laterally facing acetabulum.

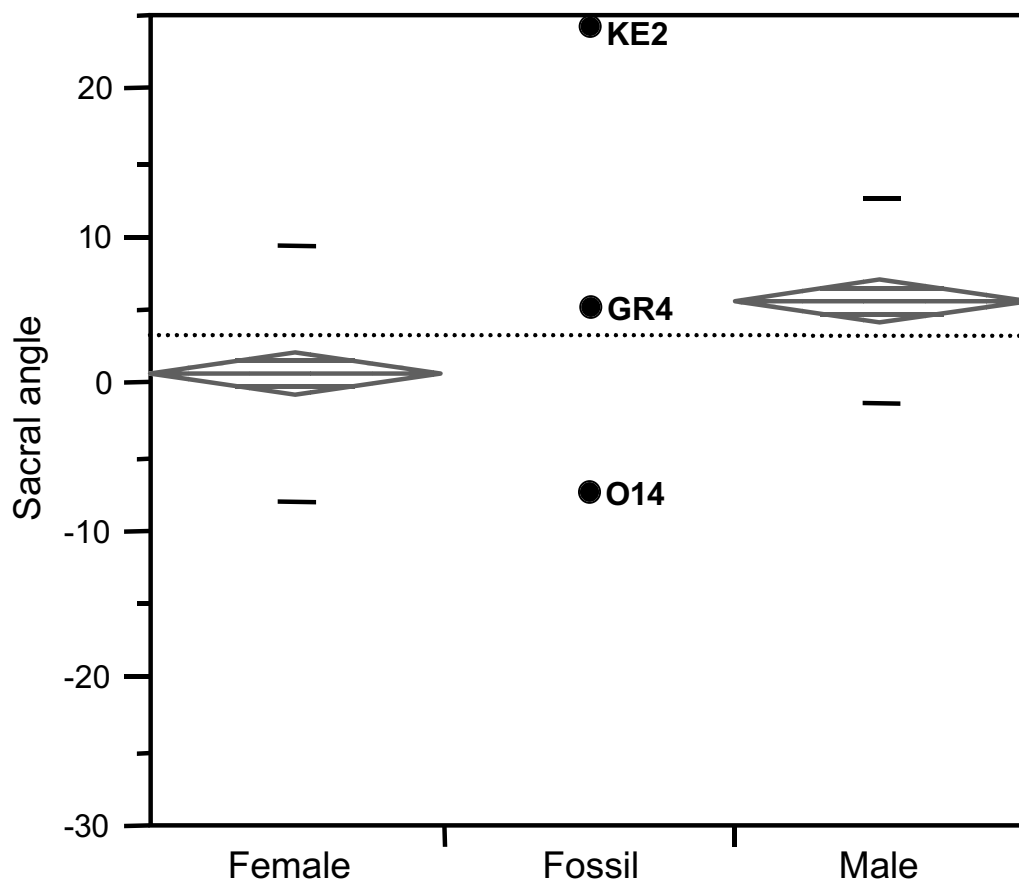


Figure 5.19 Antero-posterior sacral angle

The dotted horizontal line is the overall sample mean, and the solid, gray lines in the middle of the gray means diamonds are the group means. Non-overlapping means diamonds indicate statistical significance ($p < 0.05$). The solid, black lines are positive and negative standard deviations. Males have more anteriorly rotated sacra than females. Kebara 2 has an extremely anteriorly rotated sacrum.

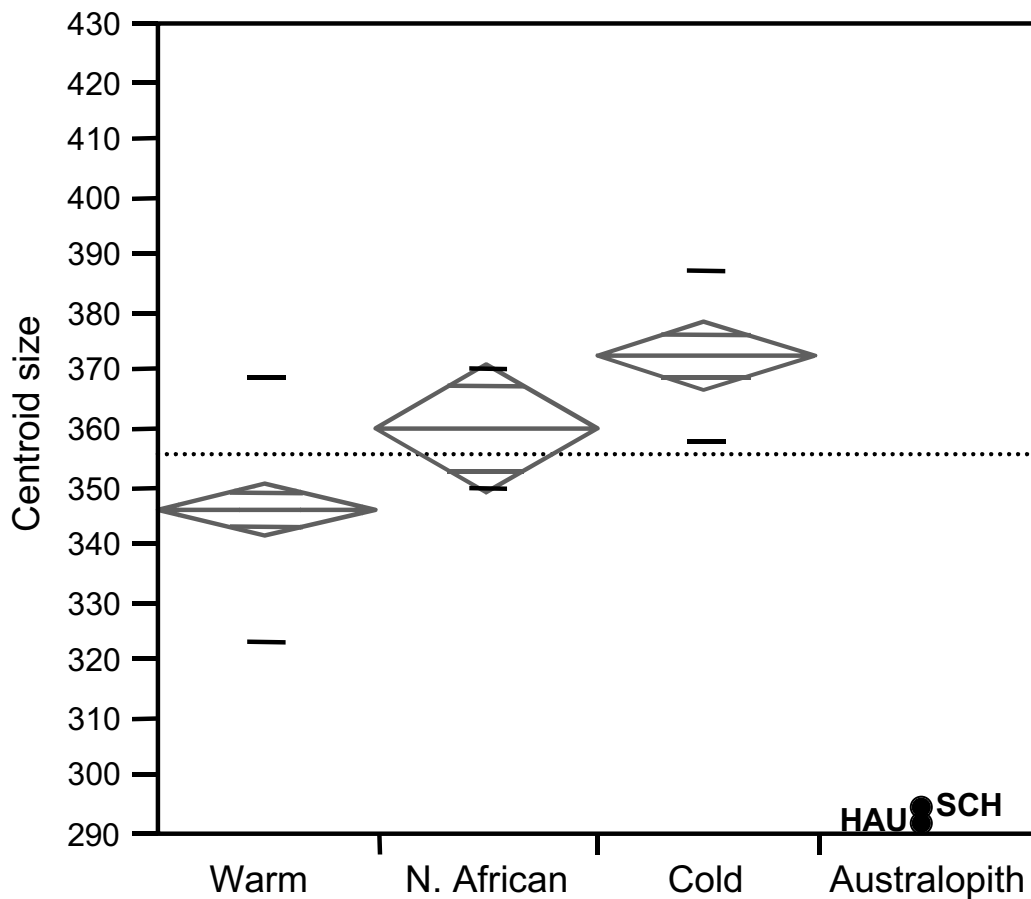


Figure 5.20 Geographically variable australopith analysis: pelvis centroid size

The dotted horizontal line is the overall sample mean, and the solid, gray lines in the middle of the gray means diamonds are the group means. Non-overlapping means diamonds indicate statistical significance ($p < 0.05$). The solid, black lines are positive and negative standard deviations. Notice the extremely small size of both reconstructions of the AL 288-1 pelvis.

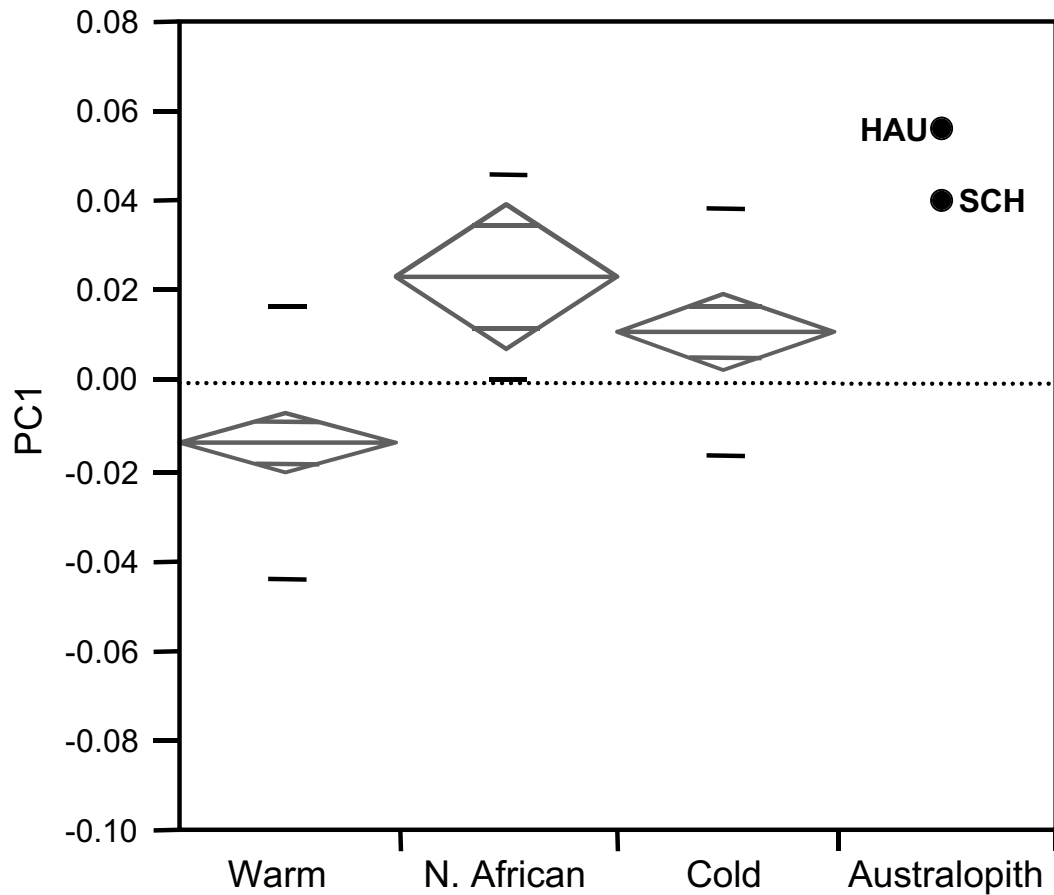


Figure 5.21 Geographically variable australopith analysis: pelvis PC1

The dotted horizontal line is the overall sample mean, and the solid, gray lines in the middle of the gray means diamonds are the group means. Non-overlapping means diamonds indicate statistical significance ($p < 0.05$). The solid, black lines are positive and negative standard deviations. Notice the high scores for both reconstructions of AL 288-1, similar to recent human northern African and cold climate individuals. Refer to Figure 4.5 for shape changes along PC1.

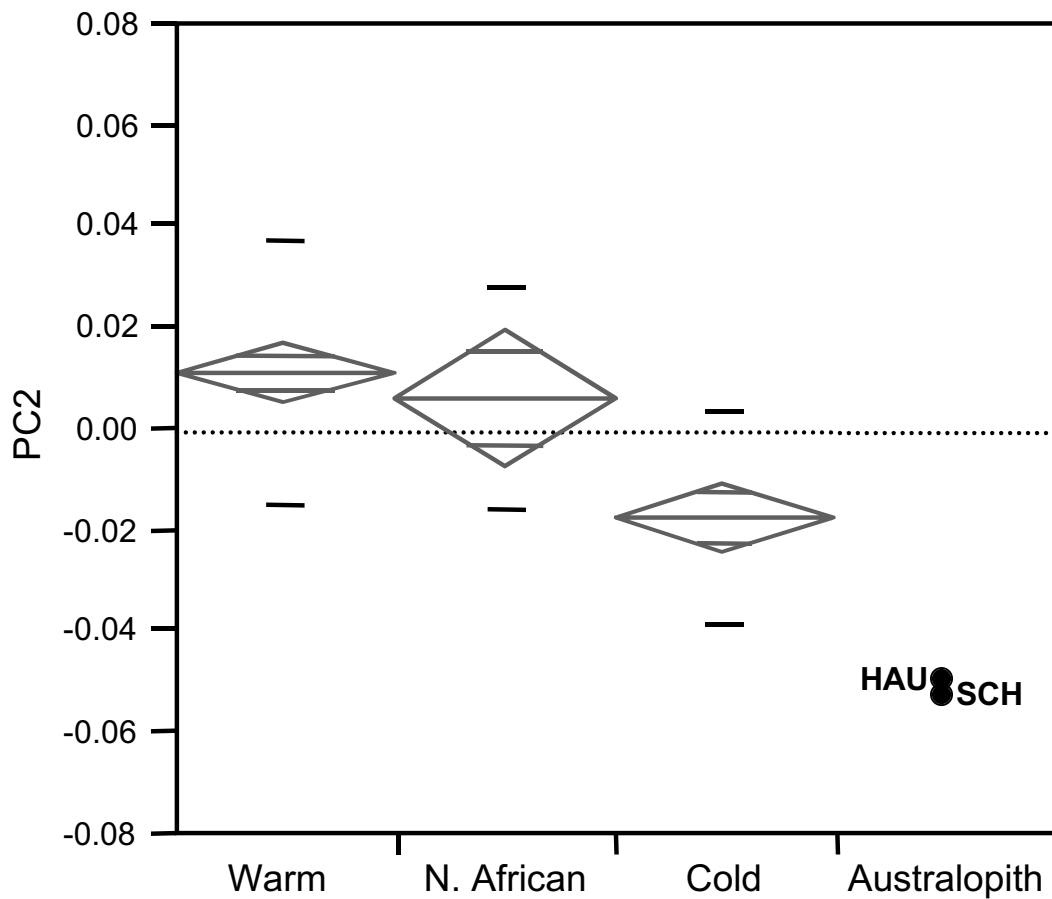


Figure 5.22 Geographically variable australopith analysis: Pelvis PC2

The dotted horizontal line is the overall sample mean, and the solid, gray lines in the middle of the gray means diamonds are the group means. Non-overlapping means diamonds indicate statistical significance ($p < 0.05$). The solid, black lines are positive and negative standard deviations. Notice that both reconstructions of AL 288-1 are even more extreme than individuals from cold climates along this principal component. Refer to Figure 4.6 for shape changes along PC2.

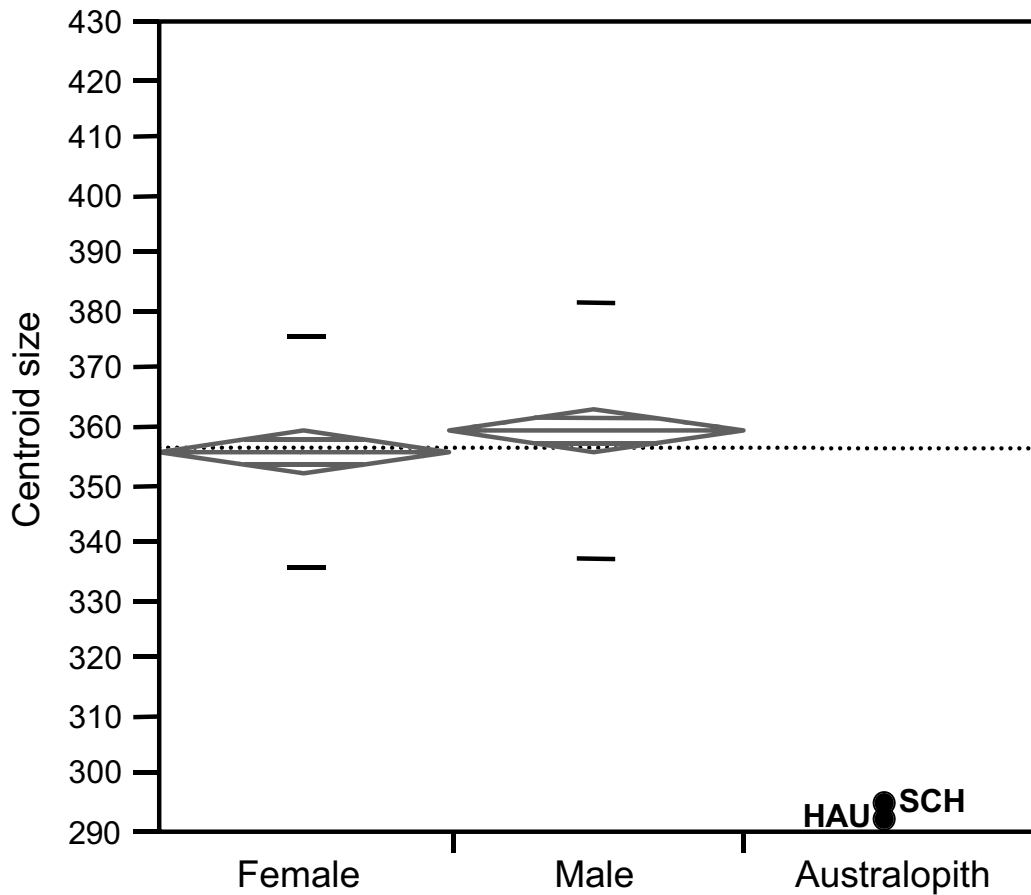


Figure 5.23 Sex balanced australopith analysis: pelvis centroid size
 The dotted horizontal line is the overall sample mean, and the solid, gray lines in the middle of the gray means diamonds are the group means. Non-overlapping means diamonds indicate statistical significance ($p < 0.05$). The solid, black lines are positive and negative standard deviations. Overall, males and females have similarly sized pelvises. Notice the extremely small sizes of the two reconstructions of AL 288-1.

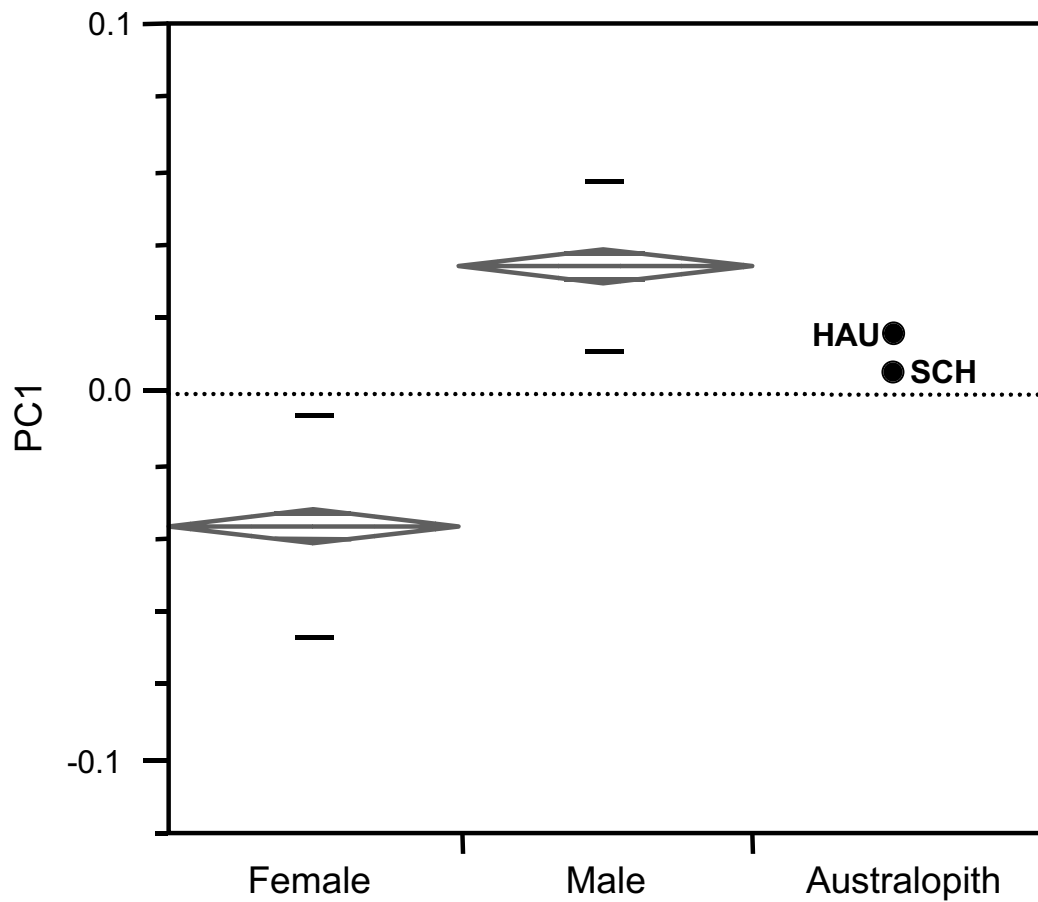


Figure 5.24 Sex balanced australopith analysis: pelvis PC1

The dotted horizontal line is the overall sample mean, and the solid, gray lines in the middle of the gray means diamonds are the group means. Non-overlapping means diamonds indicate statistical significance ($p < 0.05$). The solid, black lines are positive and negative standard deviations. Males and females are extremely sexually dimorphic in pelvic shape. Both reconstructions of AL 288-1 fall with recent human males. Refer to Figure 4.15 for shape changes along PC1.

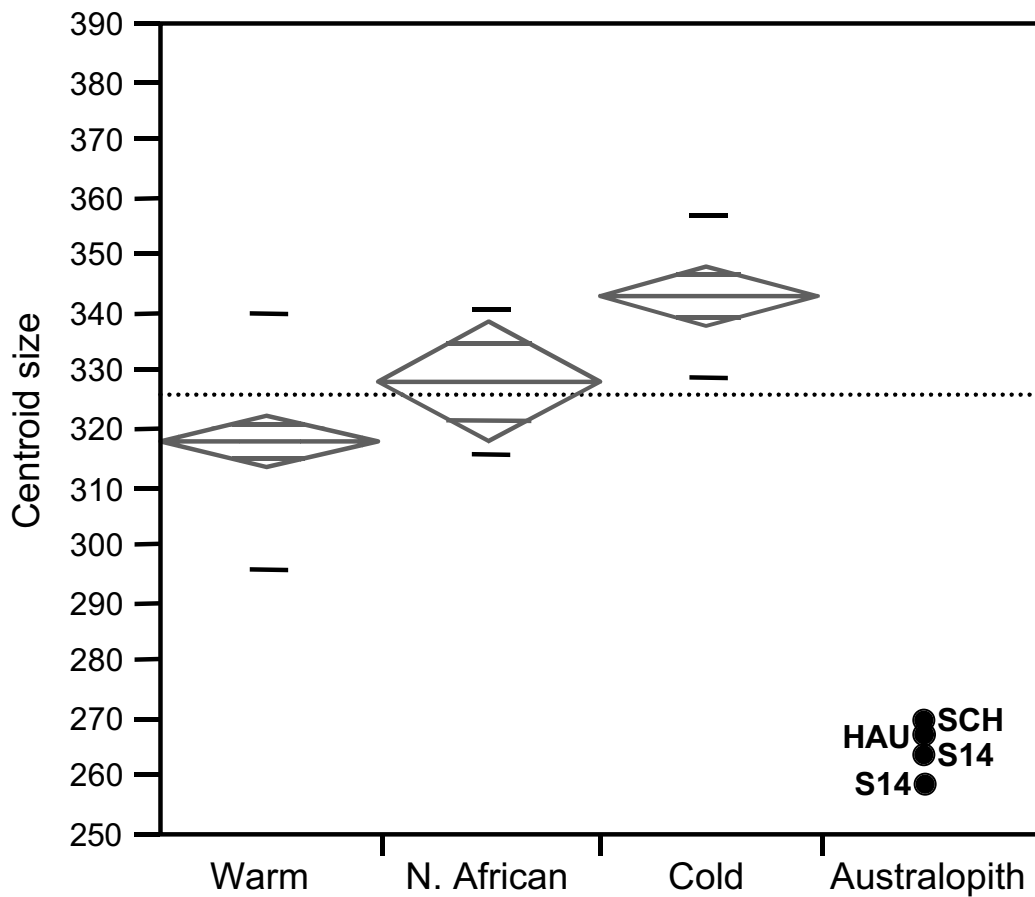


Figure 5.25 Geographically variable australopith analysis: innominate centroid size

The dotted horizontal line is the overall sample mean, and the solid, gray lines in the middle of the gray means diamonds are the group means. Non-overlapping means diamonds indicate statistical significance ($p < 0.05$). The solid, black lines are positive and negative standard deviations. Notice the extremely small sizes of the australopiths relative to recent humans.

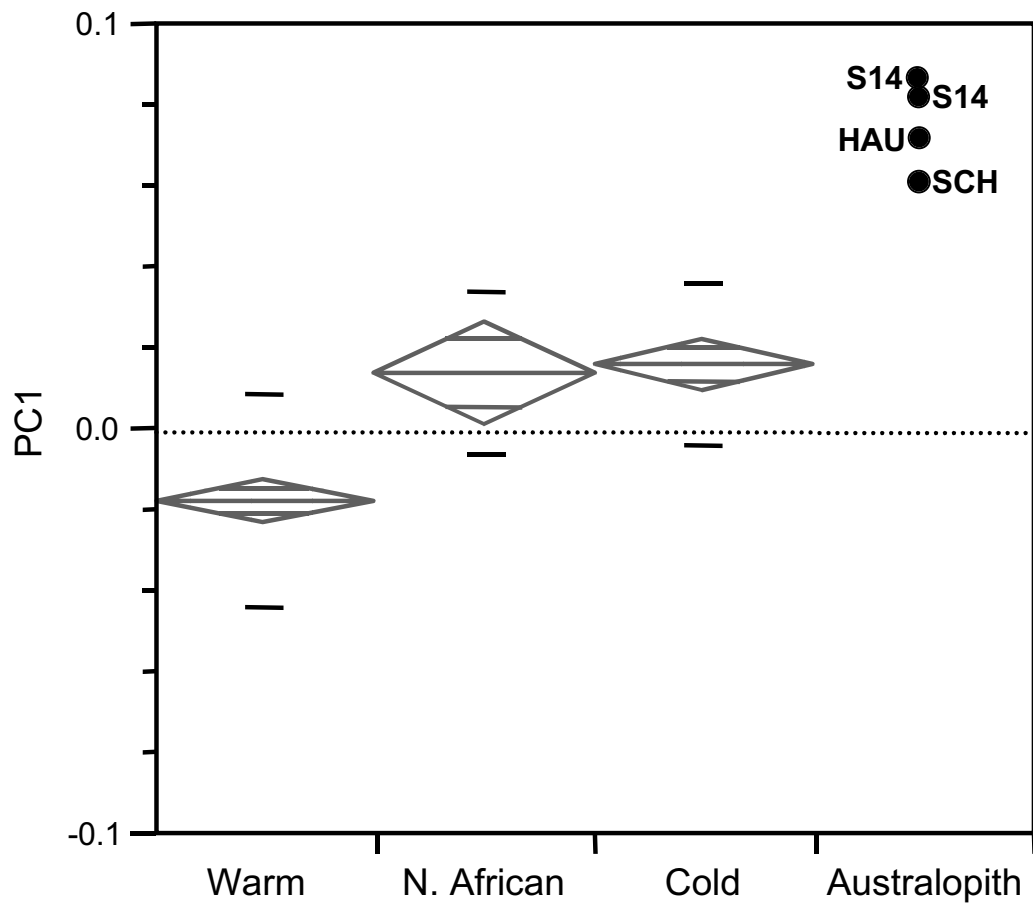


Figure 5.26 Geographically variable australopith analysis: innominate PC1

The dotted horizontal line is the overall sample mean, and the solid, gray lines in the middle of the gray means diamonds are the group means. Non-overlapping means diamonds indicate statistical significance ($p < 0.05$). The solid, black lines are positive and negative standard deviations. Notice the extreme positive position of all the australopiths along this principal component. Refer to Figure 4.9 for shape changes along PC1.

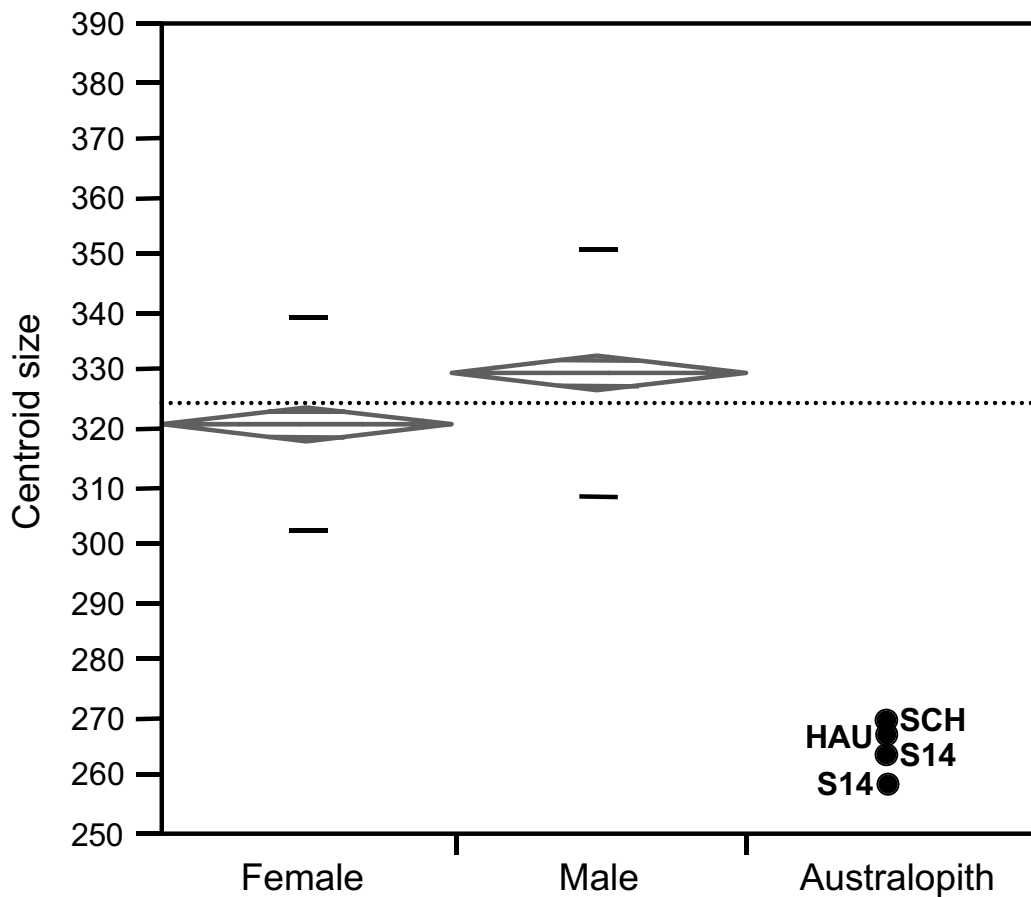


Figure 5.27 Sex balanced australopith analysis: innominate centroid size

The dotted horizontal line is the overall sample mean, and the solid, gray lines in the middle of the gray means diamonds are the group means. Non-overlapping means diamonds indicate statistical significance ($p < 0.05$). The solid, black lines are positive and negative standard deviations. Males have significantly larger innominates than females. Notice the extremely small centroid sizes of the australopiths.

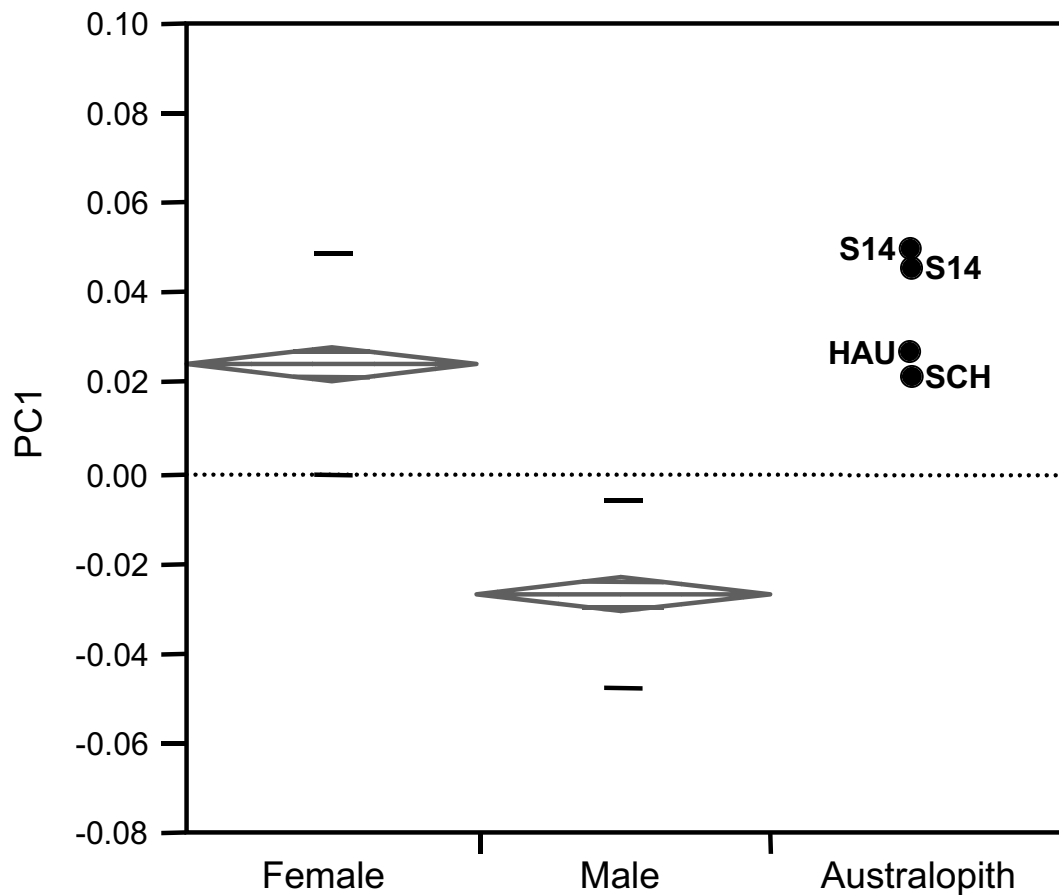


Figure 5.28 Sex balanced australopith analysis: innominate PC1
 The dotted horizontal line is the overall sample mean, and the solid, gray lines in the middle of the gray means diamonds are the group means. Non-overlapping means diamonds indicate statistical significance ($p < 0.05$). The solid, black lines are positive and negative standard deviations. Males and females are highly sexually dimorphic along this component. Notice that the australopiths group more closely with females. Refer to Figure 4.18 for shape changes along PC1.

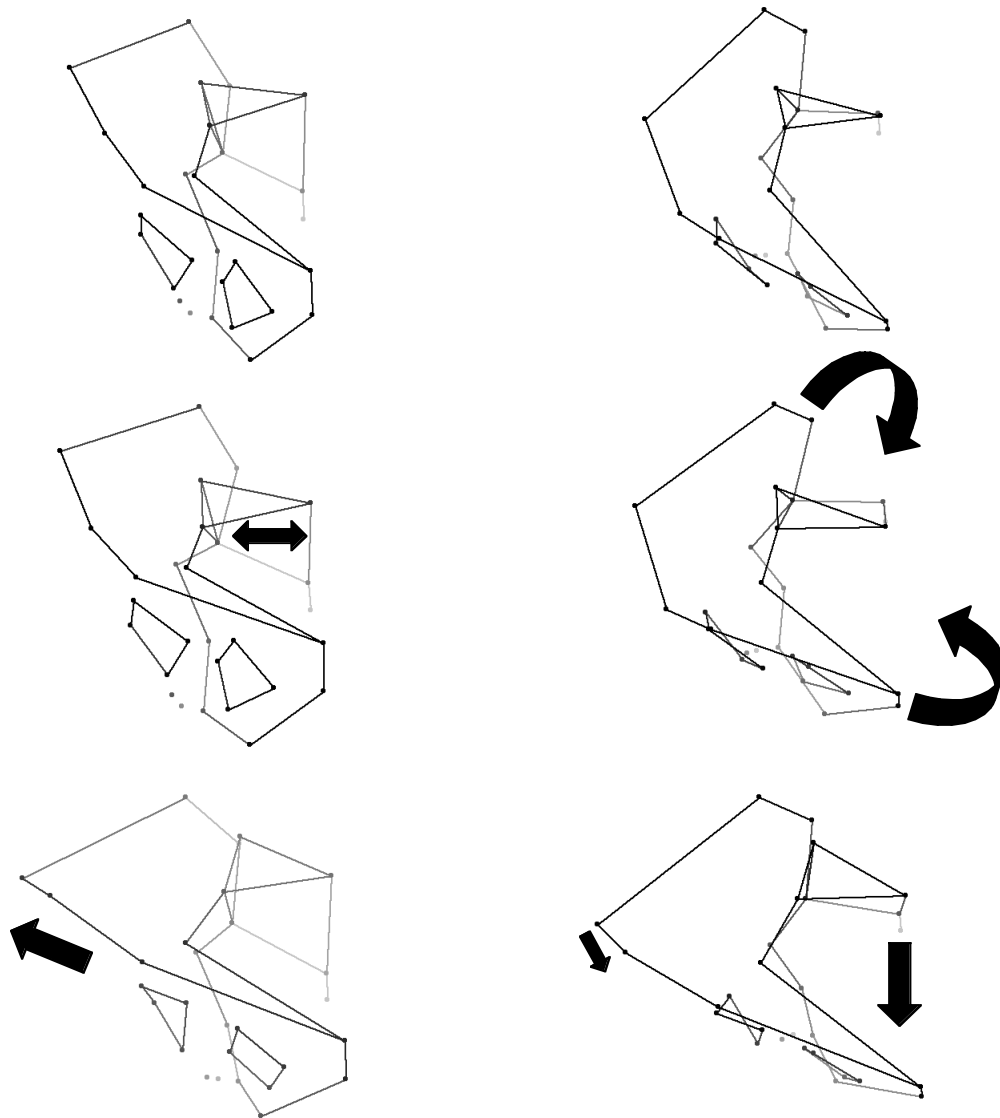


Figure 5.29 Prediction of pelvic shape based on AL 288-1's inlet shape

Anterior (left) and antero-superior (right) views

The top stick figures show the mean pelvic shape for the sex balanced sample, the middle stick figures show predicted pelvic shape based on the ratio of medio-lateral inlet breadth to antero-posterior inlet depth found in AL 288-1, and the bottom stick figures are of Häusler and Schmid's (1995) reconstruction of the AL 288-1 pelvis. The predicted shape was generated using multiple regression of the principal components of the pelvis GPA. Lighter shading indicates greater depth in the stick figures.

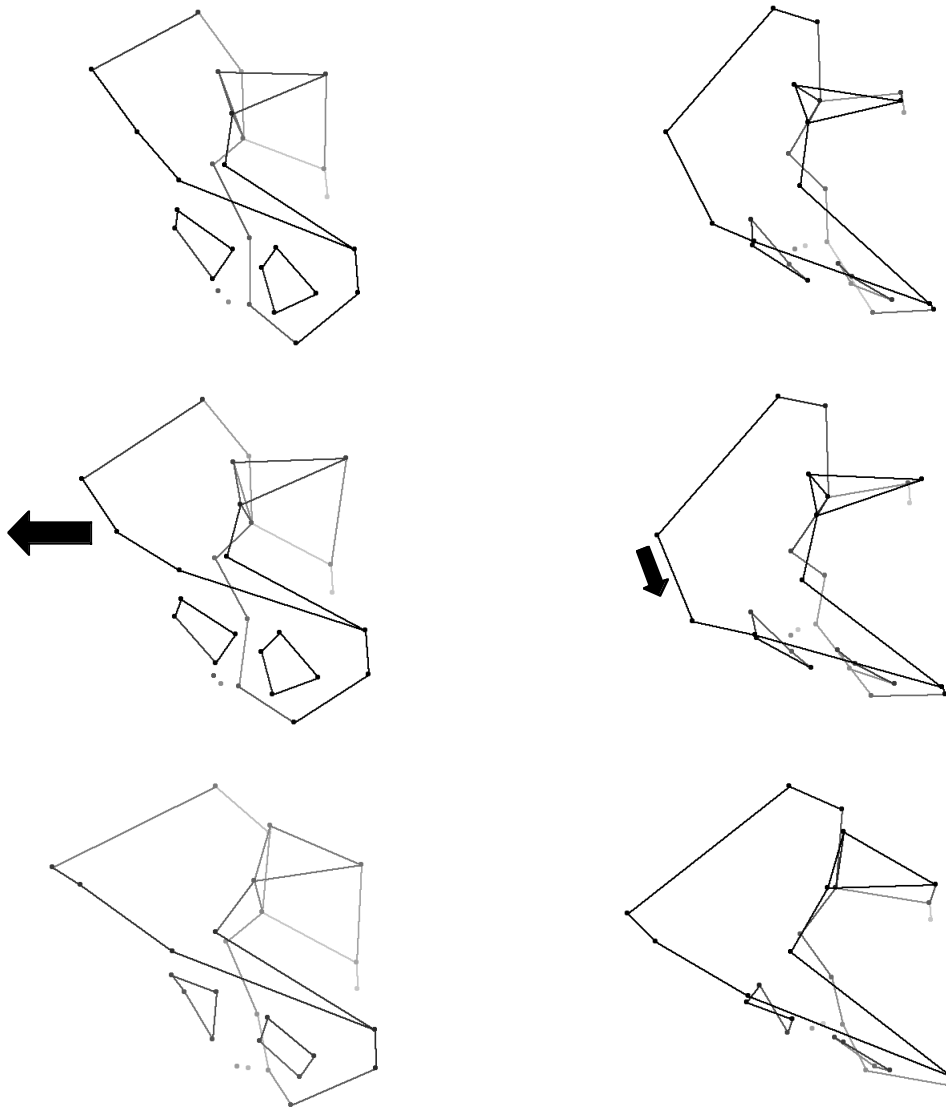


Figure 5.30 Prediction of pelvic shape based on AL 288-1's relative pelvic height

Anterior (left) and antero-superior (right) views

The top stick figures show the mean pelvic shape for the sex balanced sample, the middle stick figures show predicted pelvic shape based on the ratio of bi-iliac breadth to pelvic height found in AL 288-1, and the bottom stick figures are of Häusler and Schmid's (1995) reconstruction of the AL 288-1 pelvis. The predicted shape was generated using multiple regression of the principal components of the pelvis GPA. Lighter shading indicates greater depth in the stick figures.

C. List of fossil specimens analyzed

Code	Specimen (Locality)	Sex (?)	Date/Geologic age
<i>Near-moderns</i>			
SK4	Skhul IV (Israel) ₁	M	~100 kya (Bar-Yosef 1998)
SK5	Skhul V (Israel) ₂	M	~100 kya (Bar-Yosef 1998)
<i>Neandertals</i>			
KE2	Kebara 2 (Israel) ₃ Rak reconst.	M	~60 kya (Bar-Yosef 1998)
NE1	Neandertal 1 (Germany)	M	85-115 kya (?) (Gieseler 1971)
SP2	Spy 2 (Belgium) ₄	M	85-115 kya (?) (Twisselmann 1971)
<i>Upper Paleolithic moderns</i>			
AF2	Afalou 2 (Algeria)	M	10-15 kya (Balout 1977, Klein 1989)
GR4	Grotte des Enfants 4 (Italy)	M	<25 kya (Mussi 2001)
OH2	Ohalo 2 (Israel) ₅	M	19 kya (Hershkovitz et al. 1995)
PA1	Paviland 1 (England) ₆	M	18.5 kya (Oakley 1971)
<i>Holocene moderns</i>			
GO1	Gough's Cave 1 (England)	M	9.1 kya (Oakley 1971)
O14	Oakhurst XIV (S. Africa)	M	5.2 kya (Morris 1992)

Code	Specimen (Locality)	Sex (?)	Date/Geologic age
<i>Australopiths</i>			
HAU	AL 288-1 (Ethiopia) Häusler & Schmid reconst.	F	<3.18 mya (Kimbel, Johanson, and Rak 1994)
SCH	AL 288-1 (Ethiopia) Schmid reconst.	F	<3.18 mya (Kimbel, Johanson, and Rak 1994)
S14	STS 14 (S. Africa) Häusler & Schmid reconst.	F	2.4-2.8 mya (Vrba 1985)
<i>Middle Pleistocene Homo</i>			
JIN	Jinniushan (China) Published measurements	F	>200 kya (Chen, Yang, and Wu 1994)
SI1	Sima pelvis 1 (Spain) Published measurements	M	>320 kya (Bischoff et al. 1997)

Notes:

Landmark (point) numbers refer to those in Table 3.1.

¹Data were collected on casts made by Yoel Rak (innominate) and Mario Chech (femur), and the location of the superior acetabular margin landmark (point 27) was estimated using multiple regression (see Hartman 1989).

²The proximal and distal ends of this femur are heavily reconstructed.

³The reconstruction by Yoel Rak (cast) was analyzed for comparability with other studies, but the measurements I collected on the unreconstructed original are similar to those for the cast; morphological observations were made on the original.

⁴Multiple regression (see Hartman 1989) was used to estimate the location of the gluteal insertion landmarks (points 3 and 4).

⁵Multiple regression (see Hartman 1989) was used estimate the location of the posterior-superior iliac spine landmark (point 32) and the midpoint of superior edge of patellar surface landmark (point 9).

⁶Femur data were collected on a cast, because the original is broken in half, but measurements I collected on the original are similar to those for the cast.

D. Detailed definitions of landmarks

This appendix contains detailed definitions of the landmarks on the femur and pelvis that are listed in Table 3.1.

Femoral landmarks

1. Center of the hemispherical articular surface of the femoral head:

The center of the hip joint in a femoral reference frame (located inside the femoral head) is approximated by the average of four points (A-D) taken around the hemispherical articular surface of the femoral head. To locate these four points, start by placing the superior (A) and inferior (B) points on the lateral edges of the articular surface, making sure that points A and B are located along lines running through the middle of the superior or inferior surfaces respectively of the femoral neck. From an anterior or a posterior view, points A and B also should form a line perpendicular to the axis of the femoral neck and be maximally separated; this means that points A and B are not always located at the most lateral edges of the articular surface. Locate the other two points by placing the posterior (C) and anterior (D) points on the articular surface along a line perpendicular to both the line connecting points A and B (from a medial view) and to the axis of the femoral neck (from superior and inferior views). As for points A and B, points C and D also should be maximally separated.

2. Center of the midpoint of the femoral neck:

The center of the midpoint of the femoral neck (located inside the femoral neck) is approximated by the average of four points (A-D). To locate these four points, start by placing the superior point (A) at the minimum curvature (from anterior and posterior views) of the superior surface of the femoral neck, making sure that point A also is located on the middle axis (antero-posteriorly) of the superior surface of the femoral neck. The inferior point (B) is located on the middle axis (antero-posteriorly) of the inferior surface of the femoral neck, and it forms a line with point A that is perpendicular to the axis of the femoral neck (from anterior and posterior views). Locate the other two points by placing the posterior (C) and anterior (D) points on the femoral neck along a line perpendicular to both the line connecting points A and B (from a medial view) and to the axis of the femoral neck (from superior and inferior views). Points C and D also are located at the minimum curvature (from superior and inferior views) of the posterior and anterior surfaces respectively of the femoral neck.

3. Middle of the insertion area for gluteus minimus:

This point is located on the antero-inferior surface of the greater trochanter, just medial to the lateral border, in the center of the oval insertion area for gluteus minimus. The insertion area may extend as a thinner strip superiorly and medially, but record the point in the center of the lateral oval portion.

4. Middle of the insertion area for gluteus medius:

This point is located on the postero-superior surface of the greater trochanter, in the center of the oval insertion area for gluteus medius. The insertion area extends as a thinner strip inferiorly and anteriorly, but record the point in the center of the most superior oval portion.

5. Tip of the lesser trochanter:

This point is located where the lesser trochanter projects maximally (local maximum of a curved surface).

6. Center of the femoral shaft at the eighty-percent of the total shaft length level:

Points 6 and 7 are located using a flexible measuring tape that is aligned along the axis of the femoral shaft on the posterior surface. The 0% shaft level is defined as the most inferior edge of the middle of the intercondylar notch; 100% is the midpoint of the most superior edge of the femoral neck (between the femoral head and greater trochanter). Point 6 (located inside the femoral shaft) is approximated by the average of four points (A-D) at the 80% level (just inferior to the lesser trochanter). To locate these four points, start by placing the posterior point (A) midway between the gluteal and spiral lines at the 80% level and the anterior point (B) in the middle (medio-laterally) of the anterior surface of the shaft at the 80% level. Locate the other two points by placing the medial (C) and lateral (D) points at the 80% level on the femoral shaft and along a line perpendicular to the line connecting points A and B (from superior or inferior views).

7. Center of the femoral shaft at the mid-shaft level:

See point 6 above for a definition of shaft percentage (shaft level). Point 7 (located inside the femoral shaft) is approximated by the average of four points (A-D) at the 50% level (mid-shaft). To locate these four points, start by placing the posterior point (A) on the linea aspera at the 50% level and the anterior point (B) in the middle (medio-laterally) of the anterior surface of the shaft at the 50% level. Locate the other two points by placing the medial (C) and lateral (D) points at the 50% level on the femoral shaft and along a line perpendicular to the line connecting points A and B (from superior or inferior views).

8. Tip of the adductor tubercle:

This point is located where the adductor tubercle projects maximally (local maximum of a curved surface).

9. Midpoint of the antero-superior edge of the patellar surface of the distal femur:

This point is located on the superior edge of the patellar surface midway between the medial and lateral borders of the superior portion of the patellar surface. This point also lies on a line that passes through the middle of the axis of the distal femoral shaft.

10. Midpoint of the medial edge of the inferior surface of the medial condyle:

This point is defined as the midpoint, from an inferior view, of the medial edge of the inferior surface of the medial condyle. See point 11 for further information.

11. Midpoint of the lateral edge of the inferior surface of the lateral condyle:

This point is defined as the midpoint, from an inferior view, of the lateral edge of the inferior surface of the lateral condyle. There is usually a slight notch or depression at point 11. Points 10 and 11 should connect to form a line that is horizontal when the femur is held in anatomical position. Points 11 and 12 usually fall just anterior to the anterior edge of the intercondylar notch.

12. Midpoint of the medial edge of the posterior surface of the medial condyle:

This point is defined as the midpoint, from a posterior view, of the medial edge of the posterior surface of the medial condyle. See point 13 for further information.

13. Midpoint of the lateral edge of the posterior surface of the lateral condyle:

This point is defined as the midpoint, from a posterior view, of the lateral edge of the posterior surface of the lateral condyle. There is usually a slight notch or depression at point 13. Points 12 and 13 should connect to form a line that is in a frontal plane when the femur is held in anatomical position.

14. Midpoint of the line between the medial and lateral epicondyles:

This point is the average of two points: the point where the medial epicondyle projects maximally (local maximum of a curved surface) and the point where the lateral epicondyle projects maximally (local maximum of a curved surface).

Pelvic landmarks

15. Point where the inferior sacral auricular surface meets the superior edge of the sciatic notch:

Points 15, 16, and 17 are defined with the innominate and sacrum physically articulated. Point 15 is located where the antero-inferior edge of the auricular surface of the innominate meets the supero-medial border of the greater sciatic notch. Point 15 is located as far inferior as possible on the auricular surface, such that the same point can be located on the auricular surfaces of both the innominate and the sacrum (i.e. the most inferior point on the anterior junction between the innominate and sacrum).

16. Most postero-superior point on the auricular surface of the ilium:

Point 16 is located on the postero-superior edge of the auricular surface of the innominate, such that the same point can be located on the auricular surfaces of both the innominate and the sacrum. Point 16 usually falls at the midpoint (antero-posteriorly) of the sacral ala. See point 15 for further details.

17. Point where the arcuate line meets the auricular surface of the ilium:

Point 17 is located on the antero-superior edge of the auricular surface of the innominate where the arcuate line meets the auricular surfaces of the innominate and the sacrum. If the arcuate line splits into superior and inferior lines, point 17 is defined to be midway between the two lines. See point 15 for further details.

18. Most superior point on the superior edge of the medial aspect of the pubic symphysis:

Points 18 and 19 are located on the edges of the symphyseal surface (where the two pubic bones articulate), and they should be maximally separated. Point 18 is defined to be the most superior point on the superior edge of the pubic symphysis where the symphyseal surface constricts to form a tip or apex. On younger individuals without clear symphyseal rims, points 18 and 19 should be estimated based on comparisons with more mature anatomy.

19. Most inferior point on the inferior edge of the medial aspect of the pubic symphysis:

Point 19 is defined to be the most inferior point on the inferior edge of the pubic symphysis where the symphyseal surface tends to constrict to form a tip or apex. See point 18 for further details.

20. Center of the obturator groove on the inferior surface of the superior pubic ramus:

This point is located in the obturator groove in the center (along a line that is perpendicular to the axis of the superior pubic ramus) of the inferior surface of the superior pubic ramus.

21. Center of the notch on the superior surface of the inferior margin of the obturator foramen:

This point is defined as the local minimum (notch) of the inferior arc of the obturator foramen (viewing the obturator foramen head on), centered on the superior surface of the ischio-pubic ramus along a line that is perpendicular to the axis of the ischio-pubic ramus.

22. Center of the posterior obturator tubercles along the posterior margin of obturator foramen:

This point is located in the center (supero-inferiorly) of the posterior obturator tubercles along the posterior margin of the obturator foramen. Point 22 usually lies directly across the obturator foramen from where the pubic body meets the ischio-pubic ramus. See point 23 for further details.

23. Center of inflection point on postero-lateral surface of the anterior margin of the obturator foramen:

This point is located on the posterior edge of the anterior margin of the obturator foramen where the pubic body meets the ischio-pubic ramus (inflection point or superior root of the ischio-pubic ramus). Point 23 usually is directly across from point 22.

24. Point on the superior edge of acetabular notch next to the lunate surface:

This point is located on the anterior edge of the acetabulum where the lunate surface ends at the acetabular notch. The acetabular notch is just inferior to point 24.

25. Point on the acetabular margin furthest away from the superior edge of the acetabular notch:

This point is located on the posterior edge of the acetabulum such that it is maximally separated from point 24. See point 24 for further details.

26. Inflection point on the inferior edge of the acetabular margin:

This point is located on the inferior edge of the acetabulum at the maximum perpendicular distance from the line between points 24 and 25. Point 26 is a local minimum (inflection point) when the acetabulum is oriented such that the line formed by points 24 and 25 is horizontal.

27. Point on acetabular margin furthest away from the inflection point on the inferior acetabular margin:

This point is located on the superior edge of the acetabulum such that it is maximally separated from point 26. Point 27 is located where the anterior-inferior iliac spine meets the margin of the acetabulum. See point 26 for further details.

28. Apex of the anterior-inferior iliac spine:

This point is located where the anterior-inferior iliac spine projects maximally (local maximum of a curved surface). When the anterior-inferior iliac spine is very elongated, point 28 is defined as the maximum projection in the center (supero-inferiorly) of the anterior-inferior iliac spine.

29. Apex of the anterior-superior iliac spine:

This point is located where the anterior-superior iliac spine projects maximally (local maximum of a curved surface).

30. Midpoint of the supero-lateral edge of the cristal tubercle:

This point is located on the external crest of the ilium in the middle (along the axis of the iliac crest) of the cristal tubercle. Point 30 usually is the most lateral point on the pelvis in standard anatomical position, and it usually occurs at the maximum thickness of the iliac crest.

31. Point where the lateral margin of the iliac crest meets the superior end of the posterior gluteal line:

This point is located where the external crest of the ilium meets the most superior end of the posterior gluteal line.

32. Apex of the posterior-superior iliac spine:

This point is located where the posterior-superior iliac spine projects maximally (local maximum of a curved surface). Point 32 is located on the iliac crest and not on the more medial projections of bone that are posterior to the auricular surface.

33. Point of maximum curvature in the greater sciatic notch:

This point is the deepest point in the greater sciatic notch in the middle (medio-laterally) of the surface of the notch. If the two edges of the greater sciatic notch are

extended to form an angle, point 33 is located where the bisector of this angle meets the surface of the greater sciatic notch.

34. Tip of the ischial spine:

This point is located where the ischial spine projects maximally (the tip).

35. Point where the transverse ridge meets the medial edge of the ischial tuberosity:

This point is located where the transverse ridge of the ischial tuberosity meets the medial edge of the ischial tuberosity (where the sacrotuberous ligament attaches). The transverse line runs medio-laterally and divides the ischial tuberosity into hamstring and adductor portions.

36. Center of the more proximal hamstring facet:

This point is located in the center of the lateral elongated oval facet on the hamstring portion of the ischial tuberosity.

37. Center of the more distal hamstring facet:

This point is located in the center of the small medial oval facet on the hamstring portion of the ischial tuberosity.

38. Point where the ischio-pubic ramus meets the ischial tuberosity:

This point is located where the ridge on the inferior surface of the ischial tuberosity crosses a line perpendicular to the axis of the ischio-pubic ramus at the point

where the ischial tuberosity has thinned to the same width as the root of the ischio-pubic ramus.

39. Point of maximum curvature on the arcuate line of ilium (most lateral point in anatomical position):

With the innominate held in standard anatomical position, point 39 is located on the arcuate line at the maximum perpendicular distance from the mid-sagittal plane. Point 39 is the most lateral point on the inlet rim.

40. Midpoint of the anterior edge of the superior surface of the first sacral body:

This point is located at the middle (medio-laterally) of the anterior edge of the superior surface of the first sacral body (the middle of the sacral promontory). If there is osteophytic lipping, point 40 is defined as its approximate location prior to the pathological changes.

41. Midpoint of the transverse line between the fourth and fifth sacral vertebrae:

This point is located midway between the medial edges of the 4th anterior sacral foramina along the transverse line between the 4th and 5th sacral vertebrae. If the transverse line is not sharply defined, point 41 is defined as the middle (supero-inferiorly) of the transverse line region.

42. Midpoint of the antero-inferior edge of the apex of the sacrum:

This point is located in the middle (medio-laterally) of the antero-inferior edge of the apex of the sacrum. If the 1st coccygeal element is fused or there is a 6th sacral vertebra, point 42 is defined as the middle (medio-laterally) of the fusion line.

E. Methods for calculating standard measurements

This appendix contains detailed descriptions of the how the standard measurements in Table 3.2 were calculated from landmark coordinates. All landmark numbers refer to Table 3.1 and Appendix D. Unless otherwise indicated, all distances are calculated with the pelvis or femur in standard anatomical position (as defined in the methods chapter). Euclidean distances by definition are calculated without respect to anatomical orientation. The digitized points discussed below that do not have numbers are used only to calculate standard measurements and are therefore not included in Table 3.1 or Appendix D.

BIBR (Bi-iliac breadth of the pelvis):

Twice the perpendicular distance from the sagittal plane of the middle of the cristal tubercle (point 30) to the mid-sagittal plane.

PELVD (Pelvic depth):

The perpendicular distance from the coronal plane of the posterior-superior iliac spine (point 32) to the coronal plane of the anterior-superior iliac spine (point 29).

FEML (Bicondylar length of the femur):

The perpendicular distance from the transverse plane of the inferior surfaces of the femoral condyles (points 10 and 11) to the transverse plane of the most superior point on the femoral head (point estimated with the femur held in standard anatomical position).

MLIN (Transverse diameter of the pelvic inlet):

Twice the perpendicular distance from the sagittal plane of the most lateral point on the arcuate line (point 39) to the mid-sagittal plane.

MLMID (Transverse diameter of the pelvic mid-plane):

Twice the perpendicular distance from the sagittal plane of the tip of the ischial spine (point 34) to the mid-sagittal plane.

MLOUT (Transverse diameter of the pelvic outlet):

Twice the perpendicular distance from the sagittal plane where the transverse ridge meets the medial edge of the ischial tuberosity (point 35) to the mid-sagittal plane.

APIN (Sagittal diameter of the pelvic inlet):

The Euclidean distance from the sacral promontory (point 40) to the tip of the most superior point on the superior edge of the medial aspect of the pubic symphysis (point 18).

APMID (Sagittal diameter of the pelvic mid-plane):

The Euclidean distance from the midpoint of the transverse line between the fourth and fifth sacral vertebrae (point 41) to the tip of the most inferior point on the inferior edge of the medial aspect of the pubic symphysis (point 19).

APOUT (Sagittal diameter of the pelvic outlet):

The Euclidean distance from the midpoint of the antero-inferior edge of the apex of the sacrum (point 42) to the tip of the most inferior point on the inferior edge of the medial aspect of the pubic symphysis (point 19).

SACBR (Maximum breadth between the margins of the sacral alae):

Twice the perpendicular distance from the sagittal plane of the sacral promontory (point 40) to the sagittal plane of a point in the middle of the lateral edge of the sacral ala.

ILBR (Maximum breadth of the iliac crest):

The distance, perpendicular to the axis of the iliac crest, from the middle of the supero-lateral lip of the cristal tubercle (point 30) to a point on the internal lip of iliac crest.

PUBH (Superior pubic ramus height):

The distance, perpendicular to the axis of the superior pubic ramus, from the center of the obturator groove (point 20) to a point on the superior surface of the superior pubic ramus.

PUBB (Superior pubic ramus breadth):

The distance, perpendicular to and even with (medi-laterally along the axis of the superior pubic ramus) superior pubic ramus height, from a point on the medial side to a point on the lateral side of the superior pubic ramus.

NECK (Femoral neck-shaft angle):

In a frontal plane, the angle between the line formed by the center of the femoral head (point 1) and the midpoint of the femoral neck (point 2) and the line formed by the center of the femoral shaft at the 80% level (point 6) and the center of the femoral shaft at the mid-shaft level (point 7).

TORS (Femoral torsion angle):

In a transverse plane, the angle between the line formed by the center of the femoral head (point 1) and the midpoint of the femoral neck (point 2) and a coronal plane.

BICON (Femoral bicondylar angle):

In a frontal plane, the angle between the line formed by the center of the femoral shaft at mid-shaft (point 7) and the midpoint of the femoral epicondyles (point 14) and a sagittal plane.

NECKL (Femoral biomechanical neck length):

The perpendicular distance from the sagittal plane of the gluteal insertions (average of points 3 and 4) to the sagittal plane of the center of the femoral head (point 1).

FHDIA (Femoral head diameter):

The Euclidean distance between superior and inferior points on the hemisphere of articular surface of femoral head (see definition of point 1 in Appendix D).

EPIBR (Epicondylar width):

The Euclidean distance between the medial and lateral femoral epicondyles (see definition of point 14 in Appendix D).

RAML (Superior pubic ramus length):

The Euclidean distance between the superior edge of the acetabular notch (point 24) and the most superior point on the superior edge of the medial aspect of the pubic symphysis (point 18).

PUBL (Pubic length):

The Euclidean distance between a point at the developmental center of the acetabulum (junction of the ilium, ischium, and pubis) and the most superior point on the superior edge of the medial aspect of the pubic symphysis (point 18).

ISCHL (Ischium length):

The Euclidean distance between a point at the developmental center of the acetabulum (junction of the ilium, ischium, and pubis) and the ischial hamstring facets (average of points 36 and 37).

BWMA (Body weight moment arm):

The perpendicular distance from the sagittal plane of the center of the acetabulum (average of points 24, 25, 26, and 27) to the mid-sagittal plane.

ACET (Acetabulum diameter):

The Euclidean distance between the superior (point 26) and inferior (point 27) margins of the acetabulum (see definitions of points 26 and 27 in Appendix D).

MLMS (Transverse femoral mid-shaft diameter):

The Euclidean distance between the medial and lateral margins of the femoral mid-shaft (see definition of point 7 in Appendix D).

APMS (Antero-posterior femoral mid-shaft diameter):

The Euclidean distance between the anterior and posterior margins of the femoral mid-shaft (see definition of point 7 in Appendix D).

F. Original software

This appendix contains brief descriptions of the software that I wrote to collect and analyze the data discussed in this dissertation. This software is composed of multiple components/programs that are designed to work together while still allowing for maximum analytical flexibility. This flexibility made it possible for me to integrate the programs that I wrote with JMP 3.0, particularly for the discriminant and multiple regression analyses and for basic statistical tests such as calculating correlation coefficients, t-tests, etc. All the components are written in the C programming language and are for Macintosh computers. However, because C is a cross-platform programming language that is reasonably portable, all the components other than the visualization program could be converted easily to run under other operating systems. The software and information about input and output file formats are available by contacting me.

Data collection

The data collection program is designed for use with a Microscribe digitizer, and it communicates with the digitizer via the serial port using routines in the Software Development Kit (SDK) that are available free-of-charge from Immersion Corporation. This component allows a user to save the three-dimensional (3-D) coordinate locations of a sequence of landmarks to an ASCII text file. This raw data can be used as input to the programs discussed below or to other morphometrics software.

For reference and troubleshooting, the application window of the data collection program continuously displays the x-y-z coordinate location of the tip of the digitizing stylus. As discussed in the methods chapter, points are recorded with the left foot pedal

and confirmed with the right foot pedal. Although this feature was not used in this dissertation, the program also can be used record a series of points as the stylus is moved across the surface of an object. To confirm that the object being did not move during digitizing, the user can collect a subset of points at both the beginning and the end of the digitizing session. At the end of the digitizing session, the coordinates in millimeters of the landmarks that were digitized are saved sequentially to a text file.

Rearticulation and anatomical orientation

The rearticulation and anatomical orientation program reads as input a text file containing the 3-D coordinates of landmarks on arbitrarily oriented sacra, innominates, and femora from a sample of individuals. As output the program creates a new text file containing the 3-D coordinates of rearticulated and anatomically oriented hip joints (as described in the methods chapter). The mean “docking” errors between the sacrum and innominate for each individual are written to a separate text file. I also adapted this program to orient a pelvis so that the inlet rim was horizontal to duplicate Rak’s (1991) measurements of relative acetabular positioning.

Calculation of standard measurements

The standard measurement calculation program reads as input a text file containing the 3-D coordinate locations of landmarks on rearticulated and anatomically oriented hip joints from a sample of individuals. As output the program creates a new text file containing a row for each individual and a column containing values for each of the standard measurements listed in Table 3.2. Measurements that cannot be calculated due to missing data are given values of -1000.

Morphometric analysis

A suite of programs together can perform a variety of morphometric analyses. The initial input is a text file containing the 2-D or 3-D coordinate locations of landmarks from a sample of individuals. As output the programs create text files containing centroid sizes, mean shapes or forms, Generalized Procrustes Analysis (GPA) superimposed landmarks, residuals from a mean shape or form, and scores along the most important principal components of shape for the sample. The eigenvalues and eigenvectors for the principal components also are saved to separate text files. These programs can be combined with commercial software to perform discriminant analyses or multiple regression (as discussed in the methods chapter). Size can be added back in after GPA superimposition, and data superimposed using other software packages can be read as input at any stage of the analysis. Changes along principal component axes can be visualized using the visualization program discussed below.

Interactive visualization

A computer visualization program allows any object described by 3-D coordinate landmarks with or without links between them to be interactively displayed, rotated, translated, and scaled on the computer screen. The landmarks and links can either be white, red, green, blue, or yellow and are shaded so that they become darker with increasing depth in the picture. Objects also can be displayed in grayscale only to produce black and white images for publication. Basic measurements such as the angle between three landmarks and the distance between two landmarks can be calculated. This program can be used to display shape changes along principal component or

discriminant function axes, mean shapes or forms, or the landmark coordinates of any individual in a sample. A series of shapes or forms can be read as input and then the user can interactively flip between them to better understand size and shape changes. This program is extremely flexible; all it requires is a file or series of files containing landmark coordinates, links, and color information.

Bibliography

- Abitbol, M. M. 1987a. Evolution of the lumbosacral angle. *American Journal of Physical Anthropology* 72:361-372.
- . 1987b. Obstetrics and posture in pelvic anatomy. *Journal of Human Evolution* 16:243-255.
- . 1995a. Lateral view of *Australopithecus afarensis*: primitive aspects of bipedal positional behavior in the earliest hominids. *Journal of Human Evolution* 28:211-229.
- . 1995b. Reconstruction of the STS 14 (*Australopithecus africanus*) pelvis. *American Journal of Physical Anthropology* 96:143-158.
- . 1996. The shapes of the female pelvis: Contributing factors. *Journal of Reproductive Medicine* 41:242-250.
- Akazawa, T., S. Muhesen, Y. Dodo, and Y. Mizoguchi. 1995. Neanderthal infant burial. *Nature* 377:585-586.
- Allen, J. A. 1877. The influence of physical conditions in the genesis of species. *Radical Review* 1:108-140.
- Anderson, J. Y., and E. Trinkaus. 1998. Patterns of sexual, bilateral and interpopulational variation in human femoral neck-shaft angles. *Journal of Anatomy* 192:279-285.
- Arsuaga, J.-L., and J.-M. Carretero. 1994. Multivariate analysis of the sexual dimorphism of the hip bone in a modern human population and in early hominids. *American Journal of Physical Anthropology* 93:241-257.
- Arsuaga, J.-L., C. Lorenzo, J.-M. Carretero, A. Gracia, I. Martínez, N. García, J.-M. Bermúdez de Castro, and E. Carbonell. 1999. A complete human pelvis from the Middle Pleistocene of Spain. *Nature* 399:255-258.
- Arthur, W. 2002. The emerging conceptual framework of evolutionary developmental biology. *Nature* 415:757-764.
- Ashton, K. G., M. C. Tracy, and A. de Queiroz. 2000. Is Bergmann's rule valid for mammals? *American Naturalist* 156:390-415.

- Balout, L. 1977. "Algeria," in *Catalogue of fossil hominids*, 2nd. edition, vol. 1: Africa. Edited by K. P. Oakley, B. G. Cambell, and T. I. Molleson, pp. 1-6. London: Trustees of the British Museum (Natural History).
- Bar-Yosef, O. 1998. "The chronology of the Middle Paleolithic of the Levant," in *Neandertals and modern humans in western Asia*. Edited by T. Akazawa, K. Aoki, and O. Bar-Yosef, pp. 39-56. New York: Plenum Press.
- Baskerville, R. F. 1989. On Neandertal pubic length. *Current Anthropology* 30:482-486.
- Beaupré, G. S., T. E. Orr, and D. R. Carter. 1990. An approach for time-dependent bone modeling and remodeling—application: A preliminary remodeling simulation. *Journal of Orthopaedic Research* 8:662-670.
- Berge, C. 1994. How did the australopithecines walk? A biomechanical study of the hip and thigh of *Australopithecus afarensis*. *Journal of Human Evolution* 26:259-273.
- Berge, C., R. Orban-Segebarth, and P. Schmid. 1984. Obstetrical interpretation of the Australopithecine pelvic cavity. *Journal of Human Evolution* 13:573-587.
- Bergmann, C. 1847. Über die verhältnisse der wärmeökonomie der thiere zu ihrer grösse. *Göttinger Studien* 3:595-708.
- Bischoff, J. L., J. A. Fitzpatrick, L. León, J.-L. Arsuaga, C. Falguères, J. J. Bahain, and T. Bullen. 1997. Geology and preliminary dating of the hominid-bearing sedimentary fill of the Sima de los Huesos Chamber, Cueva Mayor of the Sierra de Atapuerca, Burgos, Spain. *Journal of Human Evolution* 33:129-154.
- Bookstein, F. L. 1991. *Morphometric tools for landmark data: Geometry and biology*. Cambridge: Cambridge University Press.
- . 1996. "Combining the tools of geometric morphometrics," in *Advances in morphometrics, NATA Advanced Science Institutes Series*. Edited by L. F. Marcus, M. Corti, A. Loy, G. J. P. Naylor, and D. E. Slice, pp. 131-151. New York: Plenum Press.
- Boule, M. 1912. l'Homme fossile de La Chapelle-aux-Saints. *Annales de Paléontologie* 7:105-192.
- Brand, R. A., R. D. Crowninshield, C. E. Wittstock, D. R. Pedersen, C. R. Clark, and F. M. Van Krieken. 1982. A model of lower extremity muscular anatomy. *Journal of Biomechanical Engineering* 104:304-310.

- Brien, E. W., J. M. Lane, and J. Healey. 1995. Progressive coxa valga after childhood excision of the hip abductor muscles. *Journal of Pediatric Orthopedics* 15:95-97.
- Carter, D. R. 1987. Mechanical loading history and skeletal biology. *Journal of Biomechanics* 20:1095-1109.
- Carter, D. R., and G. S. Beaupré. 2001. *Skeletal function and form: Mechanobiology of skeletal development, aging, and regeneration*. Cambridge: Cambridge University Press.
- Chen, T., Q. Yang, and E. Wu. 1994. Antiquity of *Homo sapiens* in China. *Nature* 368:55-56.
- Churchill, S. E. 1996. Particulate versus integrate evolution of the upper body in Late Pleistocene humans: A test of two models. *American Journal of Physical Anthropology* 100:559-583.
- Cohn, M. J., and P. E. Bright. 2000. "Development of vertebrate limbs: insights into pattern, evolution and dysmorphogenesis," in *Development, growth, and evolution: Implications for the study of the hominid skeleton*, vol. 20, *Linnean Society Symposium Series*. Edited by P. O'Higgins and M. J. Cohn, pp. 41-55. London: Academic Press.
- Day, M. H. 1971. Postcranial remains of *Homo erectus* from Bed IV, Olduvai Gorge, Tanzania. *Nature* 232:383-387.
- Day, M. H., M. H. C. Twist, and S. C. Ward. 1991. Les vestiges post-crâniens d'Omo I (Kibish). *L'Anthropologie* 95:595-610.
- de Lumley, M.-A. 1972. L'Os iliaque anténéandertalien de la Grotte du Prince (Grimaldi, Ligurie italienne). *Bulletin du Musée d'Anthropologie Préhistorique du Monaco* 18:89-112.
- Dean, M. C., C. B. Stringer, and T. G. Bromage. 1986. A new age at death for the Neanderthal child from Devil's Tower, Gibraltar and the implications for studies of general growth and development in Neanderthals. *American Journal of Physical Anthropology* 70:301-309.
- Delp, S. L. 1990. Surgery simulation: A computer graphics system to analyze and design musculoskeletal reconstructions of the lower limb. Ph.D., Stanford University.
- Dryden, I. L., and K. V. Mardia. 1998. *Statistical shape analysis*. New York: John Wiley & Sons.

- Endo, B., and T. Kimura. 1970. "Postcranial skeleton of the Amud man," in *The Amud man and his cave site*. Edited by H. Suzuki and F. Takai, pp. 231-406. Tokyo: Academic Press of Japan.
- Eveleth, P. B., and J. M. Tanner. 1976. *Worldwide variation in human growth*, 1st edition. Cambridge: Cambridge University Press.
- . 1990. *Worldwide variation in human growth*, 2nd edition. Cambridge: Cambridge University Press.
- Gambier, D. 1989. "Fossil hominids from the early Upper Palaeolithic (Aurignacian) of France," in *The human revolution*. Edited by P. Mellars and C. B. Stringer, pp. 194-211. Edinburgh: Edinburgh University Press.
- Gelvin, B. R., and G. H. Albrecht. 1989. Gestation length in Neandertals. *American Journal of Physical Anthropology* 78:226.
- Gieseler, W. 1971. "Germany," in *Catalogue of fossil hominids*, vol. 2: Europe. Edited by K. P. Oakley, B. G. Cambell, and T. I. Molleson, pp. 189-215. London: Trustees of the British Museum (Natural History).
- Gilbert, S. F., J. M. Opitz, and R. A. Raff. 1996. Resynthesizing evolutionary and developmental biology. *Developmental Biology* 173:357-372.
- Gower, J. C. 1975. Generalized procrustes analysis. *Psychometrika* 40:33-50.
- Grine, F. E., W. L. Jungers, P. V. Tobias, and O. M. Pearson. 1995. Fossil *Homo* femur from Berg Aukas, Northern Namibia. *American Journal of Physical Anthropology* 97:151-185.
- Hager, L. D. 1996. Sex differences in the sciatic notch of great apes and modern humans. *American Journal of Physical Anthropology* 99:287-300.
- Hartman, S. E. 1989. Stereophotogrammetric analysis of occlusal morphology of extant hominoid molars: Phenetics and function. *American Journal of Physical Anthropology* 80:145-166.
- Häusler, M., and L. Berger. 2001. Stw 441/465: A new fragmentary ilium of a small-bodied *Australopithecus africanus* from Sterkfontein, South Africa. *Journal of Human Evolution* 40:411-417.

- Häusler, M., and P. Schmid. 1995. Comparison of the pelves of Sts 14 and AL 288-1: Implications for birth and sexual dimorphism in australopithecines. *Journal of Human Evolution* 29:363-383.
- . 1998. Assessing the pelvis of AL 288-1: A reply to Wood and Quinney. *Journal of Human Evolution* 32:99-102.
- Heim, J.-L. 1983. Les variations du squelette post-crânien des hommes de Néandertal suivant le sexe. *L'Anthropologie* 87:5-26.
- Heimkes, B., P. Posel, W. Plitz, and V. Jansson. 1993. Forces acting on the juvenile hip joint in the one-legged stance. *Journal of Pediatric Orthopedics* 13:431-436.
- Heimkes, B., P. Posel, W. Plitz, and M. Zimmer. 1997. Age relevant distribution of forces at the proximal end of the femur of the normally developing-child. *Zeitschrift für Orthopaedie und Ihre Grenzgebiete* 135:17-23.
- Hennessy, R. J., and C. B. Stringer. 2002. Geometric morphometric study of the regional variation of modern human craniofacial form. *American Journal of Physical Anthropology* 117:37-48.
- Hershkovitz, I., M. S. Speirs, D. Frayer, D. Nadel, S. Wish-Baratz, and B. Arensburg. 1995. Ohalo II H2: A 19,000-year-old skeleton from a water-logged site at the Sea of Galilee, Israel. *American Journal of Physical Anthropology* 96:215-234.
- Holliday, T. W. 1995. Body size and proportions in the Late Pleistocene Western Old World and the origins of modern humans. Ph.D., University of New Mexico.
- . 1997a. Body proportions in Late Pleistocene Europe and modern human origins. *Journal of Human Evolution* 32:423-447.
- . 1997b. Postcranial evidence of cold adaptation in European Neandertals. *American Journal of Physical Anthropology* 104:245-258.
- Houston, C. S., and W. A. Zaleski. 1967. The shape of vertebral bodies and femoral necks in relation to activity. *Radiology* 89:59-66.
- Hublin, J.-J. 1992. Le fémur humain pléistocène moyen de l'Aïn Maarouf (El Hajeb, Maroc). *Comptes rendus de l'Académie des sciences. Série II* 314:975-980.
- Ingman, M., H. Kaessmann, S. Pääbo, and U. Gyllensten. 2000. Mitochondrial genome variation and the origin of modern humans. *Nature* 408:708-713.

- Johanson, D. C., C. O. Lovejoy, W. H. Kimbel, T. D. White, S. C. Ward, M. E. Bush, B. M. Latimer, and Y. Coppens. 1982. Morphology of the Pliocene partial hominid skeleton (A.L. 288-1) from the Hadar Formation, Ethiopia. *American Journal of Physical Anthropology* 57:403-451.
- Johnson, R. A., and D. W. Wichern. 1998. *Applied multivariate statistical analysis*, 4th edition. Upper Saddle River: Prentice-Hall.
- Kendall, D. G. 1984. Shape manifolds, procrustean metrics and complex projective spaces. *Bulletin of the London Mathematical Society* 16:81-121.
- Kennedy, G. E. 1983. Some aspects of femoral morphology in *Homo erectus*. *Journal of Human Evolution* 12:587-616.
- . 1984. The emergence of *Homo sapiens*: The post cranial evidence. *Man* 19:94-110.
- Kimbel, W. H., D. C. Johanson, and Y. Rak. 1994. The first skull and other new discoveries of *Australopithecus afarensis* at Hadar, Ethiopia. *Nature* 368:449-451.
- Klein, R. G. 1989. *The human career: Human biological and cultural origins*. Chicago: University of Chicago Press.
- . 1999. *The human career: Human biological and cultural origins*, 2nd edition. Chicago: University of Chicago Press.
- . 2000. Archeology and the evolution of human behavior. *Evolutionary Anthropology* 9:17-36.
- Knight, A., M. Batzer, M. Stoneking, H. Tiwari, W. D. Scheer, R. J. Herrera, and P. L. Deininger. 1996. DNA sequences of Alu elements indicate a recent replacement of the human autosomal genetic complement. *Proceedings of the National Academy of Sciences of the United States of America* 93:4360-4364.
- Kormondy, E. J., and D. E. Brown. 1998. *Fundamentals of human ecology*. Upper Saddle River: Prentice Hall.
- Krings, M., C. Capelli, F. Tschentscher, H. Geisert, S. Meyer, A. von Haeseler, K. Grossschmidt, G. Possnert, M. Paunovic, and S. Pääbo. 2000. A view of Neandertal genetic diversity. *Nature Genetics* 26:144-146.
- Lahr, M. M. 1995. Patterns of modern human diversification: Implications for Amerindian origins. *Yearbook of Physical Anthropology* 38:163-198.

- LaPlaza, F. J., L. Root, A. Tassanawipas, and D. B. Glasser. 1993. Femoral torsion and neck-shaft angles in cerebral palsy. *Journal of Pediatric Orthopedics* 13:192-199.
- LaVelle, M. 1995. Natural selection and developmental sexual variation in the human pelvis. *American Journal of Physical Anthropology* 98:59-72.
- Lele, S. 1991. Some comments on coordinate-free and scale-invariant methods in morphometrics. *American Journal of Physical Anthropology* 85:407-417.
- Lele, S., and J. T. Richtsmeier. 2001. *An invariant approach to statistical analysis of shapes. Interdisciplinary statistics*. Boca Raton: Chapman & Hall.
- Lieberman, D. E. 1995. Testing hypotheses about recent human evolution from skulls. *Current Anthropology* 36:159-178.
- Lordkipanidze, D., and A. Vekua. 2002. A new hominid mandible from Dmanisi (Georgia). *Journal of Human Evolution* 42:A20.
- Lovejoy, C. O. 1979. Reconstruction of the pelvis of AL 288-1 (Hadar Formation, Ethiopia). *American Journal of Physical Anthropology* 50:460.
- . 1988. Evolution of human walking. *Scientific American* 259:118-125.
- Lovejoy, C. O., M. J. Cohn, and T. D. White. 1999. Morphological analysis of the mammalian postcranium: A developmental perspective. *Proceedings of the National Academy of Sciences of the United States of America* 96:13247-13252.
- . 2000. "The evolution of mammalian morphology: A developmental perspective," in *Development, growth, and evolution: Implications for the study of the hominid skeleton*, vol. 20, *Linnean Society Symposium Series*. Edited by P. O'Higgins and M. J. Cohn, pp. 41-55. London: Academic Press.
- Lovejoy, C. O., K. G. Heiple, and A. H. Burstein. 1973. The gait of *Australopithecus*. *American Journal of Physical Anthropology* 38:757-779.
- Lovejoy, C. O., D. C. Johanson, and Y. Coppens. 1982. Hominid lower limb bones recovered from the Hadar Formation: 1974-1977 collections. *American Journal of Physical Anthropology* 57:679-700.
- Maquet, P. G. J. 1985. *Biomechanics of the hip: As applied to osteoarthritis and related conditions*. New York: Springer-Verlag.
- McCollum, M. A. 1999a. Response to Strait and Grine. *Science* 285:1211.

- . 1999b. The robust Australopithecine face: A morphogenetic perspective. *Science* 284:301-305.
- McCown, T. D., and A. Keith. 1939. *The stone age of Mount Carmel: The fossil human remains from the Levallois-Mousterian. Vol II.* Oxford: Clarendon Press.
- McHenry, H. M. 1975a. The ischium and hip extensor mechanism in human evolution. *American Journal of Physical Anthropology* 43:39-46.
- . 1975b. A new pelvic fragment from Swartkrans and the relationship between the robust and gracile Australopithecines. *American Journal of Physical Anthropology* 43:245-262.
- McHenry, H. M., and K. Coffing. 2000. *Australopithecus to Homo: Transformations in body and mind. Annual Review of Anthropology* 29:125-146.
- McHenry, H. M., and R. S. Corruccini. 1978. The femur in early human evolution. *American Journal of Physical Anthropology* 49:473-488.
- McLeish, R. D., and J. Charnley. 1970. Abduction forces in the one-legged stance. *Journal of Biomechanics* 3:191-209.
- Molleson, T., and M. Cox. 1993. *The Spitalfields project. Volume 2: The anthropology. CBA research report 86.* Vol. 86. York: Council for British Archaeology.
- Morris, A. G. 1992. *A master catalogue: Holocene human skeletons from South Africa.* Johannesburg: Witwatersrand University Press.
- Mussi, M. 2001. *Earliest Italy: An overview of the Italian Paleolithic and Mesolithic. Interdisciplinary contributions to archaeology.* New York: Kluwer Academic/Plenum.
- Newman, R. W. 1975. "Human adaptation to heat," in *Physiological anthropology.* Edited by A. Damon. New York: Oxford University Press.
- O'Higgins, P. 2000. The study of morphological variation in the hominid fossil record: Biology, landmarks, and geometry. *Journal of Anatomy* 197:103-120.
- O'Higgins, P., and N. Jones. 1998. Facial growth in *Cercocebus torquatus*: An application of three-dimensional geometric morphometric techniques to the study of morphological variation. *Journal of Anatomy* 193:251-272.

- Oakley, K. P. 1971. "British Isles," in *Catalogue of fossil hominids*, vol. 2: Europe. Edited by K. P. Oakley, B. G. Cambell, and T. I. Molleson, pp. 15-43. London: Trustees of the British Museum (Natural History).
- Orban, R. 1982. A biometrical comparative study of the os coxae of hominidae, pongidae and Australopithecus Sts 14. *Man and His Origins* 21:61-72.
- Ovchinnikov, I. V., A. Götherström, G. P. Romanova, V. M. Kharitonov, K. Lidén, and W. Goodwin. 2000. Molecular analysis of Neanderthal DNA from the northern Caucasus. *Nature* 404:490-493.
- Pasqualetti, M., and F. M. Rijli. 2002. The plastic face. *Nature* 416:493-494.
- Pauwels, F. 1980. *Biomechanics of the locomotor apparatus: Contributions on the functional anatomy of the locomotor apparatus*. New York: Springer-Verlag.
- Pearson, O. M. 2000a. Activity, climate, and postcranial robusticity. *Current Anthropology* 41:569-607.
- . 2000b. Postcranial remains and the origins of modern humans. *Evolutionary Anthropology* 9:229-247.
- Penin, X., and M. Baylac. 1999. Comparaison tridimensionnelle des crânes de *Pan* et *Pongo* par superpositions procrustéennes. *Comptes Rendus de l'Academie des Sciences. Serie III, Sciences de la Vie* 322:1099-1104.
- Radovic, J., F. H. Smith, E. Trinkaus, and M. H. Wolpoff. 1988. *The Krapina hominids: An illustrated catalog of skeletal collection*. Zagreb: Mladost Publishing House.
- Rak, Y. 1990. On the differences between two pelvises of Mousterian context from the Qafzeh and Kebara caves, Israel. *American Journal of Physical Anthropology* 81:323-332.
- . 1991. "The pelvis," in *Le squelette Moustérien de Kébara*. Edited by O. Bar-Yosef and B. Vandermeersch, pp. 147-166. Paris: CNRS Editions.
- . 1993. "Morphological variation in *Homo neanderthalensis* and *Homo sapiens* in the Levant: A biogeographic model," in *Species, species concepts, and primate evolution*. Edited by W. H. Kimbel and L. B. Martin, pp. 523-536. New York: Plenum Press.
- Rak, Y., and B. Arensburg. 1987. Kebara 2 Neanderthal pelvis: First look at a complete inlet. *American Journal of Physical Anthropology* 73:227-231.

- Roberts, D. F. 1978. *Climate and human variability*, 2nd edition. Menlo Park: Cummings.
- Robinson, J. T. 1972. *Early hominid posture and locomotion*. Chicago: University of Chicago Press.
- Rohlf, F. J. 1999. Shape statistics: Procrustes superimpositions and tangent spaces. *Journal of Classification* 16:197-223.
- Rohlf, F. J., and D. E. Slice. 1990. Extensions of the procrustes method for the optimal superimposition of landmarks. *Systematic Zoology* 39:40-59.
- Rose, M. D. 1984. A hominine hip bone, KNM-ER 3228, from East Lake Turkana, Kenya. *American Journal of Physical Anthropology* 63:371-378.
- Rosenberg, K. R. 1986. The functional significance of Neandertal pubic morphology. Ph.D., University of Michigan.
- . 1988. The functional significance of Neandertal pubic length. *Current Anthropology* 29:595-607.
- . 1989. Reply to Baskerville. *Current Anthropology* 30:486-488.
- . 1992. The evolution of modern human childbirth. *Yearbook of Physical Anthropology* 35:89-124.
- . 1998. "Morphological variation in West Asian postcrania," in *Neandertals and modern humans in Western Asia*. Edited by T. Akazawa, K. Aoki, and O. Bar-Yosef, pp. 367-379. New York: Plenum Press.
- Rosenberg, K. R., L. Zun'e, and C. B. Ruff. 1999. Body size, body proportions and encephalization in the Jinniushan specimen. *American Journal of Physical Anthropology* Supplement 28:235.
- Rosenman, B. A., C. O. Lovejoy, and L. B. Spurlock. 1999. A reconstruction of the Sts 14 pelvis, and the obstetrics of *Australopithecus*. *American Journal of Physical Anthropology* Supplement 28:235.
- Ruff, C. B. 1991. Climate and body shape in hominid evolution. *Journal of Human Evolution* 21:81-105.
- . 1993. Climatic adaptation in hominid evolution: The thermoregulatory imperative. *Evolutionary Anthropology* 2:53-60.

- . 1994. Morphological adaptation to climate in modern and fossil hominids. *Yearbook of Physical Anthropology* 37:65-107.
- . 1995. Biomechanics of the hip and birth in early *Homo*. *American Journal of Physical Anthropology* 98:527-574.
- . 1998. "Evolution of the hominid hip," in *Primate locomotion: Recent advances*. Edited by E. Strasser, pp. 449-469. New York: Plenum Press.
- . 2000. "Biomechanical analyses of archaeological human skeletons," in *Biological anthropology of the human skeleton*, 2nd edition. Edited by M. A. Katzenberg and S. R. Saunders, pp. 71-102. New York: Wiley-Liss.
- Ruff, C. B., and W. C. Hayes. 1983. Cross-sectional geometry of Pecos Pueblo femora and tibiae—a biomechanical investigation: I. Method and general patterns of variation. *American Journal of Physical Anthropology* 60:359-381.
- Ruff, C. B., E. Trinkaus, and T. W. Holliday. 1997. Body mass and encephalization in Pleistocene *Homo*. *Nature* 387:173-176.
- Ruff, C. B., and A. Walker. 1993. "Body size and body shape," in *The Nariokotome Homo erectus skeleton*. Edited by A. Walker and R. Leakey, pp. 234-265. Cambridge: Harvard University Press.
- Sarmiento, E. E. 1998. Generalized quadrupeds, committed bipeds, and the shift to open habitats: An evolutionary model of hominid divergence. *Novitates* 3250:1-78.
- Schultz, A. H. 1926. Fetal growth in man and other primates. *Quarterly Review of Biology* 1:465-521.
- Segebarth-Orban, R. 1977. Comparaison de quelques dimensions de l'os coxal du chimpanze, de l'homme et d'un australopitheque (Sts 14). *Bulletin de la Société royale belge d'Anthropologie et de Préhistoire* 88:101-116.
- . 1980. An evaluation of the sexual dimorphism of the human innominate bone. *Journal of Human Evolution* 9:601-607.
- Senut, B., M. Pickford, D. Gommery, P. Mein, K. Chebio, and Y. Coppens. 2001. First hominid from the Miocene (Lukeino formation, Kenya). *Comptes Rendus de L'Academie des Sciences. Serie II, Fascicule A-Sciences de la Terre et des Planetes* 322:137-144.

- Shea, J., J. G. Fleagle, F. Brown, and Z. Assefa. 2002. Archaeological reconnaissance of the Omo Kibish Formation, Ethiopia. *Journal of Human Evolution* 42:A33.
- Shefelbine, S. J., C. Tardieu, and D. R. Carter. 2002. Development of the femoral bicondylar angle in hominid bipedalism. *Bone* 30:765-770.
- Sigmon, B. A. 1982. "Comparative morphology of the locomotor skeleton of *Homo erectus* and the other fossil hominids, with special reference to the Tautavel innominate and femora," in *L'Homo erectus et la place de l'Homme de Tautavel parmi les Hominidés fossiles*, vol. 1, Editions du CNRS. Edited by M.-A. de Lumley, pp. 422-446. Nice: Premier Congrès International de Paléontologie Humaine.
- Smith, F. H. 1978. Some conclusions regarding the morphology and significance of the Krapina Neandertal remains. *Krapinski pracojvek i evolucija hominida*:103-118.
- Smith, R. J. 1996. Biology and body size in human evolution: Statistical inference misapplied. *Current Anthropology* 37:451-481.
- Sokal, R. R., and F. J. Rohlf. 1995. *Biometry: The principals and practice of statistics in biological research*, 3rd edition. New York: W.H. Freeman and Company.
- Stegmann, A. T. 1975. "Human adaptation to cold," in *Physiological anthropology*. Edited by A. Damon, pp. 130-166. New York: Oxford University Press.
- Steele, D. G., and C. A. Bramblett. 1988. *The anatomy and biology of the human skeleton*. College Station: Texas A&M University Press.
- Stern, J. T. 2000. Climbing to the top: A personal memoir of *Australopithecus afarensis*. *Evolutionary Anthropology* 9:113-133.
- Stern, J. T., and R. L. Susman. 1983. The locomotor anatomy of *Australopithecus afarensis*. *American Journal of Physical Anthropology* 60:279-317.
- Stewart, T. D. 1960. Form of the pubic bone in Neanderthal man. *Science* 131:1437-1438.
- Stringer, C. B. 1986. An archaic character in the Broken Hill innominate E. 719. *American Journal of Physical Anthropology* 71:115-120.
- Tague, R. G. 1992. Sexual dimorphism in the human bony pelvis, with a consideration of the Neandertal pelvis from Kebara Cave, Israel. *American Journal of Physical Anthropology* 88:1-21.

- . 2000. Do big females have big pelves? *American Journal of Physical Anthropology* 112:377-393.
- Tague, R. G., and C. O. Lovejoy. 1986. The obstetric pelvis of A.L. 288-1 (Lucy). *Journal of Human Evolution* 15:237-255.
- . 1998. AL 288-1—Lucy or Lucifer: Gender confusion in the Pliocene. *Journal of Human Evolution* 35:75-94.
- Tardieu, C. 1998. Short adolescence in early hominids: Infantile and adolescent growth of the human femur. *American Journal of Physical Anthropology* 107:163-178.
- Tishkoff, S. A., E. Dietzsch, W. Speed, A. J. Pakstis, J. R. Kidd, K. Cheung, B. Bonn -Tamir, A. S. Santachiara-Benerecetti, P. Moral, M. Krings, S. P  bo, E. Watson, N. Risch, T. Jenkins, and K. K. Kidd. 1996. Global patterns of linkage disequilibrium at the CD4 locus and modern human origins. *Science* 271:1380-1387.
- Tompkins, R. L., and E. Trinkaus. 1987. La Ferrassie 6 and the development of Neandertal pubic morphology. *American Journal of Physical Anthropology* 73:233-239.
- Trinkaus, E. 1981. "Neanderthal limb proportions and cold adaptation," in *Aspects of human evolution*, vol. 21, *Symposia of the society for the study of human biology*. Edited by C. B. Stringer, pp. 187-224. London: Taylor and Francis.
- . 1983. *The Shanidar Neandertals*. New York: Academic Press.
- . 1984. Neandertal pubic morphology and gestation length. *Current Anthropology* 25:509-514.
- . 1993a. Femoral neck-shaft angles of the Qafzeh-Skhul early modern humans, and activity levels among immature Near Eastern Paleolithic hominids. *Journal of Human Evolution* 25:393-416.
- . 1993b. A note on the KNM-ER 999 hominid femur. *Journal of Human Evolution* 24:493-504.
- . 1995. Near Eastern late archaic humans. *Pal orient* 21:9-23.
- . 1996. The M-obturator internus sulcus on Middle and Late Pleistocene human ischia. *American Journal of Physical Anthropology* 101:503-513.

- . 1997. Appendicular robusticity and the paleobiology of modern human emergence. *Proceedings of the National Academy of Sciences of the United States of America* 94:13367-13373.
- Trinkaus, E., S. E. Churchill, and C. B. Ruff. 1994. Postcranial robusticity in *Homo*. II: Humeral bilateral asymmetry and bone plasticity. *American Journal of Physical Anthropology* 93:1-34.
- Trinkaus, E., C. B. Ruff, and S. E. Churchill. 1998. "Upper limb versus lower limb loading patterns among Near Eastern Middle Paleolithic hominids," in *Neanderthals and modern humans in Western Asia*. Edited by T. Akazawa, O. Bar-Yosef, and K. Aoki. New York: Plenum Press.
- Trinkaus, E., C. B. Ruff, S. E. Churchill, and B. Vandermeersch. 1998. Locomotion and body proportions of the Saint-Césaire 1 Châtelperronian Neandertal. *Proceedings of the National Academy of Sciences of the United States of America* 95:5836-5840.
- Turnbull, C. M. 1983. *The Mbuti pygmies : Change and adaptation. Case studies in cultural anthropology*. New York: Holt, Rinehart, and Winston.
- Twisselmann, F. 1971. "Belgium," in *Catalogue of fossil hominids*, vol. 2: Europe. Edited by K. P. Oakley, B. G. Cambell, and T. I. Molleson, pp. 5-13. London: Trustees of the British Museum (Natural History).
- Underhill, P. A., G. Passarino, A. A. Lin, P. Shen, M. M. Lahr, R. A. Foley, P. J. Oefner, and L. L. Cavalli-Sforza. 2001. The phylogeography of Y chromosome binary haplotypes and the origins of modern human populations. *Annals of Human Genetics* 65:43-62.
- Van Gerven, D. P. 1972. The contribution of size and shape variation to patterns of sexual dimorphism of the human femur. *American Journal of Physical Anthropology* 37:49-60.
- Vrba, E. S. 1985. "Early hominids in southern Africa: Updated observations on chronological and ecological background.," in *Hominid evolution, past, present and future*. Edited by P. V. Tobias, pp. 63-71. New York: Allan R. Liss.
- Walker, A. 1973. New *Australopithecus* femora from East Rudolf, Kenya. *Journal of Human Evolution* 2:545-555.
- Walker, A., and R. Leakey. Editors. 1993. *The Nariokotome Homo erectus skeleton*. Cambridge: Harvard University Press.

- Walker, A., and C. B. Ruff. 1993. "The reconstruction of the pelvis," in *The Nariokotome Homo erectus skeleton*. Edited by A. Walker and R. Leakey, pp. 221-233. Cambridge: Harvard University Press.
- Weaver, T. D. 2000a. Climate induced variation in recent human hip morphology. *American Journal of Physical Anthropology* Supplement 32:162.
- . 2000b. The relationship of body proportions with femoral and pelvic shape in recent humans and Late Pleistocene to Holocene fossil hominids. *Journal of Human Evolution* 40:A24-A25.
- Weaver, T. D., R. G. Franciscus, C. D. Karlin, E. A. Burson, and K. A. Gust. 1998. 3-D coordinate analysis of the Kebara 2 pelvis. *American Journal of Physical Anthropology* Supplement 26:228.
- Weidenreich, F. 1941. The extremity bones of *Sinanthropus Pekinensis*. *Palaeontologia Sinica* New Series D:1-150.
- White, T. D., and P. A. Folkens. 1995. *Human osteology*. San Diego: Academic Press.
- Williams, P. L. 1995. *Gray's anatomy: The anatomical basis of medicine and surgery*, 38th edition. New York: Churchill and Livingstone.
- Wood, B., and P. Quinney. 1996. Assessing the pelvis of AL 288-1. *Journal of Human Evolution* 31:563-568.
- Y'Edynak, G. 1978. Long bone growth in Western Eskimo and Aleut skeletons. *American Journal of Physical Anthropology* 45:569-574.
- Zubrow, E. 1989. "The demographic modeling of Neanderthal extinction," in *The human revolution*. Edited by P. Mellars and C. B. Stringer, pp. 212-231. Edinburgh: Edinburgh University Press.